NASA TECHNICAL NOTE

NASA TN D-3192




# WIND-TUNNEL INVESTIGATION OF LONGITUDINAL AERODYNAMIC CHARACTERISTICS OF A POWERED FOUR-DUCT-PROPELLER VTOL MODEL IN TRANSITION

*by Kenneth P. Spreemann*

*Langley Research Center*
*Langley Station, Hampton, Va.*

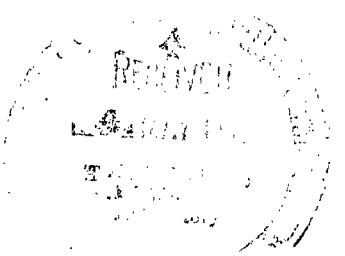

NATIONAL AERONAUTICS AND SPACE ADMINISTRATION • WASHINGTON, D. C. • APRIL 1966

NASA TN D-3192

# WIND-TUNNEL INVESTIGATION OF LONGITUDINAL AERODYNAMIC CHARACTERISTICS OF A POWERED FOUR-DUCT-PROPELLER VTOL MODEL IN TRANSITION

By Kenneth P. Spreemann

Langley Research Center
Langley Station, Hampton, Va.

NATIONAL AERONAUTICS AND SPACE ADMINISTRATION

For sale by the Clearinghouse for Federal Scientific and Technical Information
Springfield, Virginia 22151 – Price $1.55

# WIND-TUNNEL INVESTIGATION OF LONGITUDINAL AERODYNAMIC CHARACTERISTICS OF A POWERED FOUR-DUCT-PROPELLER VTOL MODEL IN TRANSITION

By Kenneth P. Spreemann
Langley Research Center

## SUMMARY

An investigation of the aerodynamic characteristics of a powered four-duct-propeller model of a VTOL airplane has been conducted in the 17-foot test section of the Langley 300-MPH 7- by 10-foot tunnel. The model was tested through an angle-of-attack and transition-speed range from hover to normal forward flight. Duct deflection angles from $-5^{\circ}$ to $90^{\circ}$ were investigated at appropriate speeds and power conditions.

The results showed that the first configuration tested was longitudinally unstable at high thrust coefficients in the cruise condition. Longitudinal stability was achieved by diminishing the destabilizing effects of the front pair of ducts by reducing the size of the front fairings between the ducts and the fuselage. Duct lip stall, which was aggravated by the low Reynolds numbers of the tests, was delayed to higher angles of attack by increasing the lower lip radius of the duct. Delaying the stall on the lower duct lip also helped to delay stalling on the upper duct surface. Trim and control requirements in the transition-speed range might best be attained by a combination of differential thrust and deflection of vanes within the ducts.

## INTRODUCTION

An investigation to study the longitudinal aerodynamic and control characteristics of a four-duct-propeller VTOL transport airplane configuration has been conducted in the 17-foot test section of the Langley 300-MPH 7- by 10-foot tunnel by using a 1/5-scale model. The four ducts were arranged in pairs at the front and rear of the model. This arrangement, as pointed out in reference 1, provides good pitch and roll control in hovering and transition by means of differential thrust of the appropriate pairs of ducted propellers. In the transition-speed range this type of aircraft can experience longitudinal and lateral instability associated with flow into the ducts and interference between ducts.

The present investigation was undertaken to study the longitudinal and lateral stability characteristics from hover through transition to normal forward flight. Included in the investigation were various types of modifications used in attempts to reduce some of the stability problems encountered, particularly in the low-transition-speed range. This paper will present only the longitudinal characteristics and the effects of the appropriate modifications.

## COEFFICIENTS AND SYMBOLS

The force and moment coefficients used in this paper are based on the dynamic pressure in the tunnel free stream. The positive sense of forces, moments, and angles is indicated in figure 1 for the complete model and in figure 2 for the isolated duct-propeller assembly. Moments of the complete model are referred to the assumed center-of-gravity location indicated in figure 3. Moments of the isolated duct-propeller assembly are referred to the individual propeller plane.

Measurements for this investigation were taken in the U.S. Customary System of Units. Equivalent values are indicated herein parenthetically in the International System (SI) in the interest of promoting use of this system in future NASA reports. Details concerning the use of SI, together with physical constants and conversion factors, are given in reference 2.

$C_L$ lift coefficient, $\frac{F_L}{qS}$

$C_D$ drag coefficient, $\frac{F_D}{qS}$

$C_m$ pitching-moment coefficient, $\frac{M_Y}{qSD}$

$C_{L,D}$ lift coefficient of duct, $\frac{F_{L,D}}{qS}$

$C_{D,D}$ drag coefficient of duct, $\frac{F_{D,D}}{qS}$

$C_{m,D}$ pitching-moment coefficient of duct, $\frac{M_{Y,D}}{qSD}$

$C_{N,p}$ propeller normal-force coefficient, $\frac{F_{N,p}}{qS}$

$C_{m,p}$ propeller pitching-moment coefficient, $\frac{M_{Y,p}}{qSD}$

$C_P$ propeller power coefficient, $\frac{2\pi Qn}{\rho n^3 D^5}$

$C_T$ propeller thrust coefficient, $\frac{T_T}{qS}$

$C_{T,l}$ propeller thrust coefficient based on free-stream dynamic pressure, $\frac{T_p}{qS}$

$C_{T,2}$ propeller thrust coefficient based on rotational speed of propeller, $\frac{T_p}{\rho n^2 D^4}$

$F_L$ lift force of complete model, lbf (N)

$F_D$ drag force of complete model, lbf (N)

$M_Y$ moment about Y-axis of complete model, ft-lbf (m-N)

$F_{L,D}$ lift force of duct alone, lbf (N)

$F_{D,D}$ drag force of duct alone, lbf (N)

$F_{N,p}$ propeller normal force, lbf (N)

$M_{Y,p}$ propeller pitching moment, ft-lbf (m-N)

$M_{Y,D}$ moment of isolated duct with respect to duct reference axis, ft-lb (m-N)

$q$ free-stream dynamic pressure, $\frac{1}{2}\rho V_\infty^2$, $lbf/ft^2$ $(N/m^2)$

$\rho$ mass density of air in free stream, slugs/cu ft $(kg/m^3)$

$D$ propeller diameter, 16.8 in. (0.427 m)

$Q$ propeller shaft torque, ft-lbf (m-N)

$b$ wing span, in. (m)

$c$ local wing chord, in. (m)

$\bar{c}$ wing mean aerodynamic chord, $\frac{2}{S}\int_0^{b/2} c^2 dy$, in. (m)

$S$ wing reference area, 9.0 sq ft (0.835 $m^2$)

$y$ spanwise distance from plane of symmetry, in. (m)

$T$ thrust, lbf (N)

$T_T$ total propeller thrust, thrust plus drag (propeller off) at $\alpha = 0^\circ$, lbf (N)

$T_p$ thrust of each propeller, lbf (N)

$n$ propeller rotational speed, rps or rpm

$\alpha$ model angle of attack with respect to fuselage reference line, deg

$\alpha_D$ isolated-duct angle of attack, deg

$\theta$ model pitch angle with respect to fuselage reference line in hovering, deg

$\delta_D$ duct deflection angle, deg

$\delta_V$ vane or elevon deflection angle, deg

$i_t$ horizontal-tail, or stabilizer, incidence angle, deg

$t_D$ thickness of front duct fairing, in. (m)

$V_\infty$ free-stream velocity, ft/sec (m/sec)

V velocity of full-scale airplane, knots

$(F_L)_{\alpha=0}$ lift force of complete model at zero angle of attack in the hovering condition out of ground effects, lbf (N)

h height of model above ground board, ft (m)

Subscripts:

F front

R rear

Model components:

$D_F$ front duct fairing between duct and fuselage

$H_t$ horizontal tail, or stabilizer

$H_{t,1}$ horizontal tail, or stabilizer, designated as number 1 (fig. 6)

$V_t$ vertical tail

## MODEL AND APPARATUS

A drawing of the basic model with pertinent dimensions is given in figure 3. The model was mounted on a sting-supported six-component strain-gage balance for measurements of the complete model forces and moments. Thrust was provided by four ducted propellers - two forward mounted close inboard and two rearward mounted on a wing at the rear of the model. Also mounted on the rear wing were four nacelles simulating engine nacelles of a full-scale airplane for powering the four propellers through shafting and gearing. However, for this

tunnel model each propeller was powered by a separate electric motor. The duct center bodies were, therefore, larger than they would be on an actual airplane. The motors were mounted on strain-gage balances to measure the forces and moments of the propellers.

The two right-hand motors were instrumented to measure normal force and pitching moment; the two left-hand motors were instrumented to measure side force and yawing moment. Each pair of ducts was mounted on a shaft with actuators attached so that the front ducts could be rotated through an angle range independent of the rear ducts. The various horizontal stabilizers, control surfaces, and modifications used on the model are shown in figures 4 to 8. The wing incidence angle was held constant at $3^{\circ}$ throughout the investigation.

## TESTS AND CORRECTIONS

The tests were conducted in the 17-foot test section of the Langley 300-MPH 7- by 10-foot tunnel. The arrangement and calibration of this test section are given in the appendix of reference 3. The tunnel velocity and the model propeller speed were held constant throughout the angle-of-attack range for a particular run. Except for the few runs noted in the figures, the various thrust coefficients were obtained by varying the tunnel velocity from one run to the next while maintaining a constant propeller speed. The thrust coefficient $C_T$ was based on the total thrust $T_T$ of the propellers, which was obtained by taking the difference between the longitudinal force with the propeller operating and the longitudinal force with the propeller removed at zero angle of attack and zero duct deflection angle. The thrust coefficients of each propeller, $C_{T,1}$ and $C_{T,2}$, were based on the measured thrust of each propeller at each angle of attack.

Corrections to the free-stream velocity to account for blockage were estimated by the method of reference 4, were found to be negligible, and thus were not applied. The jet boundary corrections were estimated by a method for rectangular tunnels (ref. 5) and by a method for square wind tunnels. The resulting corrections were applied to the cruise configuration data (figs. 10 to 17) as follows:

$$\alpha = \alpha_m + 0.322C_L$$

$$C_D = C_{D,m} + 0.0049C_L^2$$

$$C_m = C_{m,m} + 0.0047C_L$$

where $\alpha_m$, $C_{D,m}$, and $C_{m,m}$ are the measured values in the tunnel.

Because of the uncertainty of applicability of model corrections to a tandem configuration of this type at the high-lift coefficients encountered in transition, no corrections were applied to the transition and duct-alone data (figs. 18 to 27).

The Reynolds numbers for the range of thrust coefficients used based on wing chord or duct chord and free-stream velocity are given in the following table:

| $C_T$ | q | | Reynolds number based on - | |
|---|---|---|---|---|
| | $lb/ft^2$ | $N/m^2$ | Wing chord | Duct chord |
| 0 | 10 | 478.8 | $9.8 \times 10^5$ | $4.8 \times 10^5$ |
| .4 | 10 | 478.8 | 9.8 | 4.8 |
| .8 | 7 | 336.0 | 8.16 | 4.0 |
| 2.1 | 3.5 | 168.0 | 5.8 | 2.85 |
| 7.1 | 1.3 | 62.2 | 3.5 | 1.72 |
| 25.00 | .42 | 20.2 | 2.0 | .92 |
| 60.00 | .19 | 9.1 | 1.34 | .66 |

## PRESENTATION OF RESULTS

The results of the investigation are presented in the following figures:



Flow patterns indicated by tuft studies at various thrust coefficients, duct deflection angles, and angles of attack are presented as parts of figure 19. Combinations of duct deflection angles and model angle of attack are given only where significant changes in stall characteristics occurred. For some tests, propeller data were recorded and are presented as parts of the appropriate figures. For the summary figures 29 and 30, the model was treated as a 0.20-scale model of a 15 000-pound (66 720-newton) airplane.

## DISCUSSION

### Hovering Characteristics

The hovering characteristics of the model within ground effect ($h/D = 0.595$) are given in figure 9, which indicates appreciable changes in the center-of-pressure location, $M_Y/(F_L)_{\alpha=0}D$, with changes in angle of attack and a slight favorable effect of the ground on lift near zero and nose-up attitudes.

### Cruise Configuration Characteristics

The first configuration tested, indicated by the circles in figure 10, was found to have very low longitudinal stability with power off, $C_T = 0$, and became slightly unstable with power on, $C_T = 0.8$; consequently, a number of modifications were tried to alleviate this condition before the transition studies were made. Increasing the size of the outboard stabilizer helped, but greater increases in stability were obtained by reducing the size of the front duct fairings or removing them entirely. (See figs. 10 and 11.)

Since the smallest duct fairing (number 3 shown in fig. 5) gave a more stable configuration than the other fairings tried, it was, therefore, used for the rest of the investigation.

The increased stability provided by the smallest fairing can be attributed to the reduction in lift carry-over on the front ducts and fuselage caused by the fairing geometry. The effects of stabilizer incidence and the effects of removing the stabilizer are shown in figure 12.

A large improvement in linearity of the pitching-moment curves and in stability at relatively high thrust coefficients was achieved by reducing the deflection of both the front and rear ducts $5^\circ$ as shown in figure 13. Although duct deflection angles of $0^\circ$ on the front and $-5^\circ$ on the rear give a good cruise configuration, it must be realized that the aircraft will have to pass through the higher duct angles while going through transition.

From figure 14, it is seen that with power off, removing the propeller had little effect on the aerodynamic characteristics of the model. Also, with sufficient power to provide a zero drag condition at zero angle of attack, the longitudinal stability of the model was virtually the same as with power off. Data for tests showing the effects of various model components on the aerodynamic characteristics of the model are given in figure 15.

In reference 6, it was shown that rotating the propeller against the tip vortex resulted in a slight reduction in power required and pitching moment in the transition speed range for an unshrouded propeller located at the wing tip. However, with the ducted fan of this investigation, direction of propeller rotation had no effect on lift (on which power required is a direct function) and pitching moment (fig. 16).

A few tests with the engine nacelles removed indicate that the nacelles produced a slightly destabilizing contribution to the pitching moment at a thrust coefficient of 0.8 and that in general the effects of the nacelles were very small (fig. 17).

## Characteristics in Transition

Duct stall characteristics.- Tuft studies of the original configuration at a duct incidence of 15° and greater indicated separation of the flow from the duct lower lip at combinations of power and speed corresponding to steady level flight (Thrust = Drag). Similar separation problems were encountered in the study reported in reference 7. In that investigation, separation occurred much earlier on the model than on the corresponding full-scale configuration. In reference 7, it was found that nearly full-scale conditions could be simulated by increasing the lower lip radius of the duct. Consequently, a number of similar modifications were made in an effort to delay the lower duct lip separation until higher angles of attack were reached. A sketch of the most effective duct lip modification which was used throughout most of the investigation is shown in figure 4. Data for the other duct lip modifications, therefore, are not presented in this paper.

The enlarged lower duct lip delayed stalling in the duct as shown by the power-off lift curves in figure 18(a) and power-on stall boundaries in figure 28 (determined from tuft studies on the isolated duct). Moreover, with the enlarged lower duct lip, stalling in the duct was delayed to higher duct angles than stalling on the upper duct surface (fig. 28). Also, delaying flow separation on the lower duct lip helped to delay the stall on the upper duct surface above thrust coefficients of 2.0.

Increasing the lower lip radius altered the camber of the lower duct profile and resulted in a change in pitching-moment characteristics with power off (fig. 18(a)), as might be expected. However, with power on (fig. 18(b)), the effect is reduced, because some of the moment obtained is due to the flow being turned into the duct. With power on, the pitching moment is less affected by duct profile.

Trim and stability in transition.- The transition characteristics are summarized in figure 29 where the data from figures 19 and 20 have been used to calculate the characteristics of a 15 000-pound (66 720-newton) airplane by assuming the model to be 1/5 scale. In the lower transition speed range, 20 to 50 knots, the data indicate that the airplane would be unstable and have large out-of-trim pitching moments. A similar analysis of the data from reference 8 indicated that the four-duct-propeller configuration of that investigation would have almost twice the out-of-trim moment compared with that of the assumed airplane of this investigation. The lower nose-up moments of the present configuration are probably due to the cambered wing and 3° incidence compared with the symmetrical airfoil section and 0° wing incidence used on the configuration of reference 8.

The maximum moments of the airplane of this investigation would require about ±2000 pounds (±8890 newtons) of differential thrust from front to rear

ducts to trim. (See thrust required and moments in fig. 30.) A combination of both differential thrust and vane control may be a better means of providing trim for the airplane in this speed range.

Control effectiveness.- Figures 21 to 24 show the control effectiveness of the vanes within the ducts at various thrust coefficients, which correspond to the range of very low transition speeds to full forward flight speeds. The pitching-moment curves show that vane deflections of $-10^{\circ}$ to $+10^{\circ}$ provide sufficient control to trim the model in the higher transition speed range, where values of $C_T$ ranged from 0.40 to 0.80. However, in the medium and very low transition range, where values of $C_T$ were 2.1 and above and the higher duct deflection angles were required, vane deflection was inadequate and thus differential thrust between the front and rear ducts in addition to vane control will be required (figs. 21 to 24).

As previously mentioned, it was noted from tuft studies that various parts of the ducts stalled at different duct deflection angles. It was also observed that the upper vane surface behind the upward rotation side of the propeller stalled at about the same duct angles of attack as the duct upper surface, whereas the section behind the downward side was delayed $15^{\circ}$ to $20^{\circ}$ higher due to twist in the propeller slipstream. Early stalling on part of the duct vanes, of course, would be detrimental to the control effectiveness of these surfaces.

## CONCLUSIONS

A wind-tunnel investigation of a powered four-duct-propeller model of a VTOL aircraft indicated the following conclusions:

1. The first configuration tested was longitudinally unstable at high thrust coefficients in the cruise condition with the center of gravity midway between the centers of rotation of the ducts. Longitudinal stability was achieved by diminishing the destabilizing effects of the front pair of ducts. This was accomplished by reducing the size of the fairings between the ducts and the fuselage, and thus, the lift carry-over to the fuselage was reduced. Reduction of duct incidence in the cruise configuration also greatly improved the longitudinal stability.

2. Duct lip stall, which was aggravated by the low Reynolds numbers of the tests, was delayed to higher angles of attack by increasing the duct lip radius. Delaying the stall on the lower duct lip also helped to delay stalling on the upper duct surface.

3. The largest nose-up moments in transition were encountered at a duct deflection angle of about $60^{\circ}$ (approximately 40 knots on a full-scale airplane). At this condition, differential thrust between the front and rear pairs of ducts will be required to provide trim and control. Differential duct deflection and deflection of control surfaces within the ducts have very little

effectiveness at high duct deflection angles and low speeds, but provide powerful control at low duct deflection angles and high speeds.

Langley Research Center,
National Aeronautics and Space Administration,
Langley Station, Hampton, Va., October 7, 1965.

## REFERENCES


1. Newsom, William A., Jr.: Aerodynamic Characteristics of Four-Duct Tandem VTOL-Aircraft Configurations. NASA TN D-1481, 1963.

2. Mechtly, E. A.: The International System of Units - Physical Constants and Conversion Factors. NASA SP-7012, 1964.

3. Kuhn, Richard E.; and Hayes, William C., Jr.: Wind-Tunnel Investigation of Longitudinal Aerodynamic Characteristics of Three Propeller-Driven VTOL Configurations in the Transition Speed Range, Including Effects of Ground Proximity. NASA TN D-55, 1960.

4. Herriot, John G.: Blockage Corrections for Three-Dimensional-Flow Closed-Throat Wind Tunnels, With Consideration of the Effect of Compressibility. NACA Rept. 995, 1950. (Supersedes NACA RM A7B28.)

5. Gillis, Clarence L.; Polhamus, Edward C.; and Gray, Joseph L., Jr.: Charts for Determining Jet-Boundary Corrections for Complete Models in 7- by 10-Foot Closed Rectangular Wind Tunnels. NACA WR L-123, 1945. (Formerly NACA ARR L5G31.)

6. Spreemann, Kenneth P.: Investigation of a Semispan Tilting-Propeller Configuration and Effects of Ratio of Wing Chord to Propeller Diameter on Several Small-Chord Tilting-Wing Configurations at Transition Speeds. NASA TN D-1815, 1963.

7. Goodson, Kenneth W.; and Grunwald, Kalman J.: Aerodynamic Characteristics of a Powered Semispan Tilting-Shrouded-Propeller VTOL Model in Hovering and Transition Flight. NASA TN D-981, 1962.

8. Davenport, Edwin E.; and Spreemann, Kenneth P.: Transition Characteristics of a VTOL Aircraft Powered by Four Ducted Tandem Propellers. NASA TN D-2254, 1964.

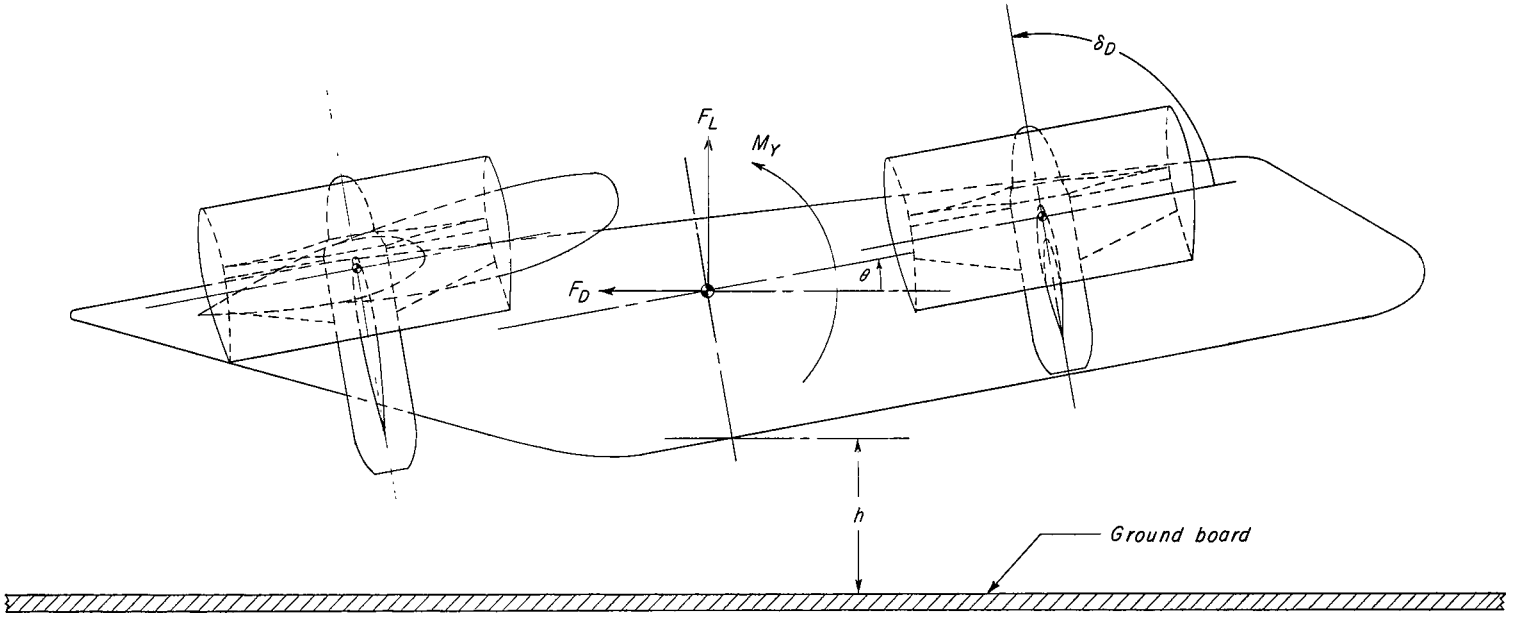


(a) Hovering tests.

Figure 1.- Conventions used to define positive sense of forces, moments, and angles for the complete model.

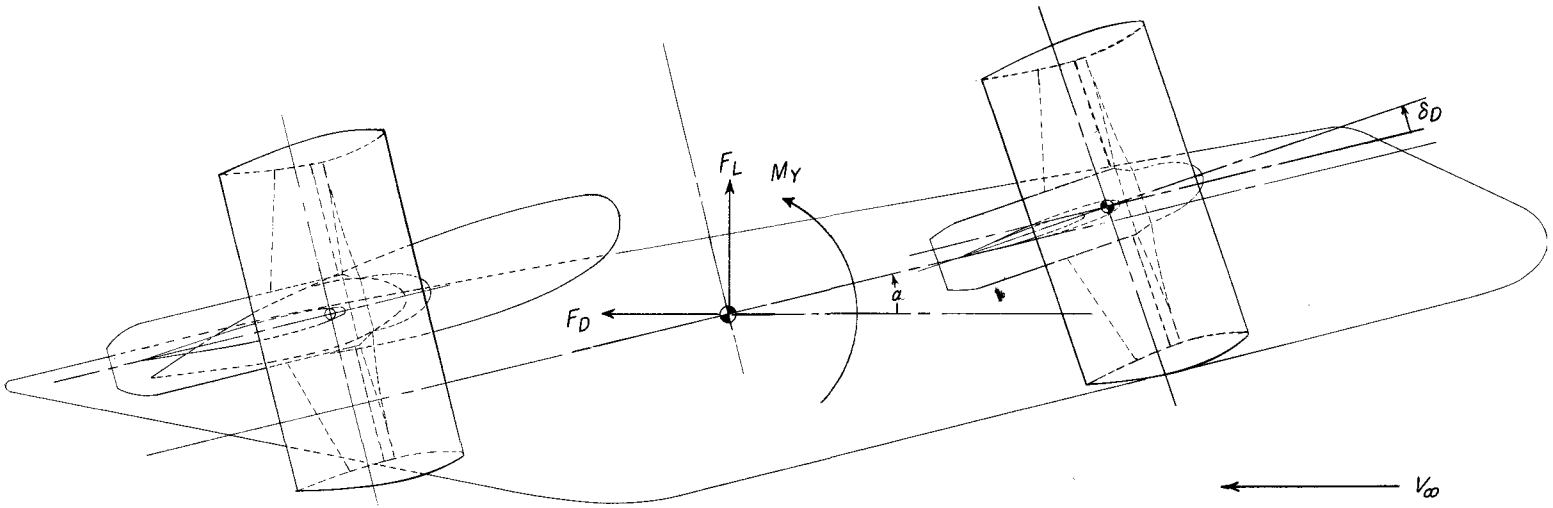


(b) Tunnel tests.

Figure 1.- Concluded.

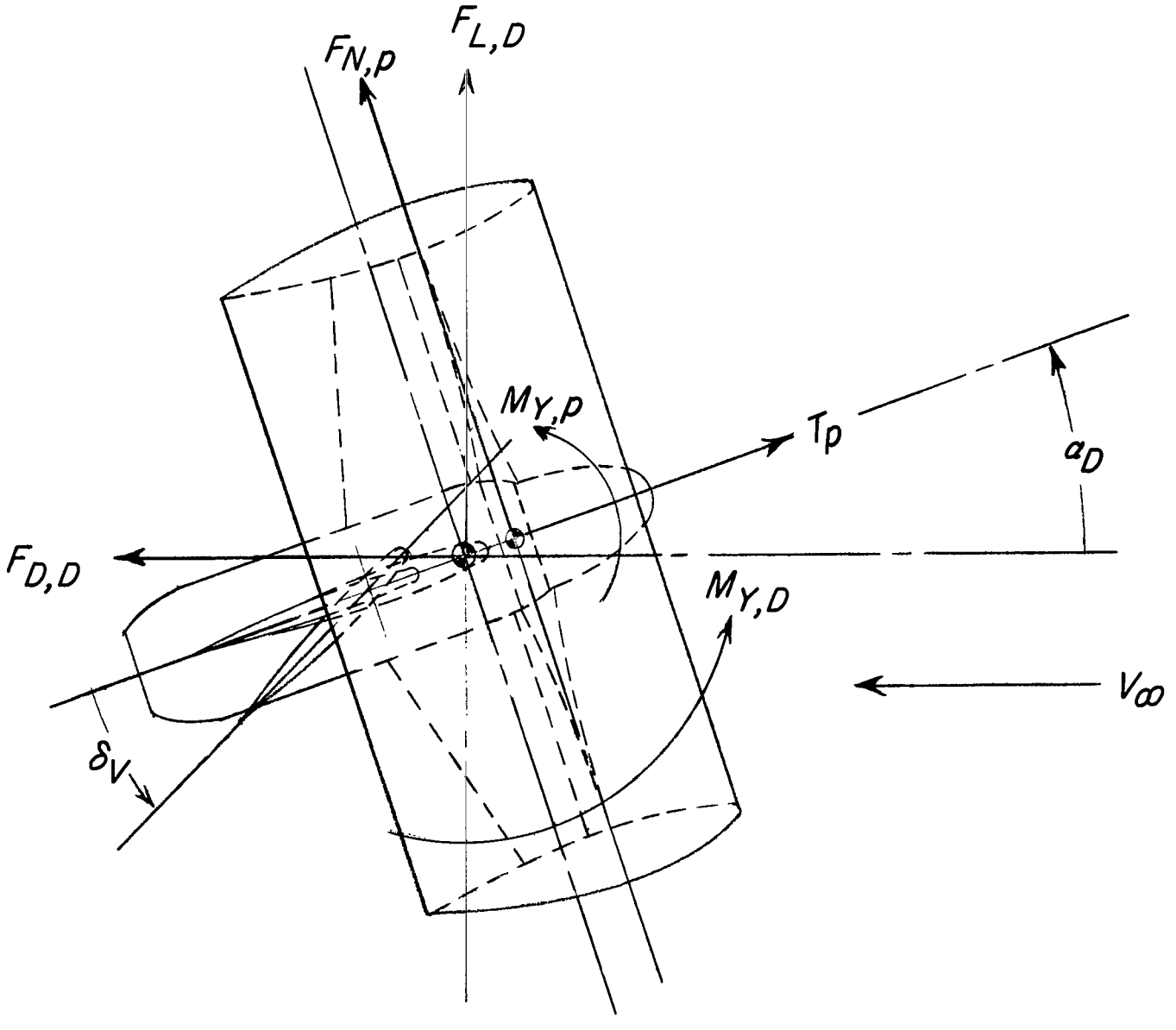


Figure 2.- Conventions used to define positive sense of forces, moments, and angles for the isolated duct with propeller.

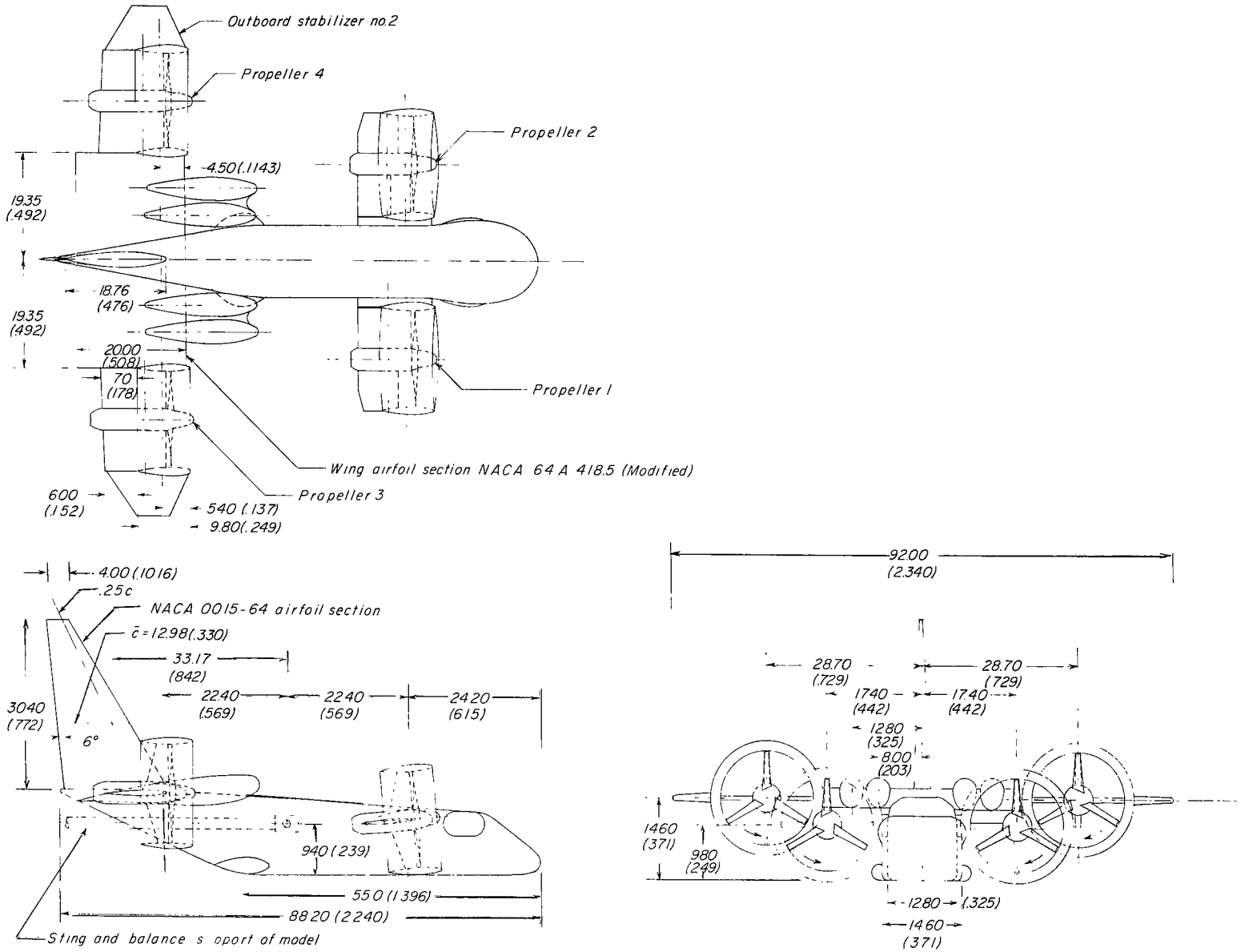


Figure 3.- Drawing of complete model. Dimensions are given first in inches and parenthetically in meters.

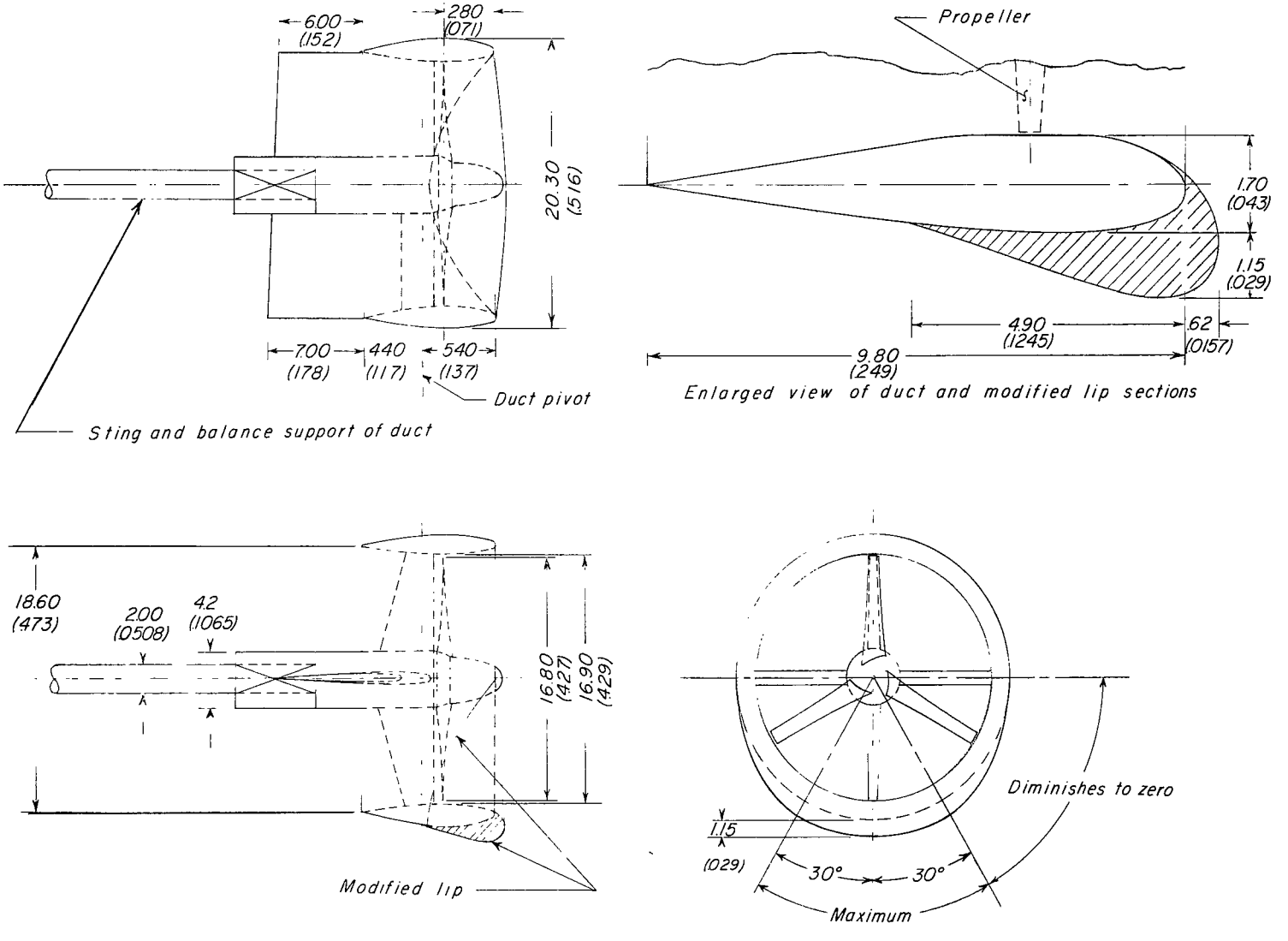


Figure 4.- Drawing of isolated duct with duct lip modifications. Dimensions are given first in inches and parenthetically in meters.

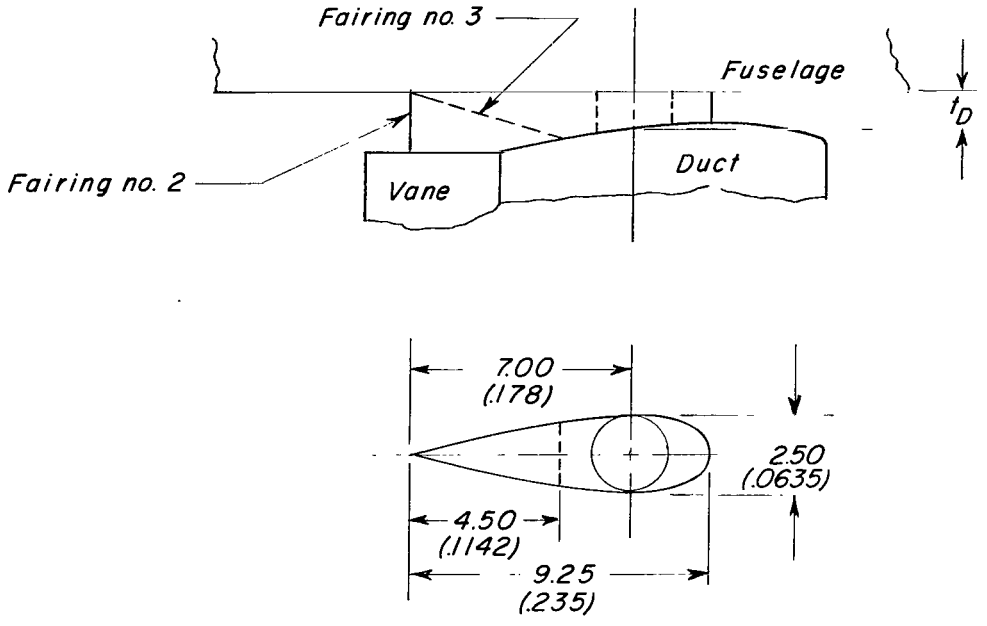


Fairings 2 and 3

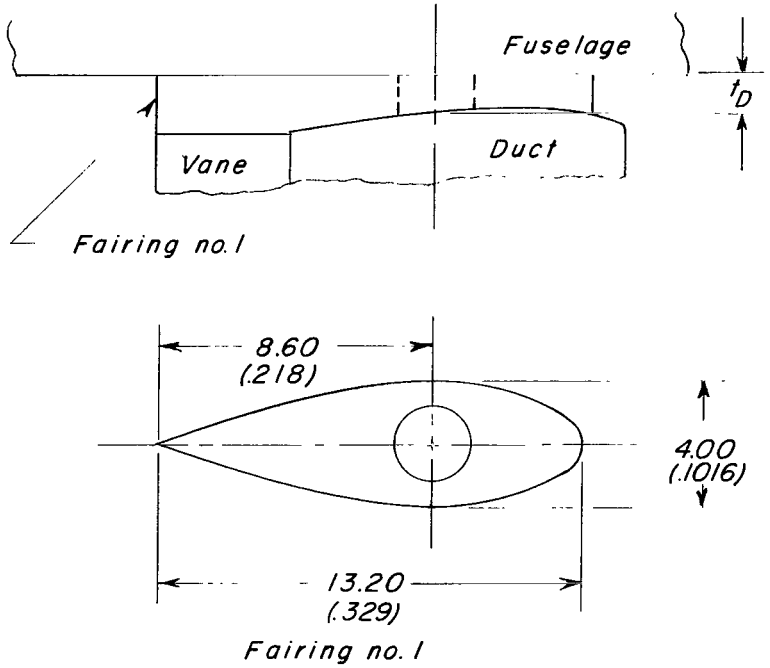


Fairing no. 1

Figure 5.- Details of fairing between duct and fuselage. Dimensions are given first in inches and parenthetically in meters.

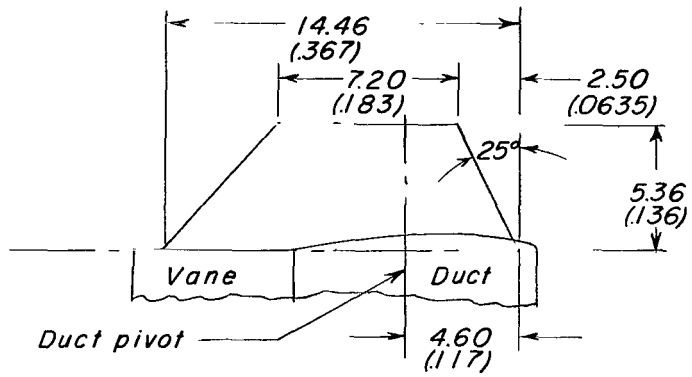


No. 3 (NACA 0015-64 section)

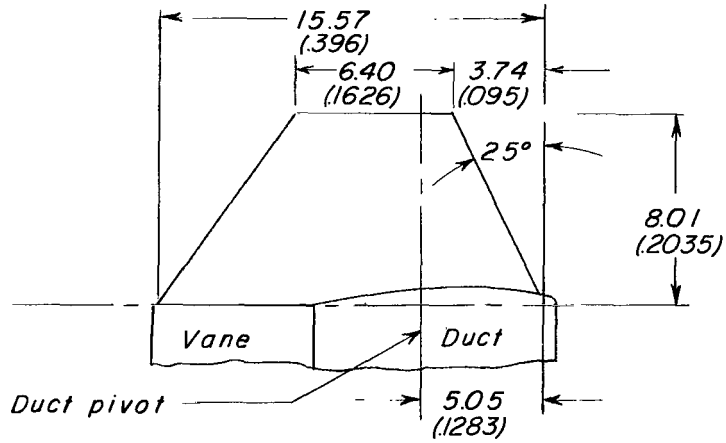


No. 2 (NACA 64 A 415 section)

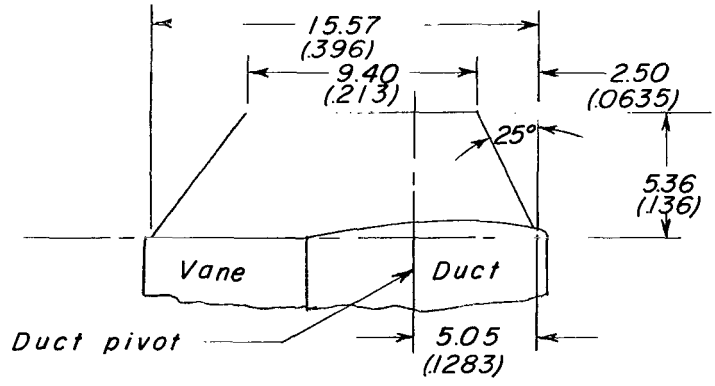


No. 1 (NACA 64 A 415 section)

Figure 6.- Details of rear-mounted outboard stabilizers. Dimensions are given first in inches and parenthetically in meters.

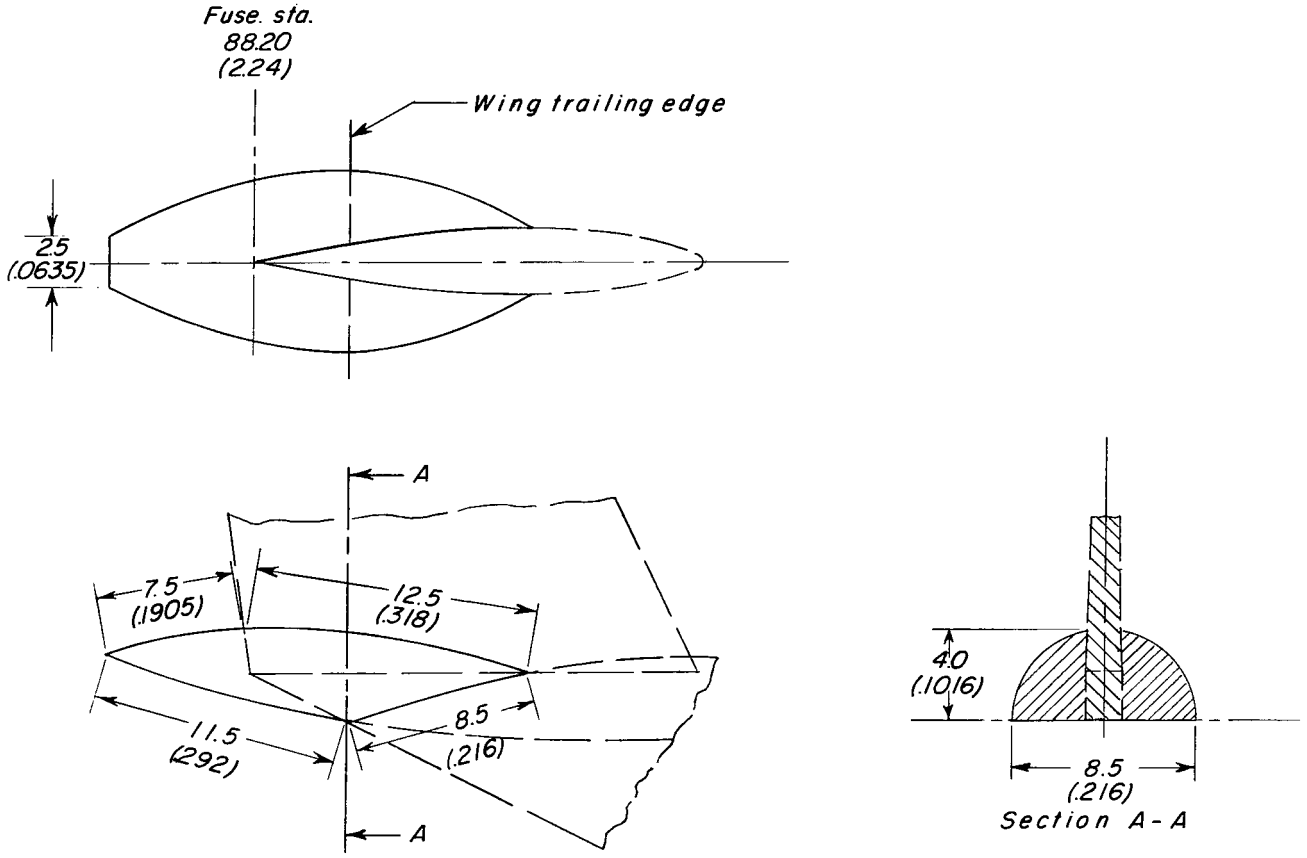


Figure 7.- Drawing of tail-fuselage fairing. Dimensions are given first in inches and parenthetically in meters.

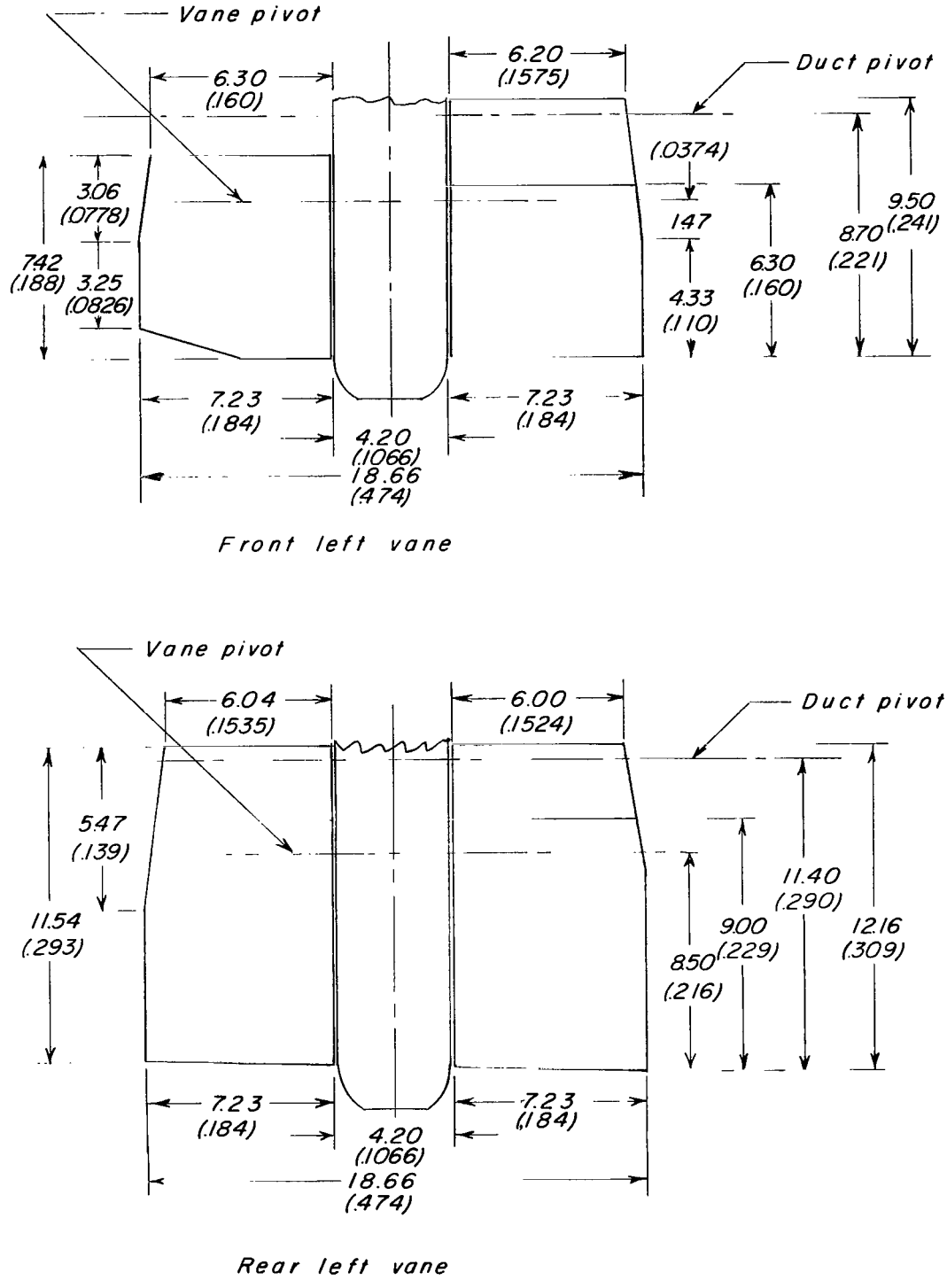


Figure 8.- Details of vanes (elevons) used in ducts. Dimensions are given first in inches and parenthetically in meters.

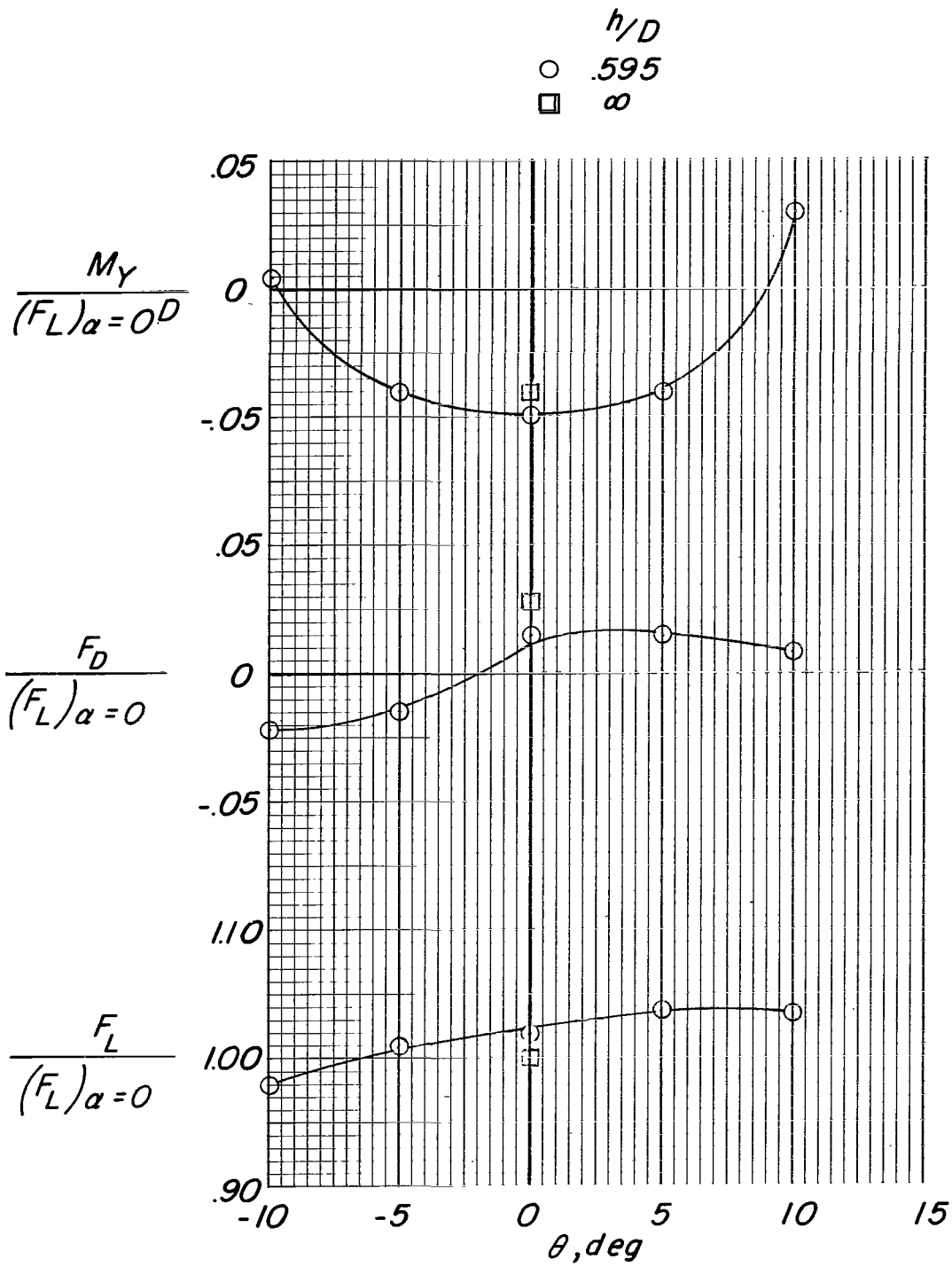


Figure 9.- Aerodynamic characteristics in hovering $\delta_{D,F} = 90^0$; $\delta_{D,R} = 90^0$; $\delta_{V,F} = 0^0$.

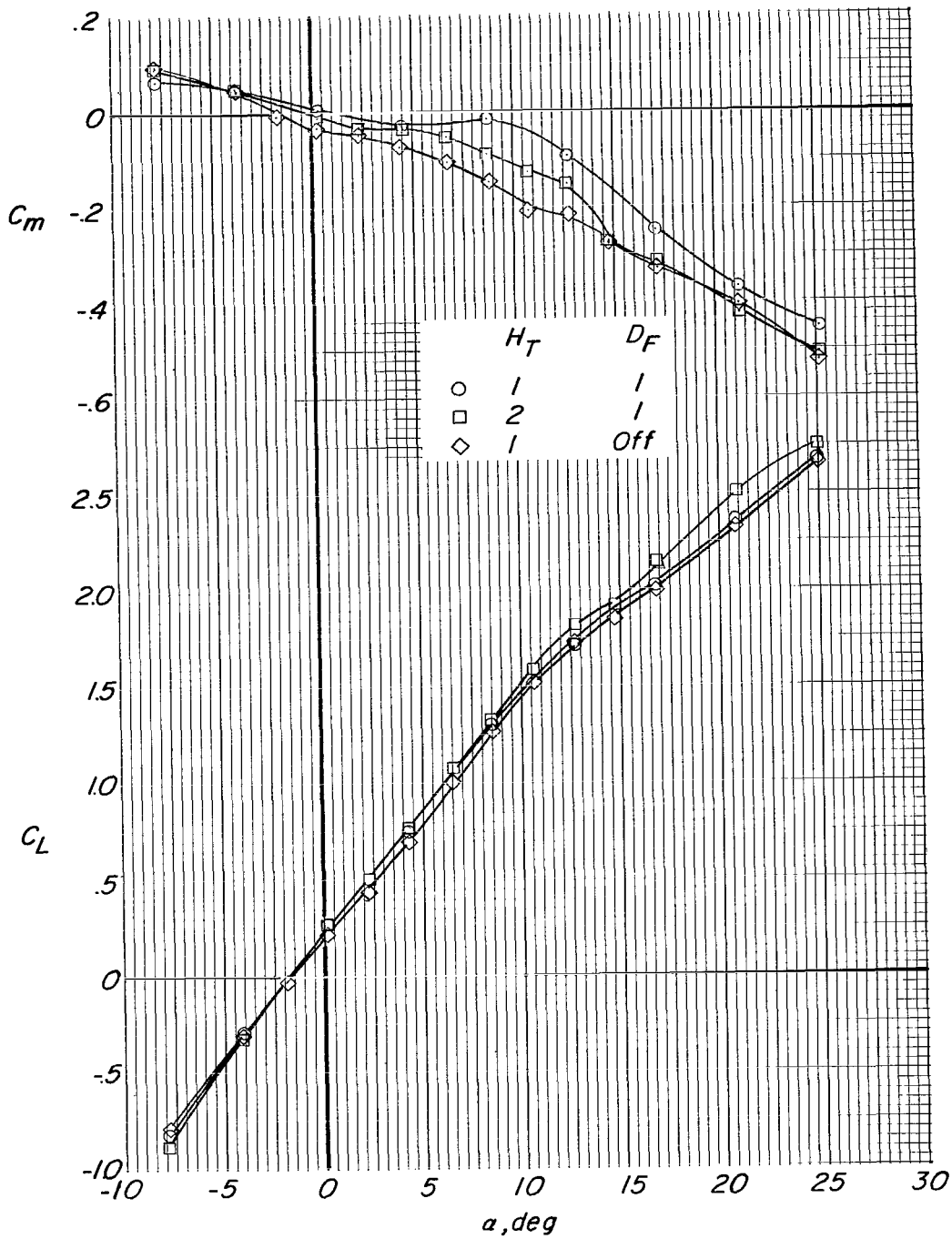


(a) $C_T = 0$; propellers windmilling.

Figure 10.- Effects of outboard stabilizer and front duct fairing on the aerodynamic characteristics of the model at two thrust coefficients. $\delta_{D,F} = 5^0$; $\delta_{D,R} = 0^0$; $\delta_{V,F} = 0^0$; $\delta_{V,R} = 0^0$; $i_t = 0^0$; $V_t$ off.

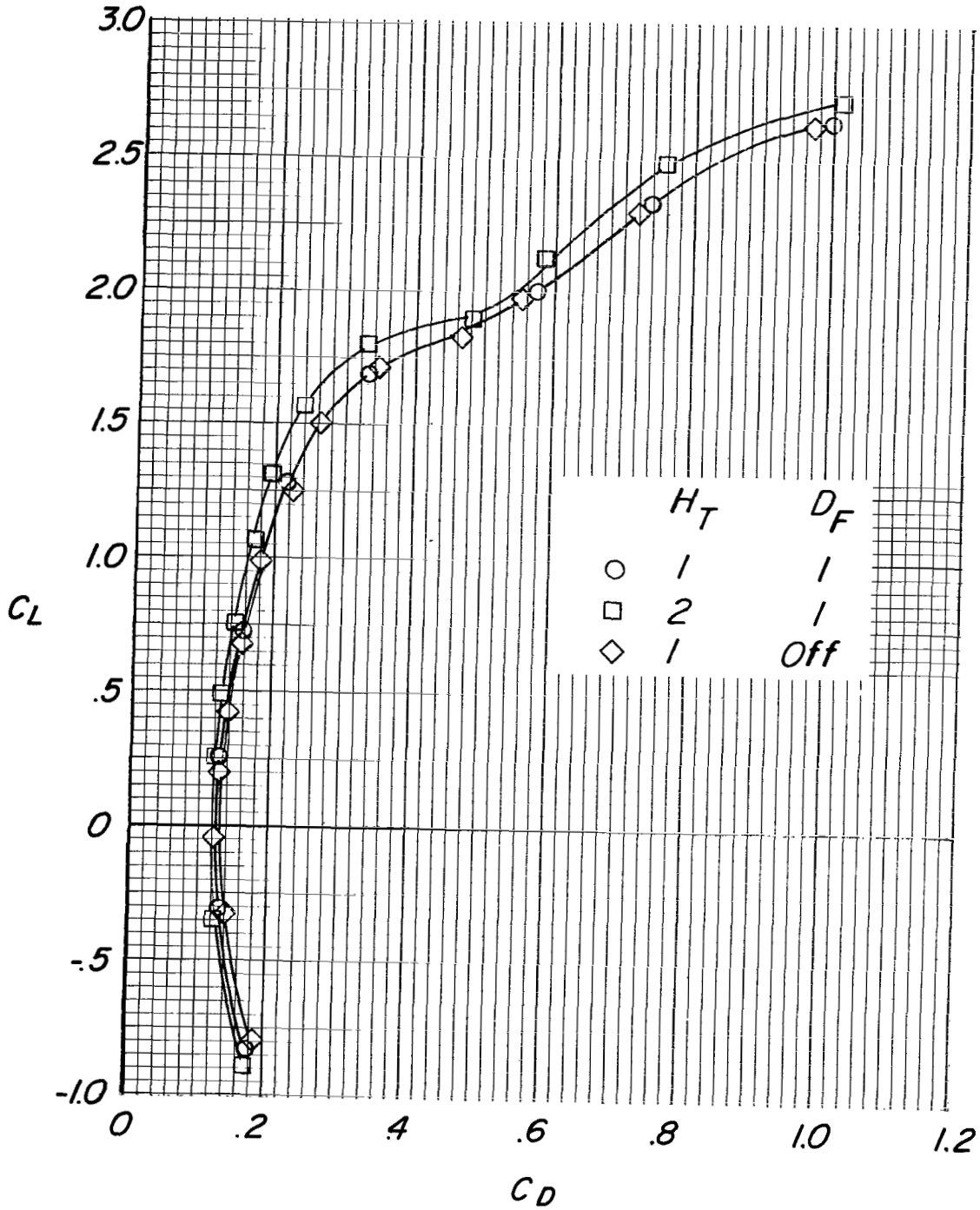


(a) Concluded.

Figure 10.- Continued.

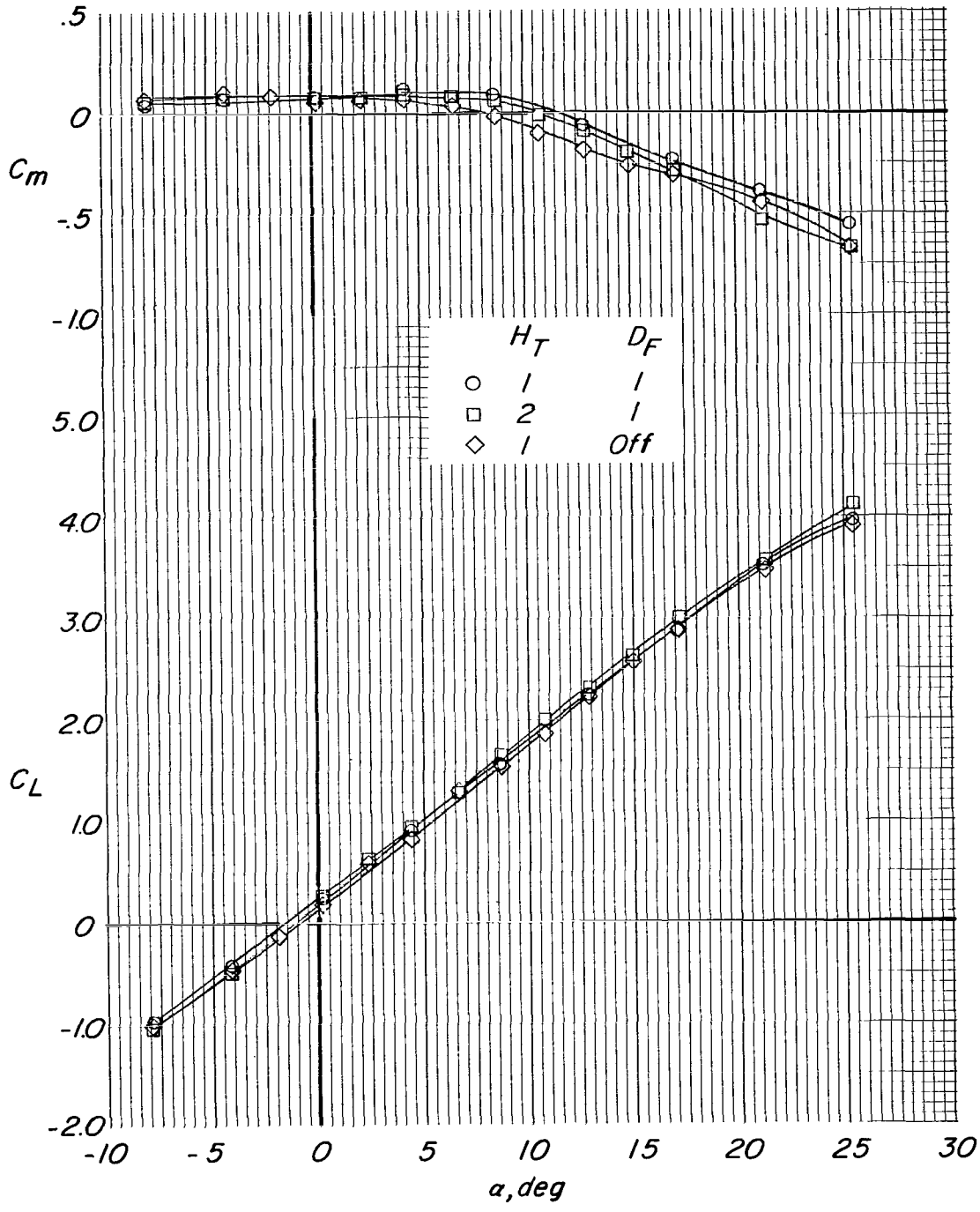


(b) $C_T = 0.8$.

Figure 10.- Continued.

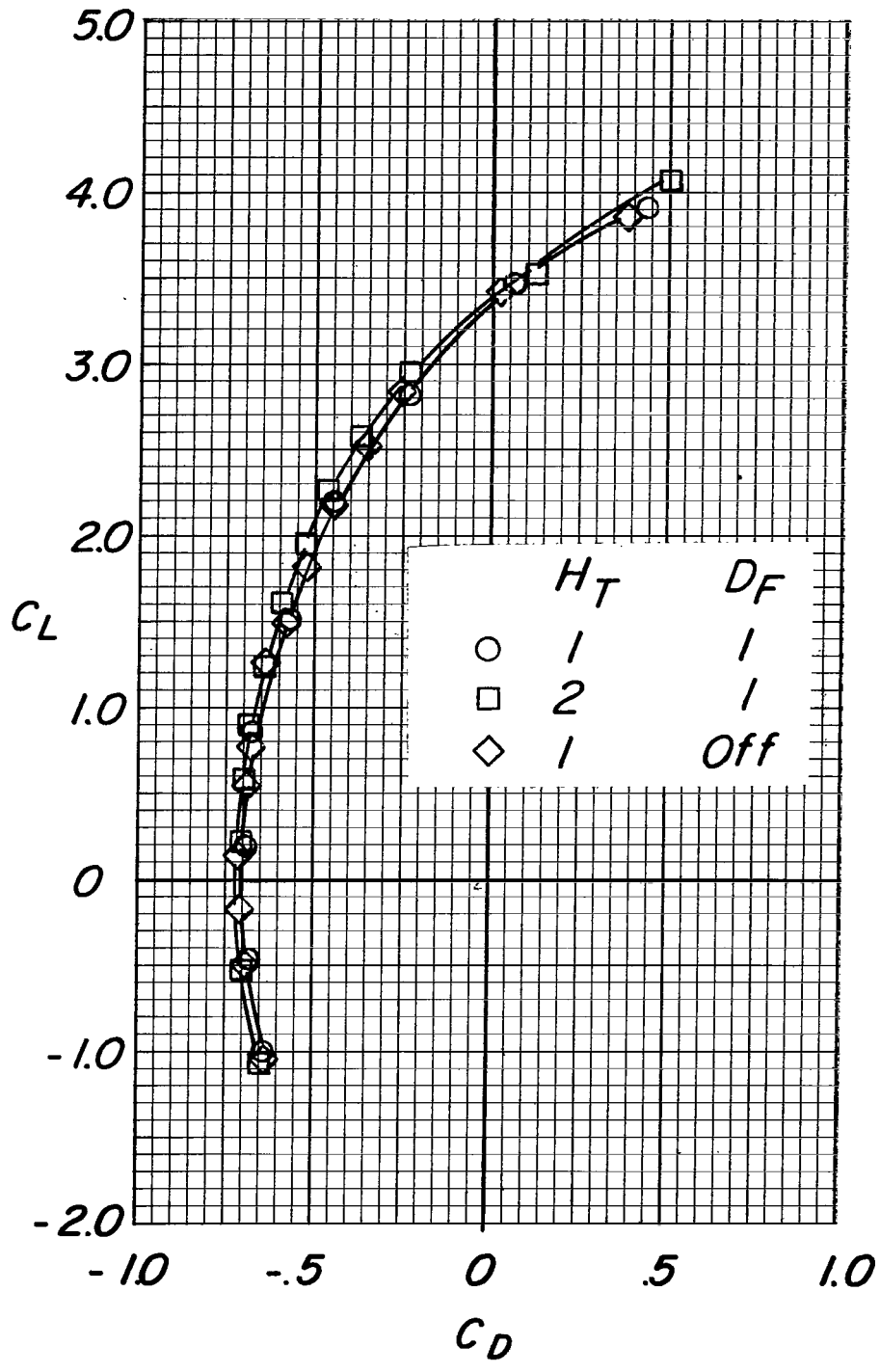


(b) Concluded.

Figure 10.- Concluded.

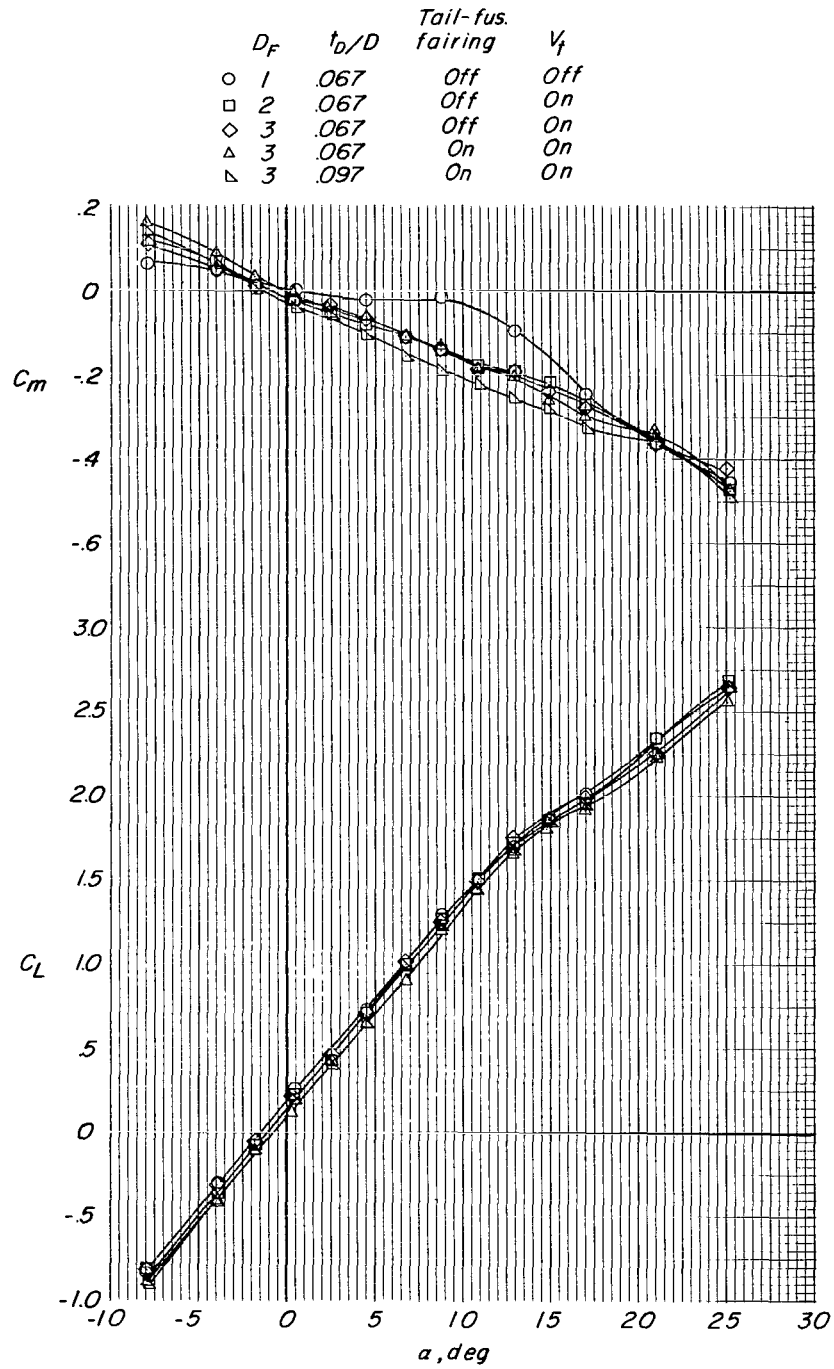


(a) $C_T = 0$; propellers windmilling.

Figure 11.- Effects of front duct fairings, distance of front duct from fuselage, and tail-fuselage fairing on the aerodynamic characteristics of the model at various thrust coefficients. $\delta_{D,F} = 5^0$; $\delta_{D,R} = 0^0$; $\delta_{V,F} = 0^0$; $\delta_{V,R} = 0^0$; $H_{t,1}$ on; $i_t = 0^0$.

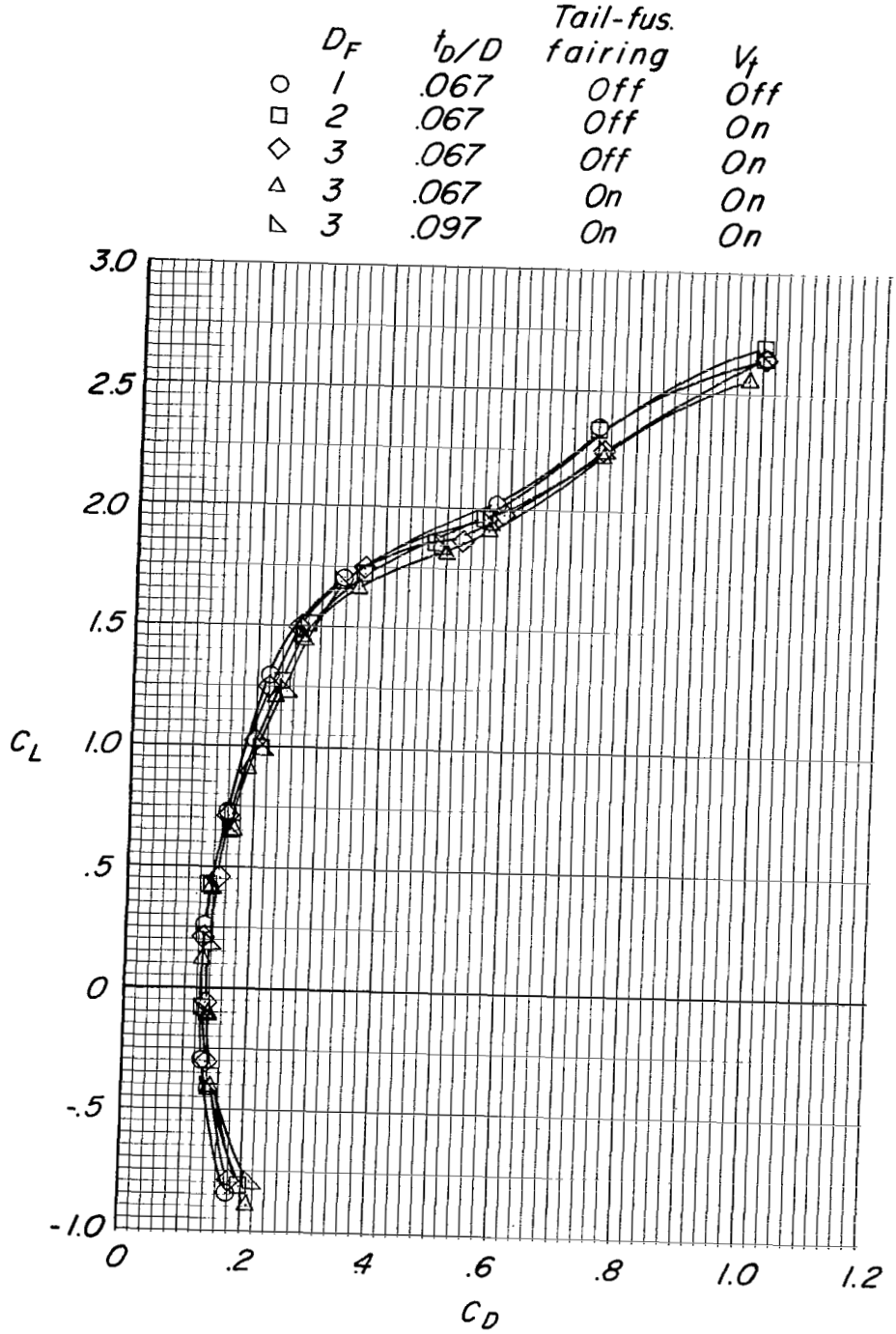


(a) Concluded.

Figure 11.- Continued.

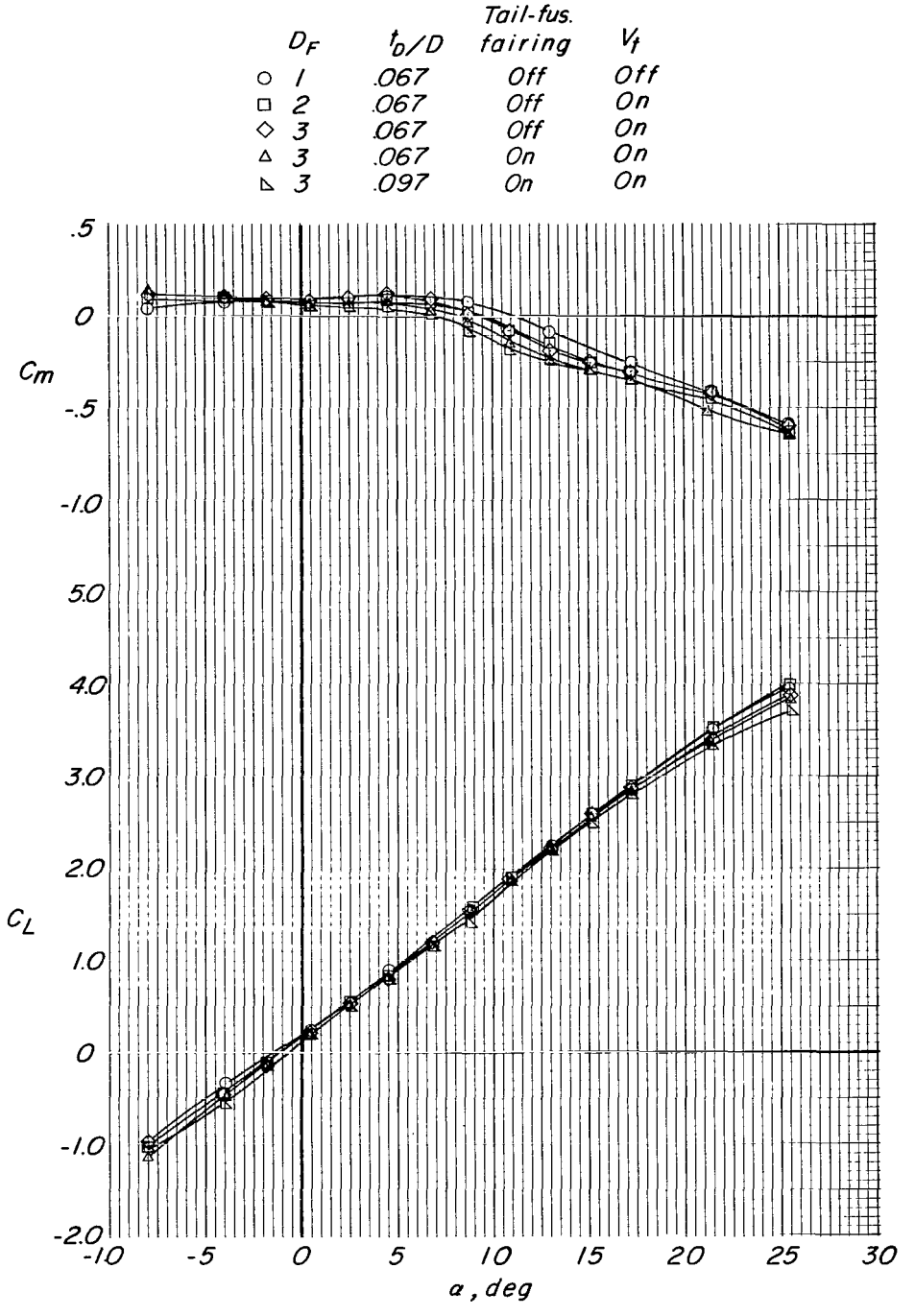


(b) $C_T = 0.8$.

Figure 11.- Continued.

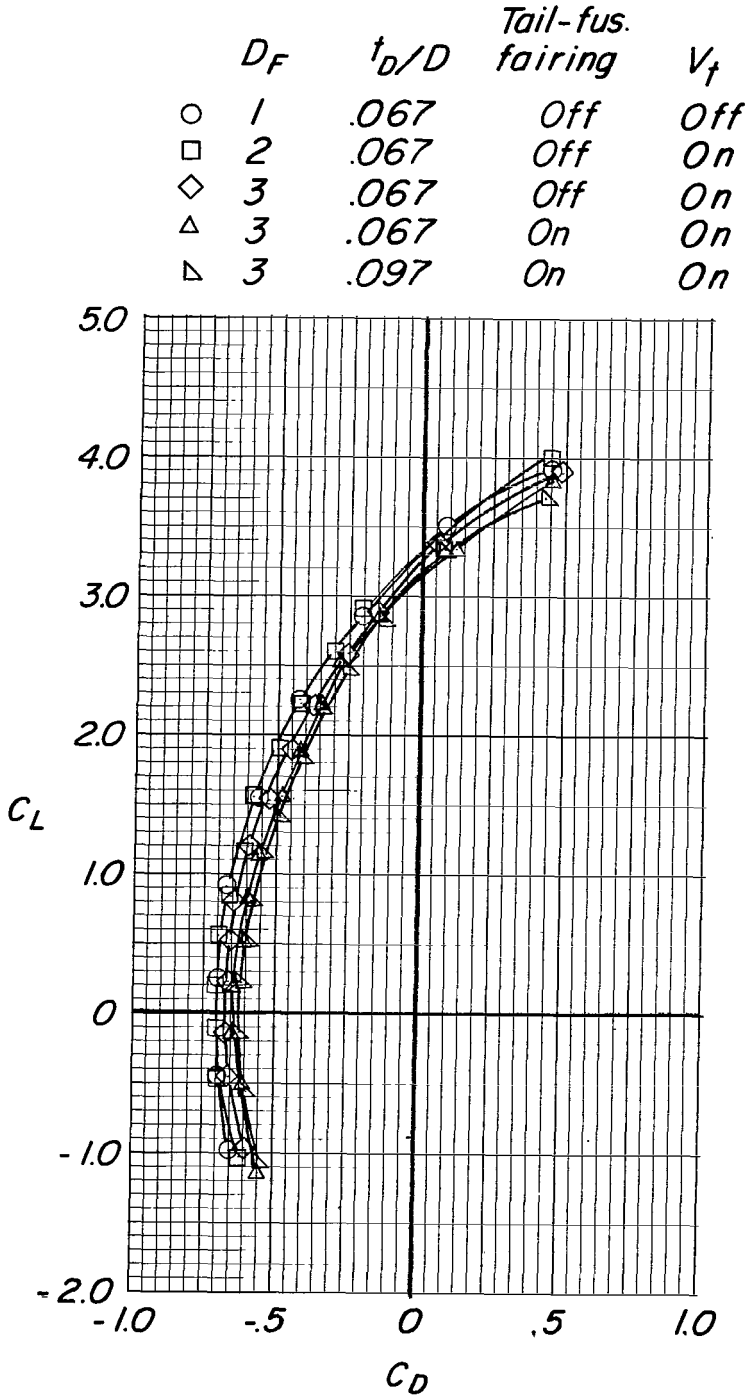


(b) Concluded.

Figure 11.- Continued.

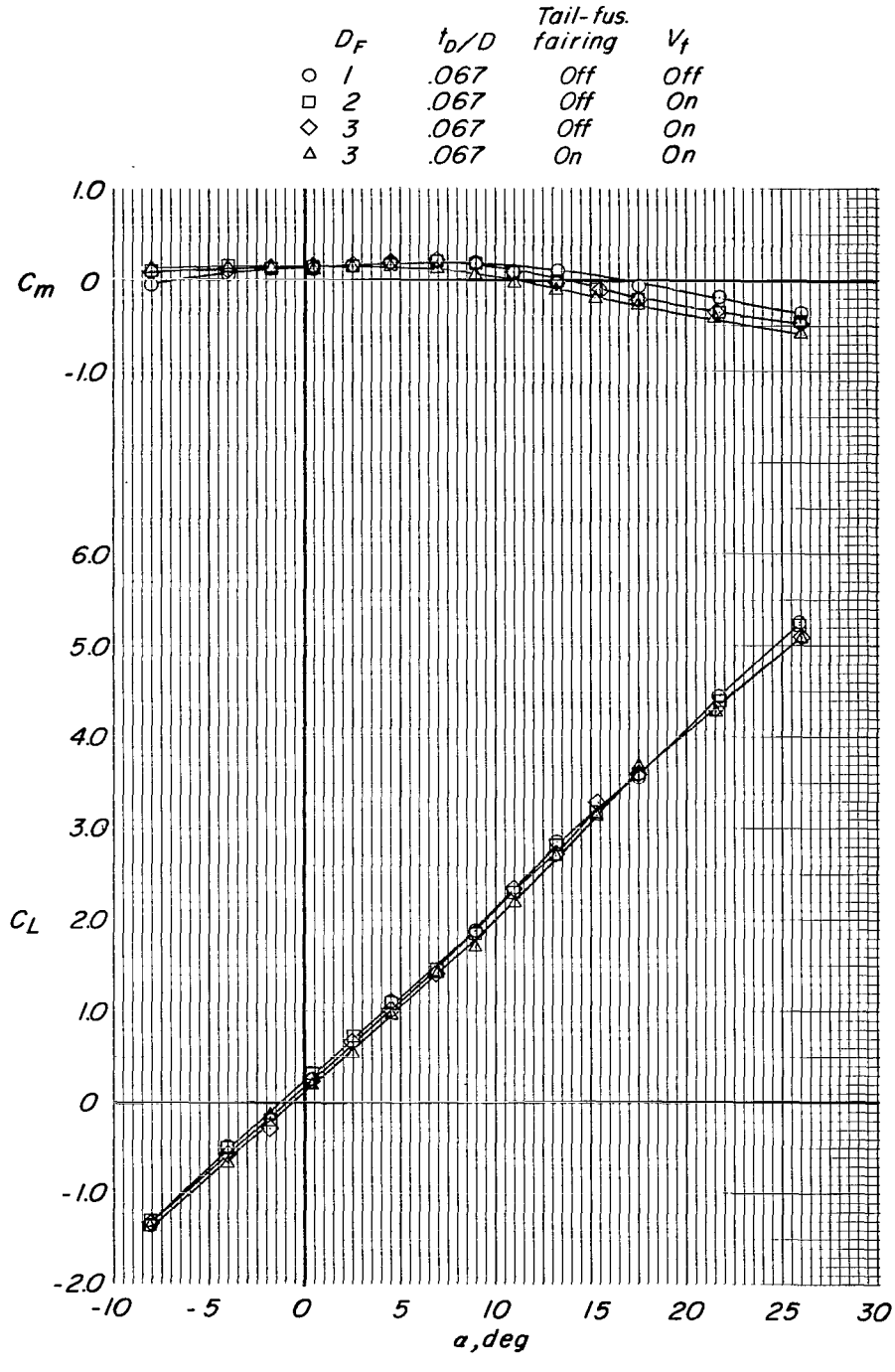


(c) $C_T = 2.1$.

Figure 11.- Continued.

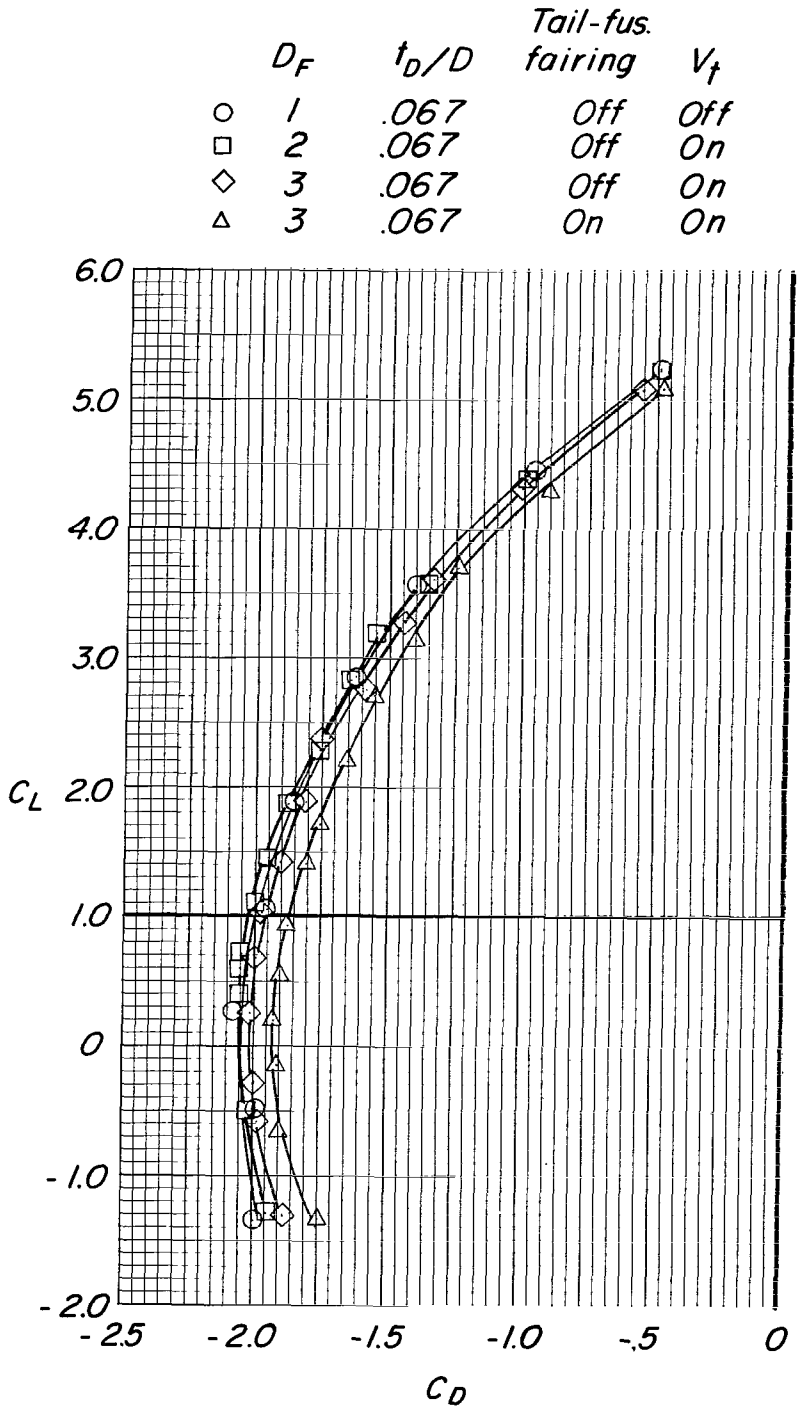


(c) Concluded.

Figure 11.- Concluded.

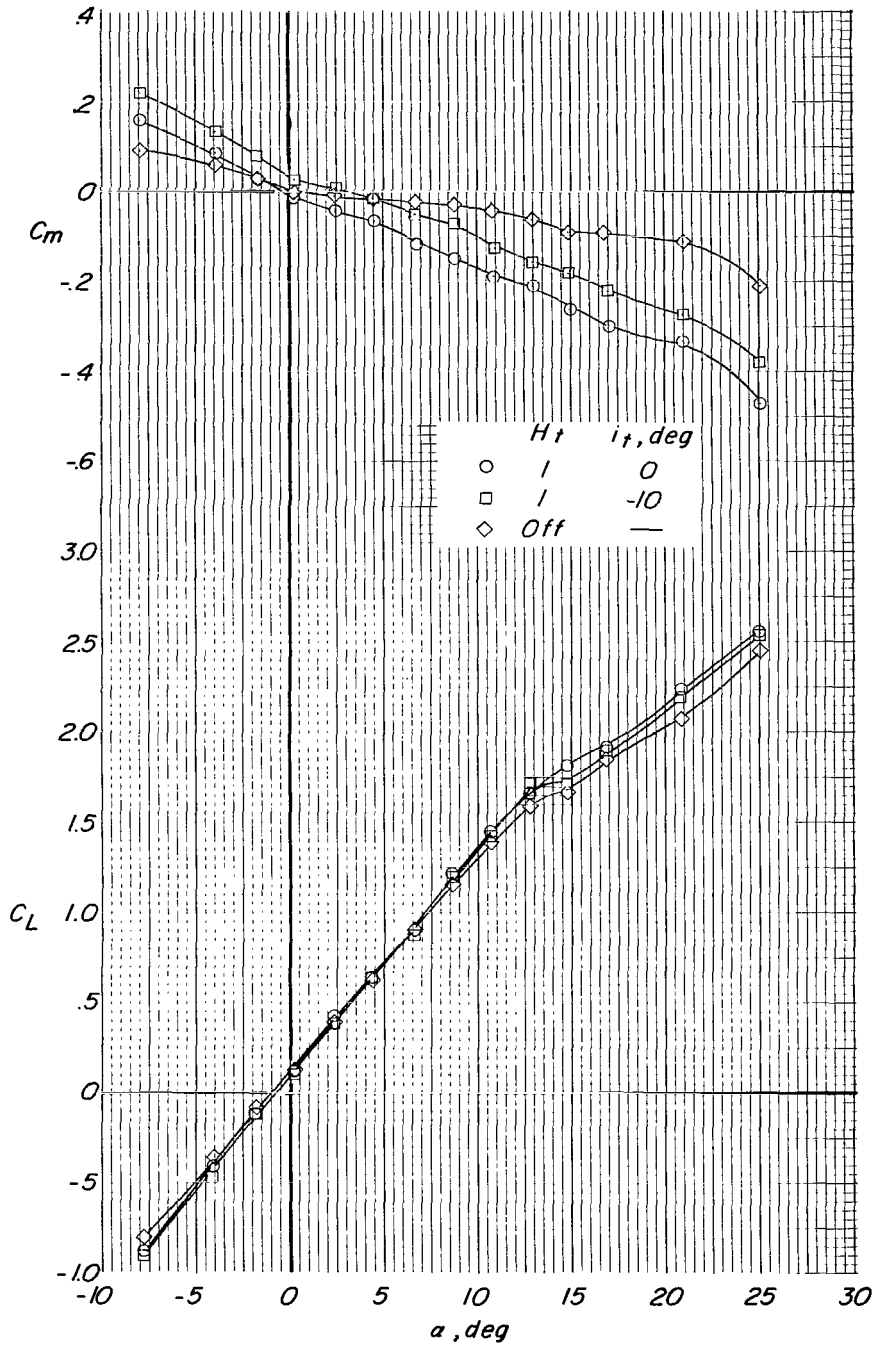


(a) $C_T = 0$; propellers windmilling.

Figure 12.- Effects of outboard stabilizer and stabilizer incidence on the aerodynamic characteristics of the model at two thrust coefficients. $\delta_{D,F} = 5^0$; $\delta_{D,R} = 0^0$; $\delta_{V,F} = 0^0$; $\delta_{V,R} = 0^0$; $V_t$ on; tail-fuselage fairing on.

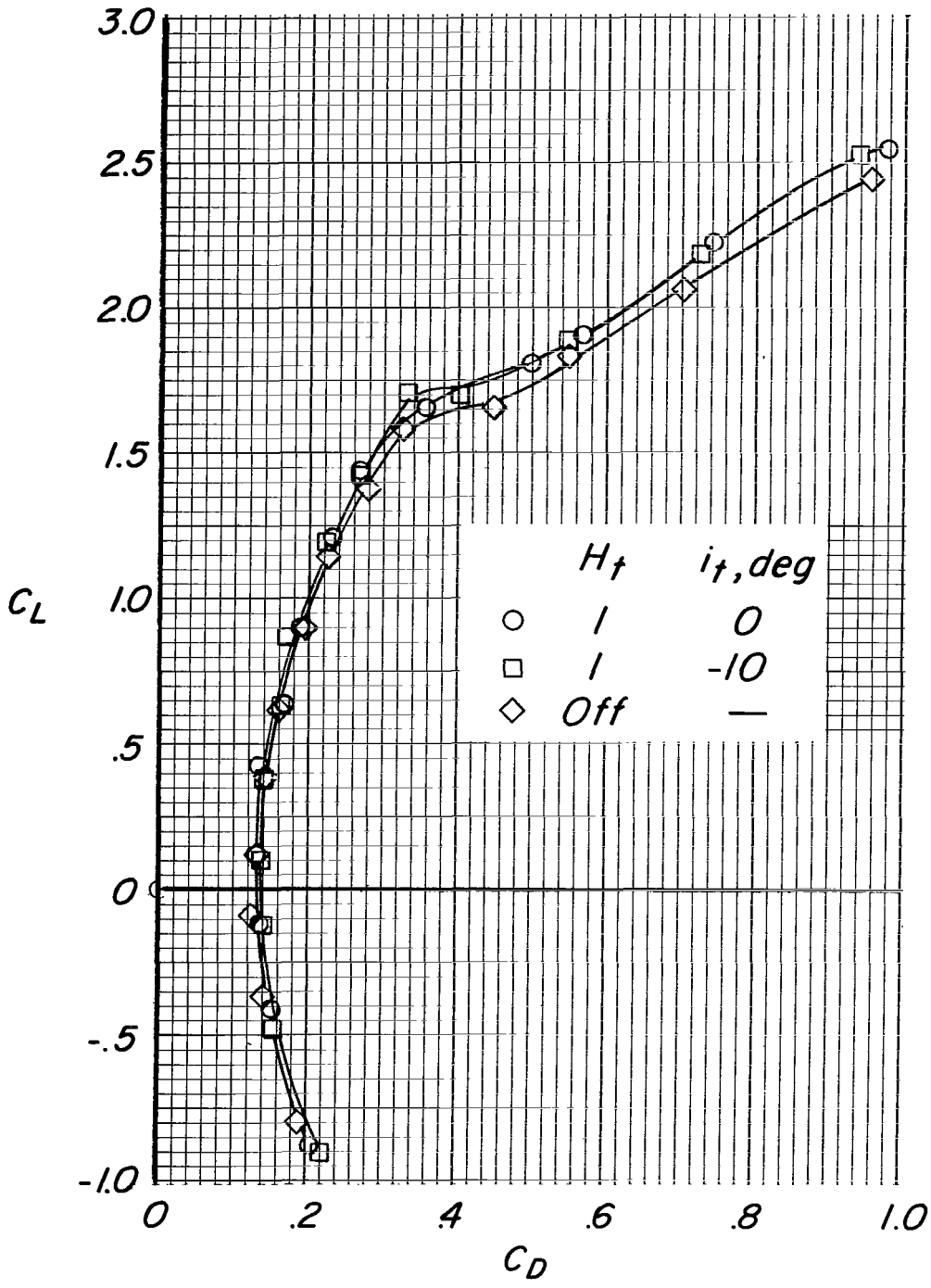


(a) Concluded.

Figure 12.- Continued.

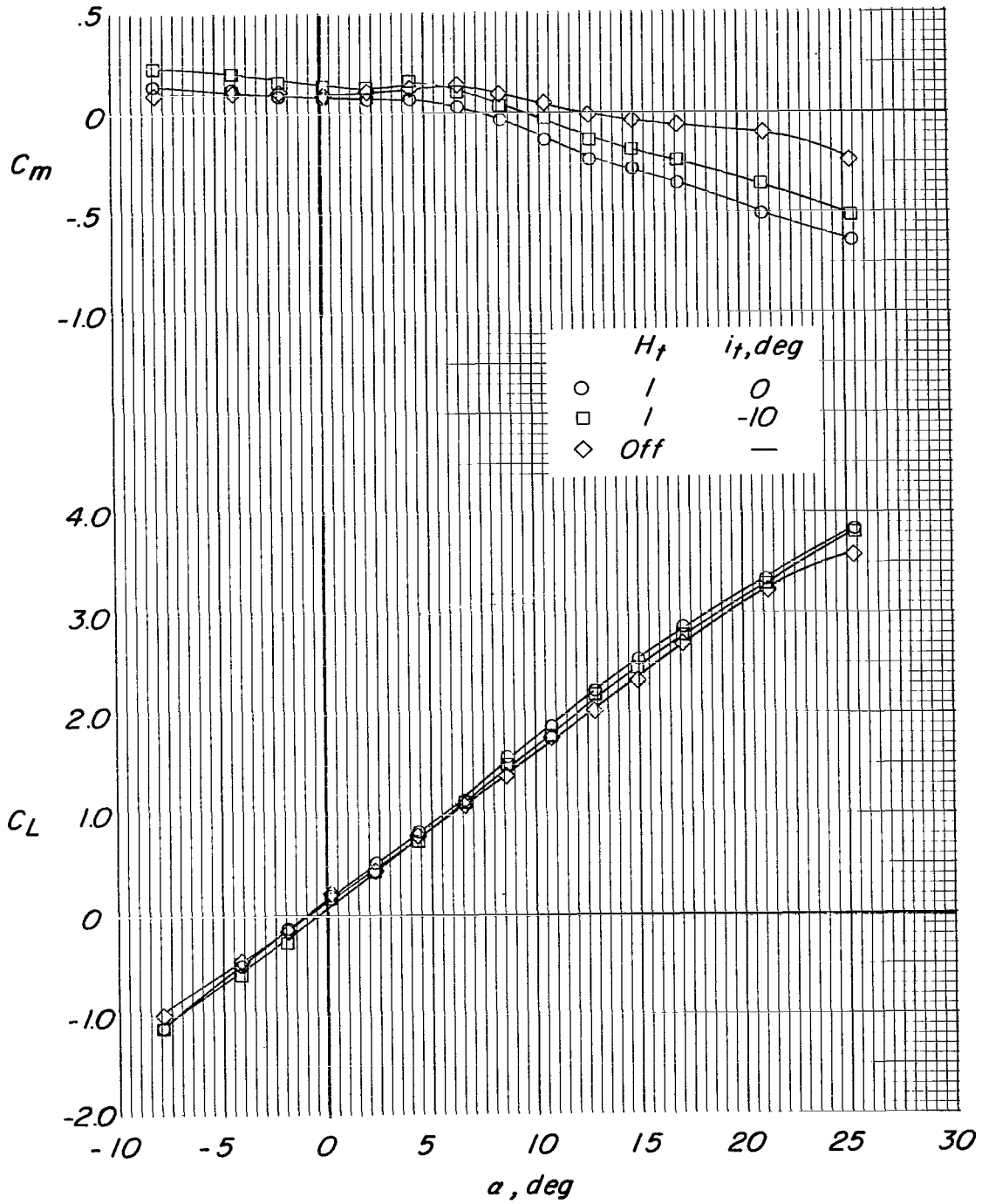


(b) $C_T = 0.8$.

Figure 12.- Continued.

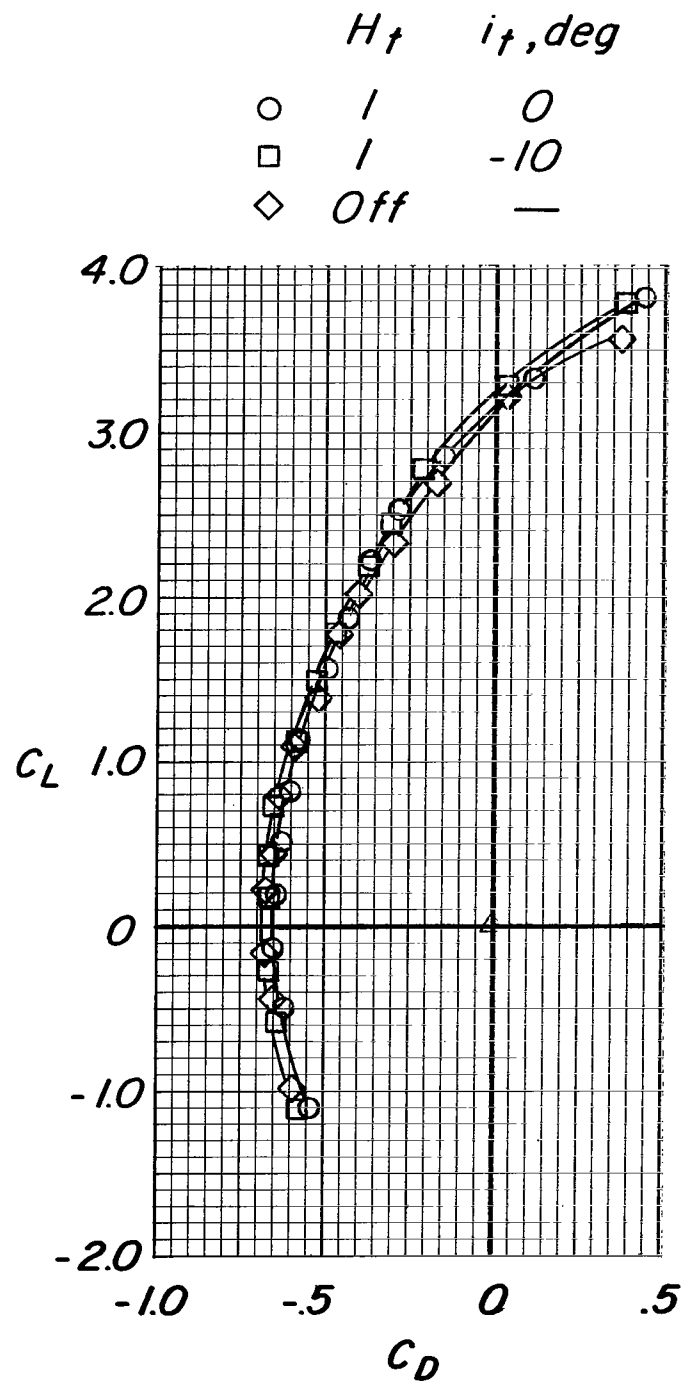


(b) Concluded.

Figure 12.- Concluded.

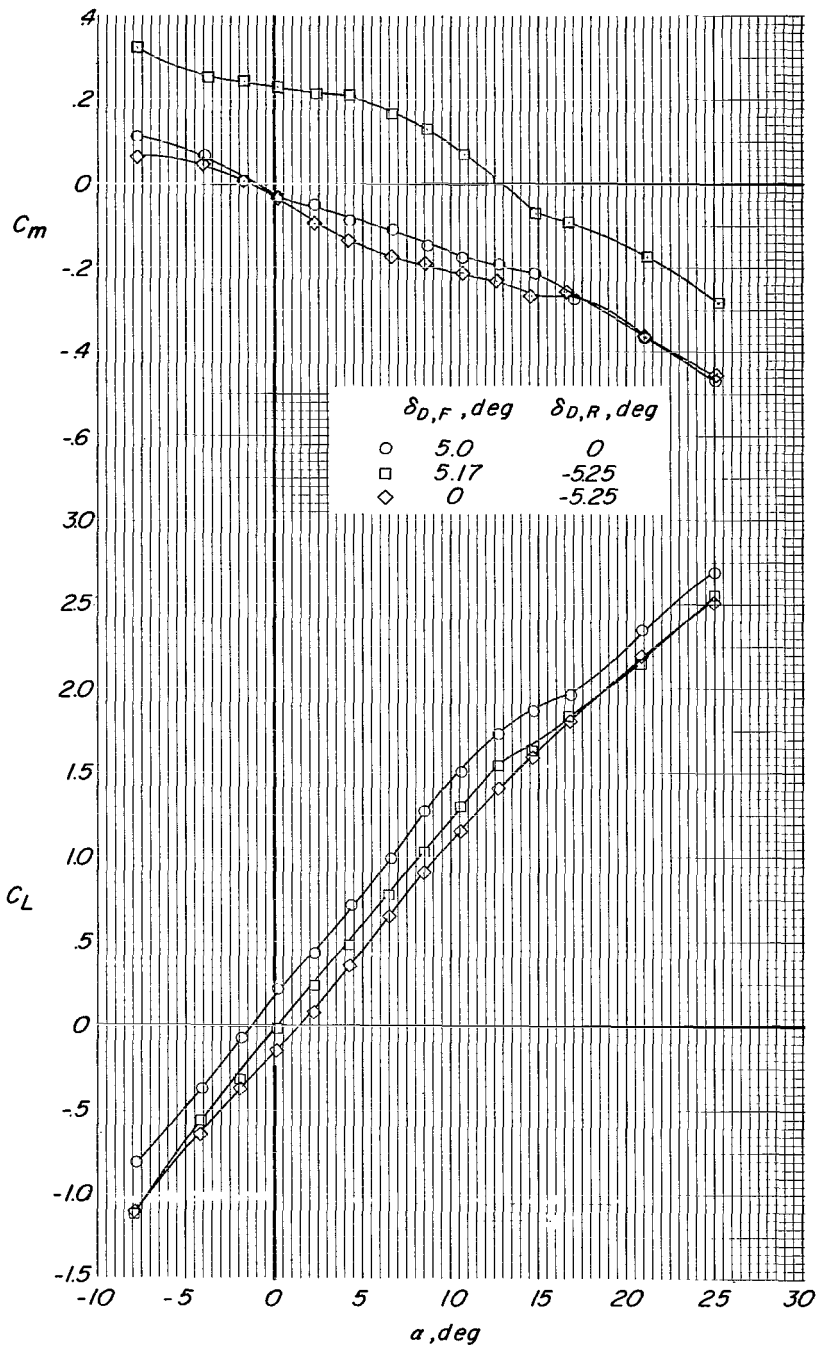


(a) $C_T = 0$; propellers windmilling.

Figure 13.- Effects of duct deflection on the aerodynamic characteristics of the model at various thrust coefficients. $\delta_{V,F} = 0^0$; $\delta_{V,R} = 0^0$; $H_{t,1}$ on; $i_t = 0^0$; $V_t$ on.

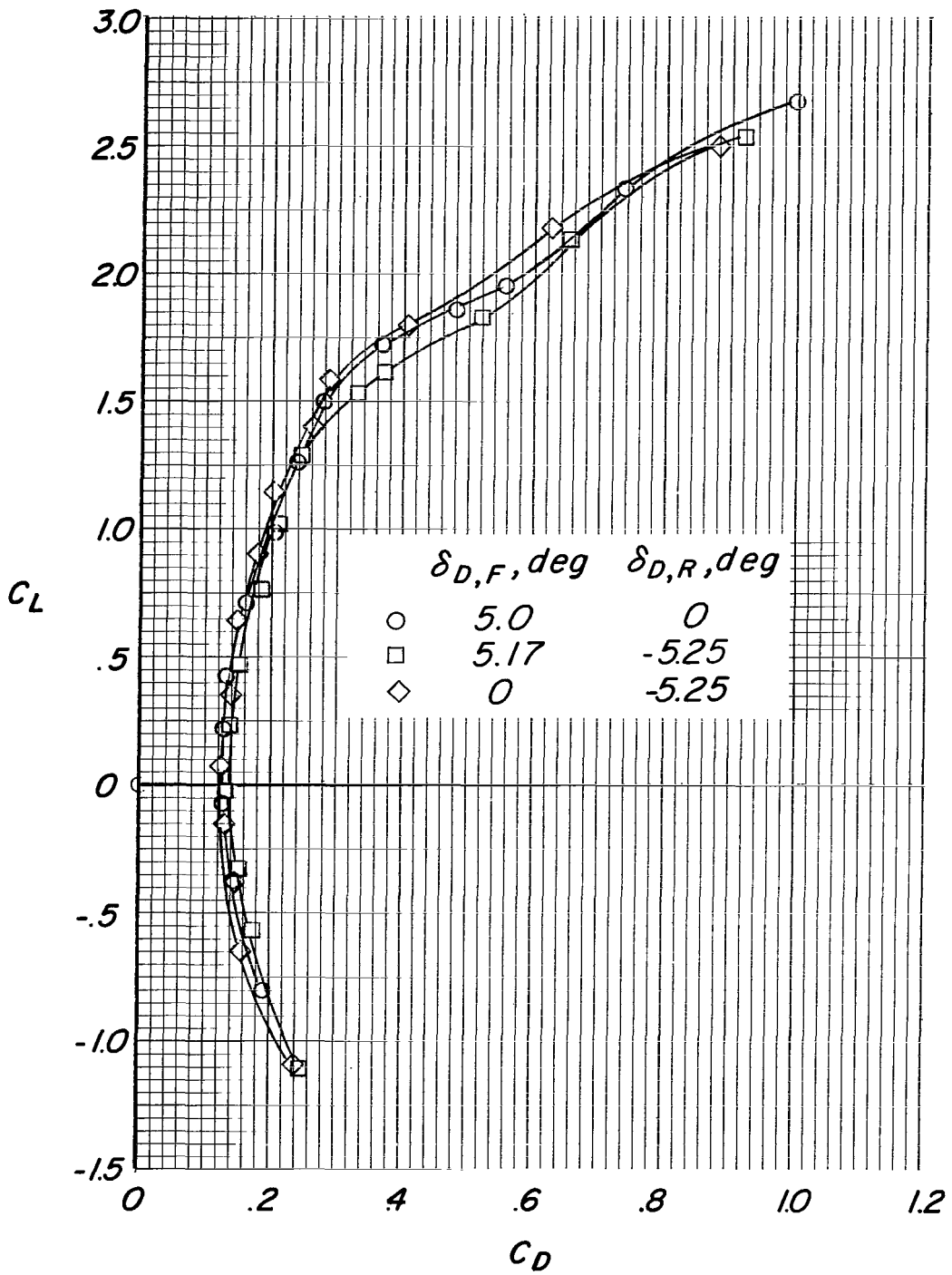


(a) Concluded.

Figure 13.- Continued.

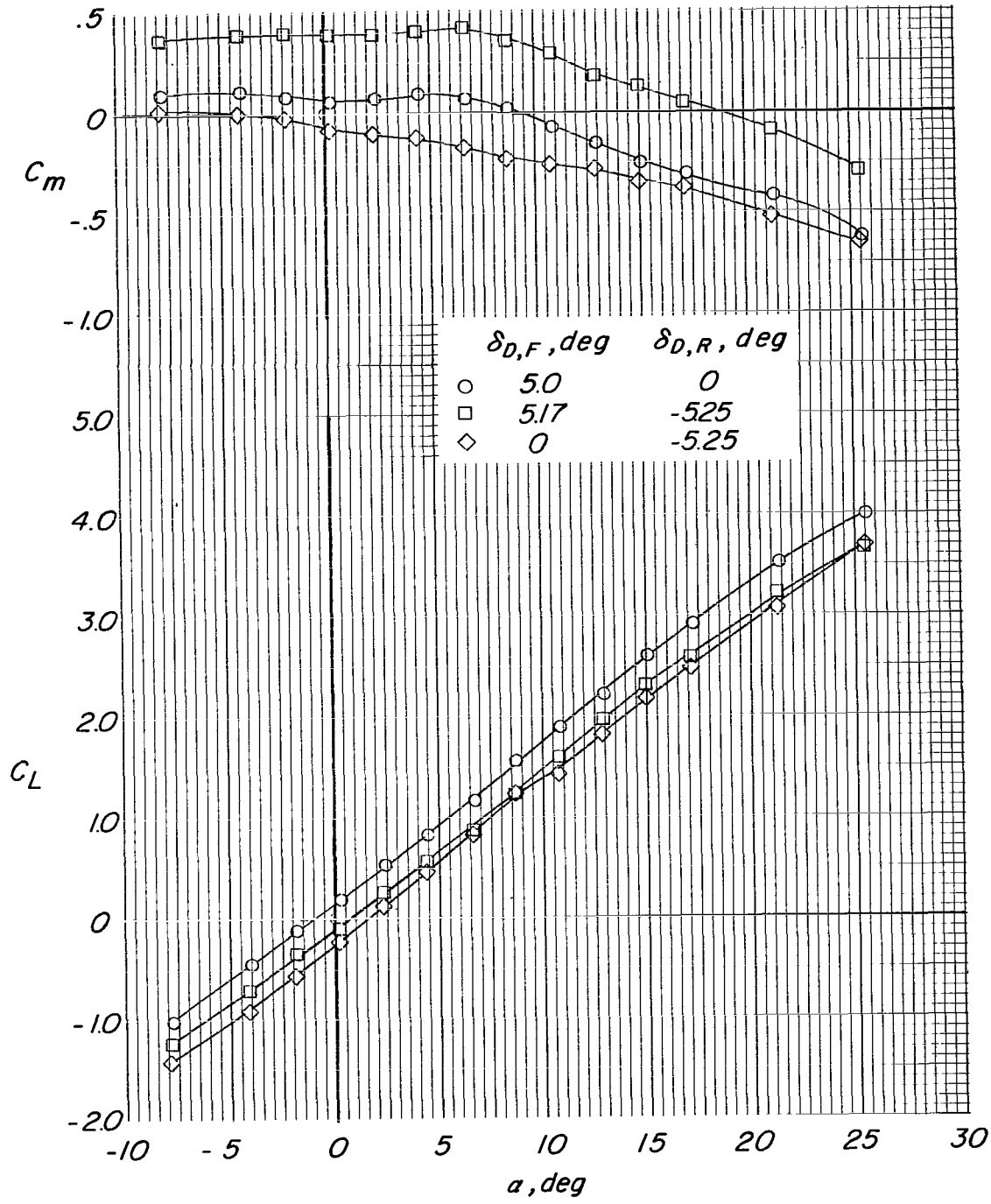


(b) $C_T = 0.8$

Figure 13.- Continued.

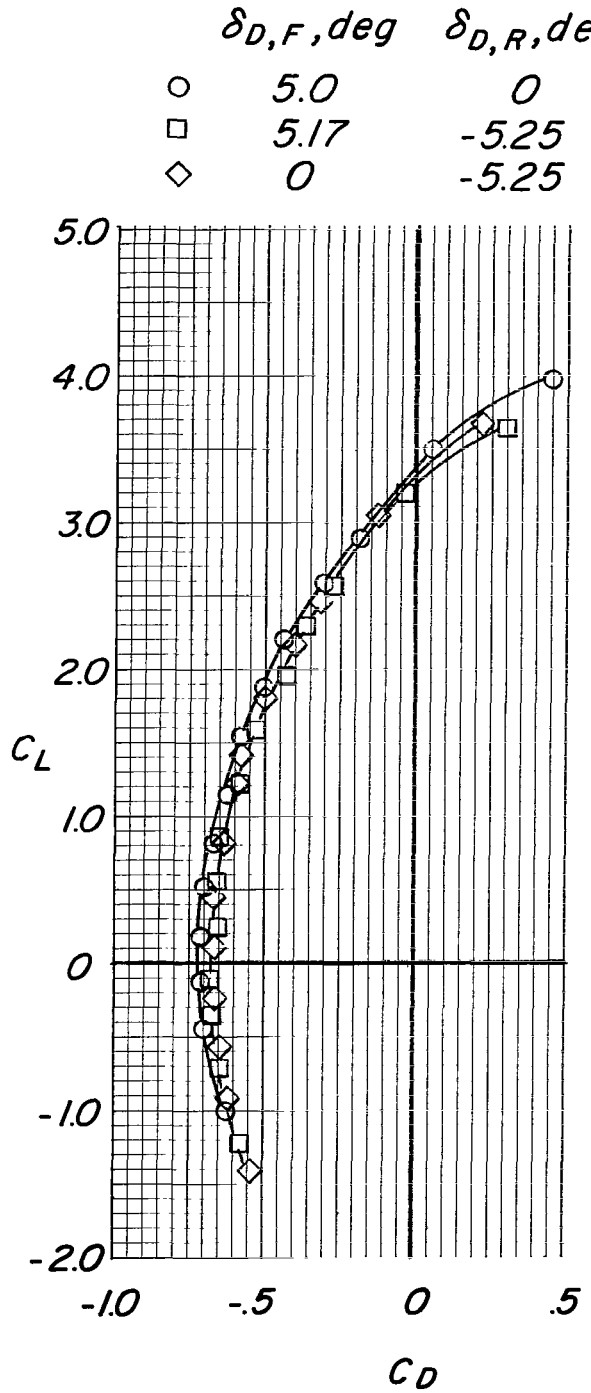


(b) Concluded.

Figure 13.- Continued.

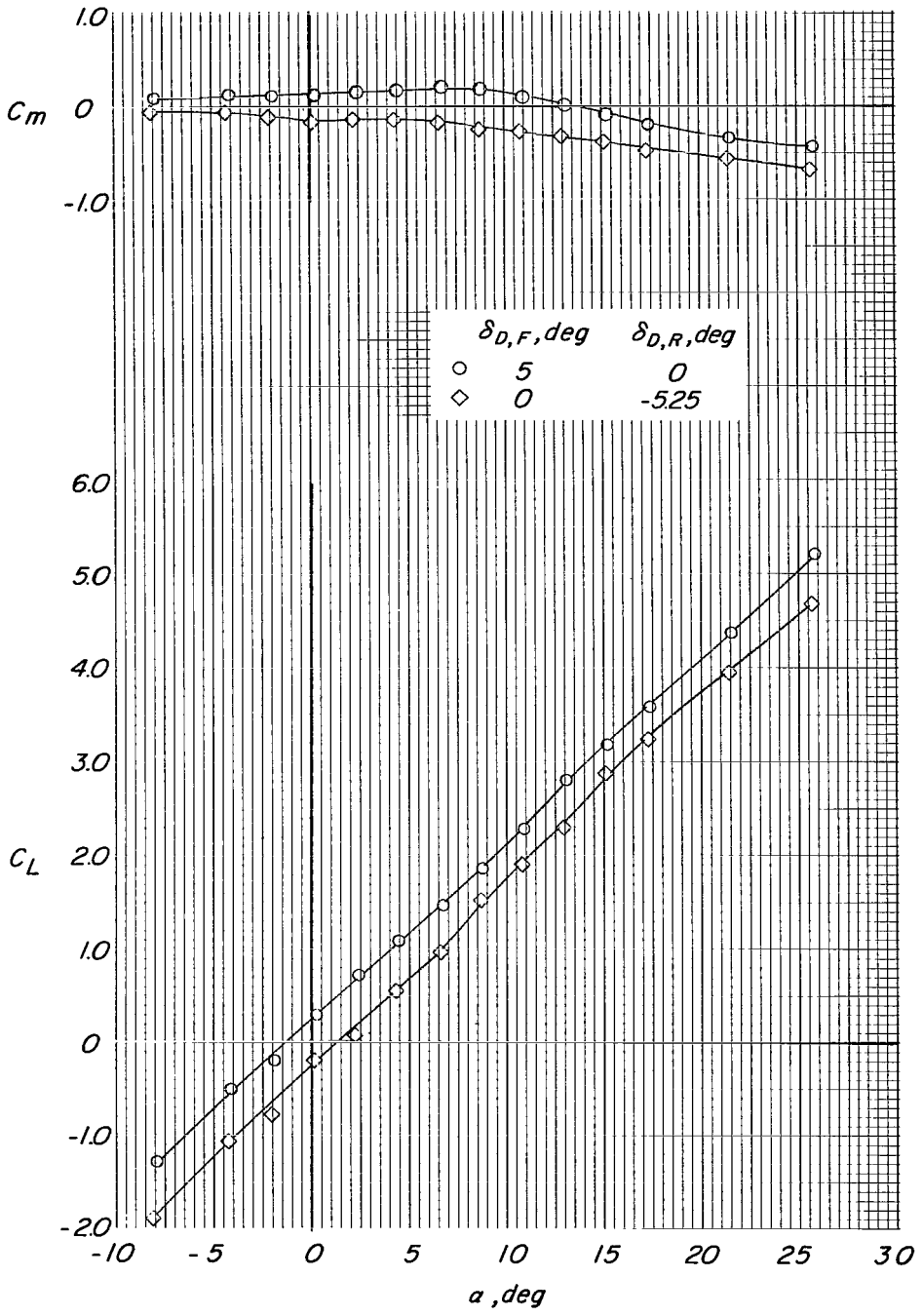


(c) $C_T = 2.1$.

Figure 13.- Continued.

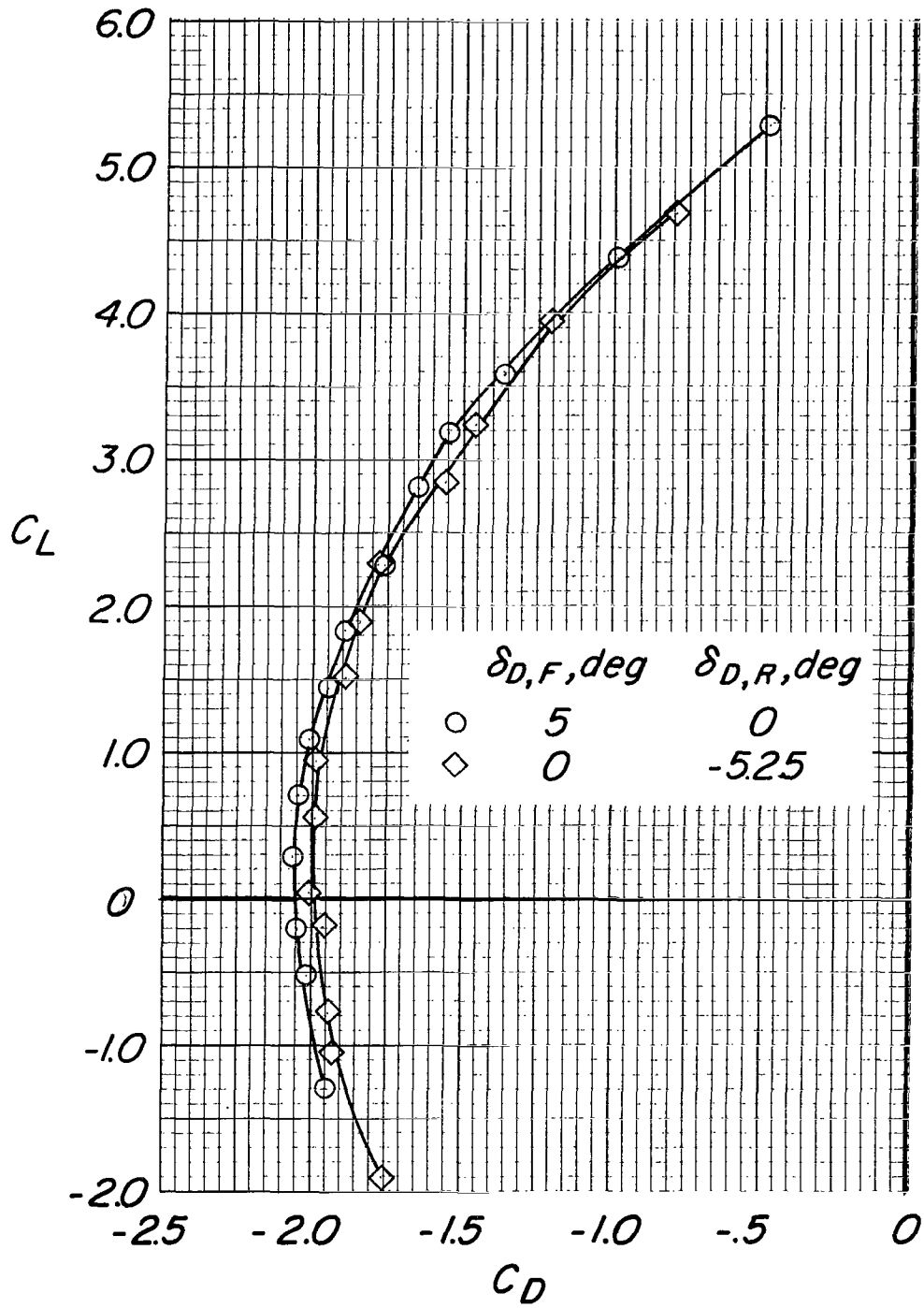


(c) Concluded.

Figure 13.- Concluded.

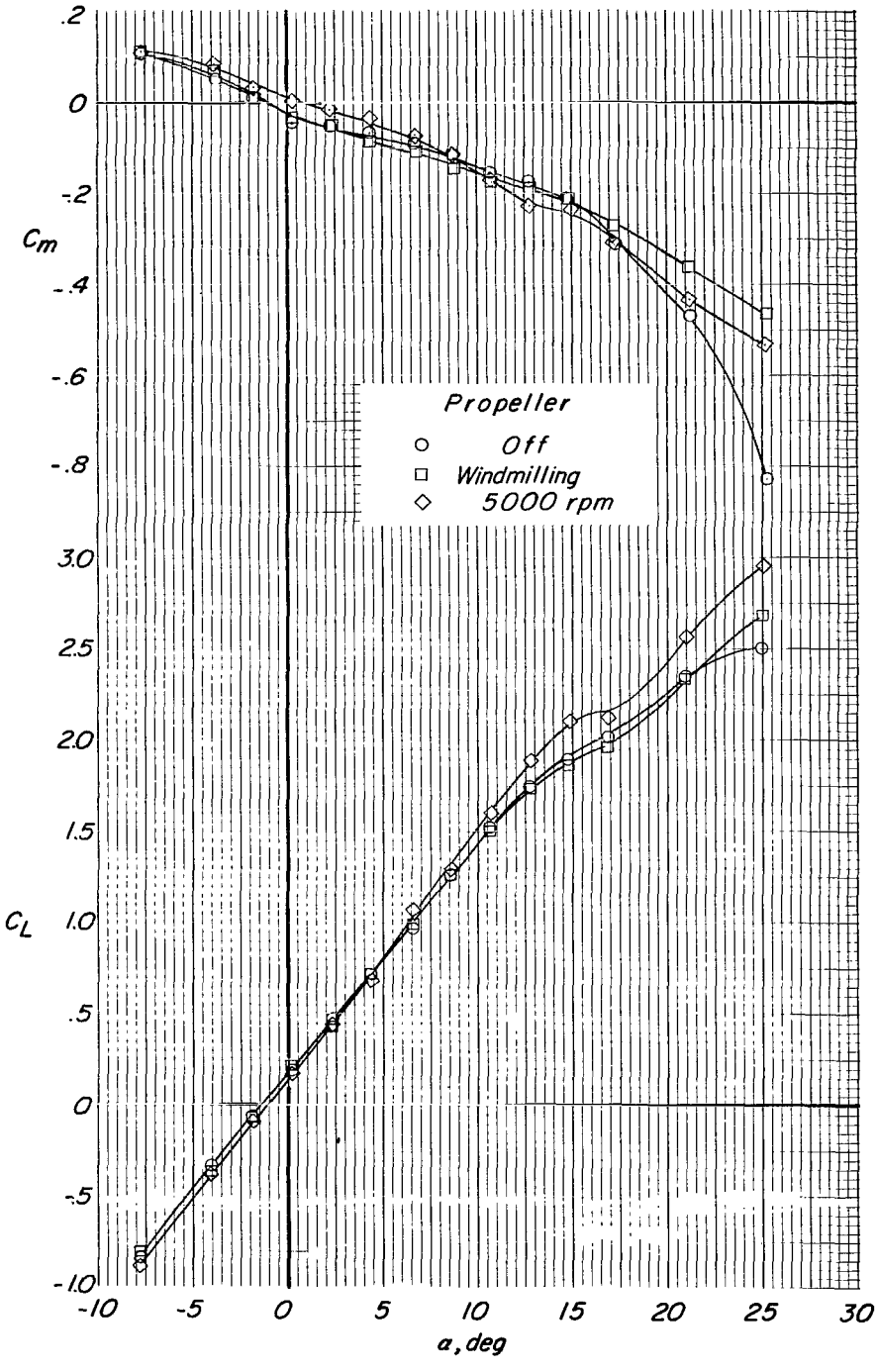


Figure 14.- Effect of propellers and sufficient thrust for zero drag on the aerodynamic characteristics of the model. $\delta_{D,F} = 5^0$; $\delta_{D,R} = 0^0$; $\delta_{V,F} = 0^0$; $\delta_{V,R} = 0^0$; $H_{t,1}$ on; $i_t = 0^0$; $V_t$ on.

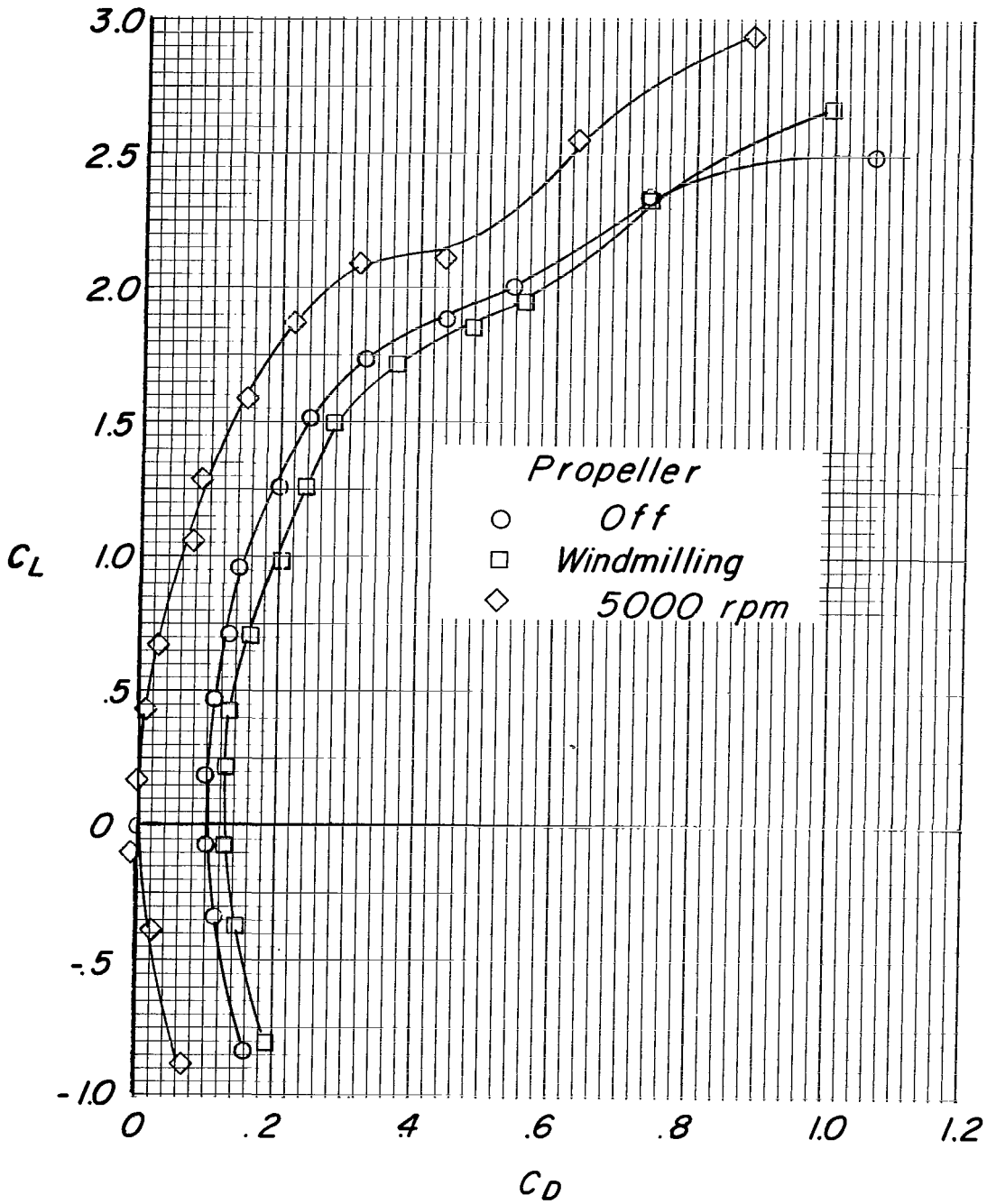


Figure 14.- Concluded.

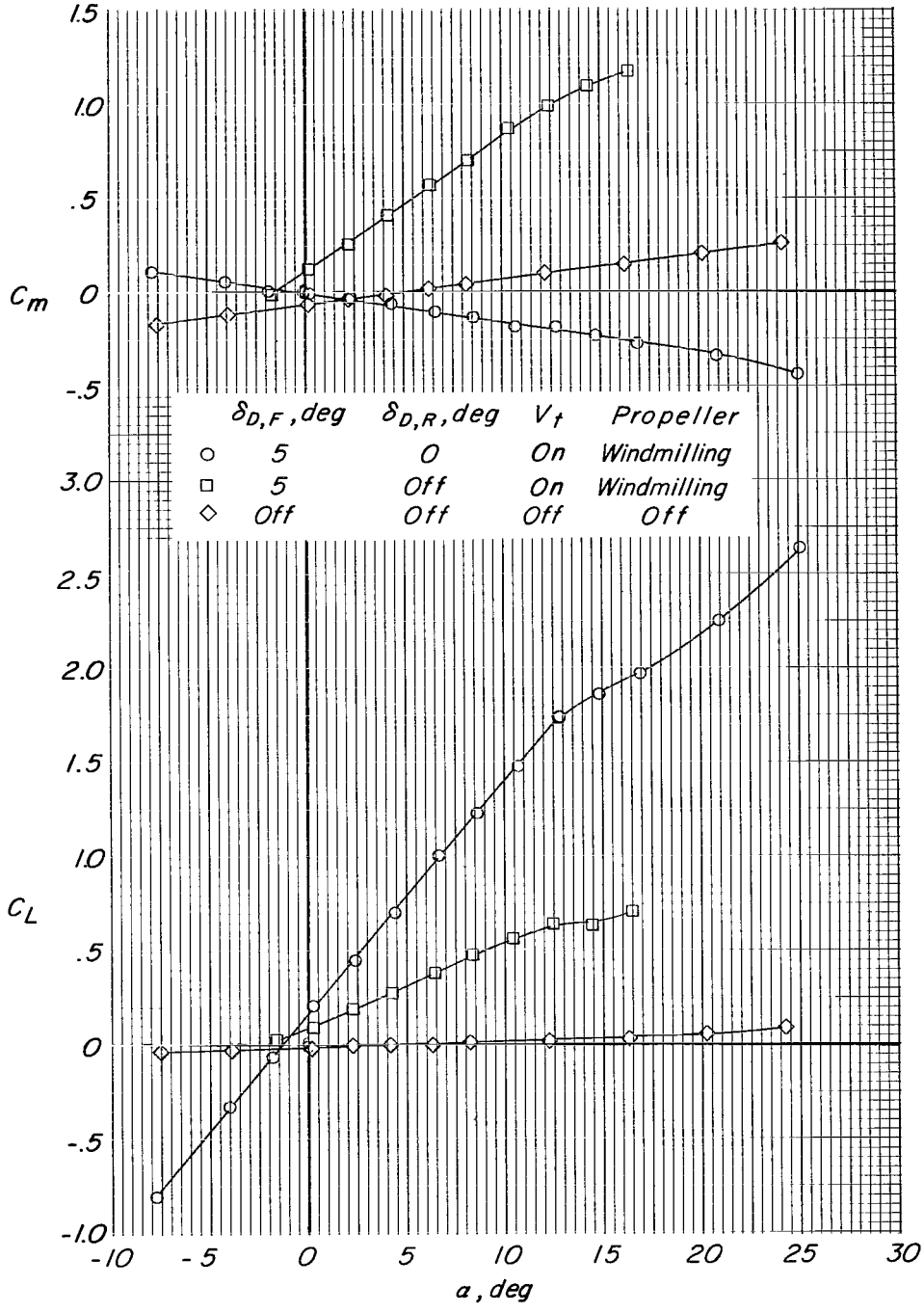


Figure 15.- Aerodynamic characteristics of the major components of the model. Power off (includes mutual interference effects); $\delta_{V,F} = 0^0$; $\delta_{V,R} = 0^0$; $H_{t,1}$ on; $i_t = 0^0$.

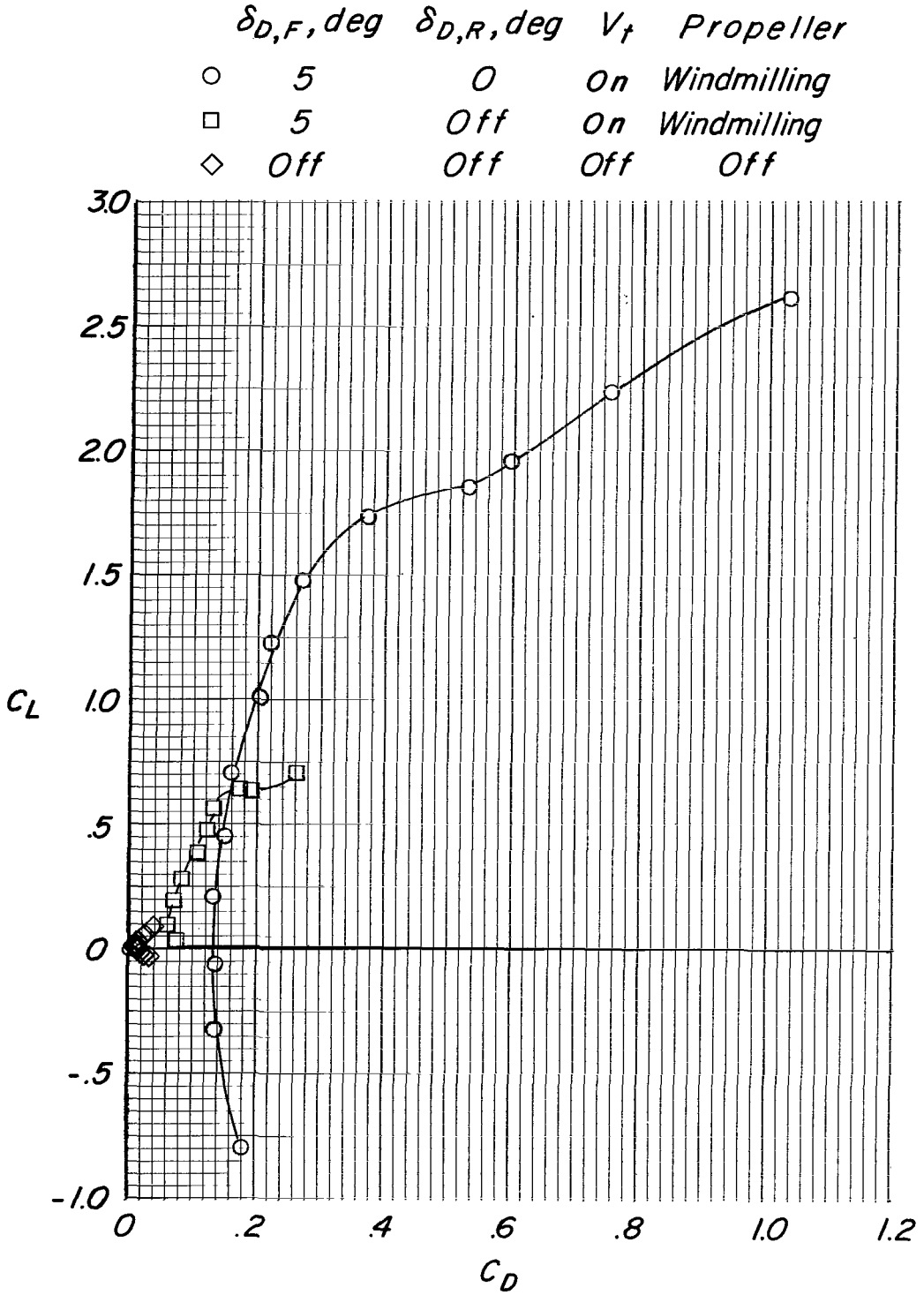


Figure 15.- Concluded.

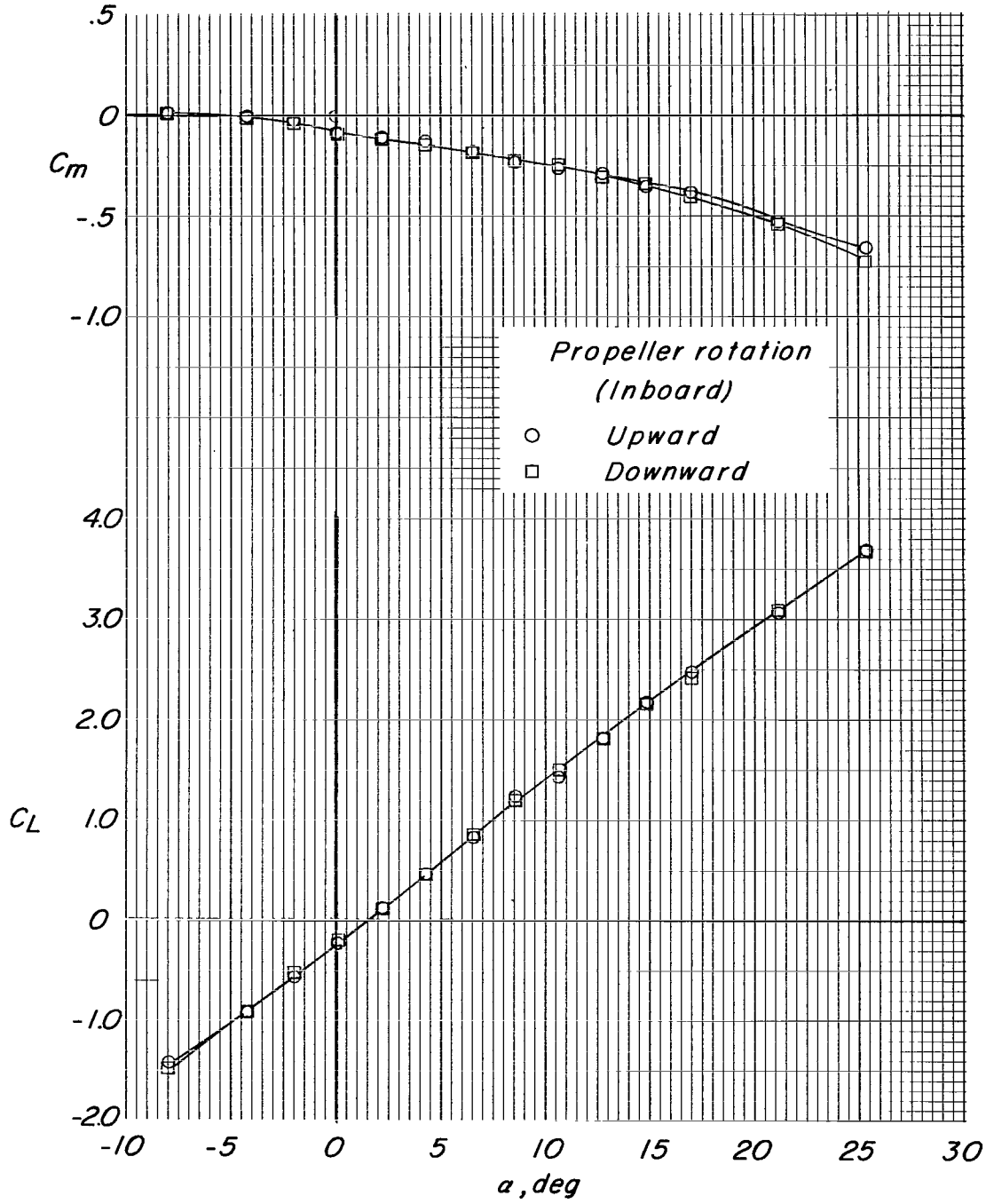


Figure 16.- Effects of direction of propeller rotation on the aerodynamic characteristics of the model. $C_T = 0.8$; $\delta_{D,F} = 0^0$; $\delta_{D,R} = -5.25^0$; $\delta_{V,F} = 0^0$; $\delta_{V,R} = 0^0$; $H_{t,1}$ on; $i_t = 0^0$; Vt on.

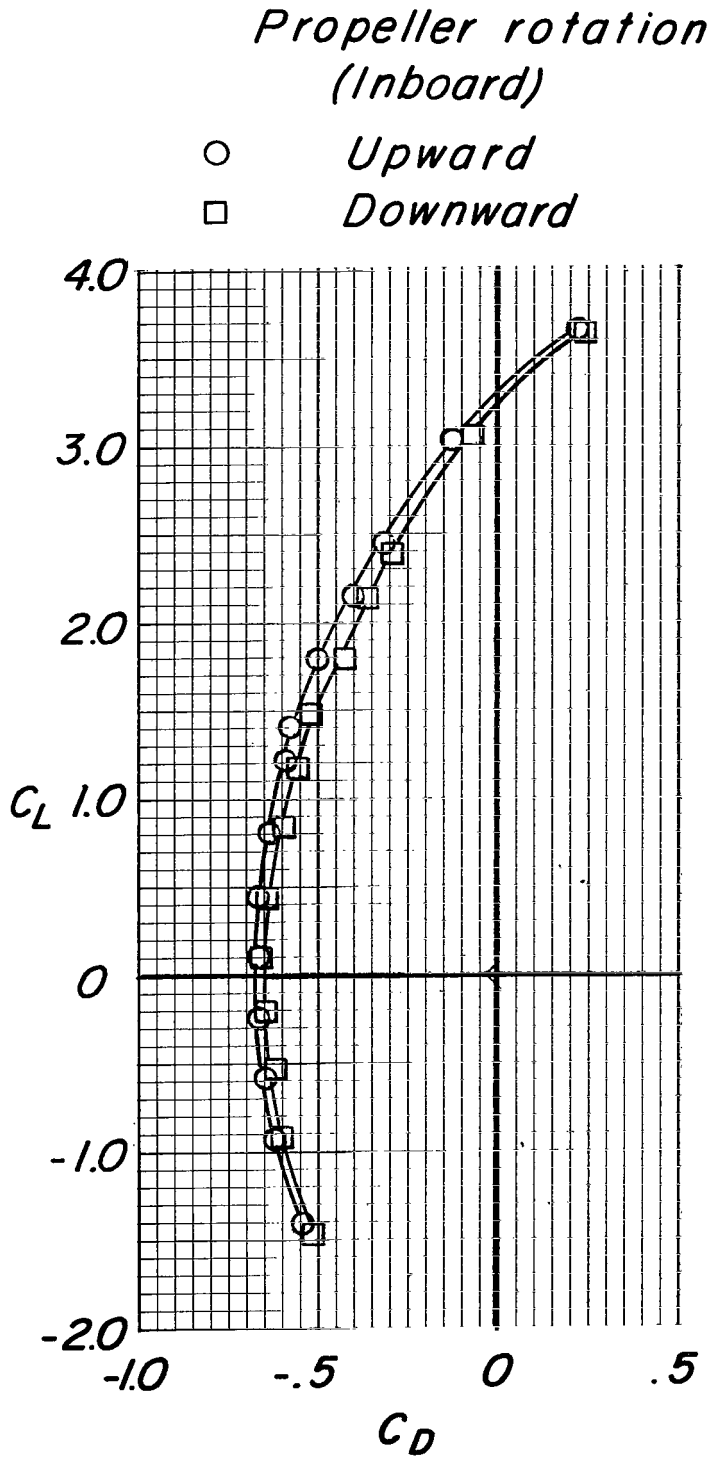


Figure 16.- Concluded.

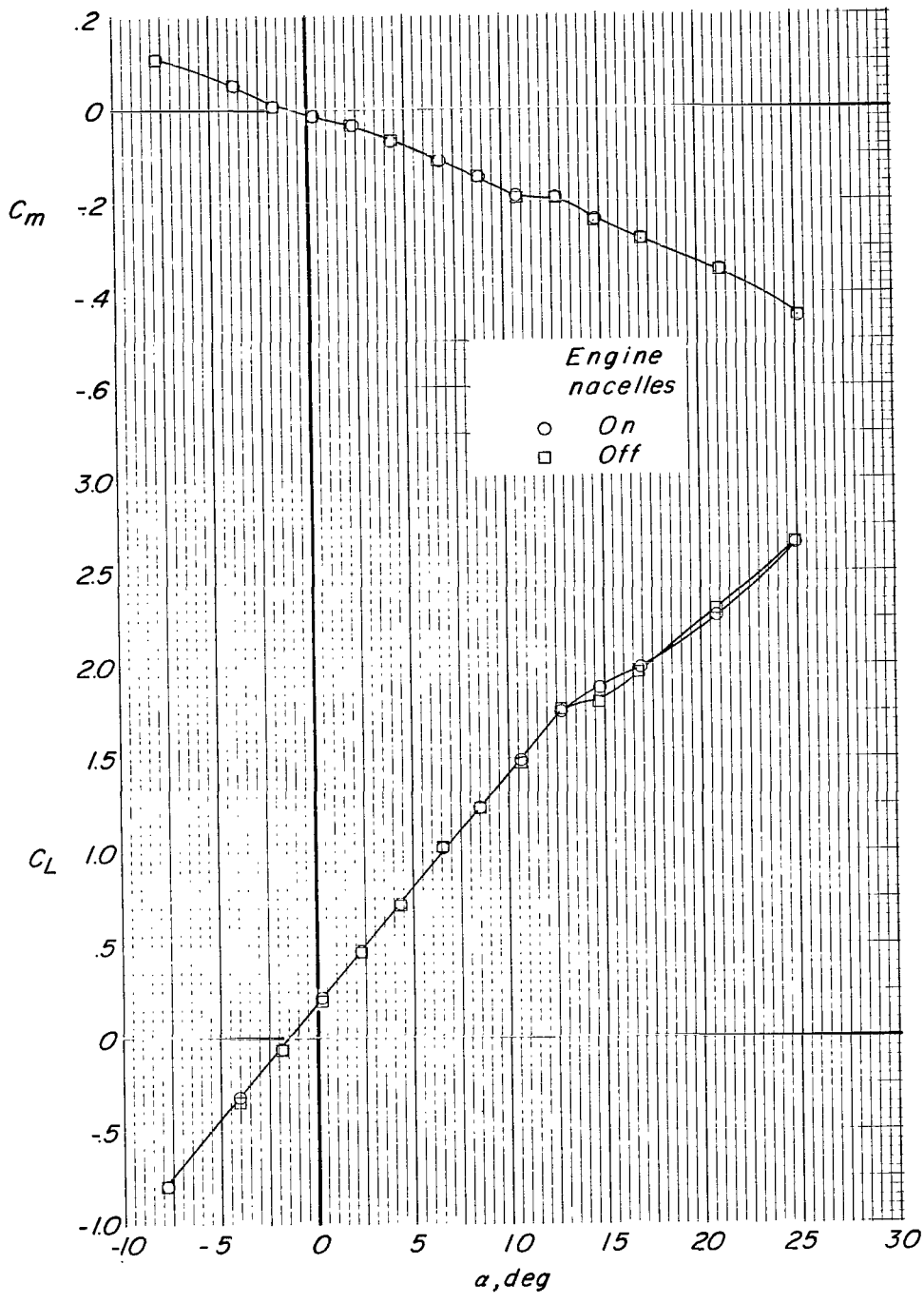


(a) $C_T = 0$; propellers windmilling.

Figure 17.- Effects of engine nacelles on the aerodynamic characteristics of the model at two thrust coefficients. $\delta_{D,F} = 5^0$; $\delta_{D,R} = 0^0$; $\delta_{V,F} = 0^0$; $\delta_{V,R} = 0^0$; $H_{t,1}$ on; $i_t = 0^0$; $V_t$ on.

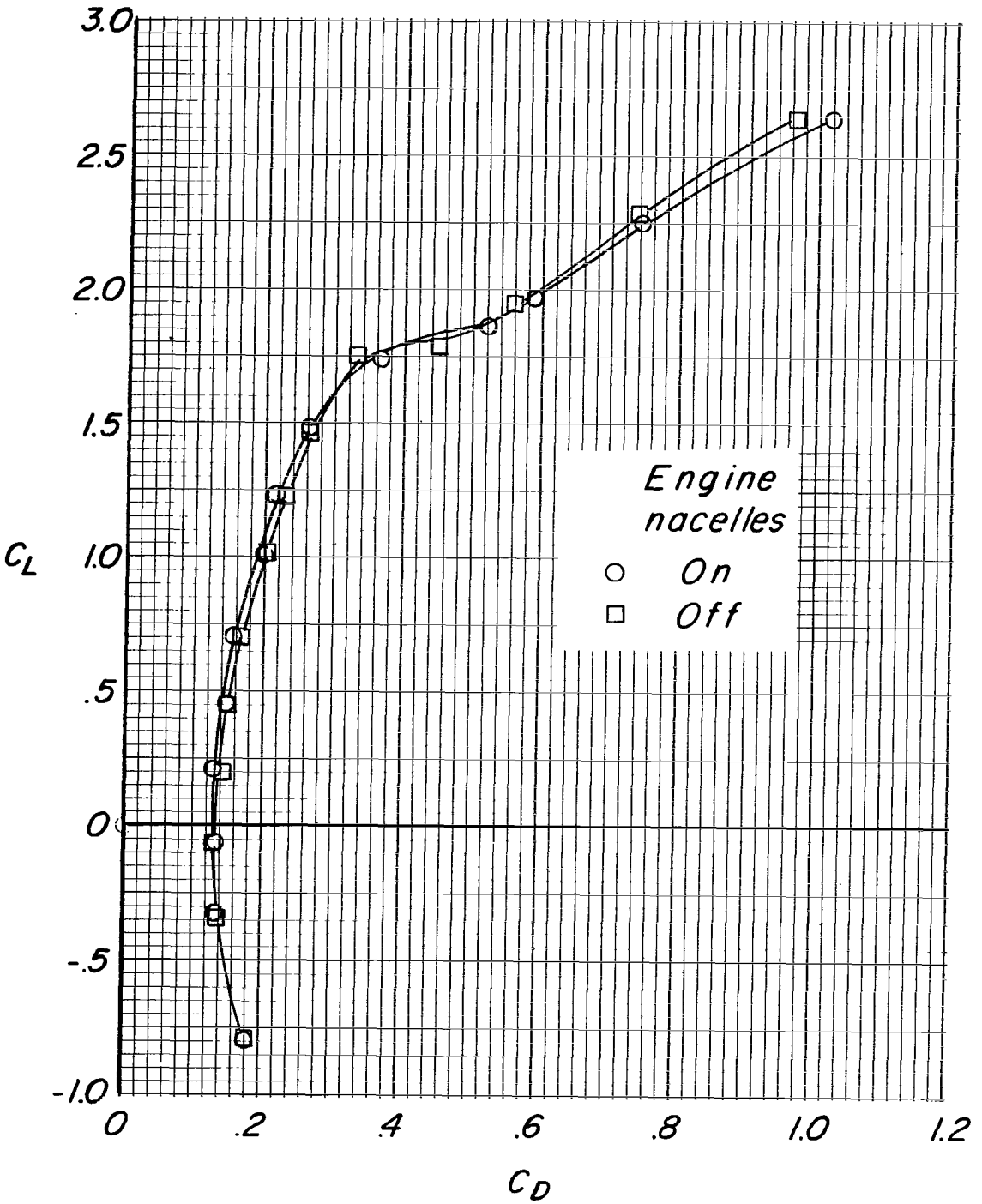


(a) Concluded.

Figure 17.- Continued.

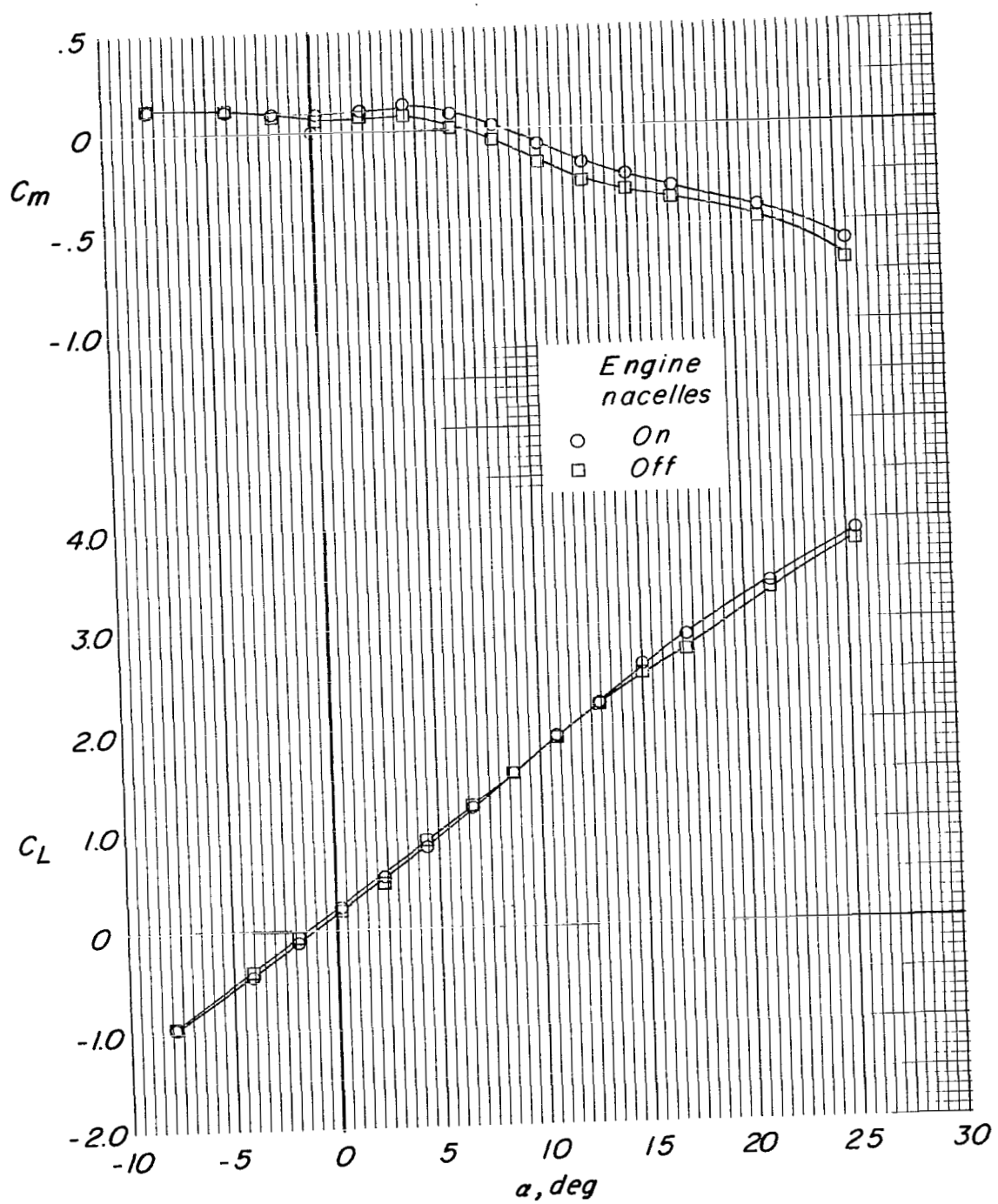


(b) $C_T = 0.8$.

Figure 17.- Continued.

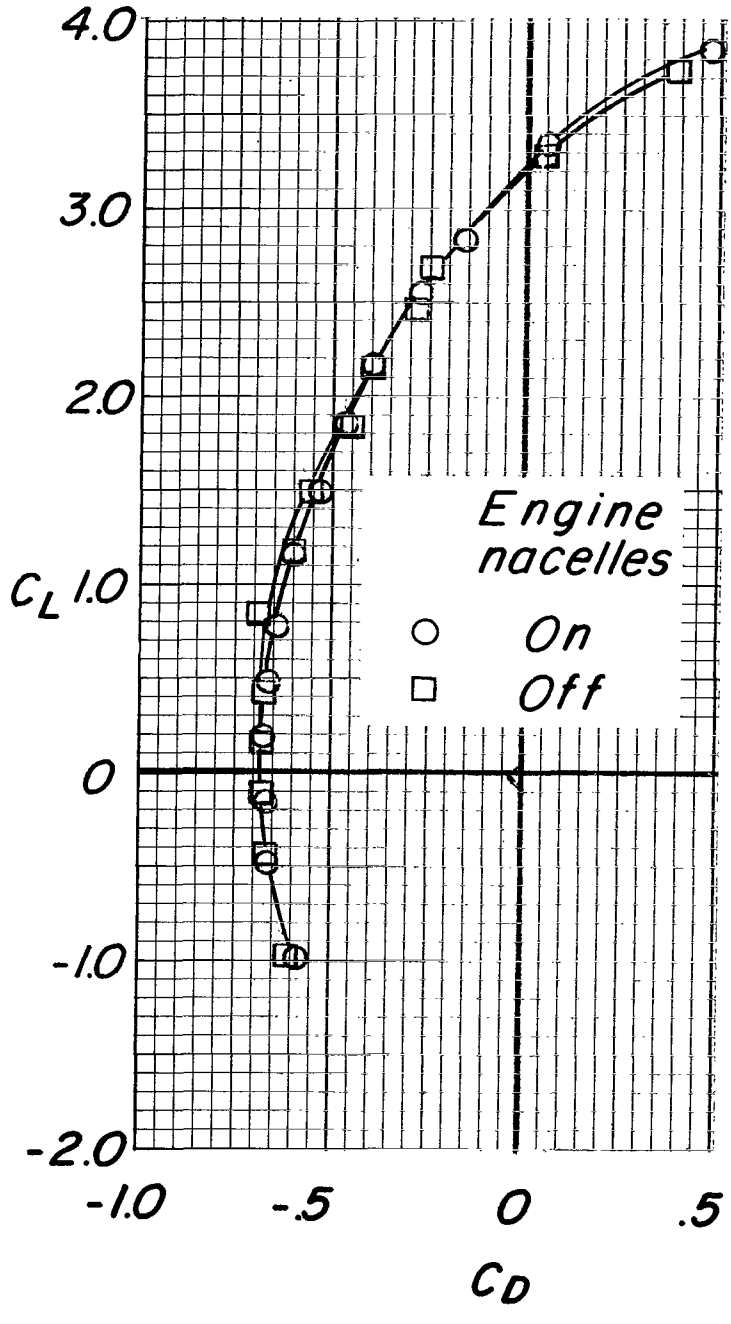


(b) Concluded.

Figure 17.- Concluded.

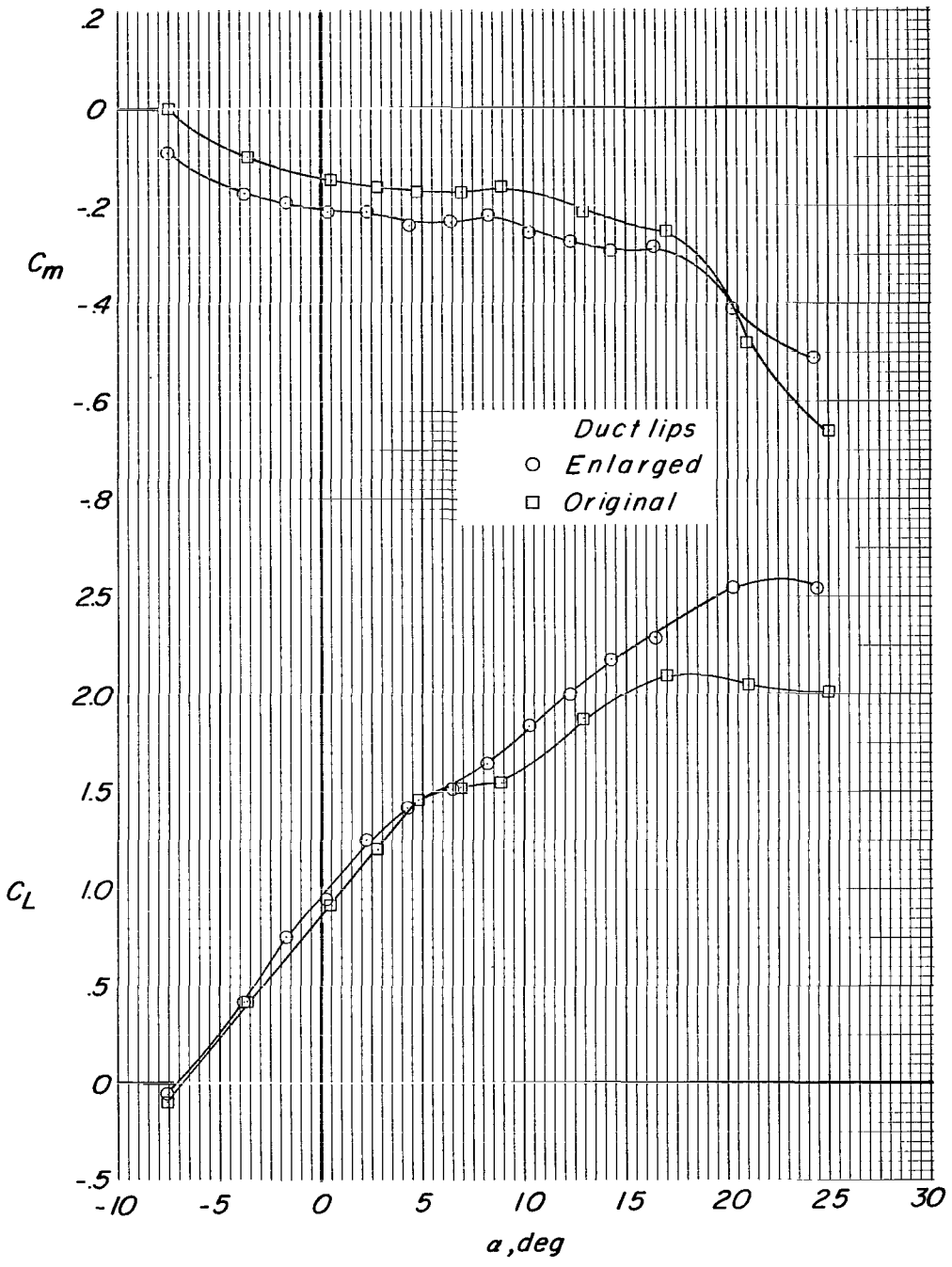


(a) $C_T = 0$; propellers windmilling.

Figure 18.- Effects of change in size of lower duct lip on the aerodynamic characteristics of the model at two thrust coefficients. $\delta_{D,F} = 15^0$; $\delta_{D,R} = 15^0$; $\delta_{V,F} = 0^0$; $\delta_{V,R} = 0^0$; $H_{t,1}$ on; $i_t = 0^0$; $V_t$ on.

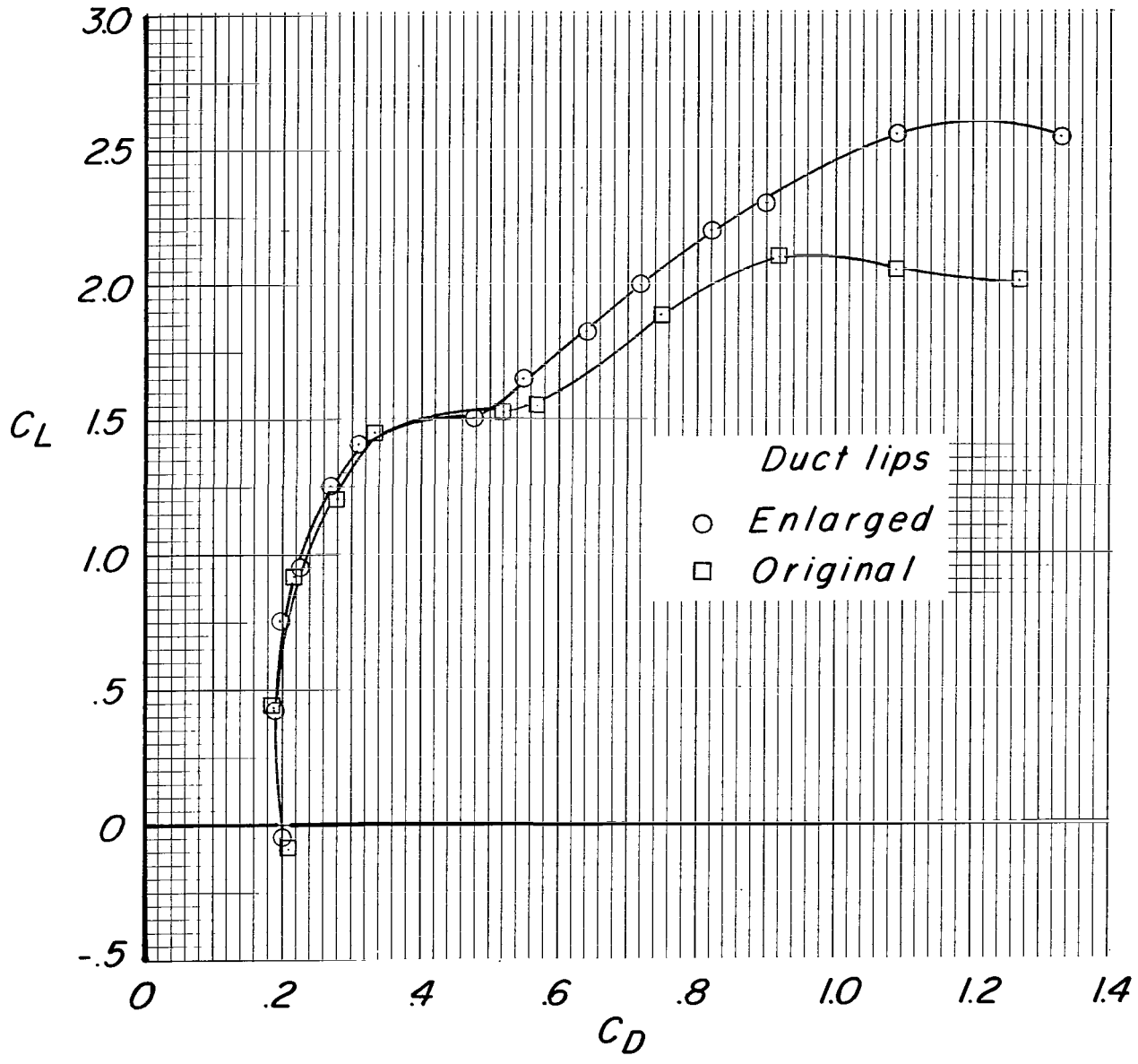


(a) Concluded.

Figure 18.- Continued.

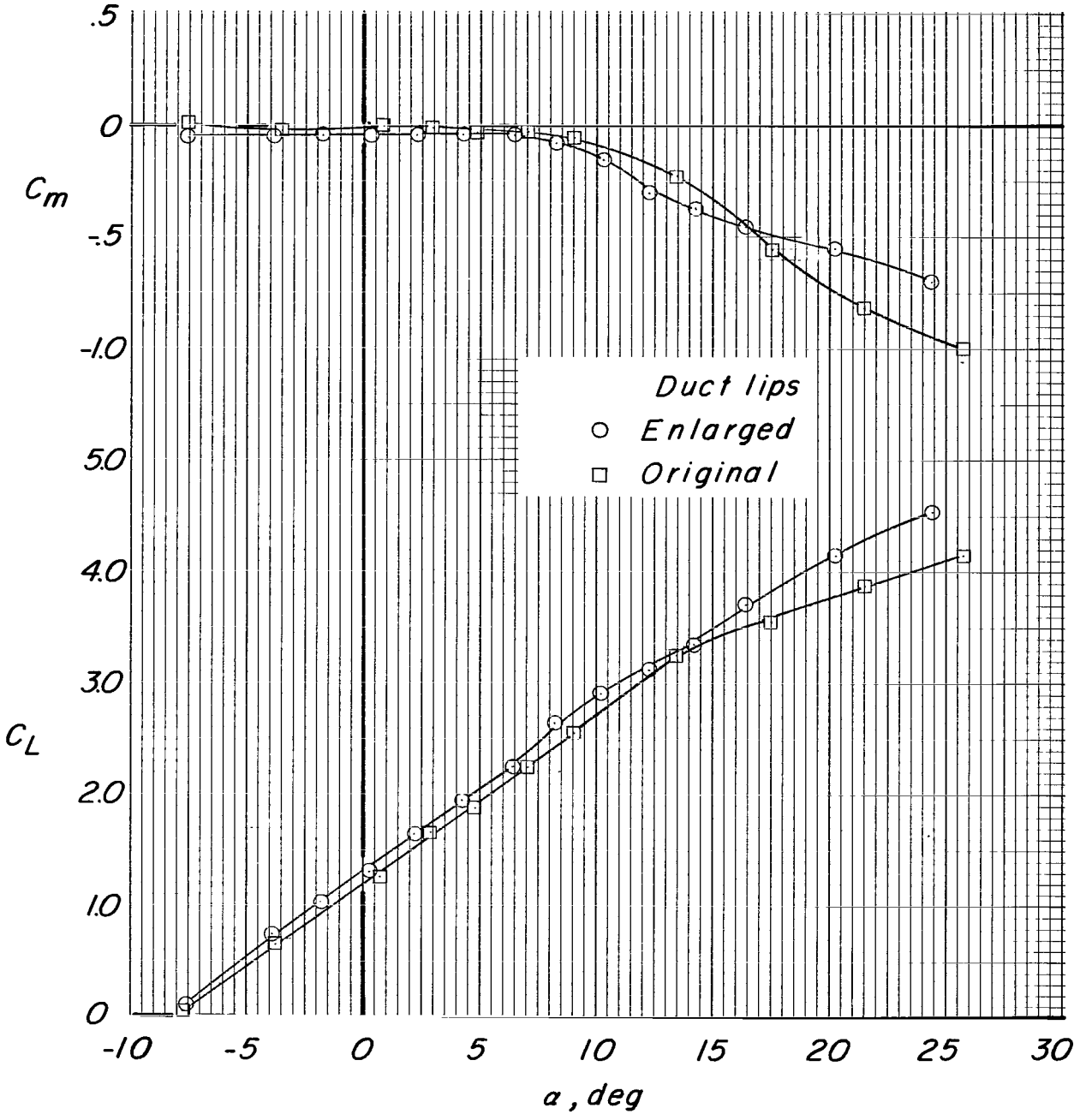


(b) $C_T = 0.8$.

Figure 18.- Continued.

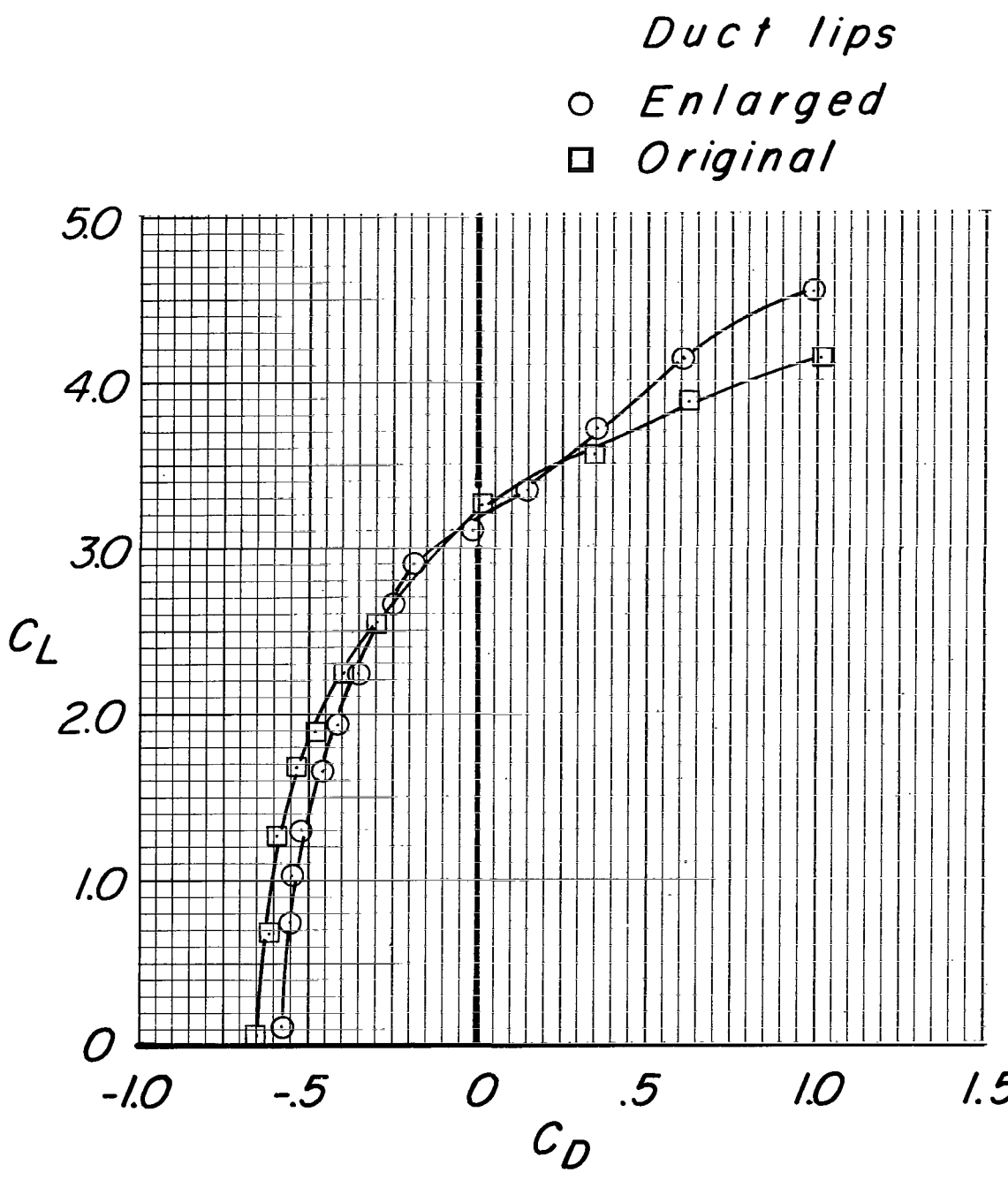


(b) Concluded.

Figure 18.- Concluded.

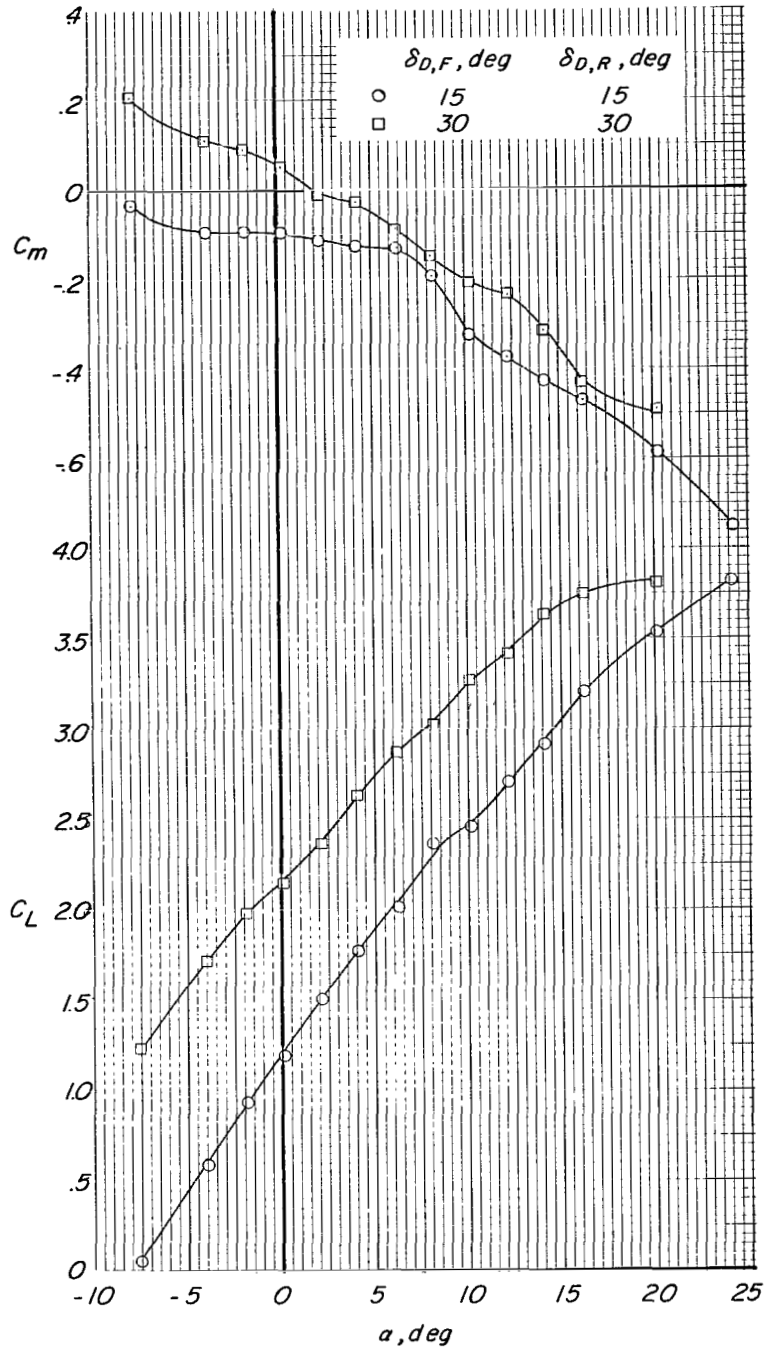


(a) $C_T = 0.4$.

Figure 19.- Effects of duct deflection angle on the aerodynamic characteristics of the model at various thrust coefficients. $\delta_{V,F} = 0^0$; $\delta_{V,R} = 0^0$; $H_{t,1}$ on; $i_t = 0^0$; $V_t$ on; modified duct lips; tail-fuselage fairing on.

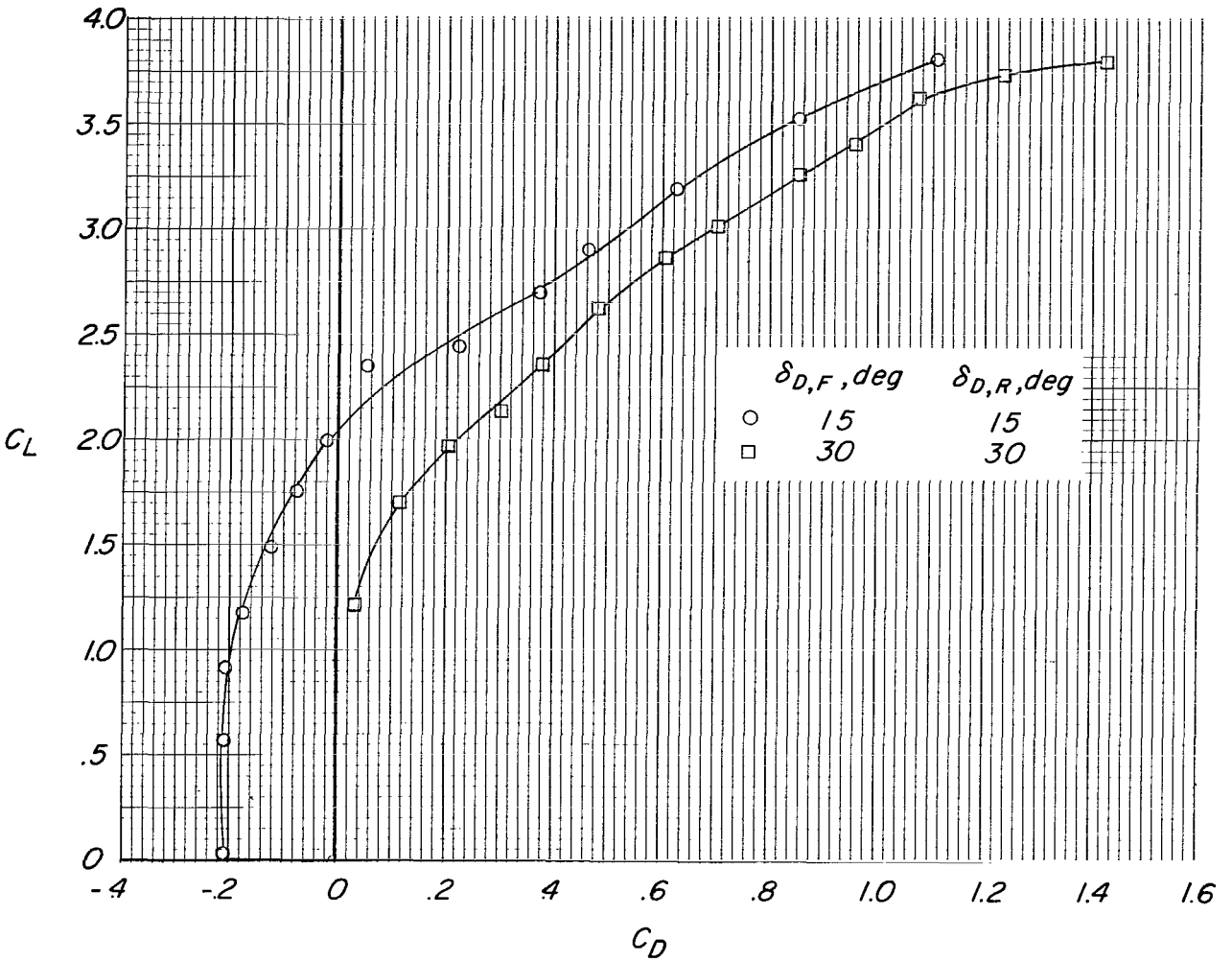


(a) Continued.

Figure 19.- Continued.

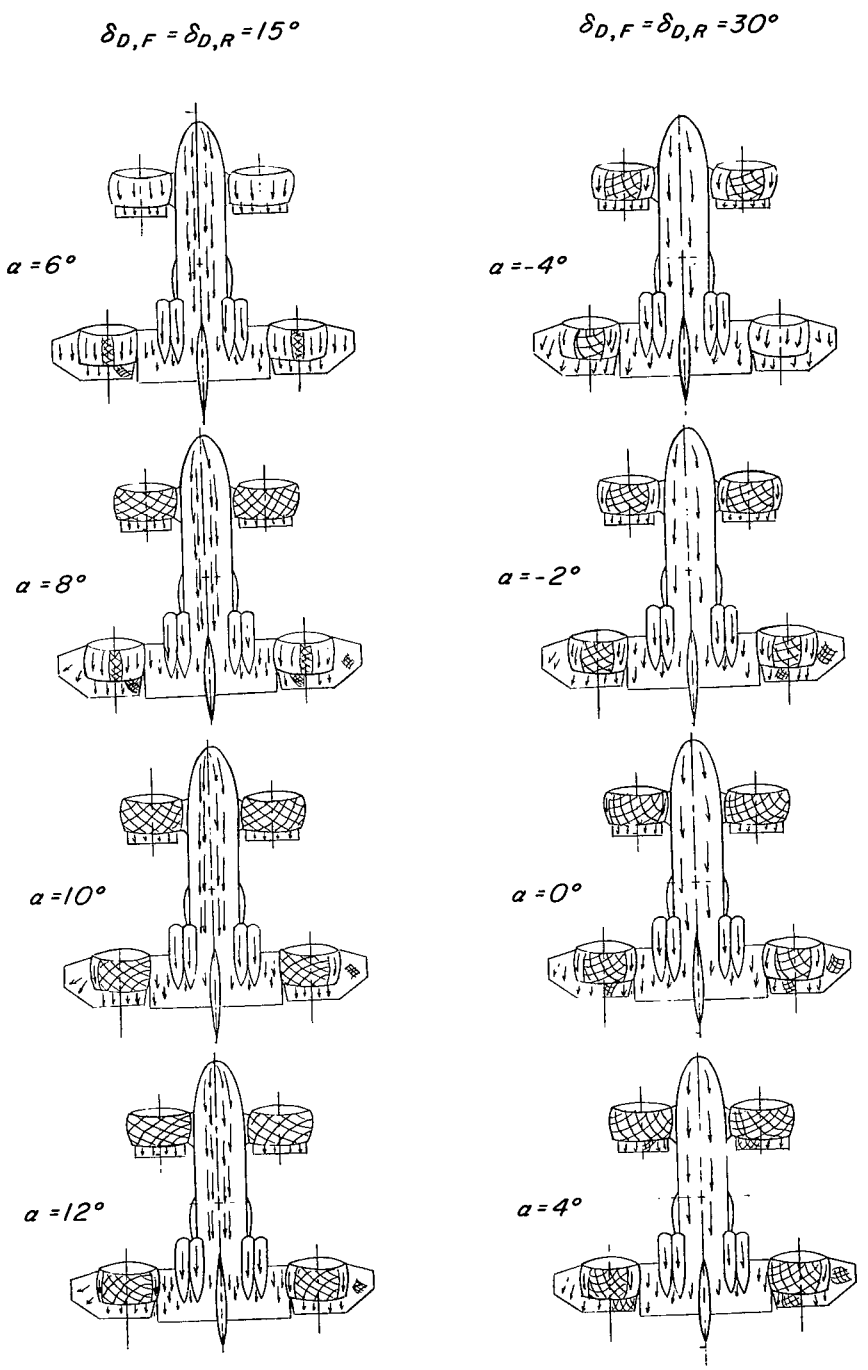


(a) Concluded.

Figure 19.- Continued.

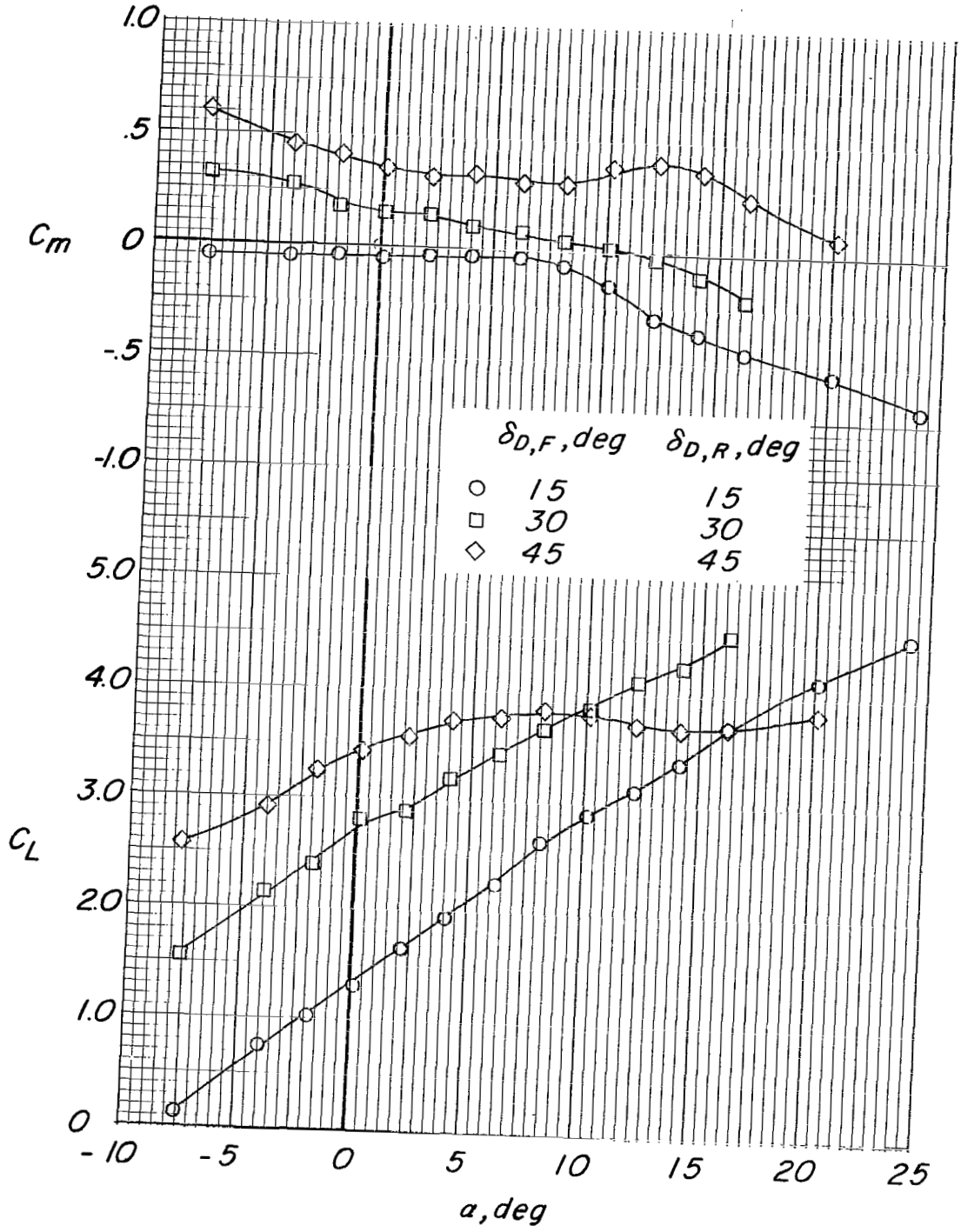


(b) $C_T = 0.8$.

Figure 19.- Continued.

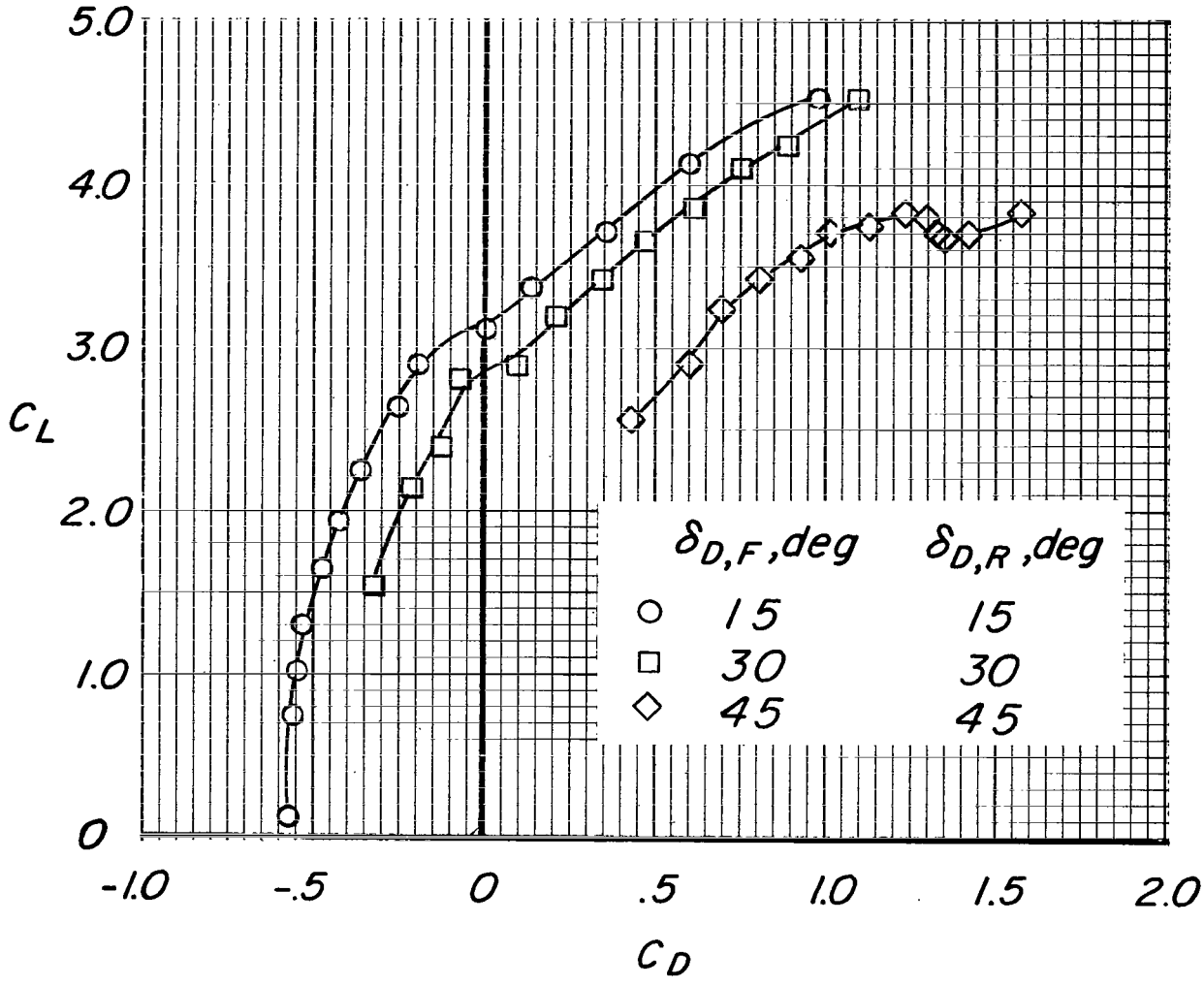


(b) Continued.

Figure 19.- Continued.

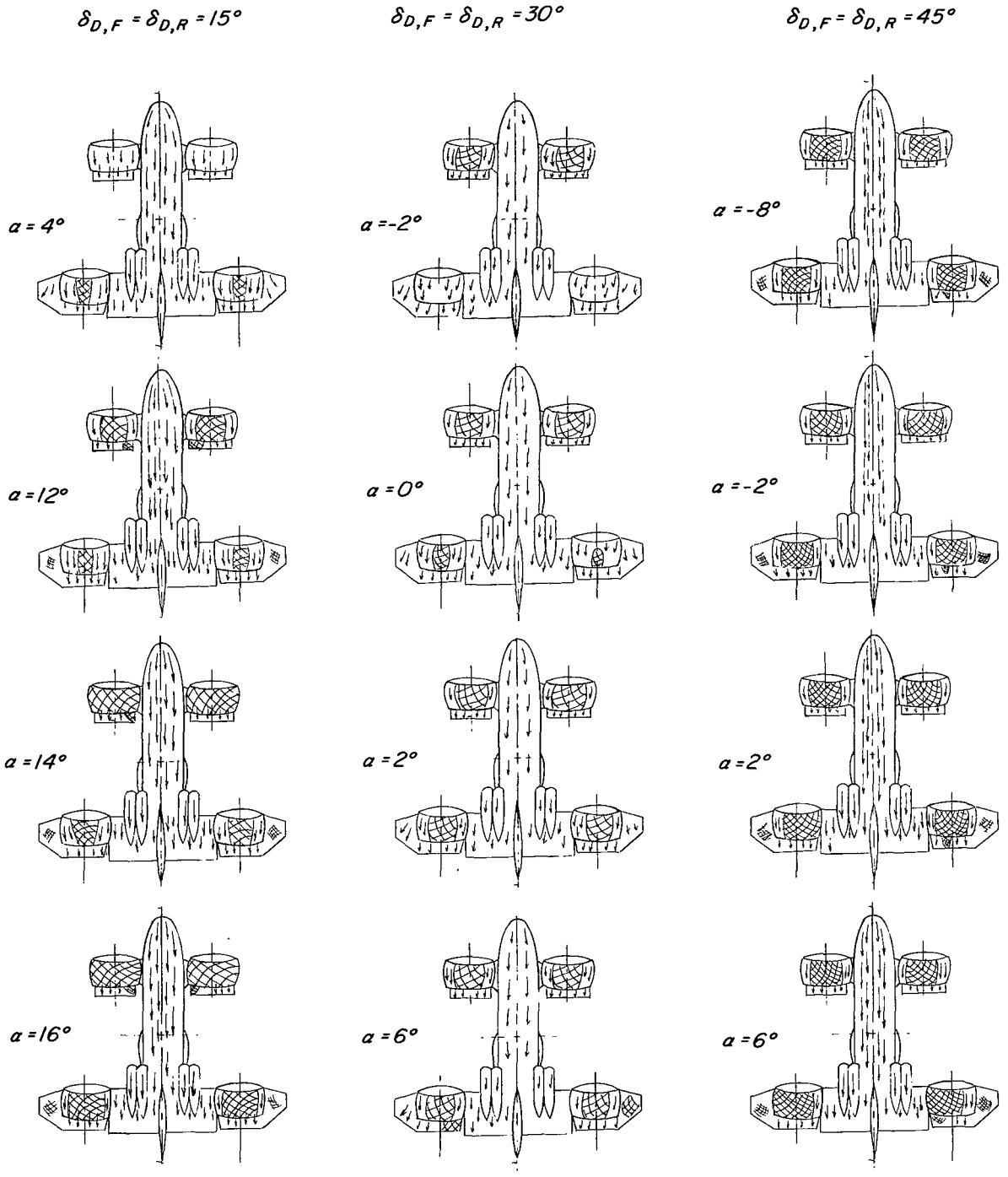


(b) Concluded.

Figure 19.- Continued.

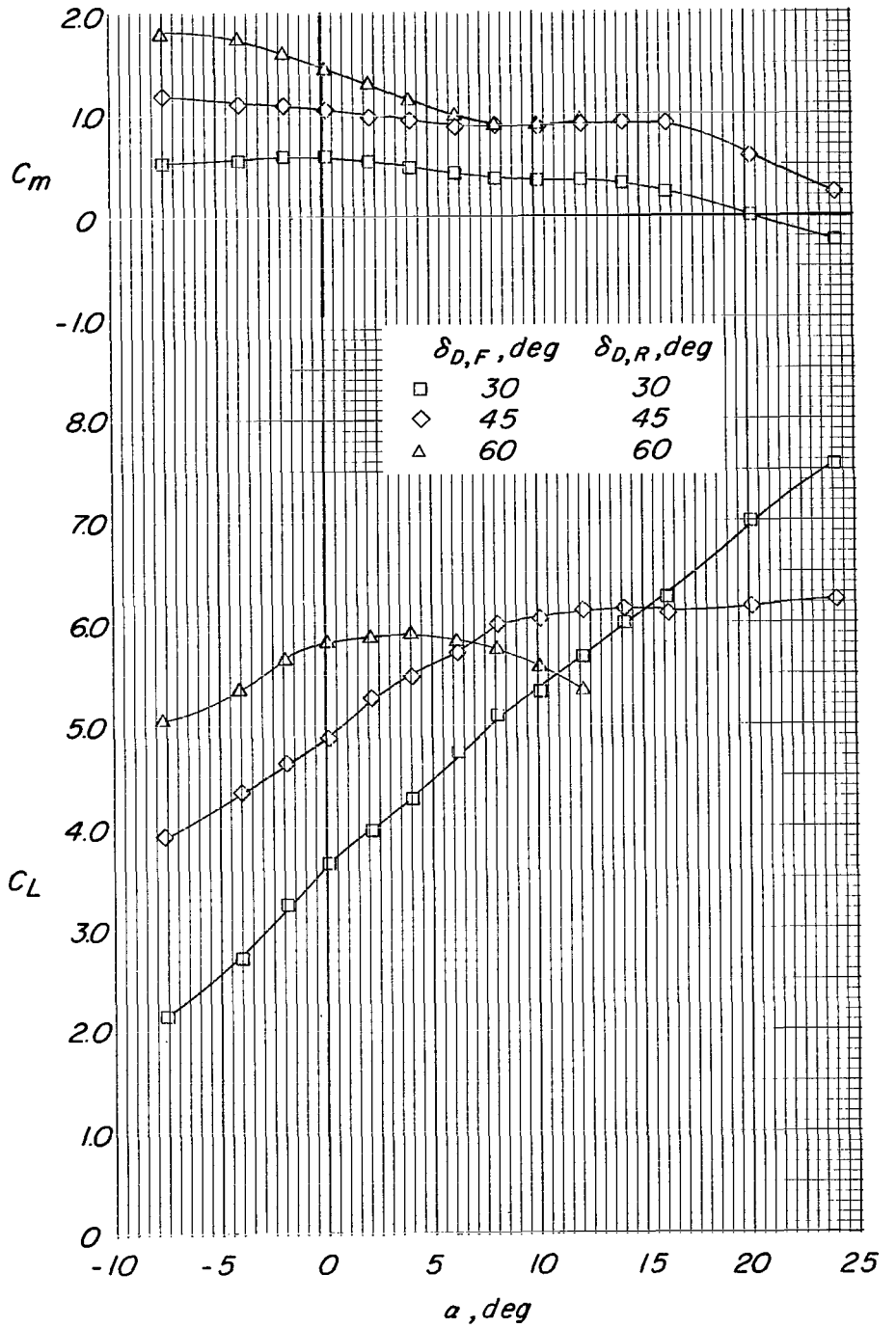


(c) $C_T = 2.1$.

Figure 19.- Continued.

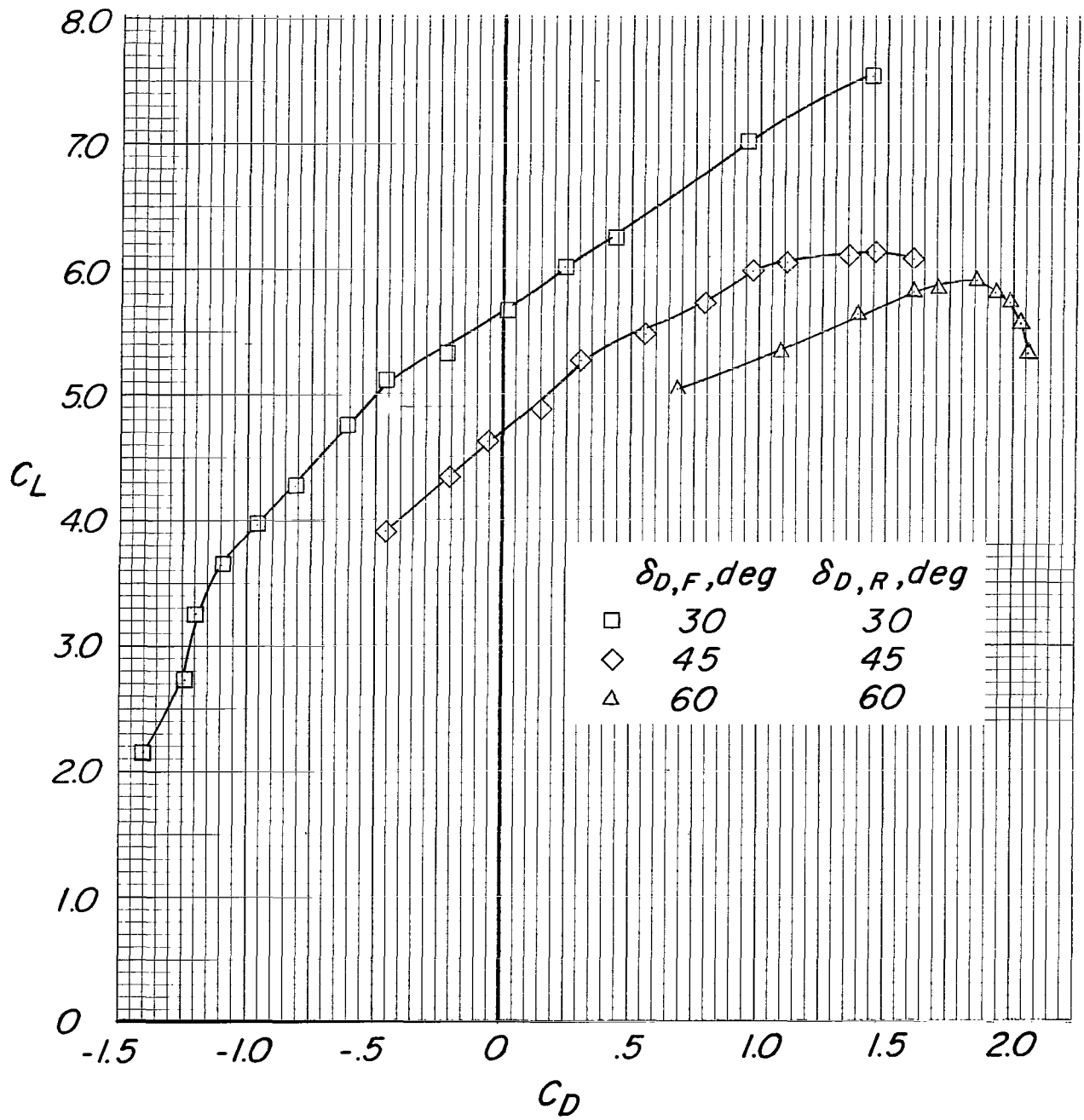


(c) Continued.

Figure 19.- Continued.

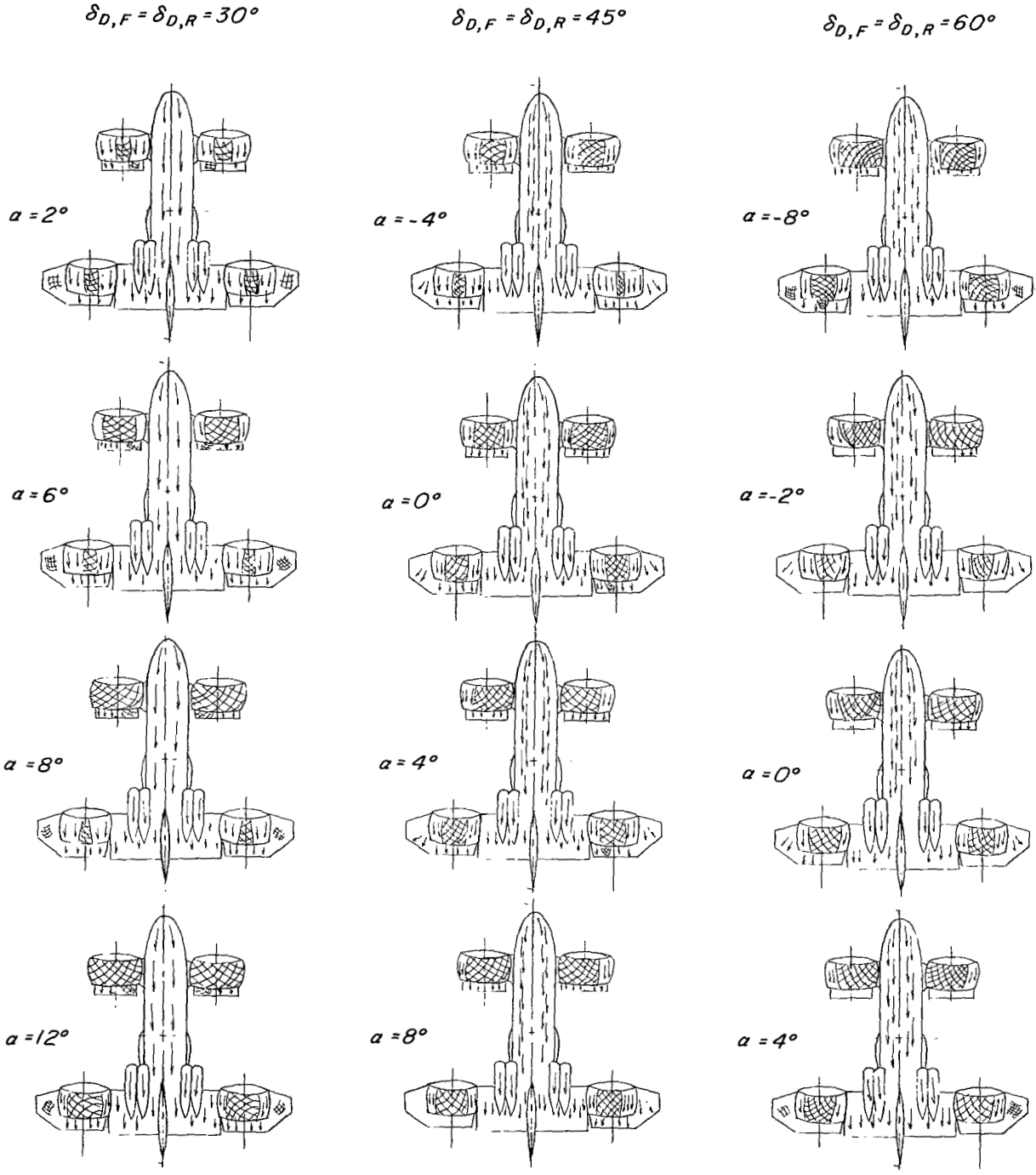


(c) Concluded.

Figure 19.- Continued.

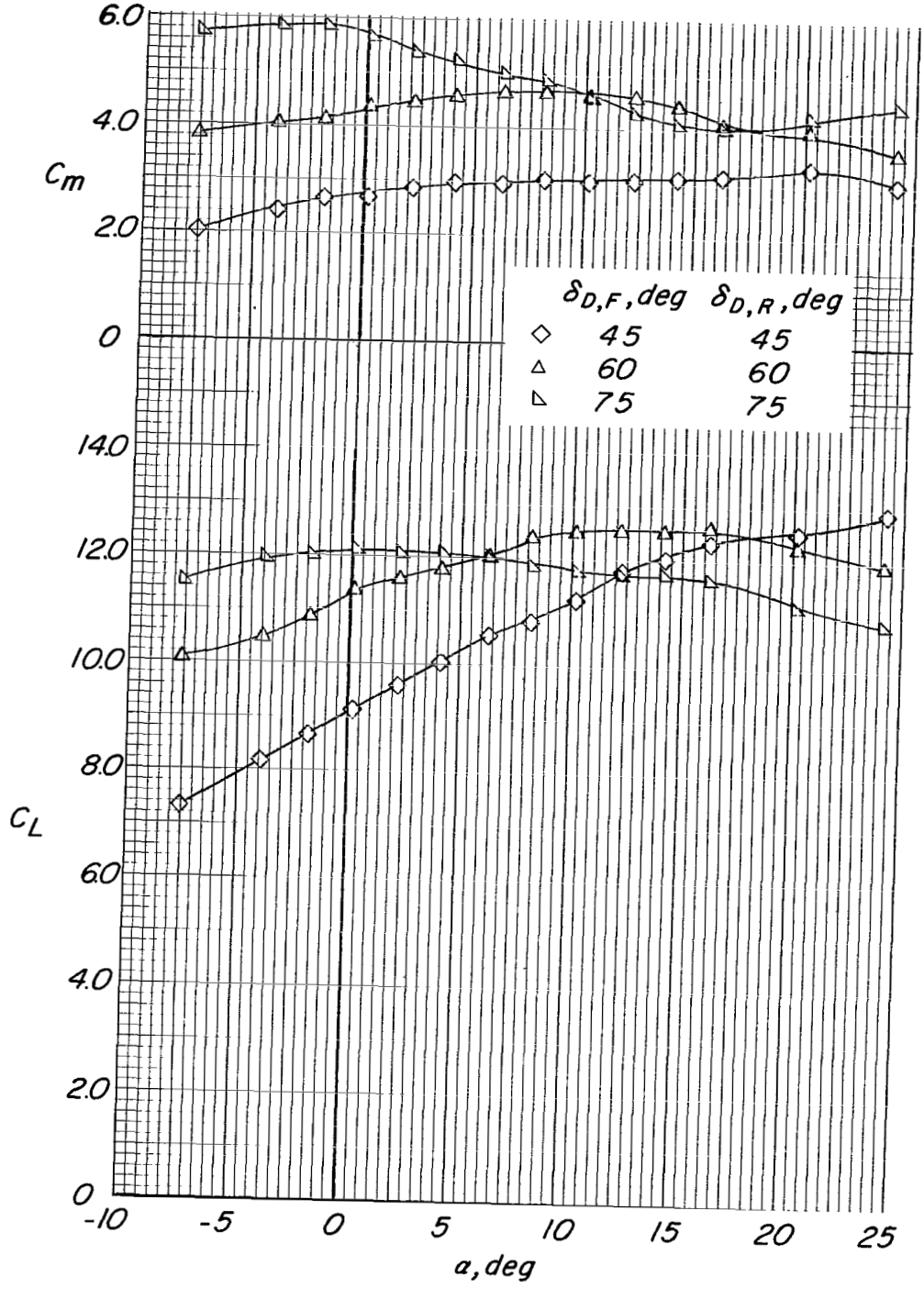


(d) $C_T = 7.0$.

Figure 19.- Continued.

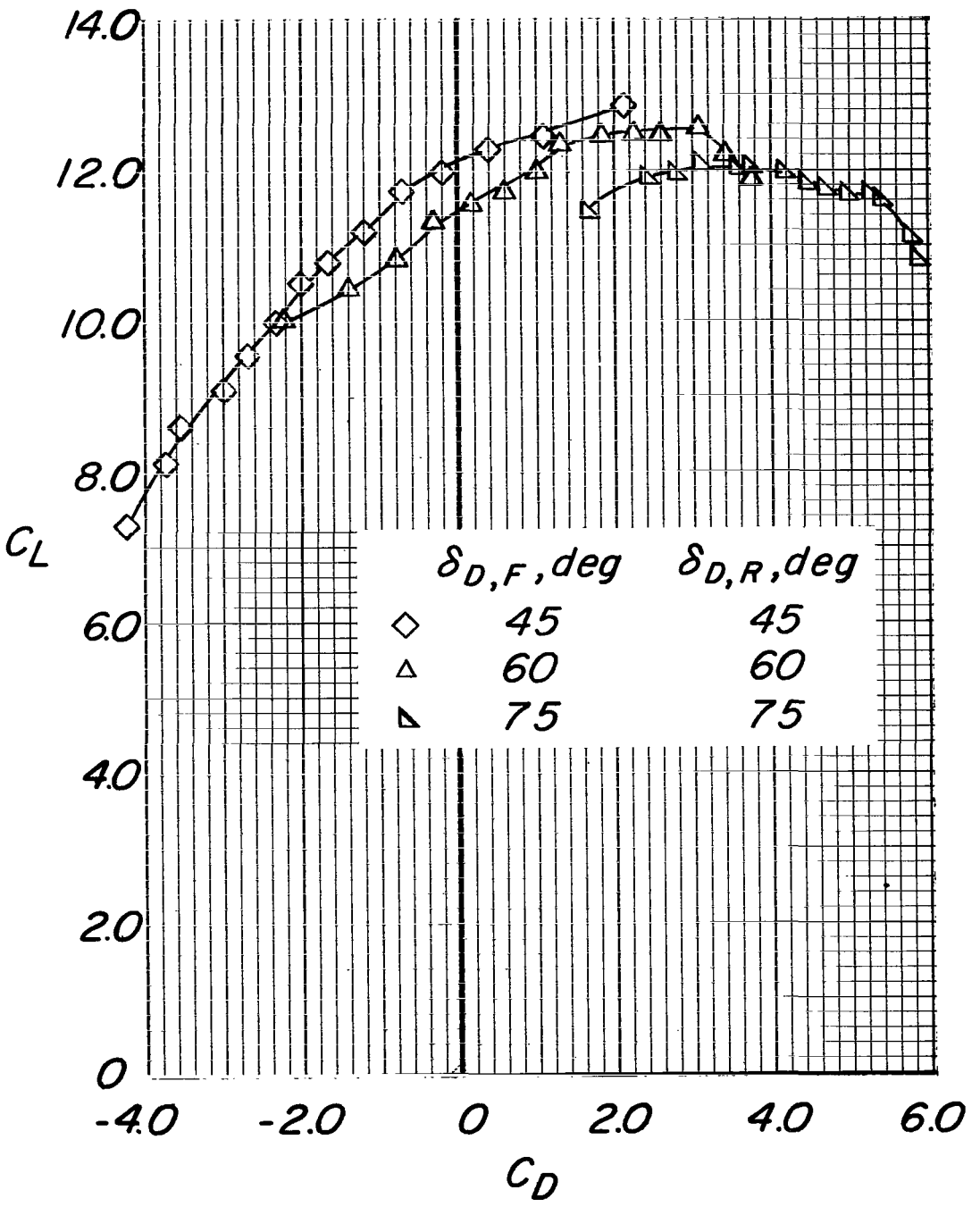


(d) Continued.

Figure 19.- Continued.

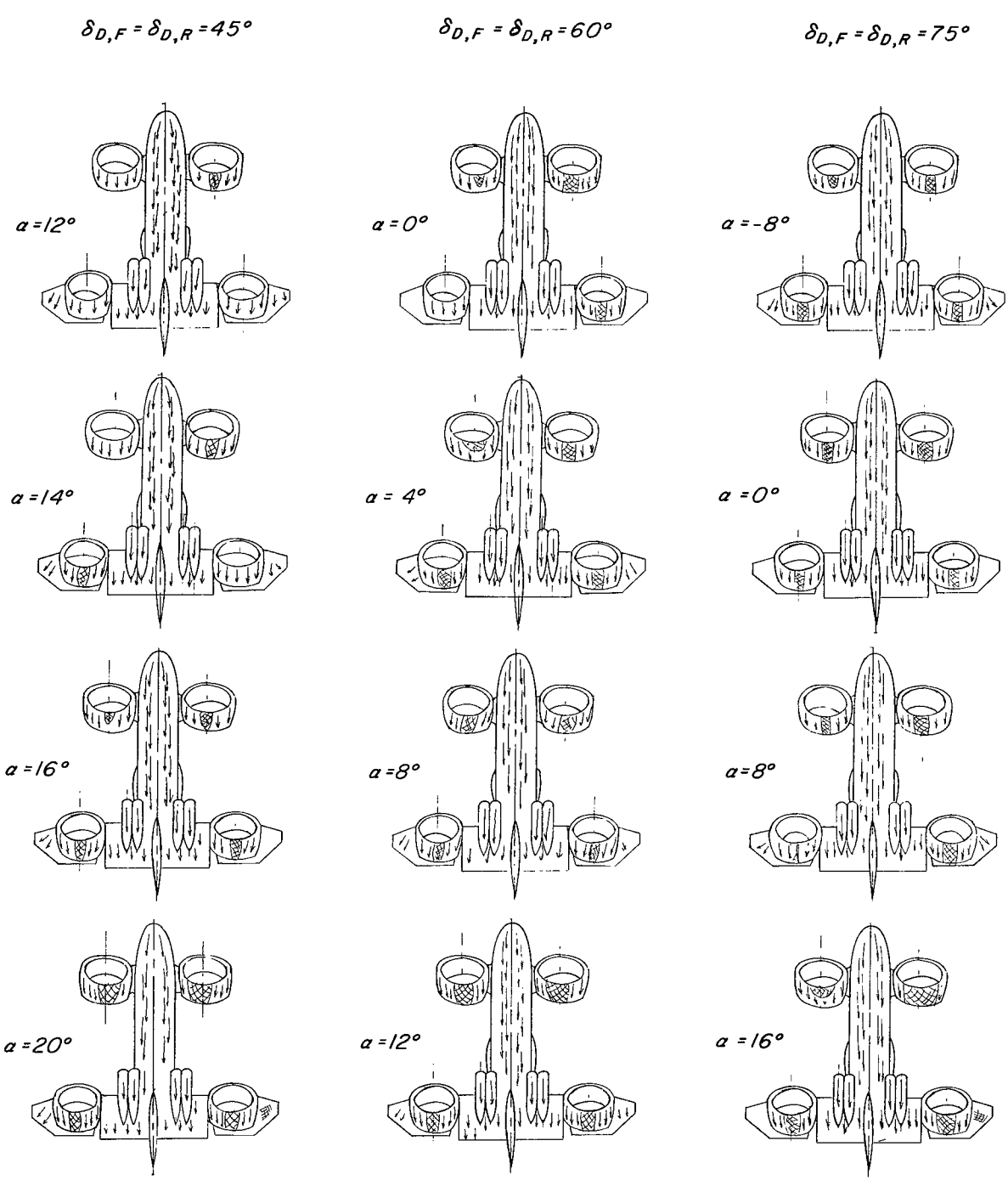


(d) Concluded.

Figure 19.- Continued.

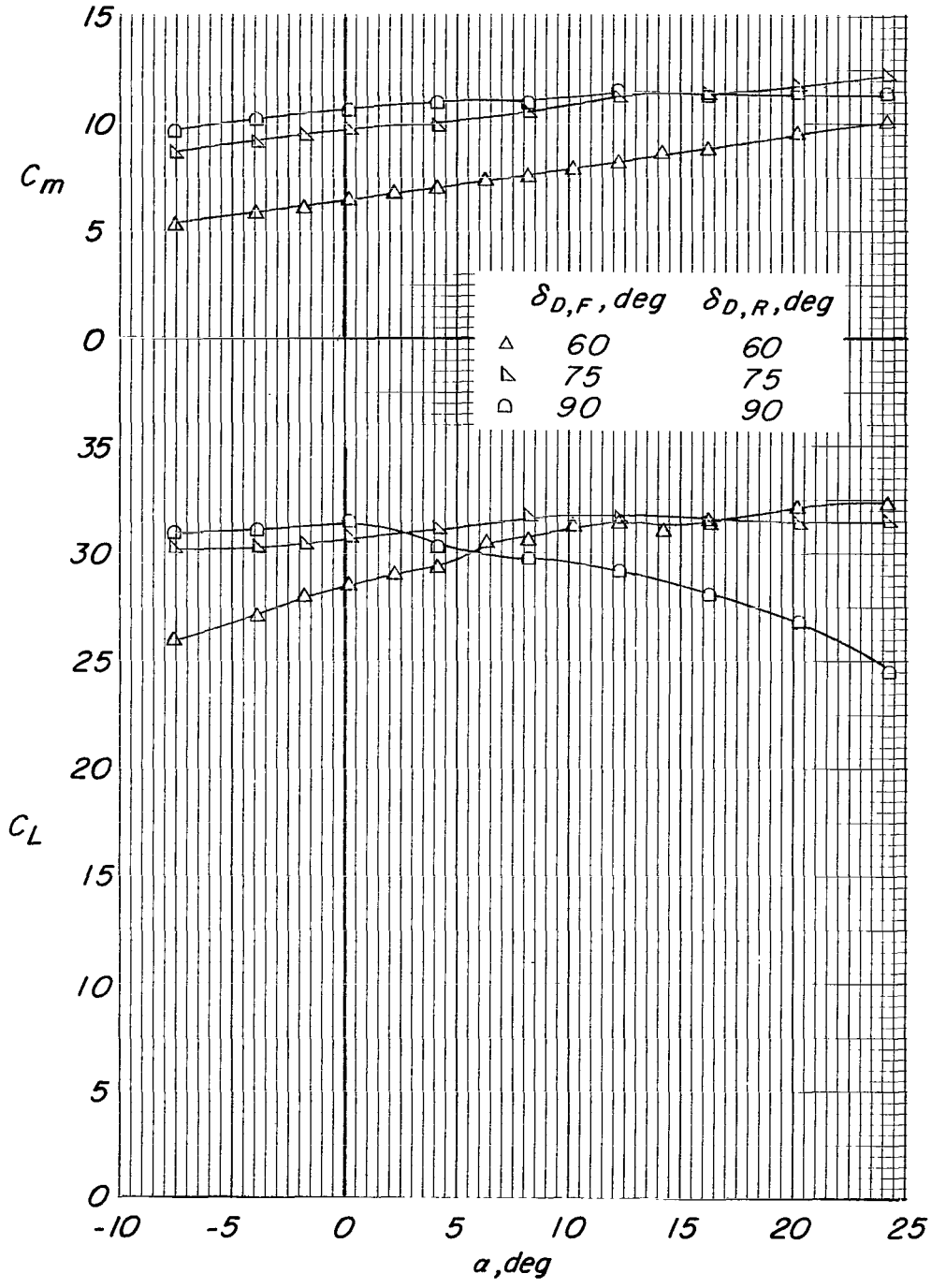


(e) $C_T = 25$.

Figure 19.- Continued.

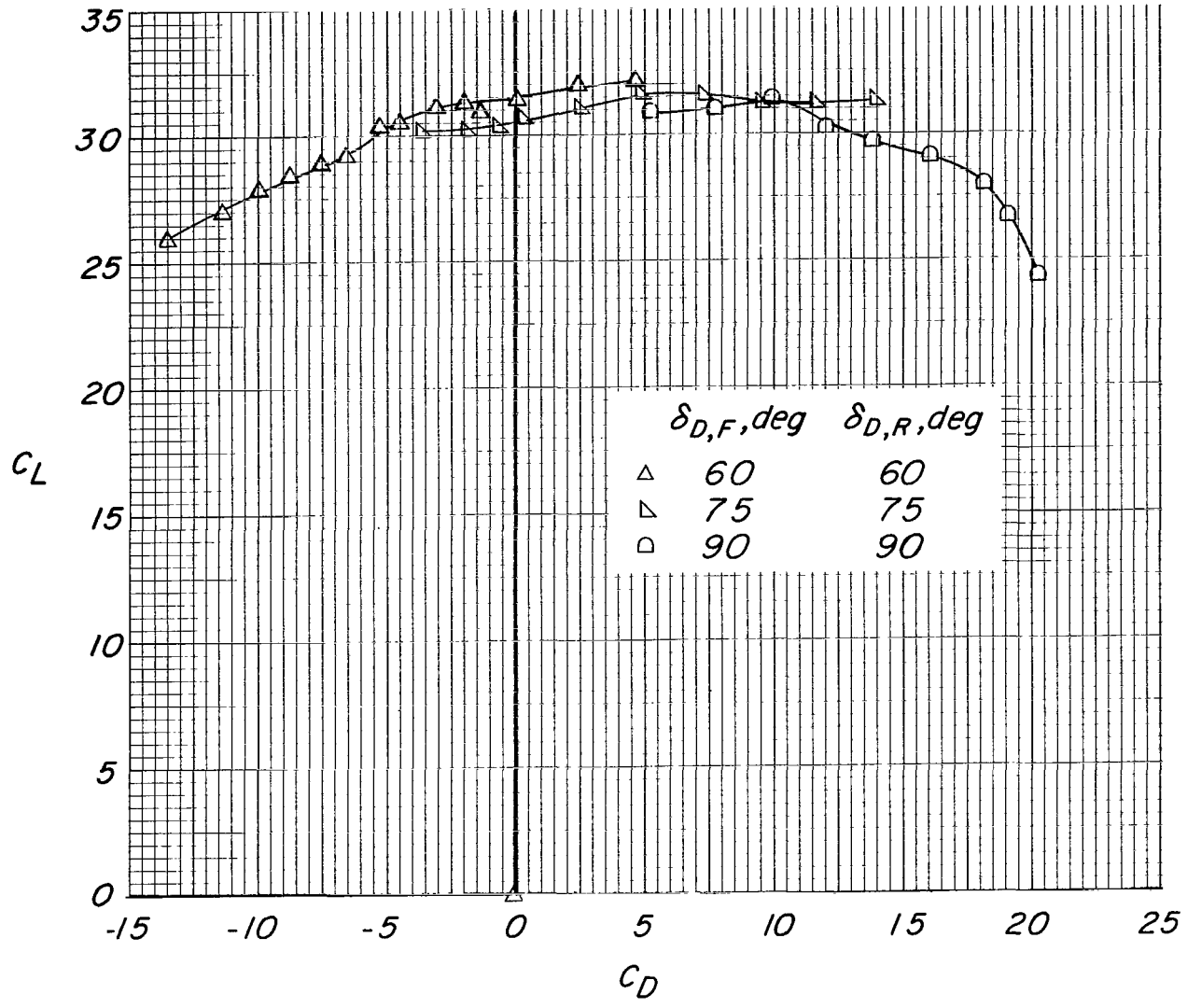


(e) Concluded.

Figure 19.- Continued.

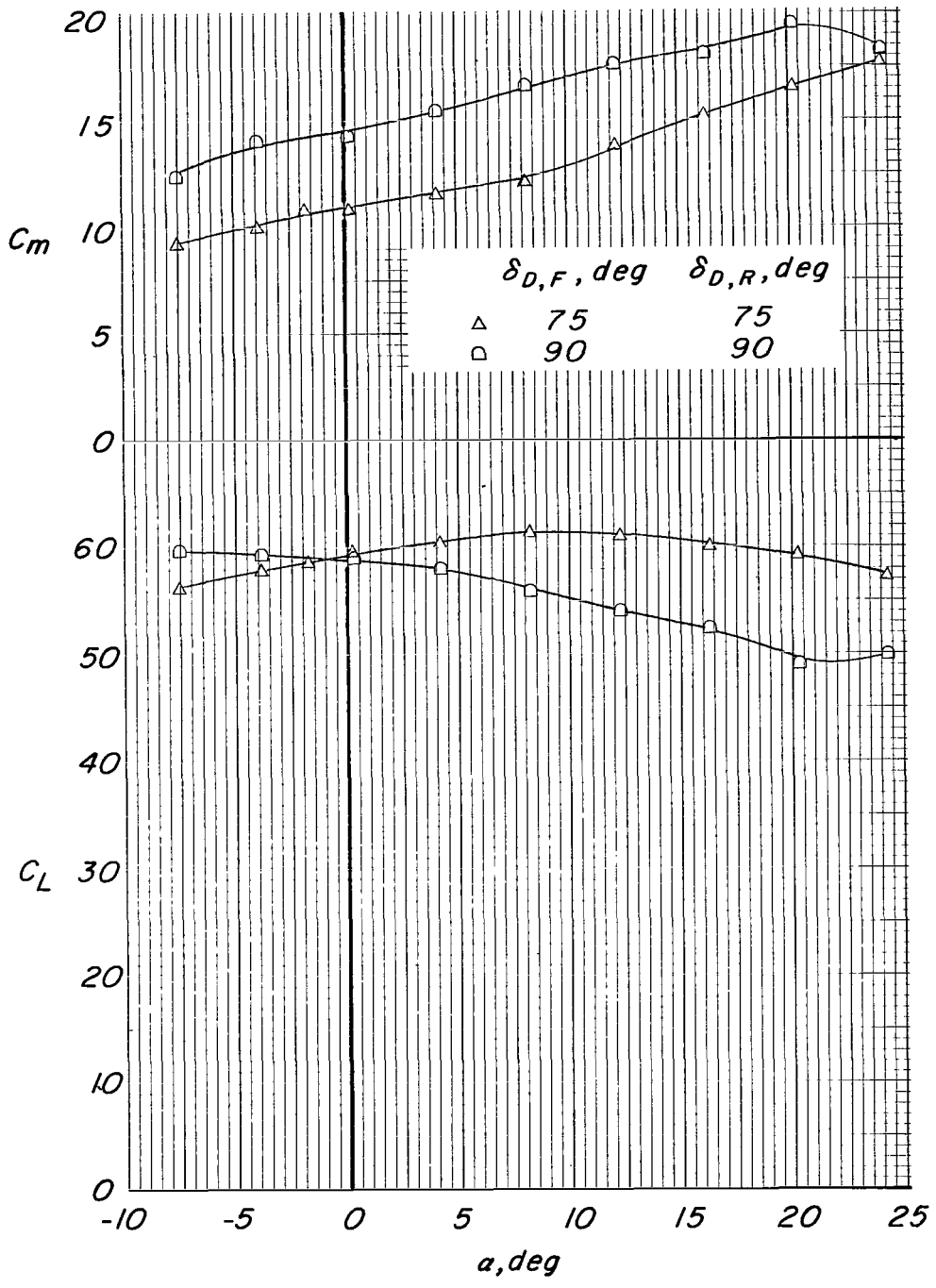


(f) $C_T = 60$.

Figure 19.- Continued.

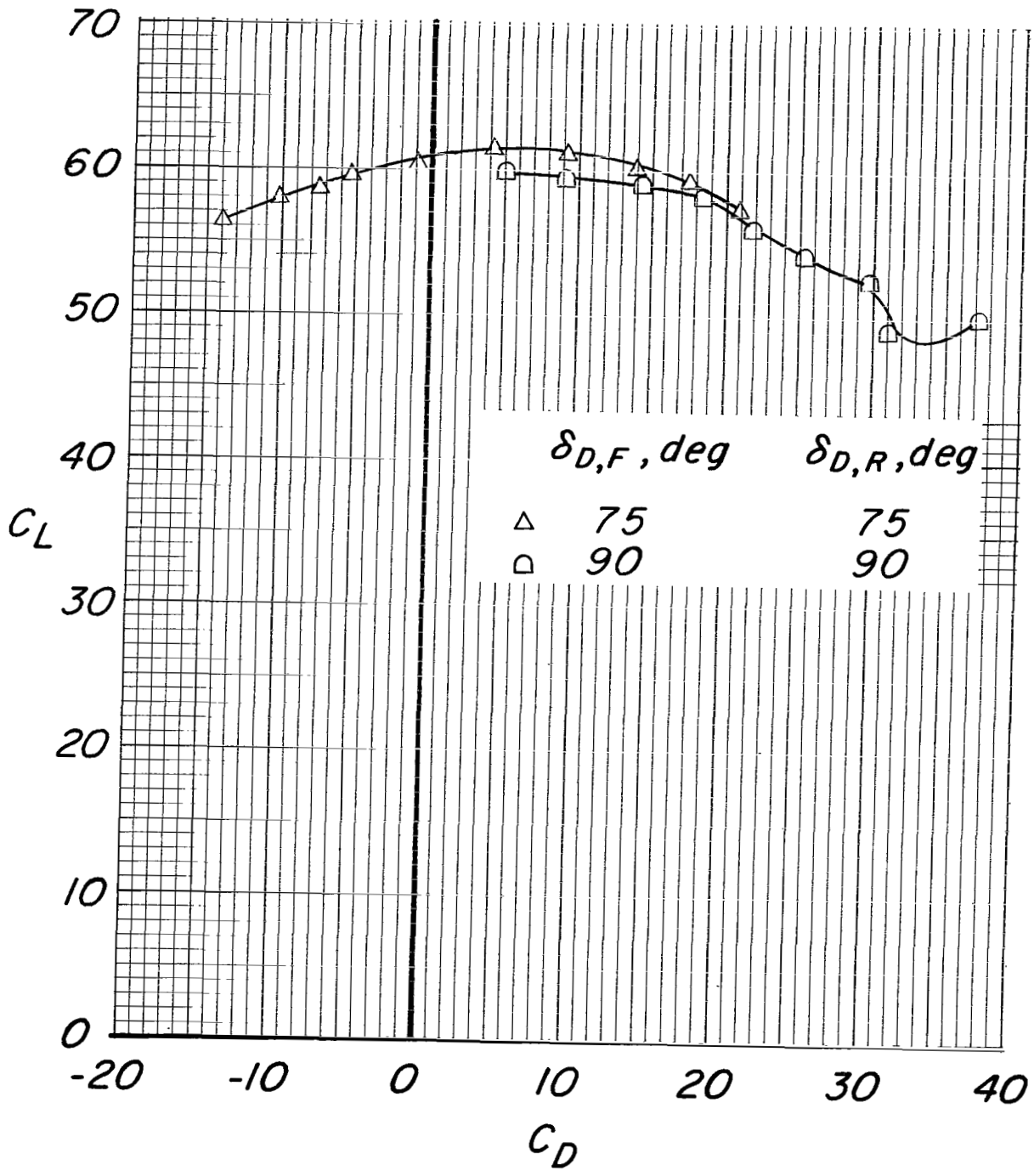


(f) Concluded.

Figure 19.- Concluded.


(a) $C_T = 0$; propellers windmilling.

Figure 20.- Effects of differential duct deflection angle on the aerodynamic characteristics of the model at two thrust coefficients. $\delta_{V,F} = 0^0$; $\delta_{V,R} = 0^0$; $H_{t,1}$ on; $i_t = 0^0$; $V_t$ on; modified duct lips; tail-fuselage fairing on.

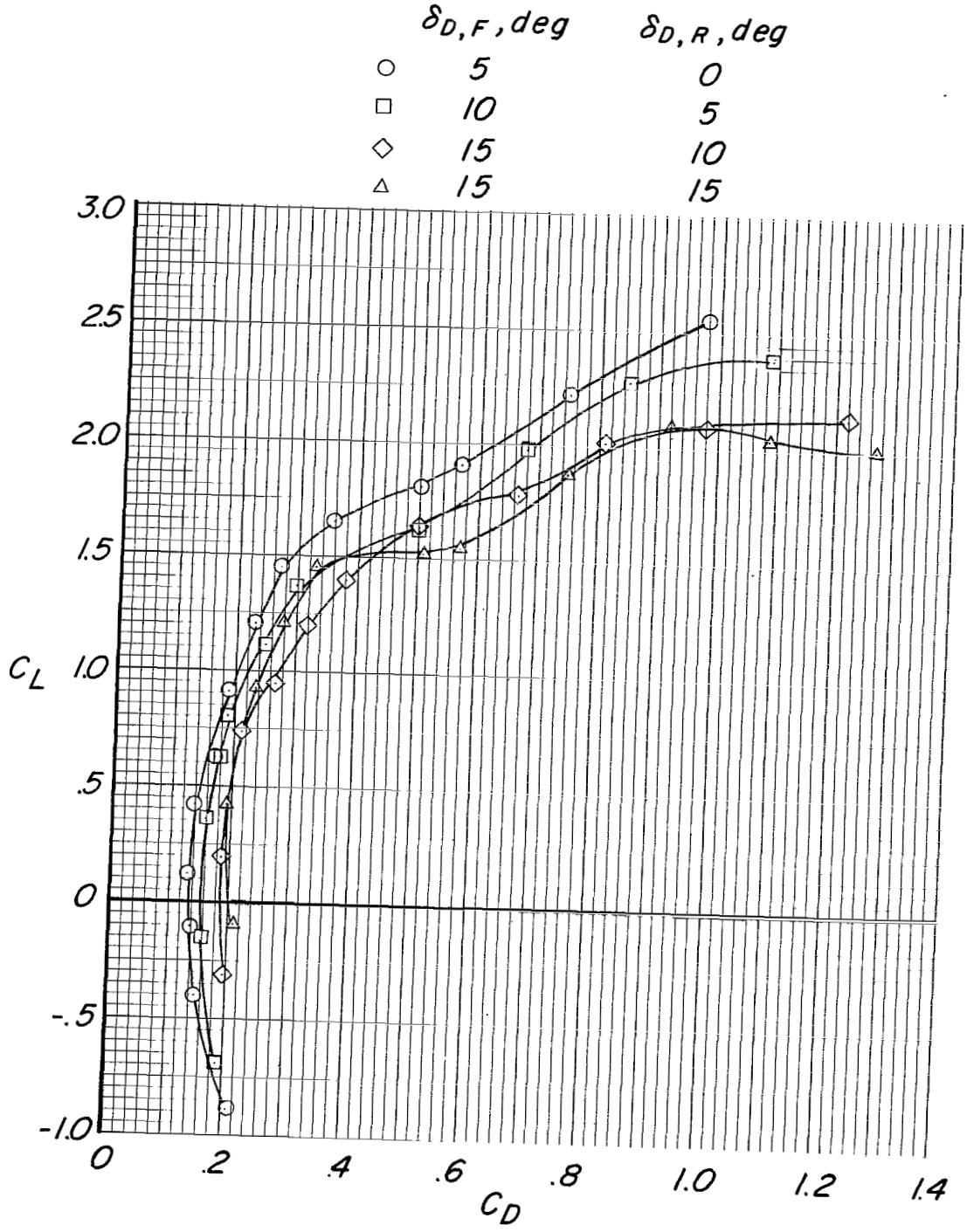


(a) Concluded.

Figure 20.- Continued.

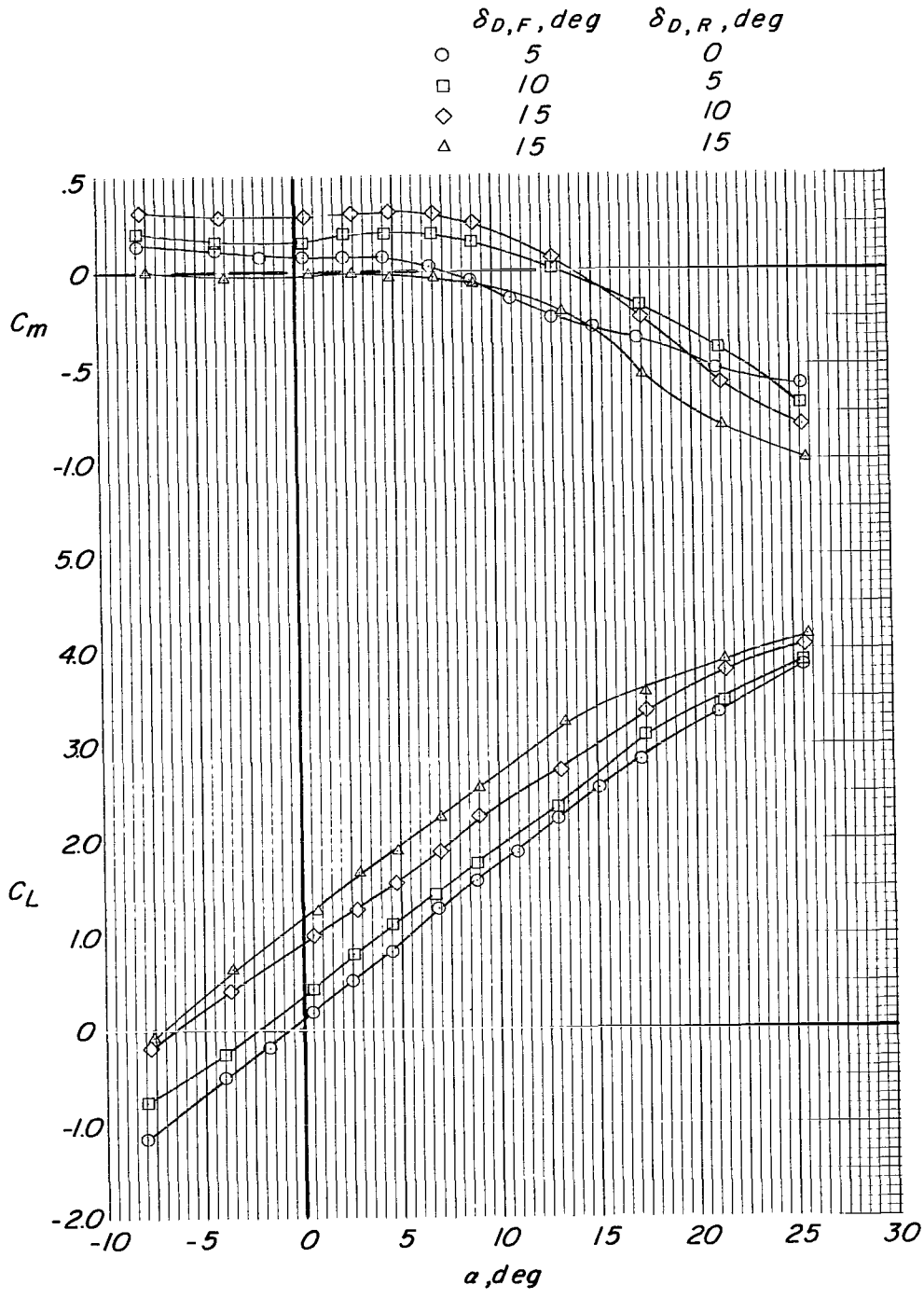


(b) $C_T = 0.8$.

Figure 20.- Continued.

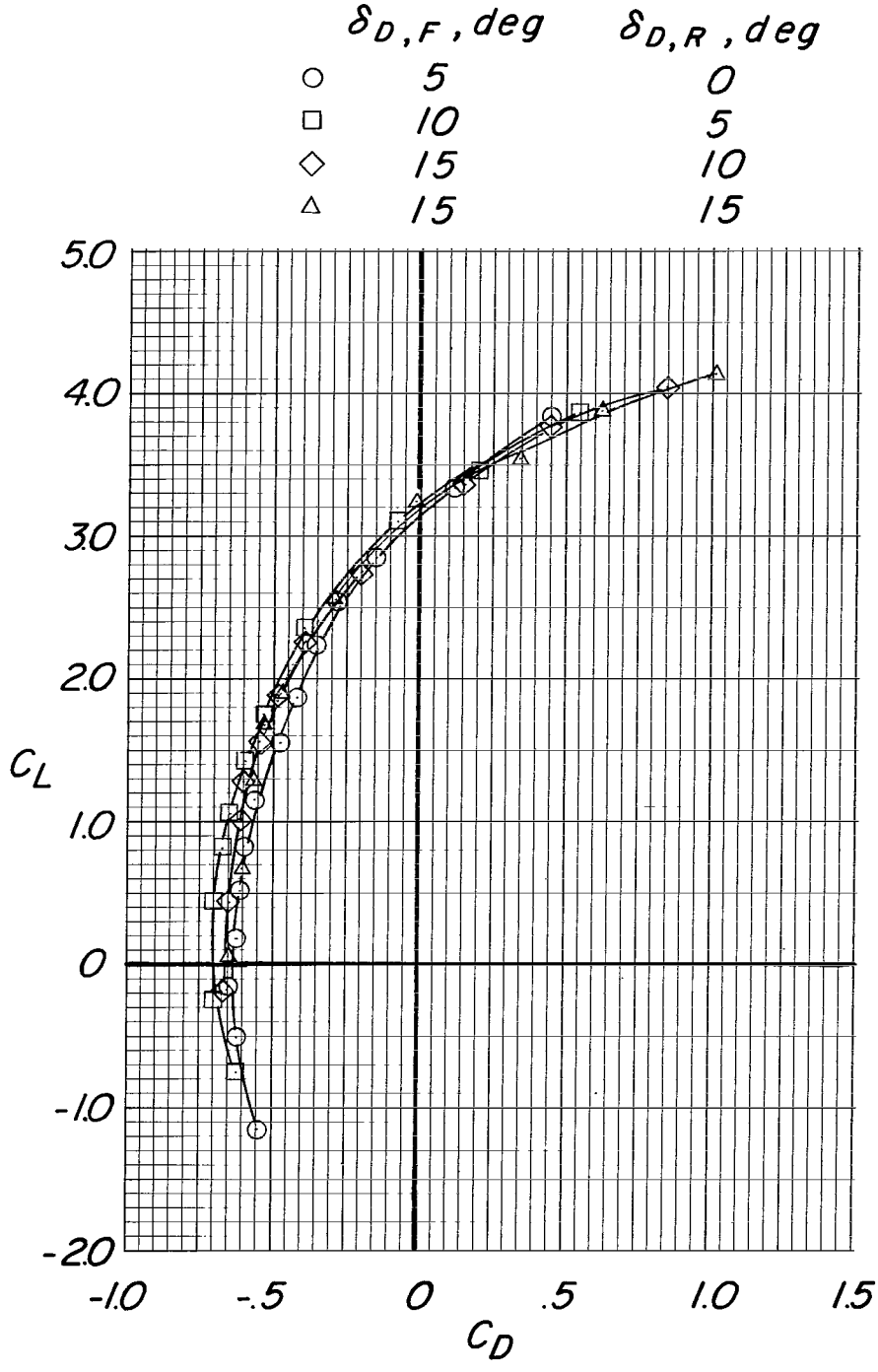


(b) Concluded.

Figure 20.- Concluded.

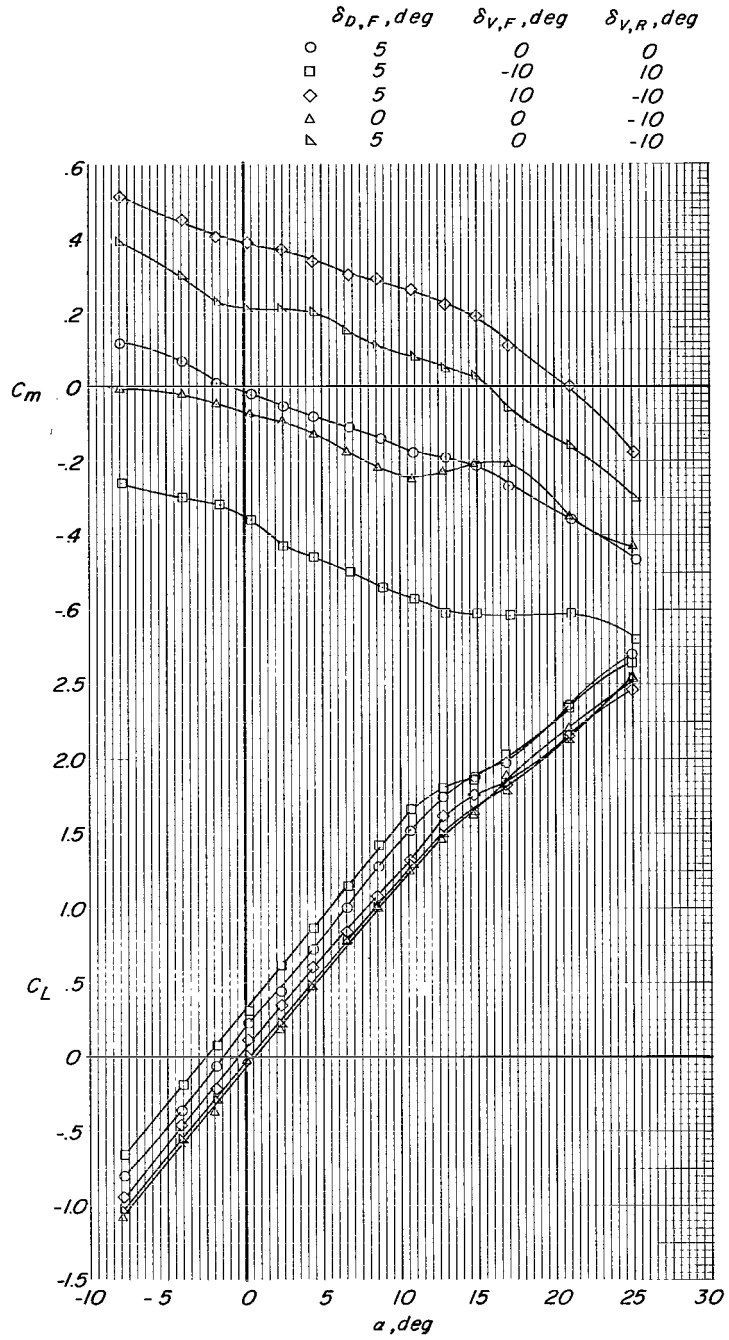


(a) $C_T = 0$; propellers windmilling.

Figure 21.- Effects of vane deflection and duct deflection on the aerodynamic characteristics of the model at various thrust coefficients. $\delta_{D,R} = 0^0$; $H_{t,1}$ on; $i_t = 0^0$; $V_t$ on; modified duct lips; tail-fuselage fairing on.

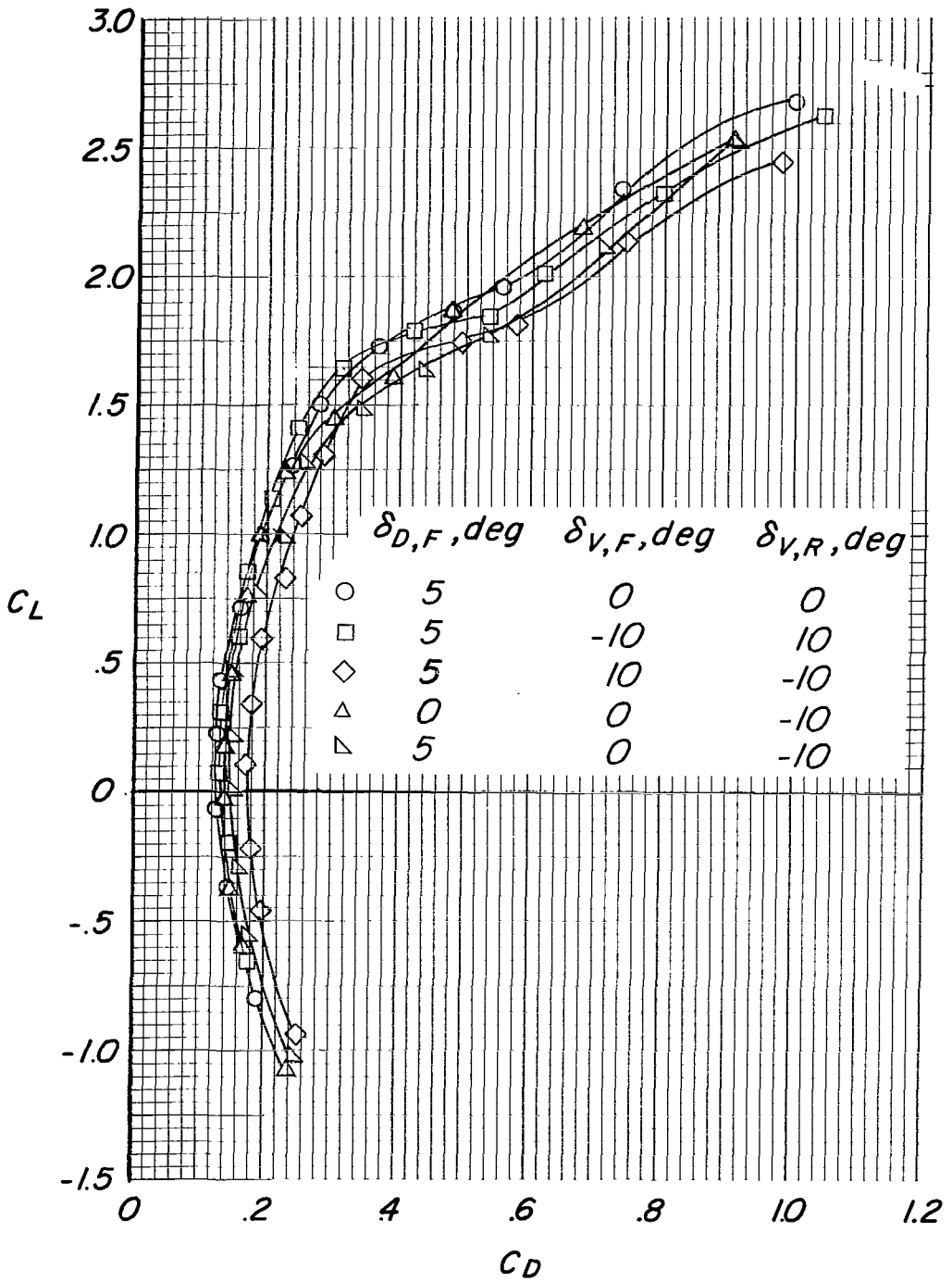


(a) Concluded.

Figure 21.- Continued.

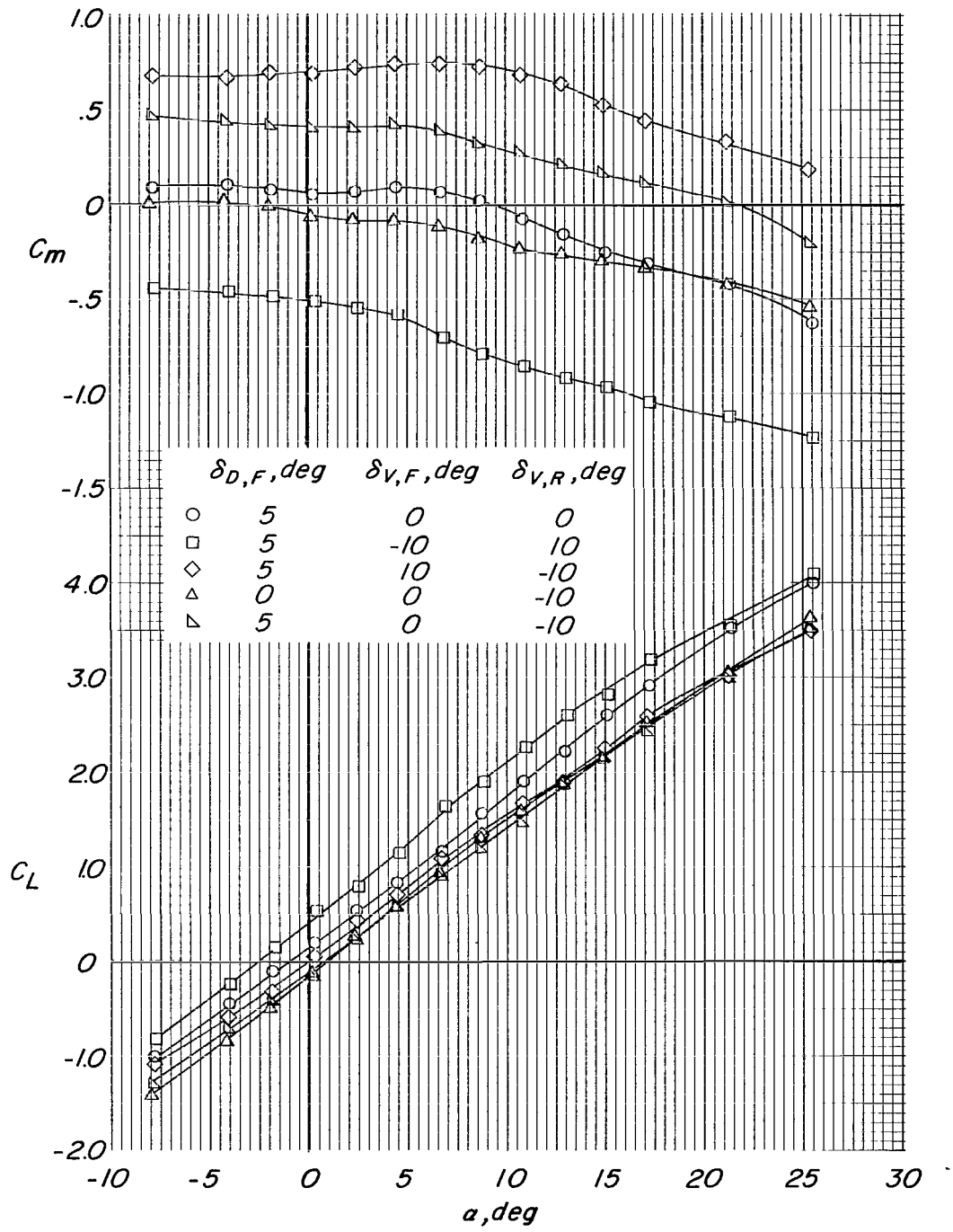


(b) $C_T = 0.8$.

Figure 21.- Continued.

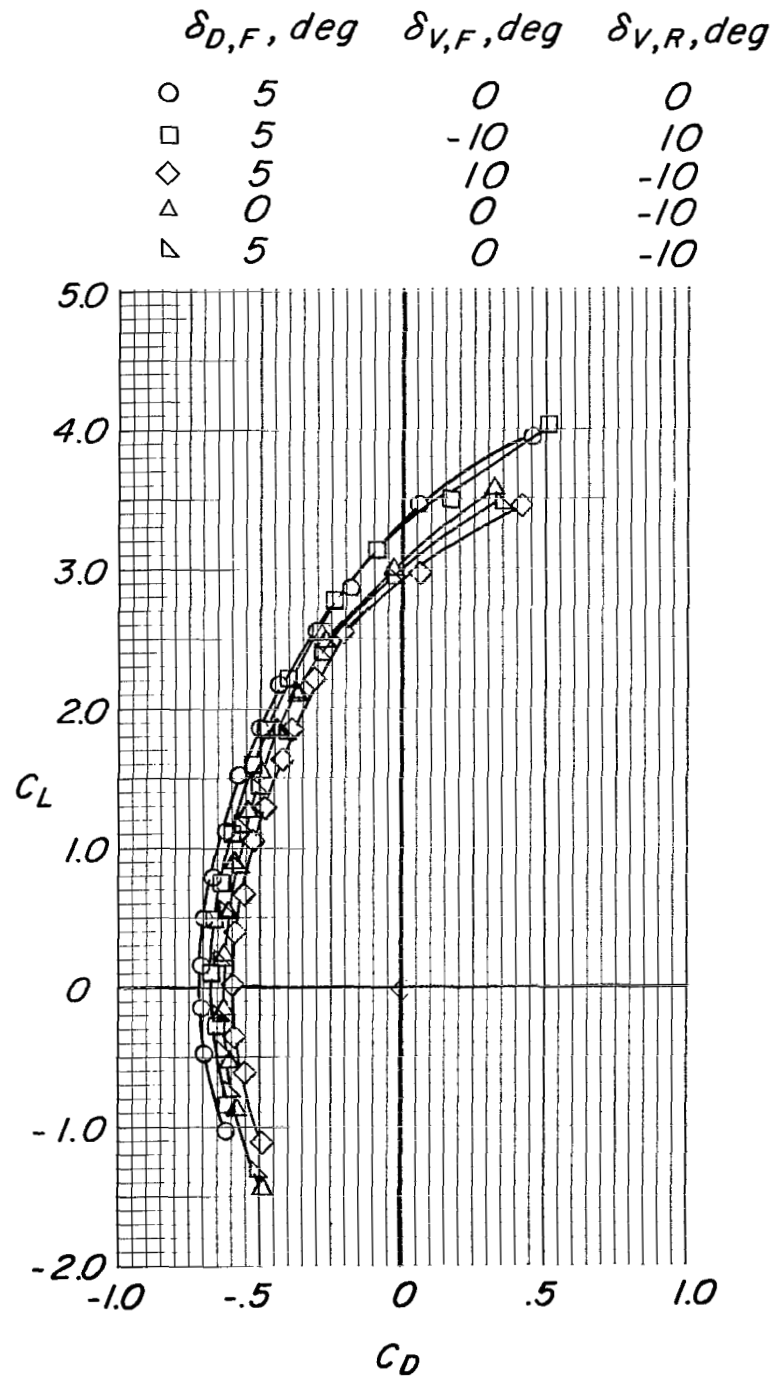


(b) Continued.

Figure 21.- Continued.

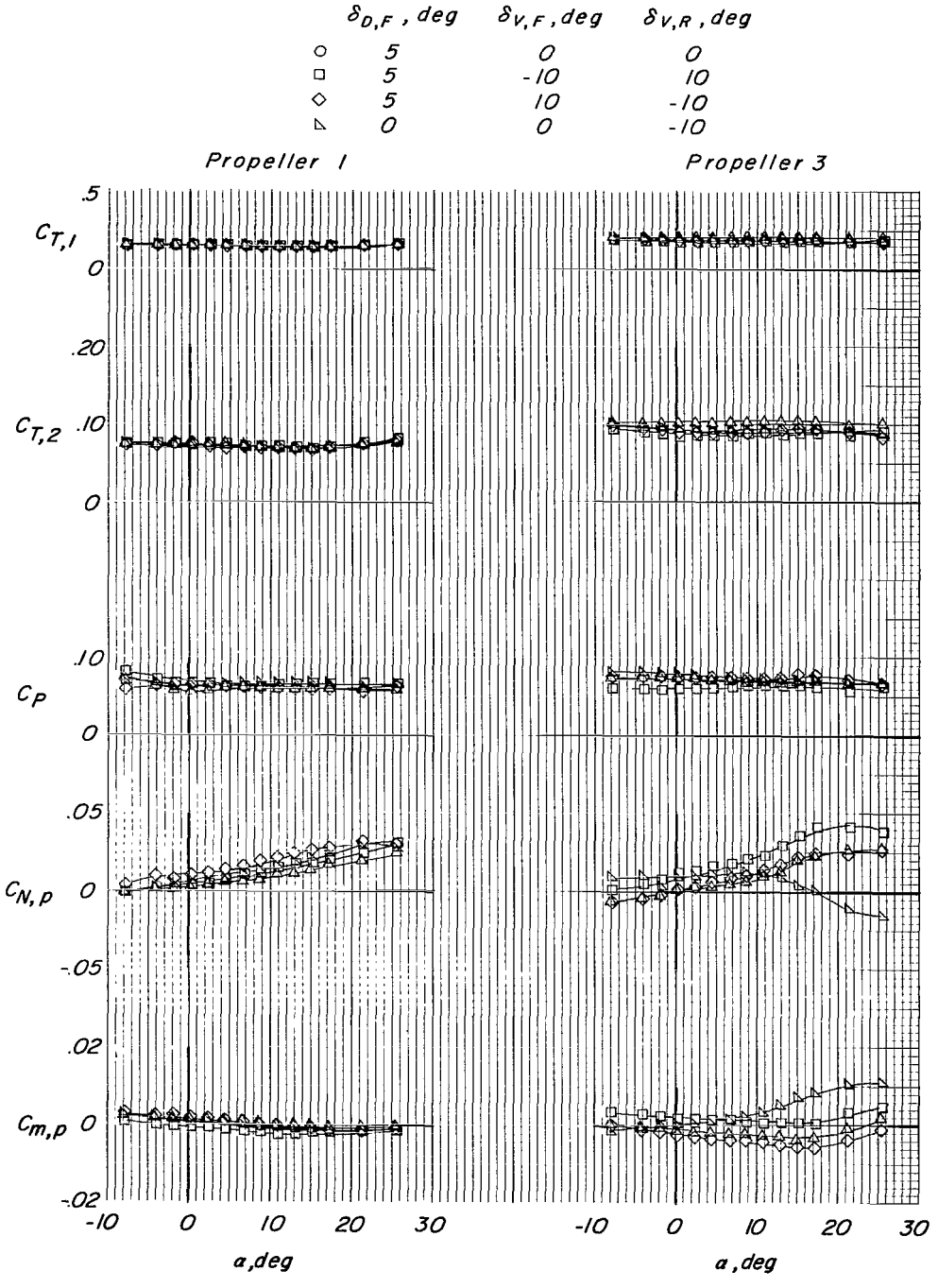


(b) Concluded.

Figure 21.- Continued.

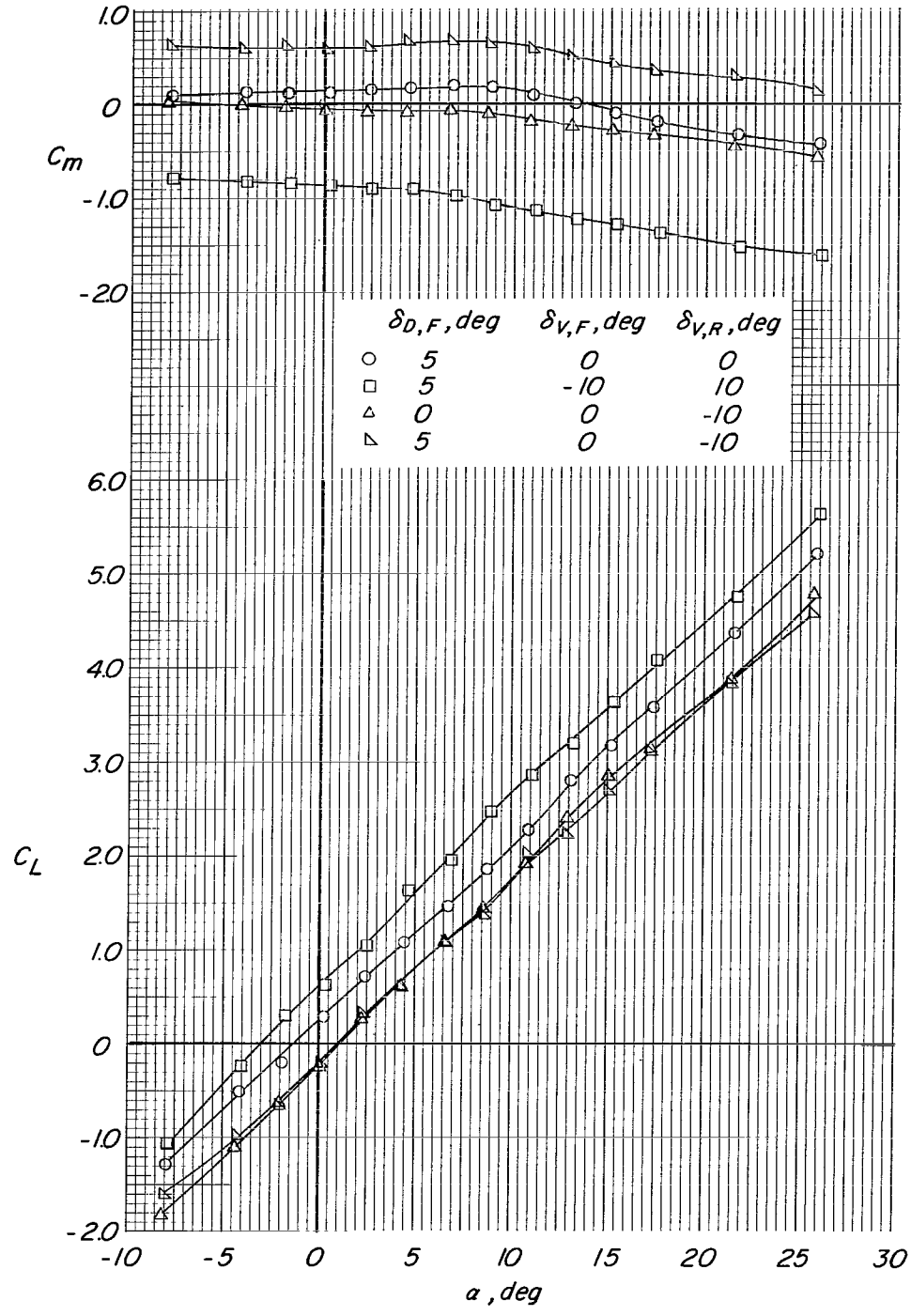


(c) $C_T = 2.1$.

Figure 21.- Continued.

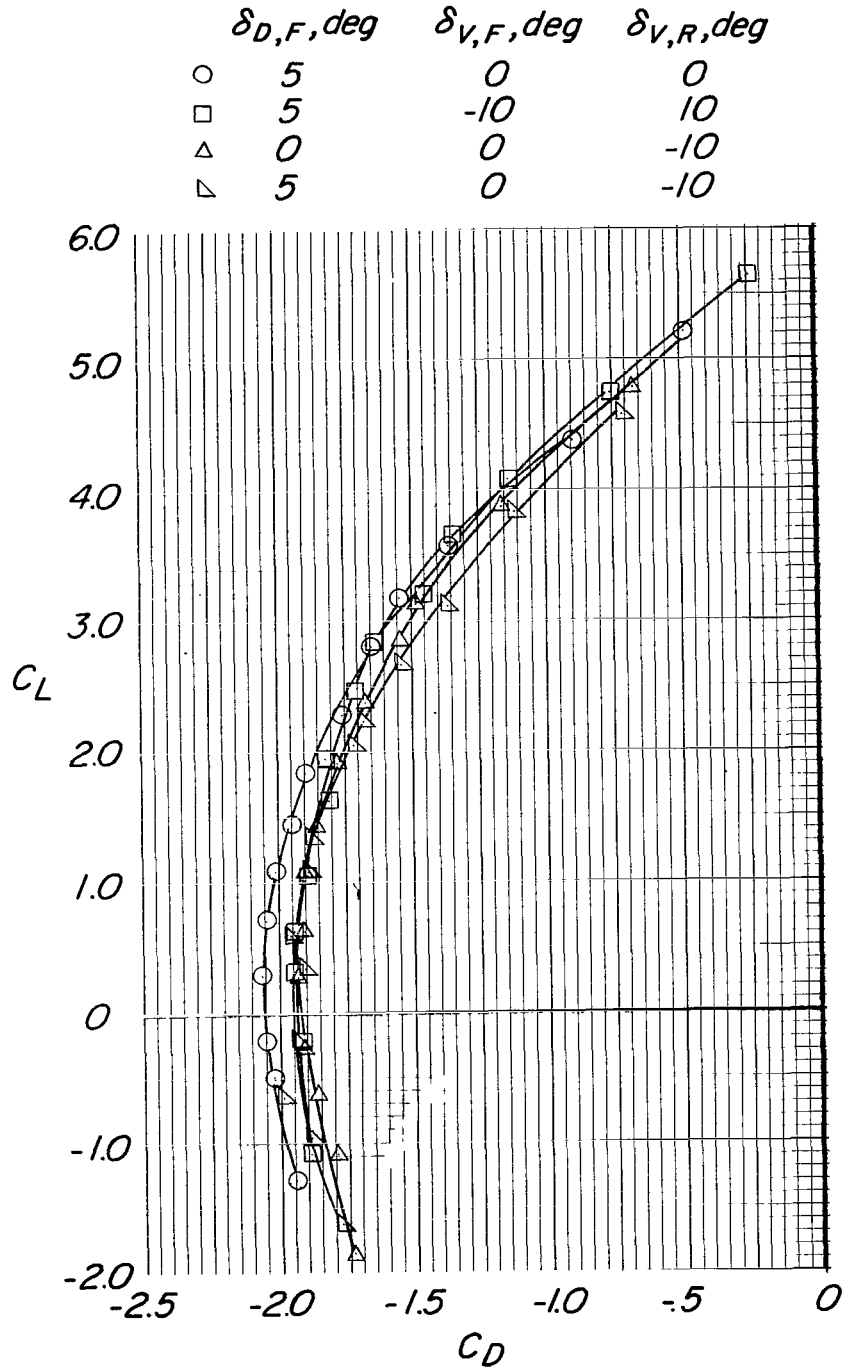


(c) Continued.

Figure 21.- Continued.

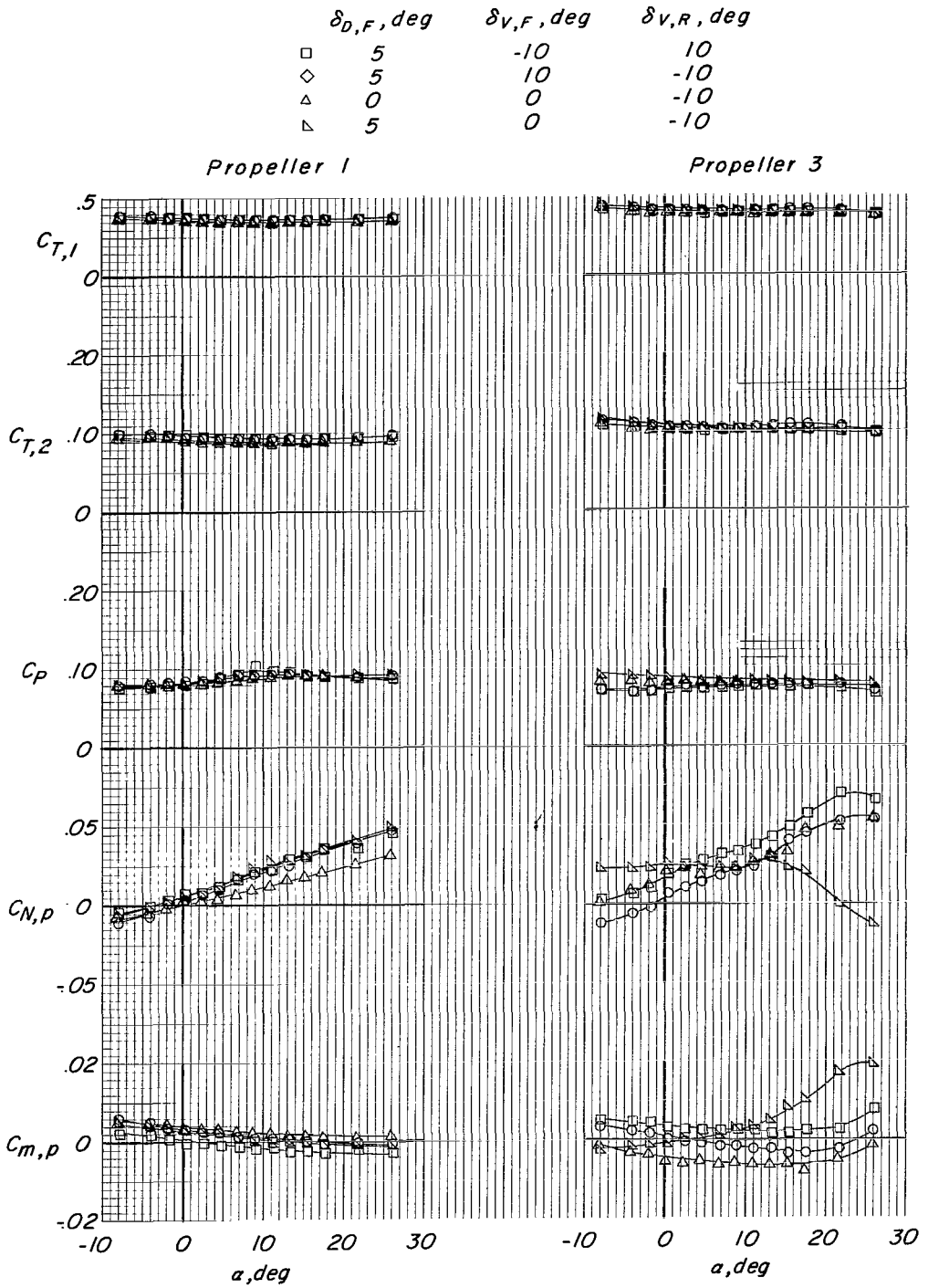


(c) Concluded.

Figure 21.- Concluded.

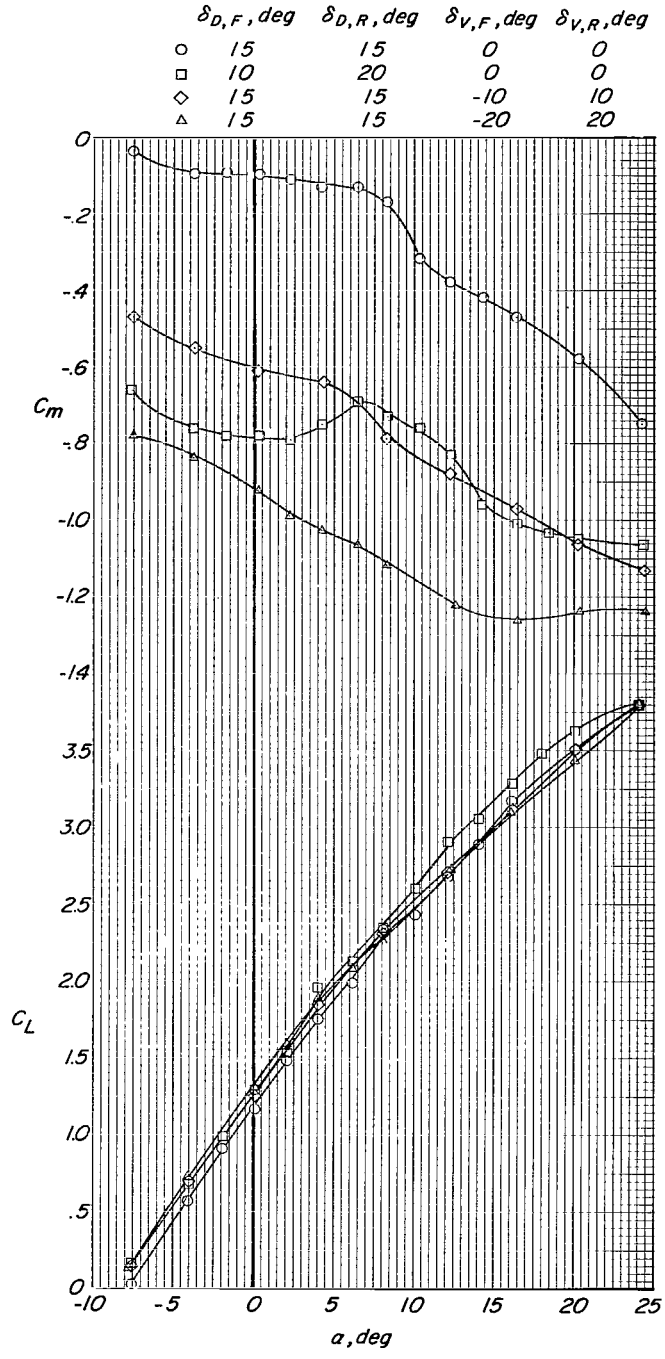


(a) $C_T = 0.4$.

Figure 22.- Effects of vane deflection and differential duct deflection angle on the aerodynamic characteristics of the model. $H_{t,1}$ on; $i_t = 0^0$; $V_t$ on; modified duct lips; tail-fuselage fairing on.

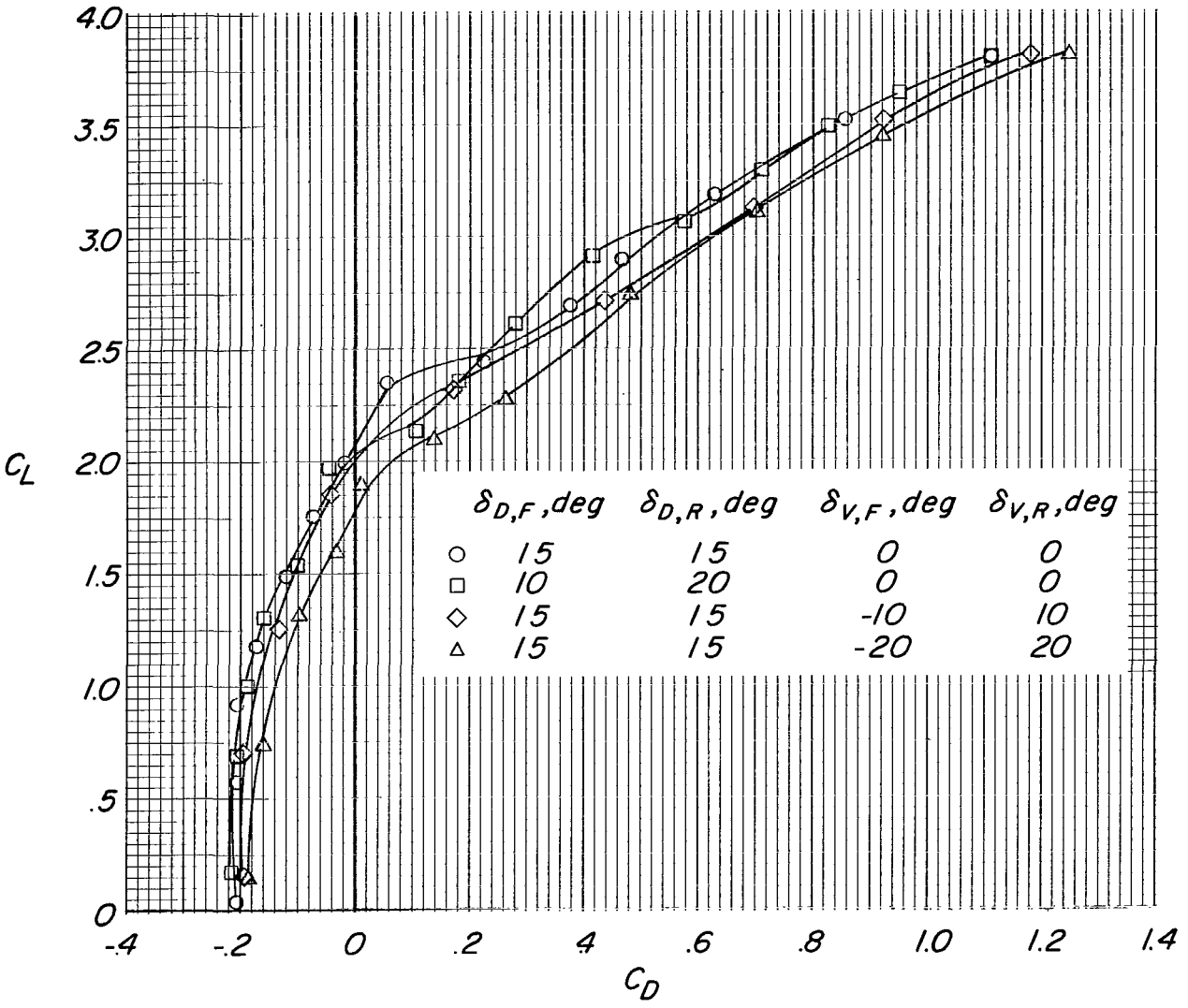


(a) Continued.

Figure 22.- Continued.

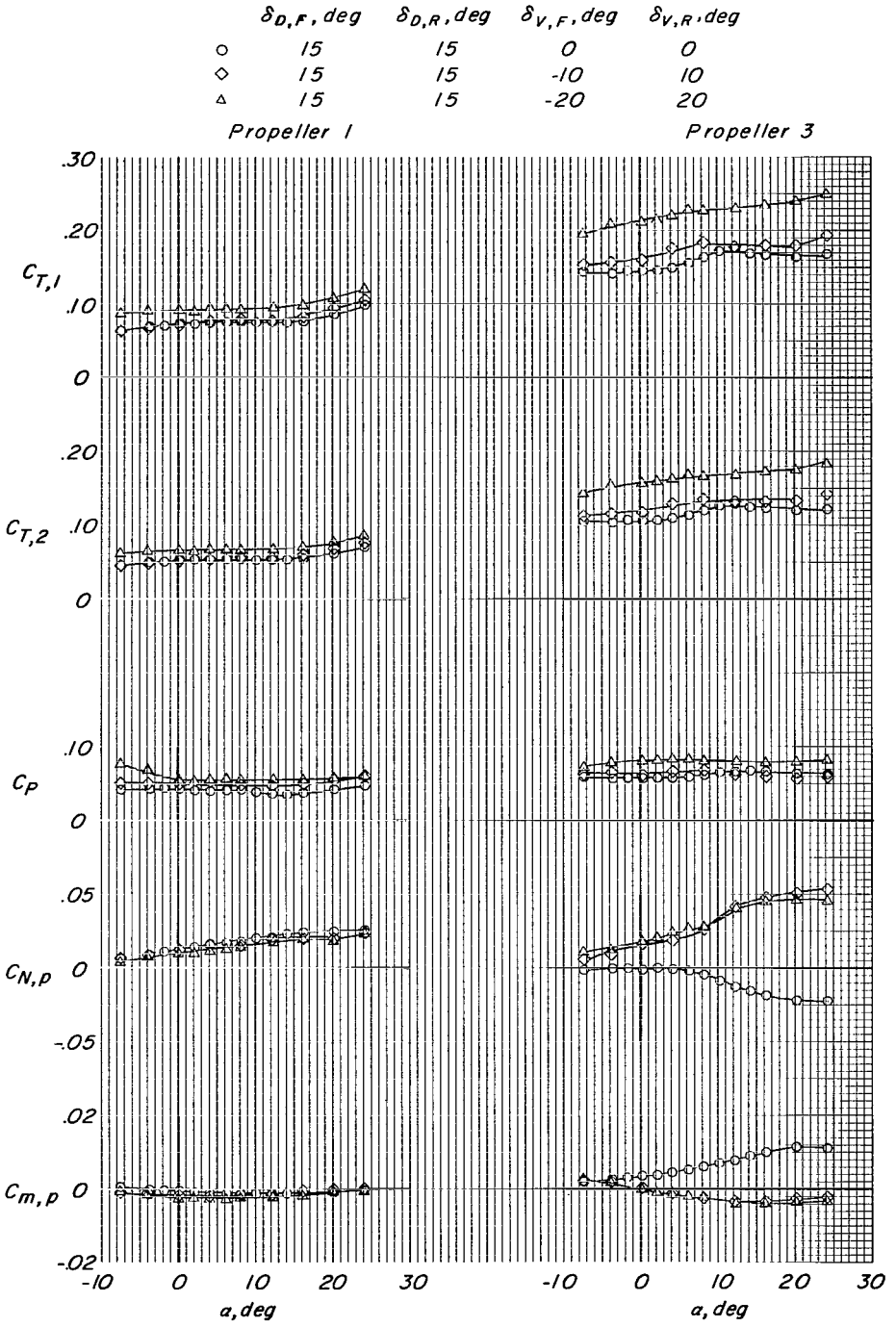


(a) Concluded.

Figure 22.- Continued.

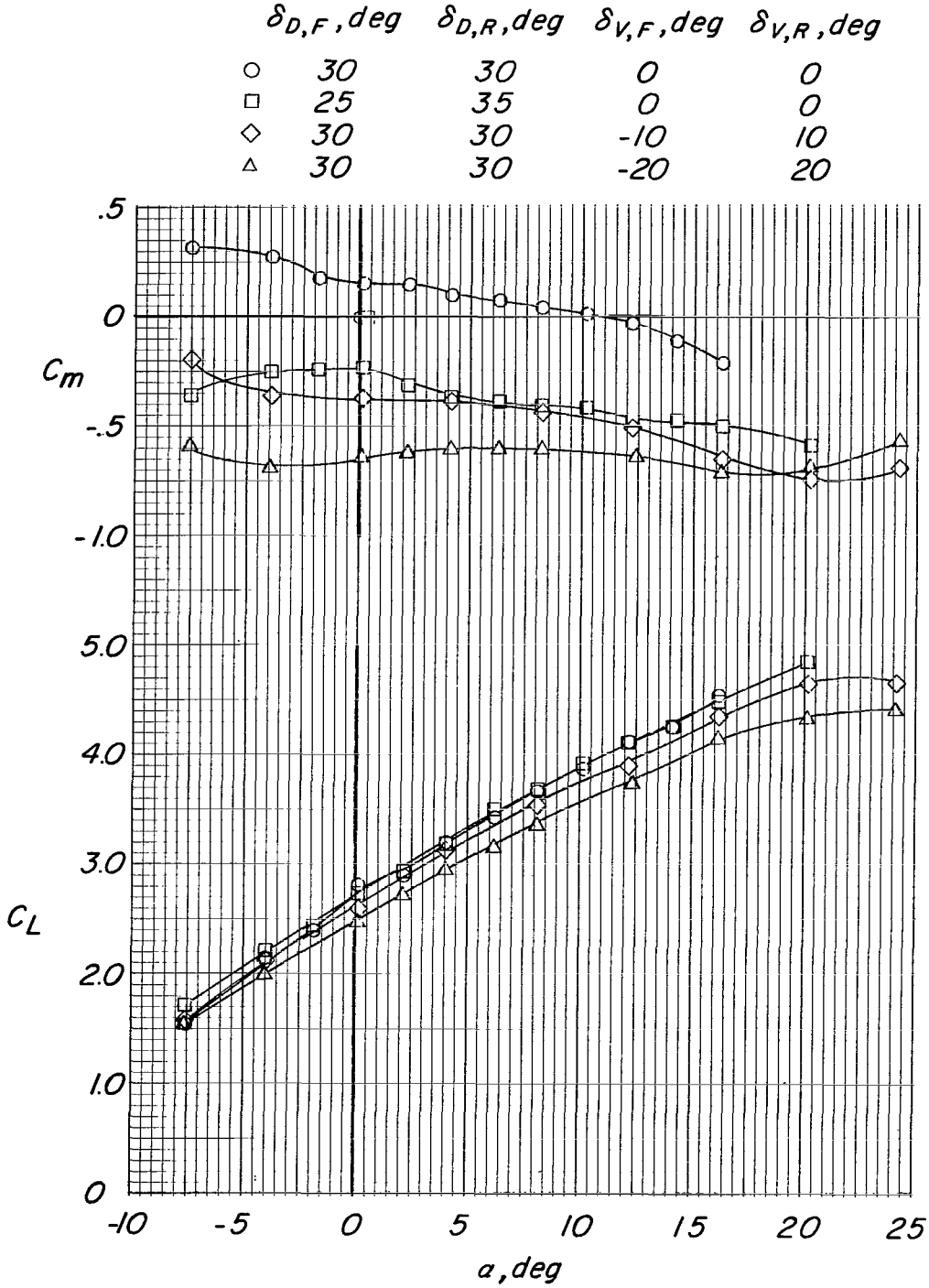


(b) $C_T = 0.8$.

Figure 22.- Continued.

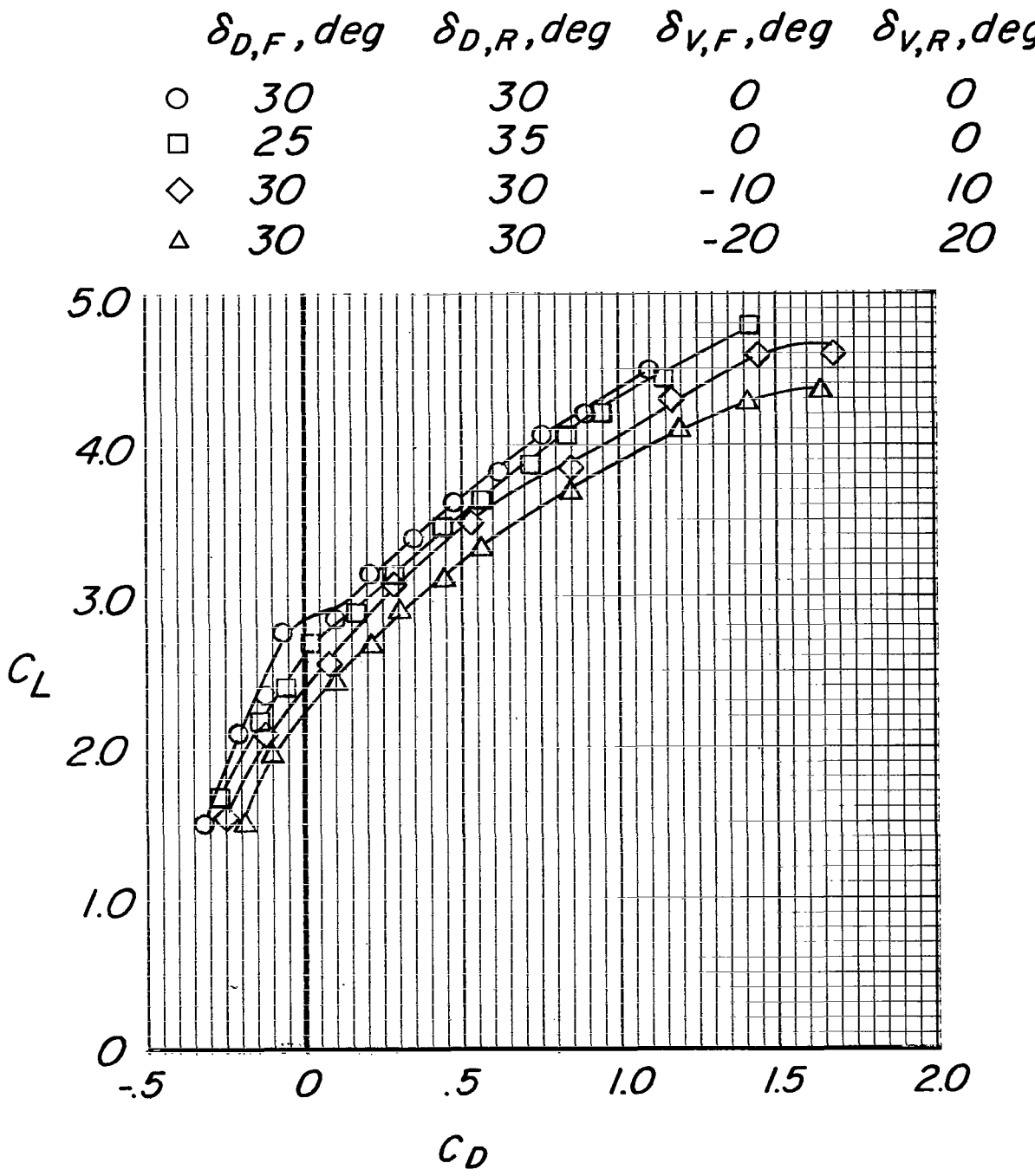


(b) Concluded.

Figure 22.- Continued.

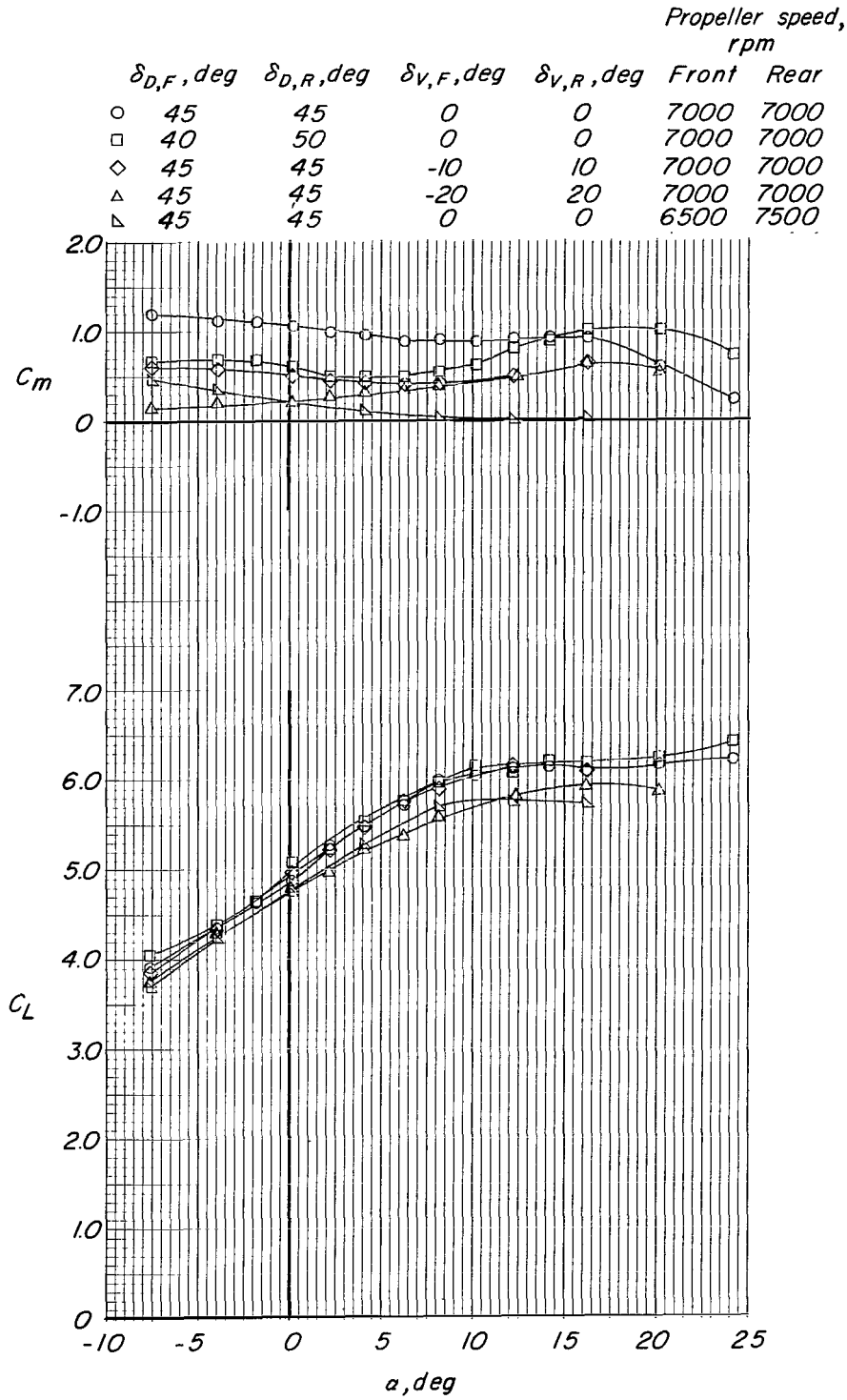


(c) $C_T = 2.1$.

Figure 22.- Continued.

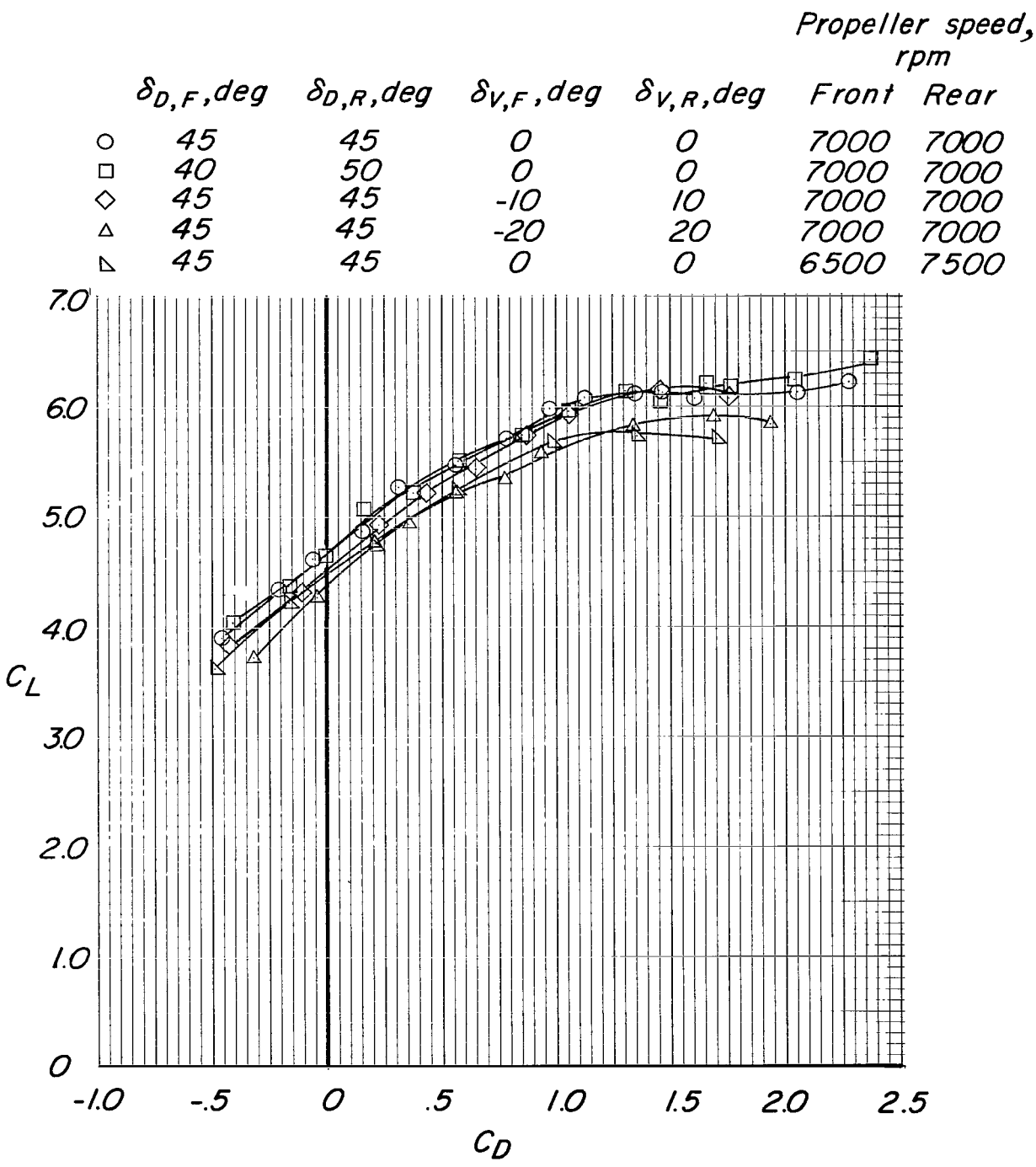


(c) Concluded.

Figure 22.- Continued.

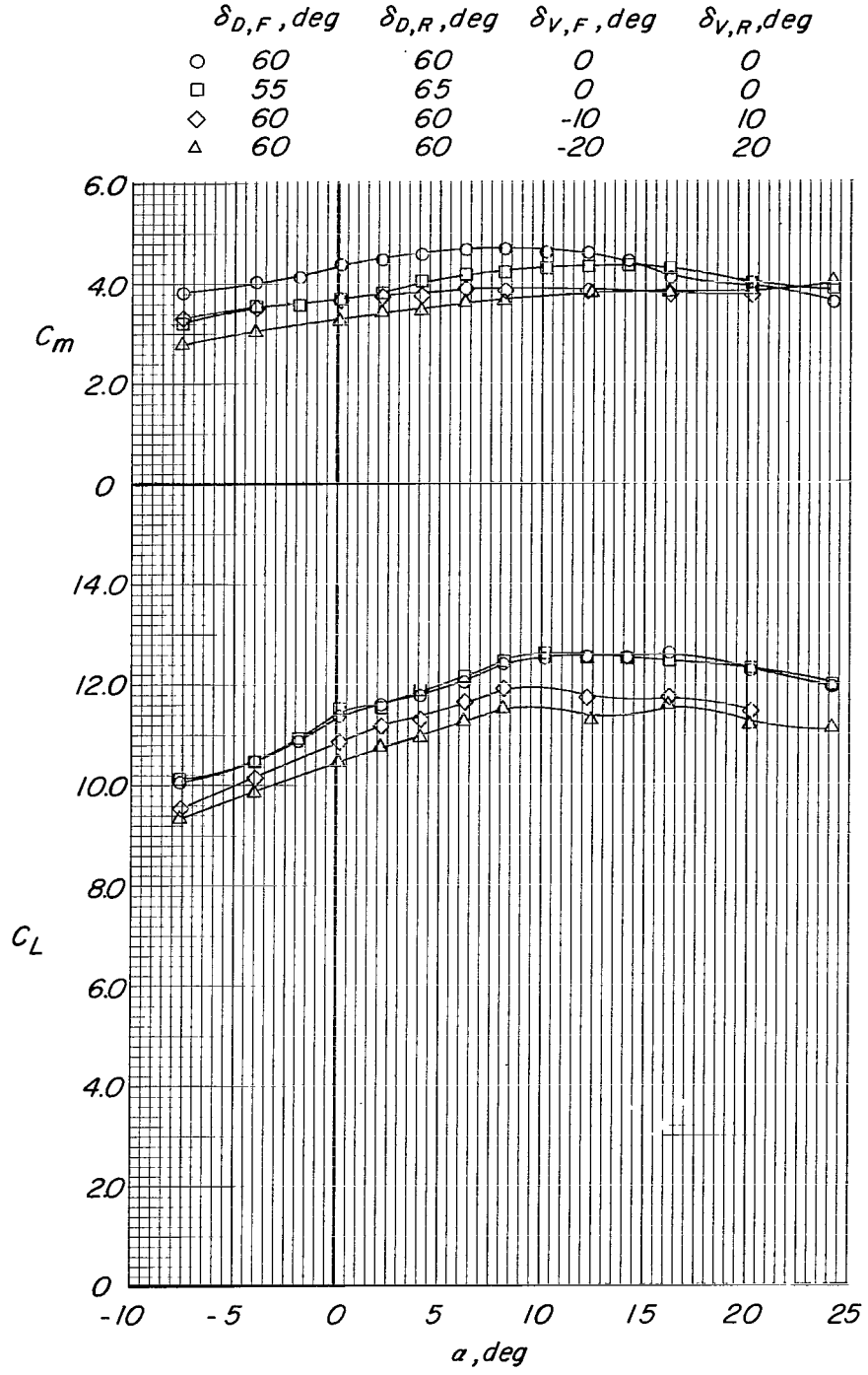


(d) $C_T = 7.0$.

Figure 22.- Continued.

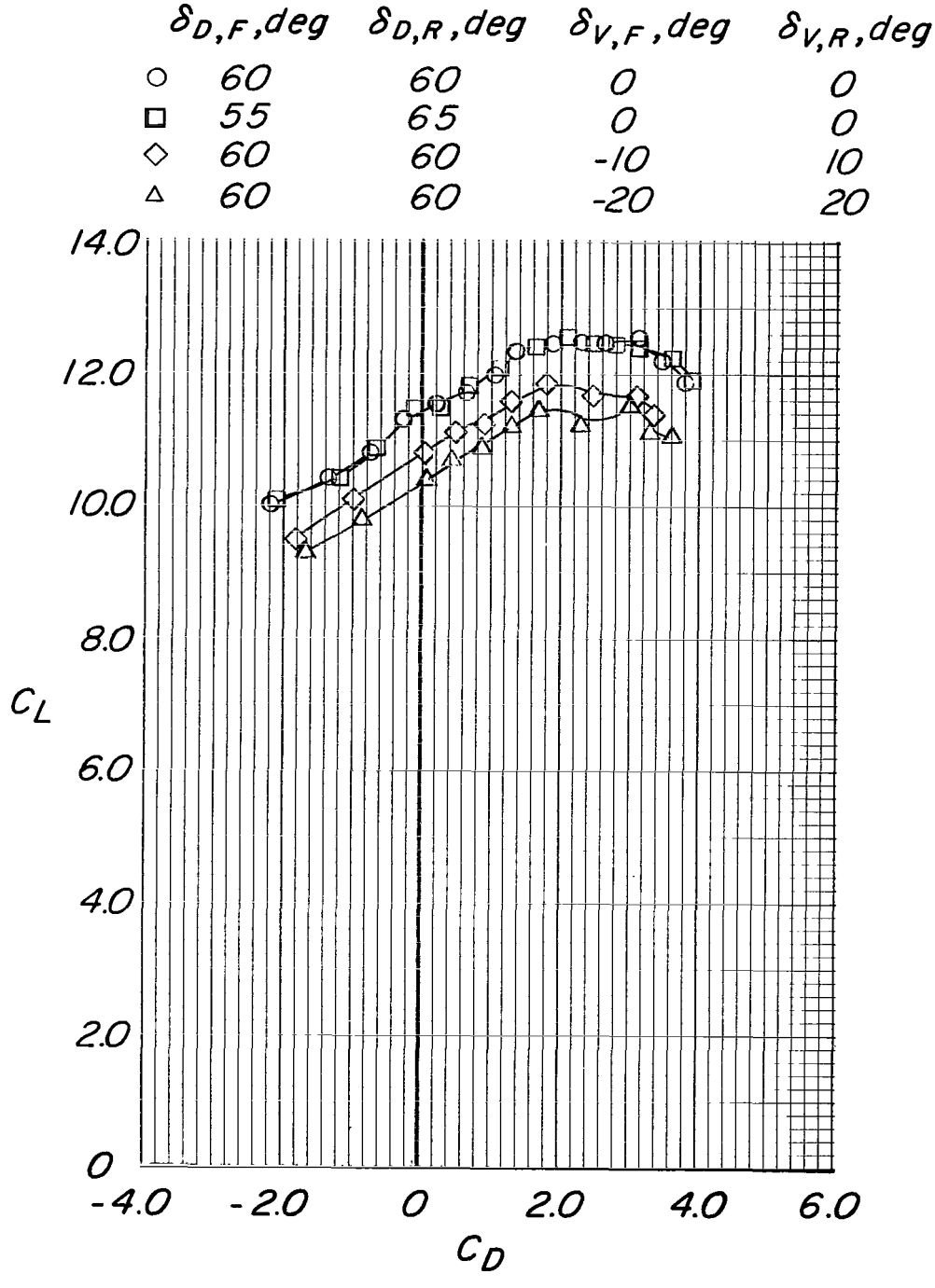


(d) Concluded.

Figure 22.- Concluded.

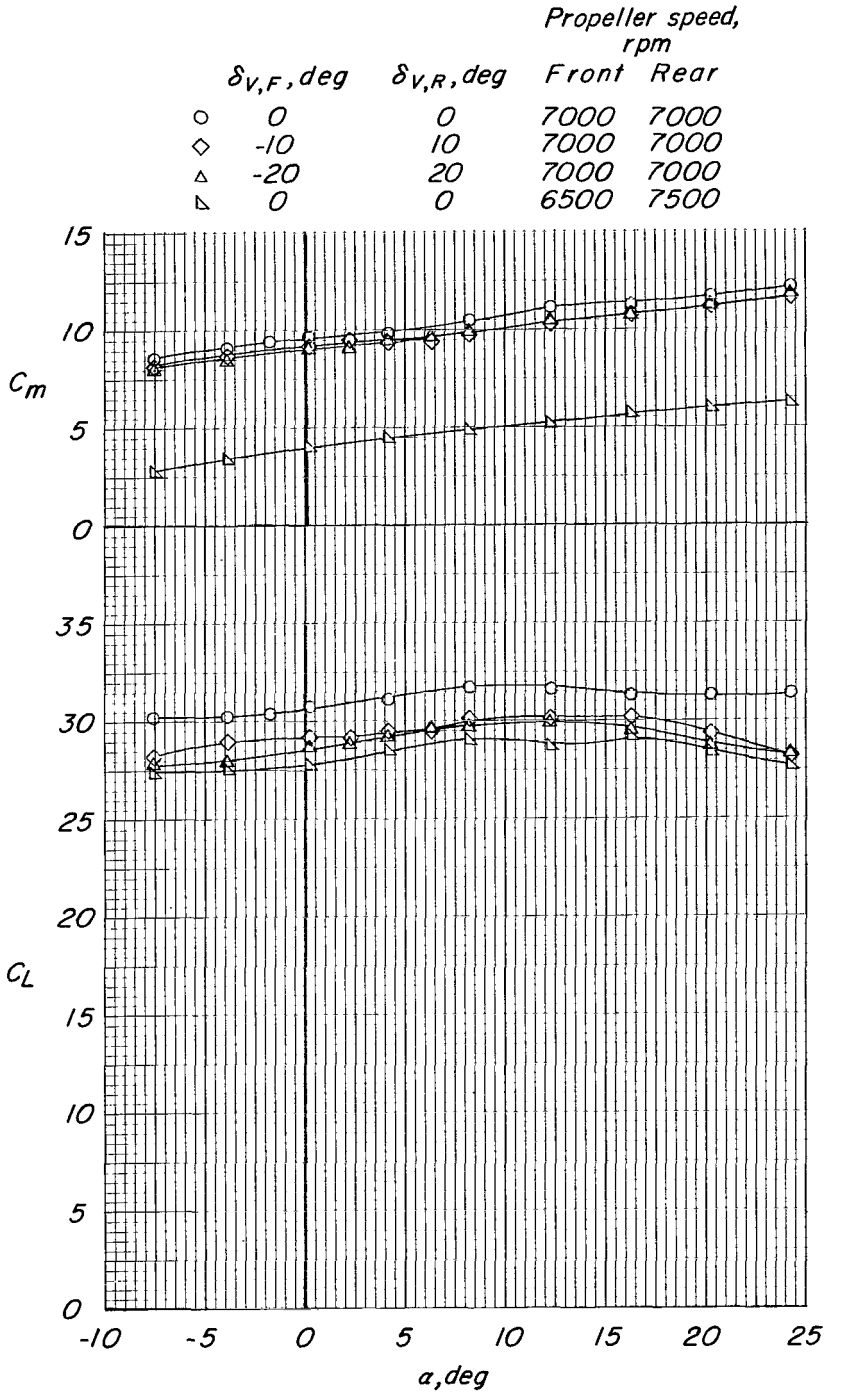


Figure 23.- Effects of vane deflection and differential thrust on the aerodynamic characteristics of the model. $C_T = 25$; $\delta_{D,F} = 75^o$; $\delta_{D,R} = 75^o$; $H_{t,1}$ on; $i_t = 0^o$; $V_t$ on; modified duct lips; tail-fuselage fairing on.

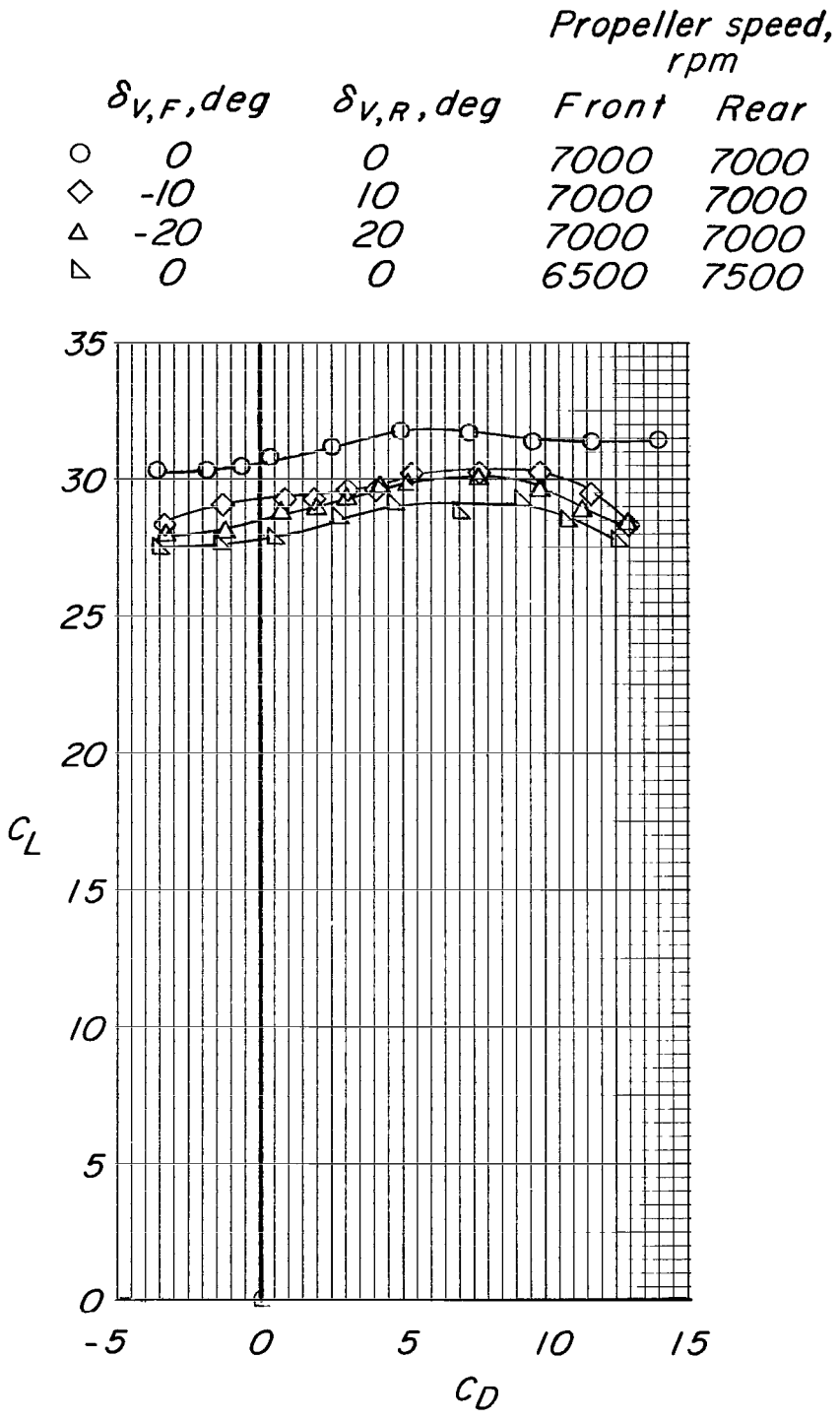


Figure 23.- Concluded.

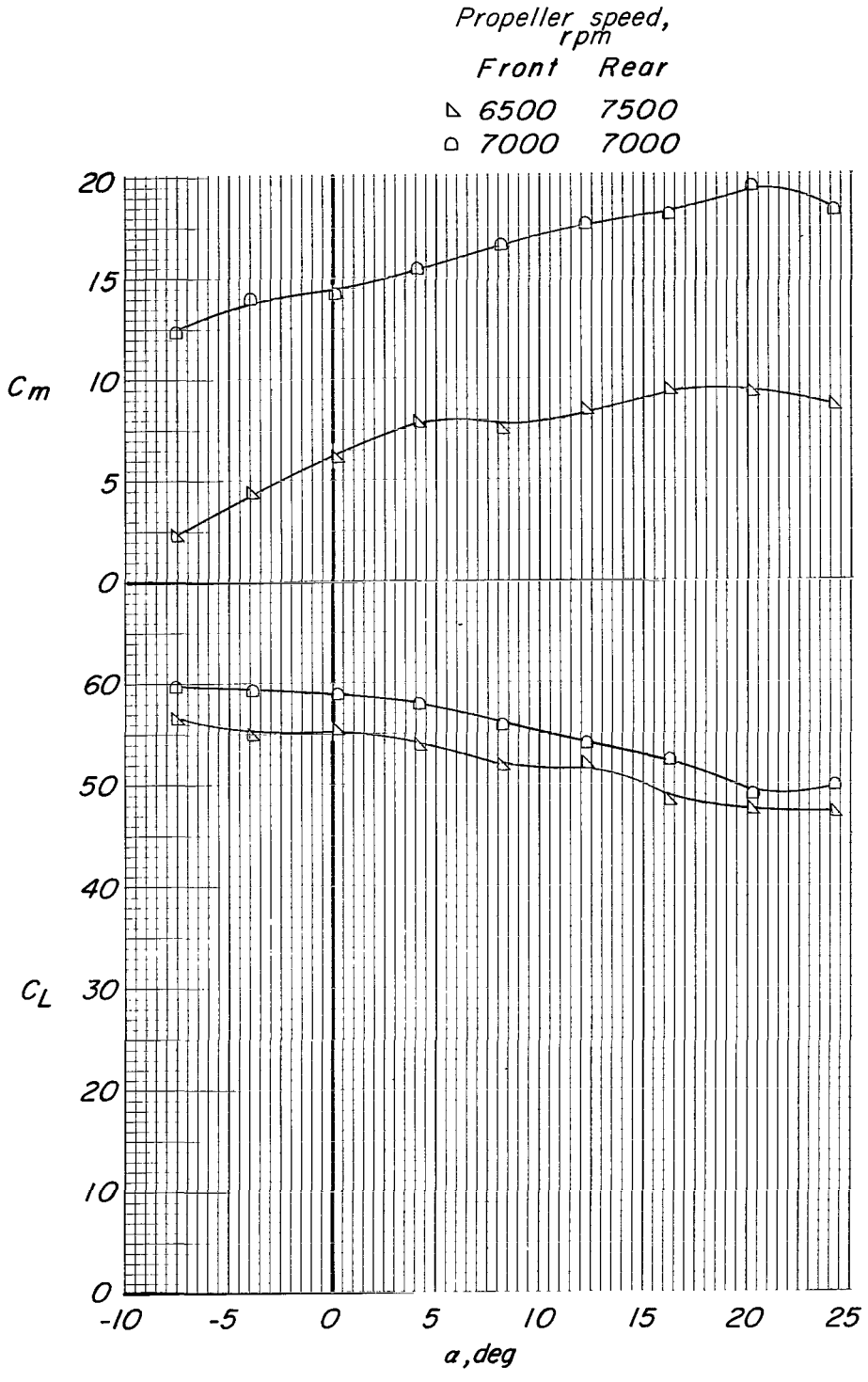


Figure 24.- Effects of differential thrust on the aerodynamic characteristics of the model. $C_T = 60$; $\delta_{D,F} = 90^0$; $\delta_{D,R} = 90^0$; $H_{t,1}$ on; $i_t = 0^0$; $V_t$ on; modified duct lips; tail-fuselage fairing on.

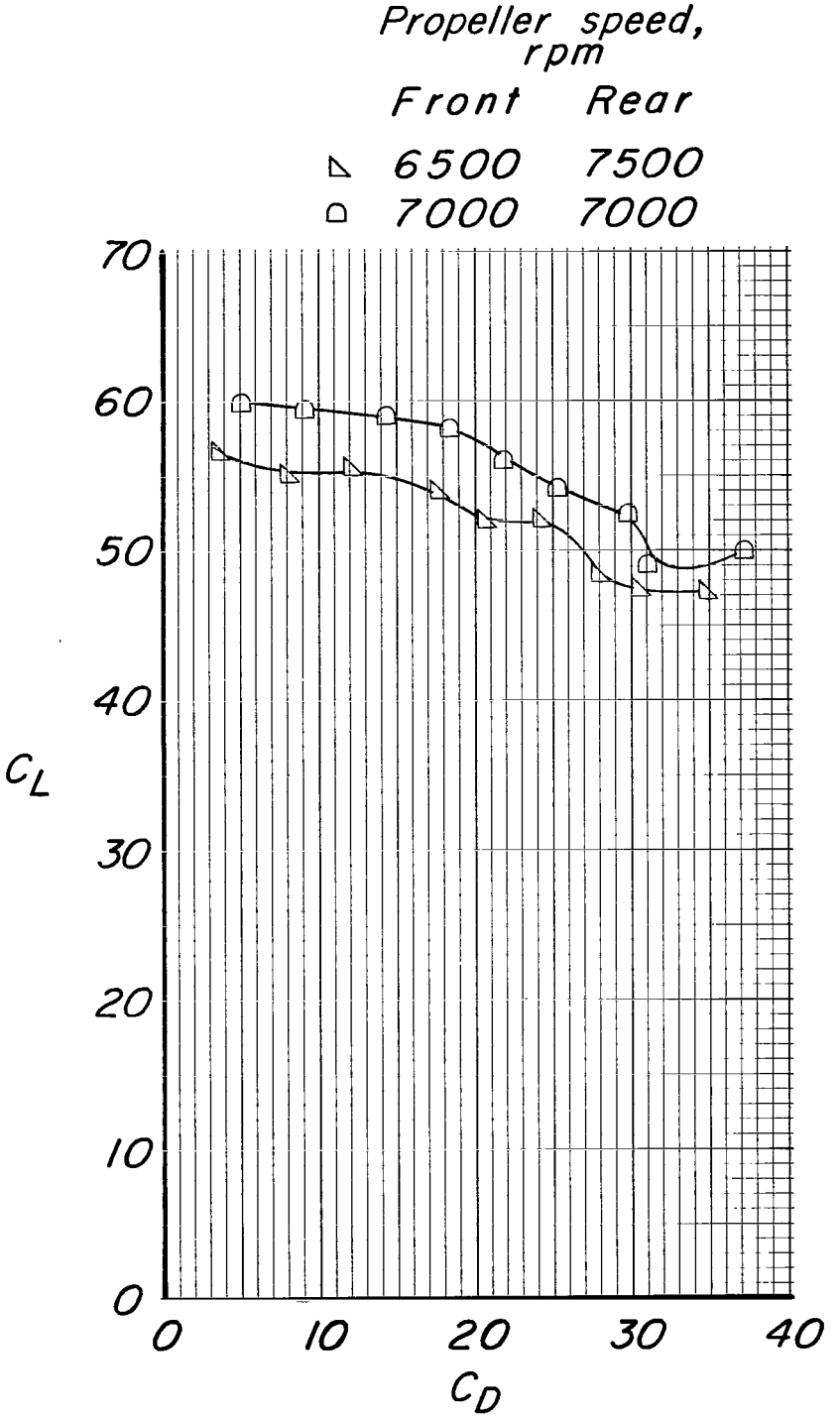


Figure 24.- Concluded.

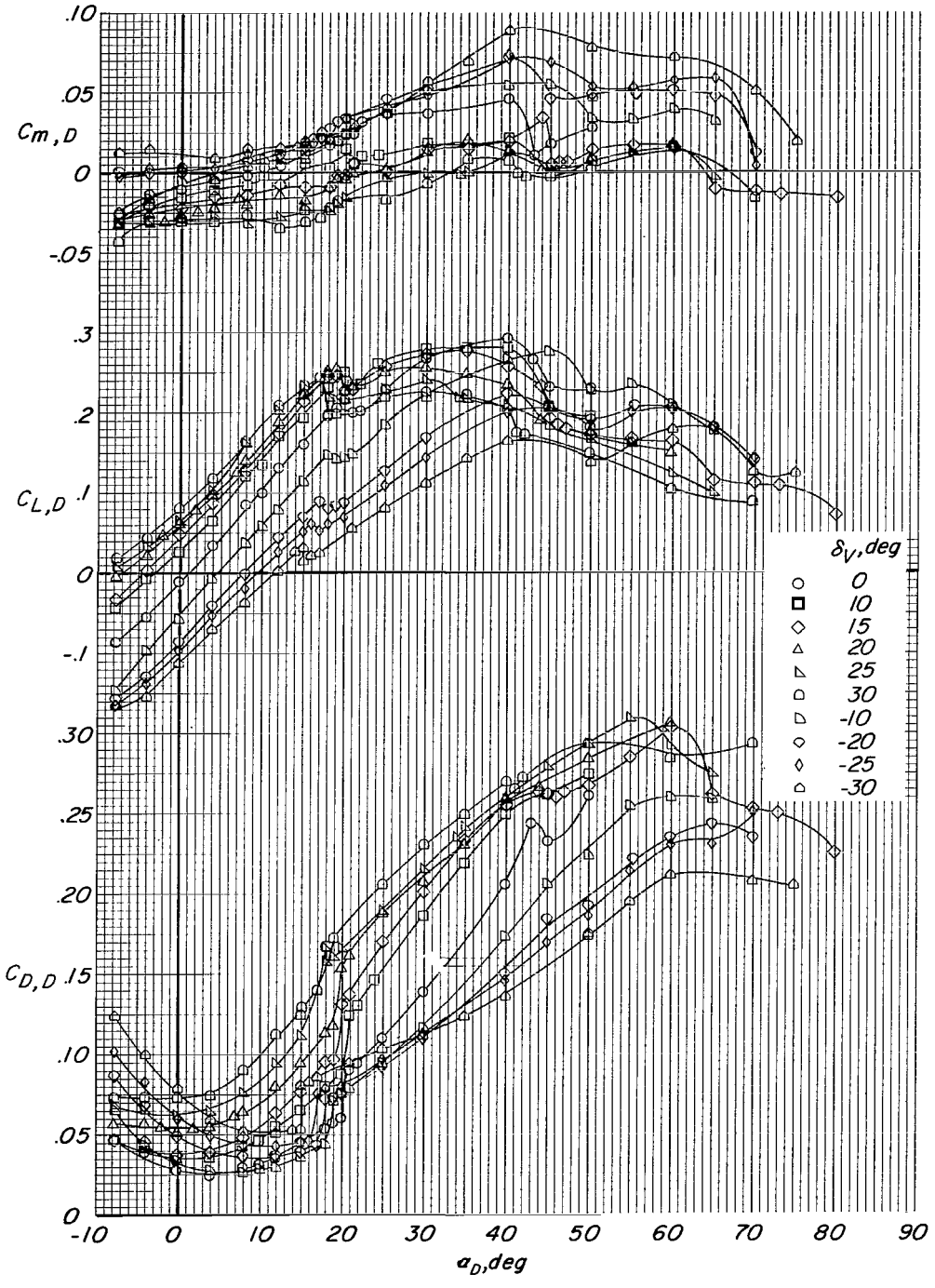


(a) $C_T = 0$; propellers windmilling.

Figure 25.- Effects of vane deflection on the aerodynamic characteristics of the isolated ducted propeller with large vane at various thrust coefficients and with modified duct lips.

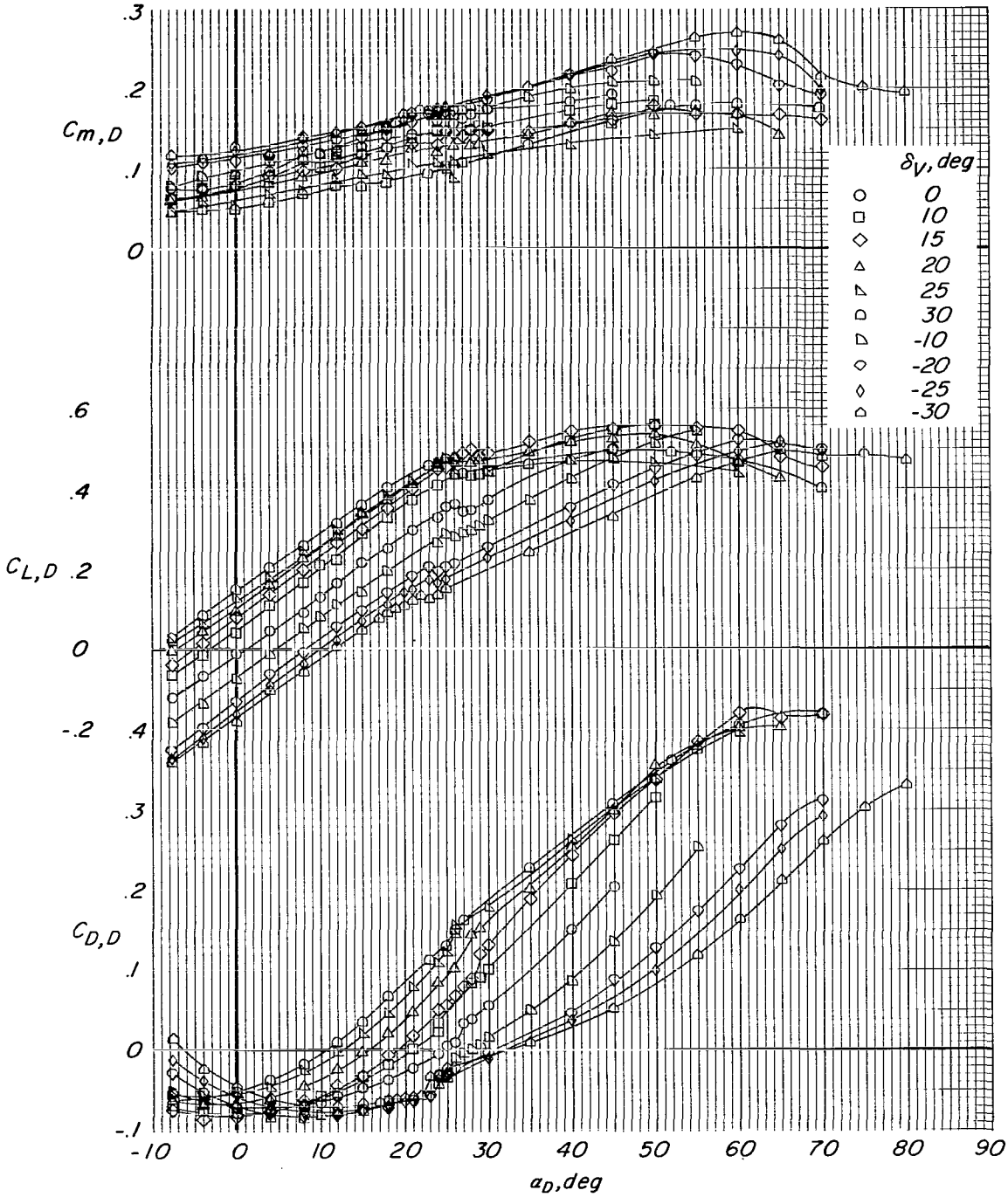


(b) $C_T = 0.4$.

Figure 25.- Continued.

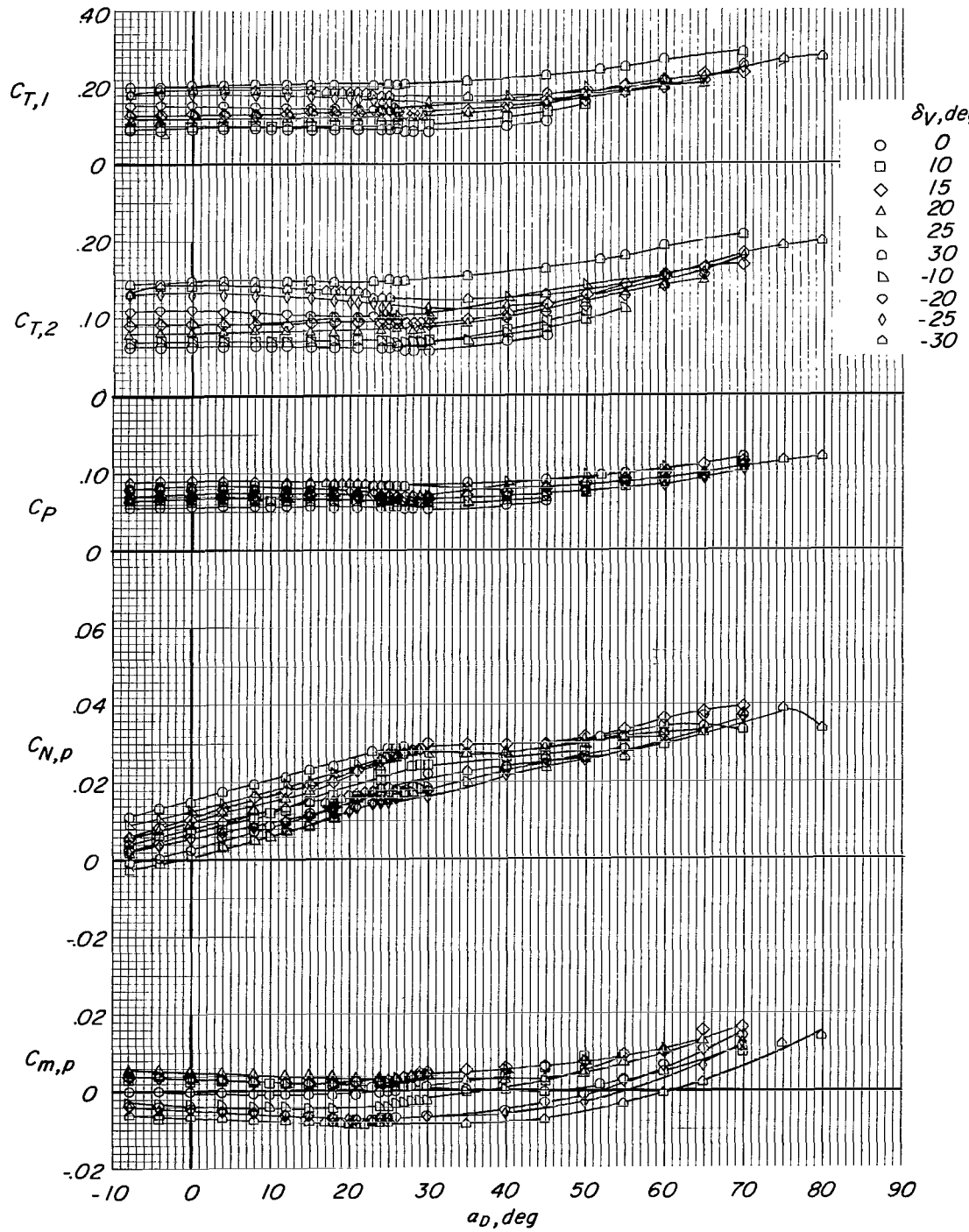


(b) Concluded.

Figure 25.- Continued.

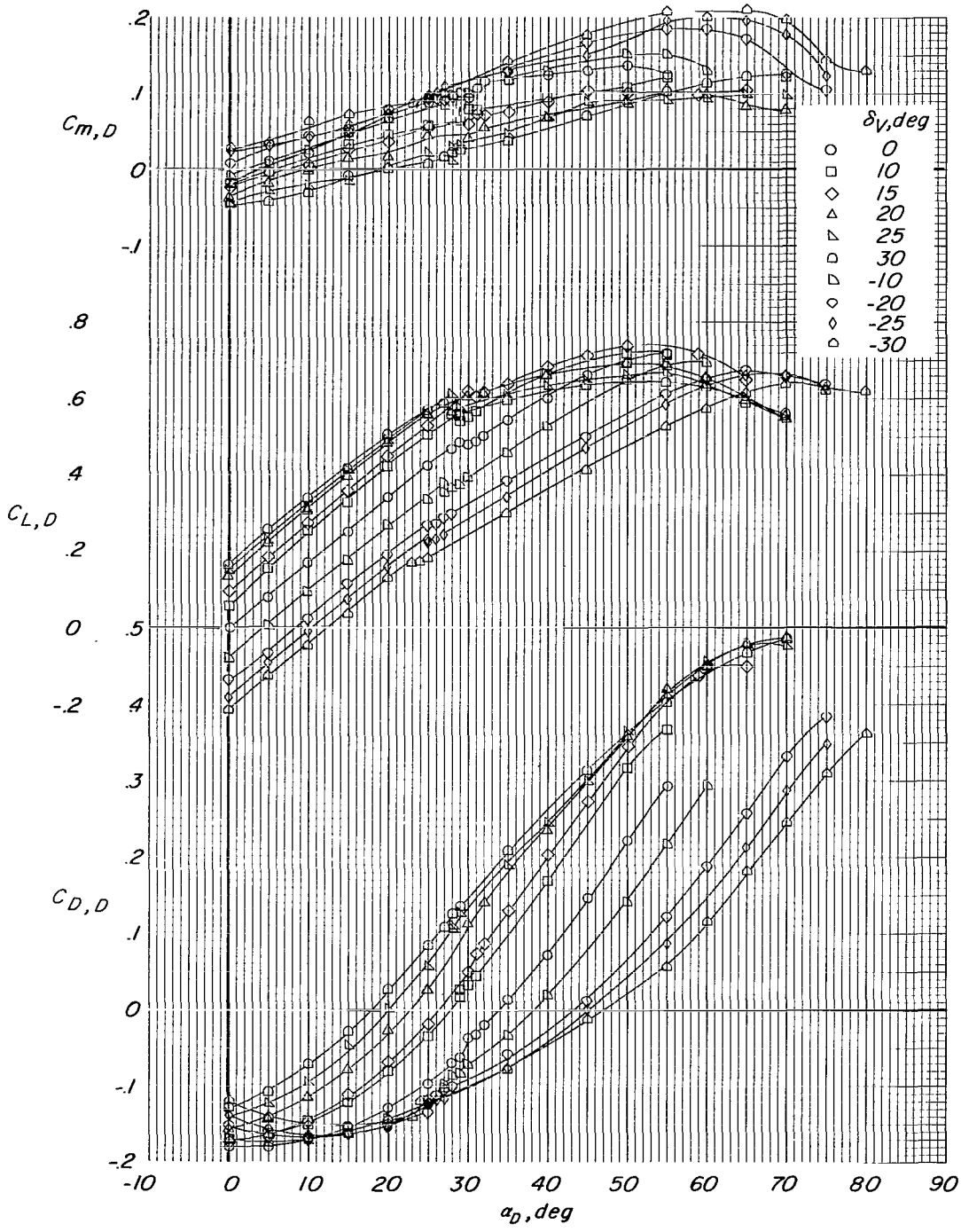


(c) $C_T = 0.80$.

Figure 25.- Continued.

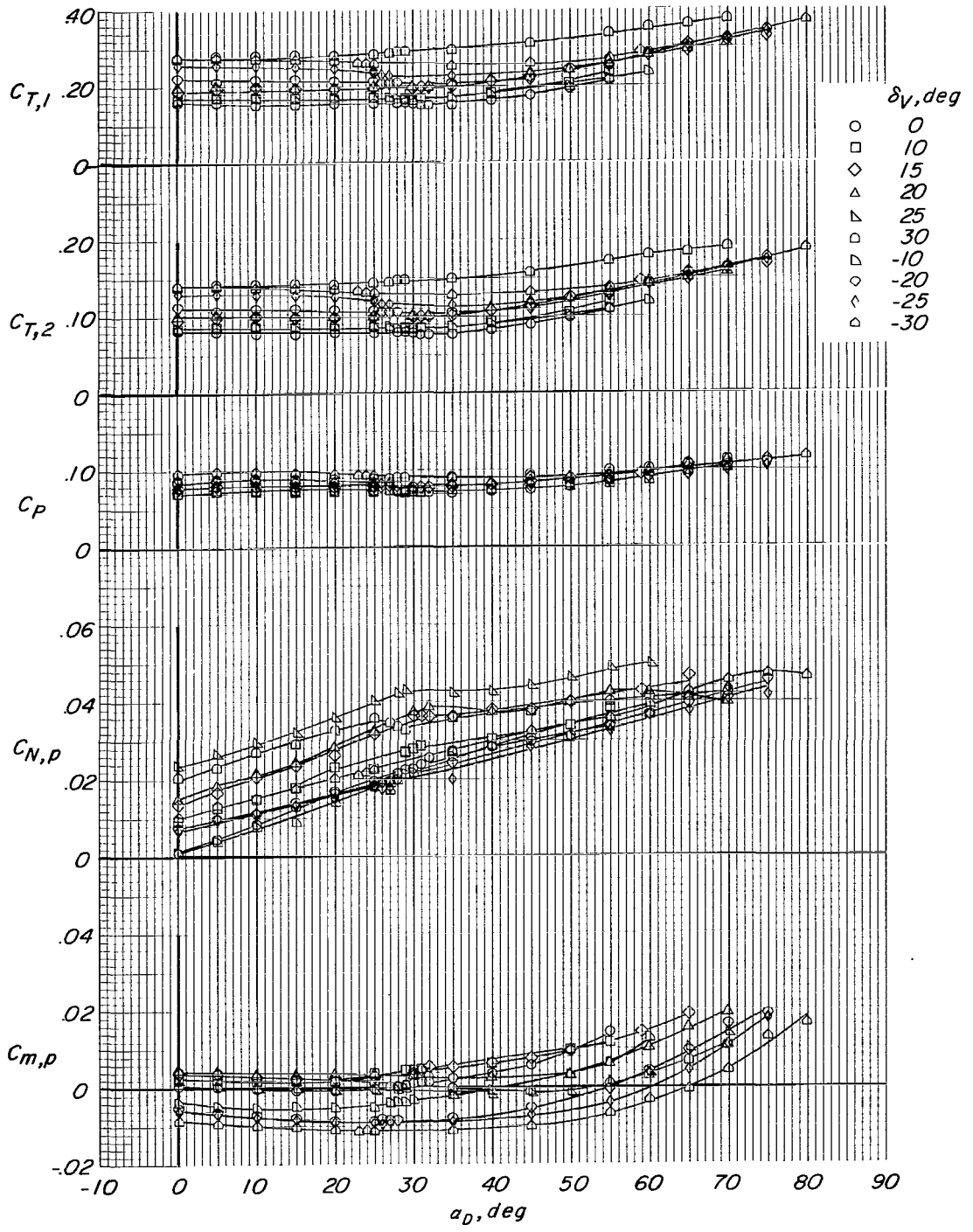


(c) Concluded.

Figure 25.- Continued.

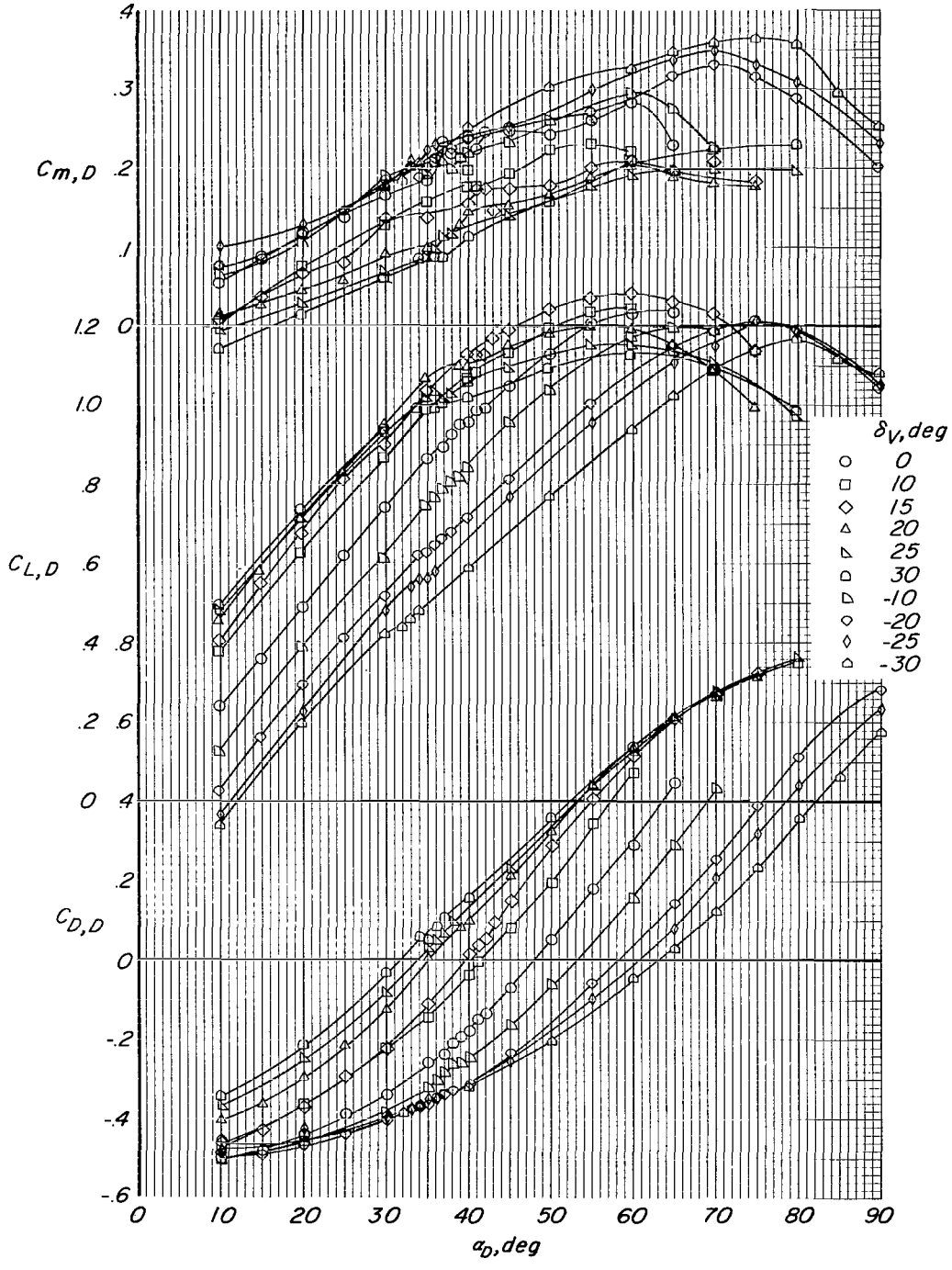


(d) $C_T = 2.1$.

Figure 25.- Continued.

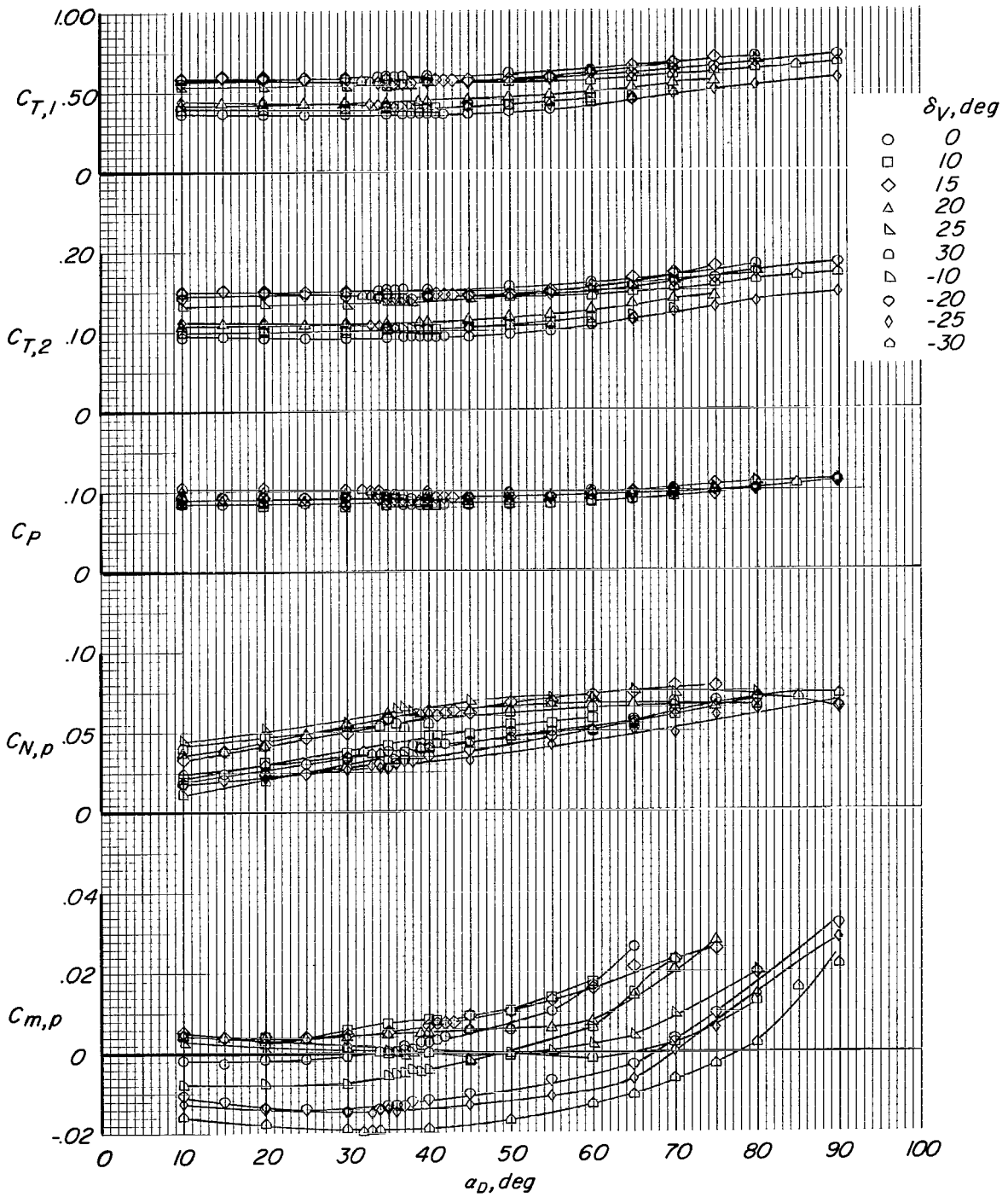


(d) Concluded.

Figure 25.- Continued.

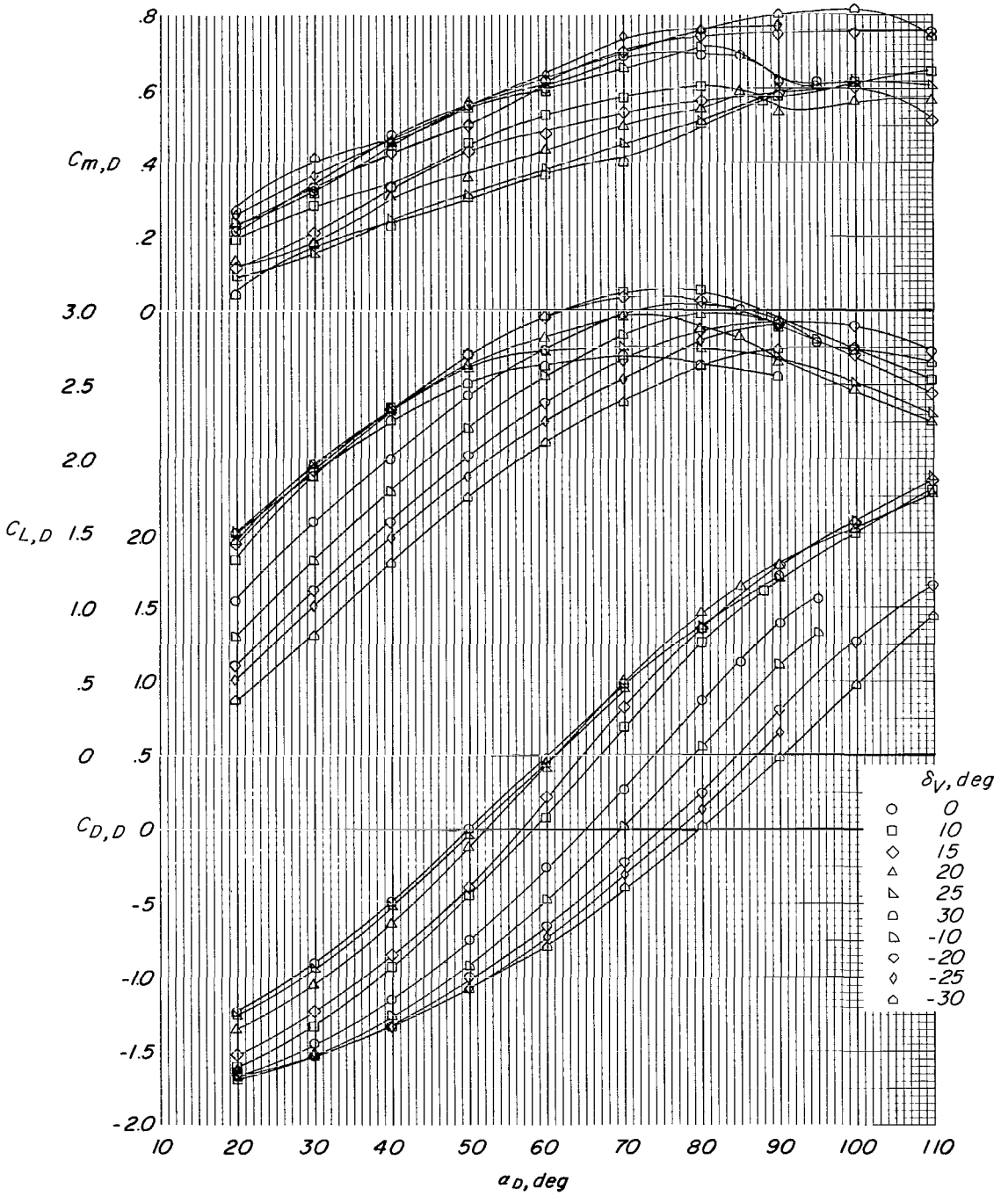


(e) $C_T = 7.0$.

Figure 25.- Continued.

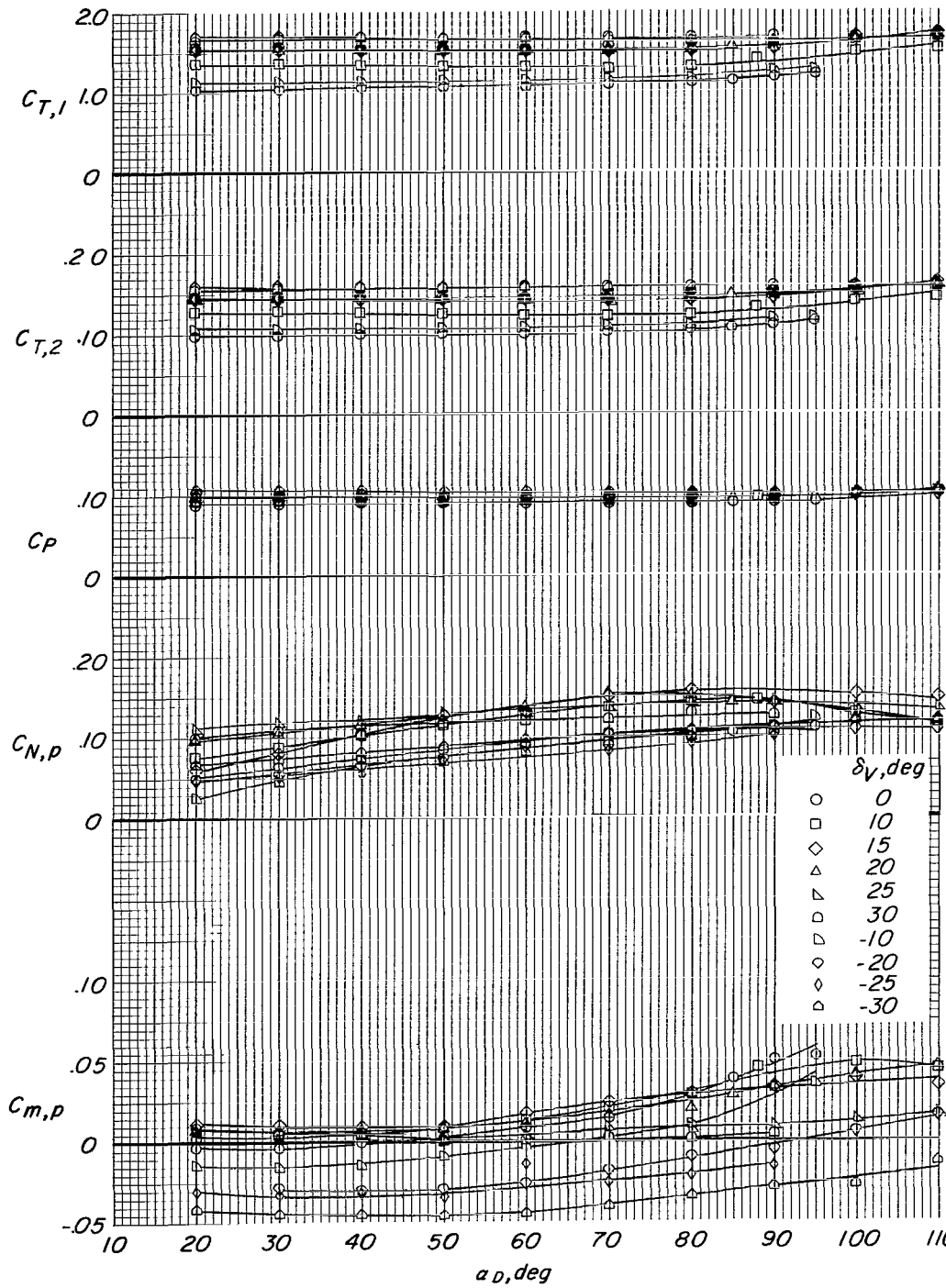


(e) Concluded.

Figure 25.- Continued.

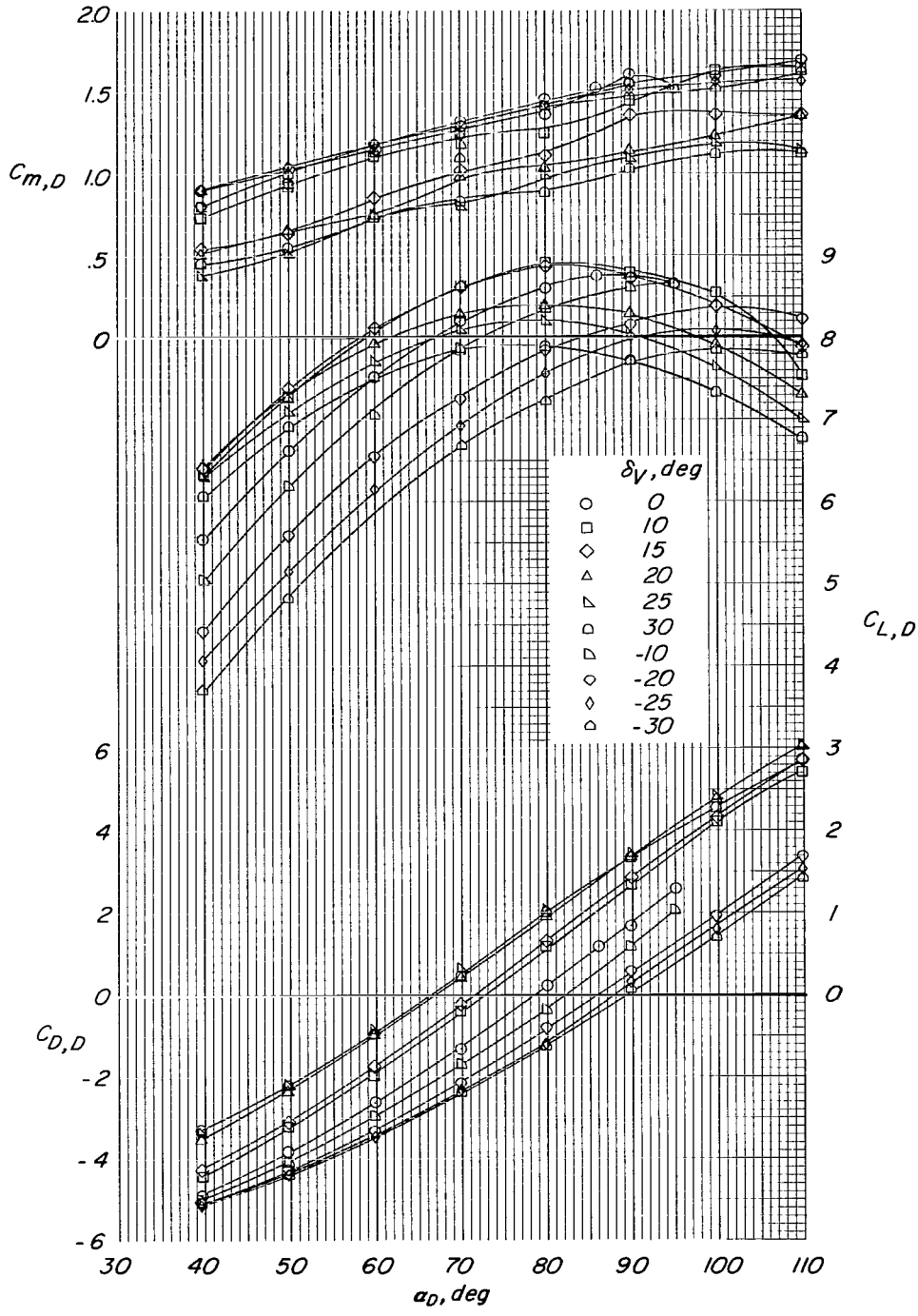


(f) $C_T = 25$.

Figure 25.- Continued.

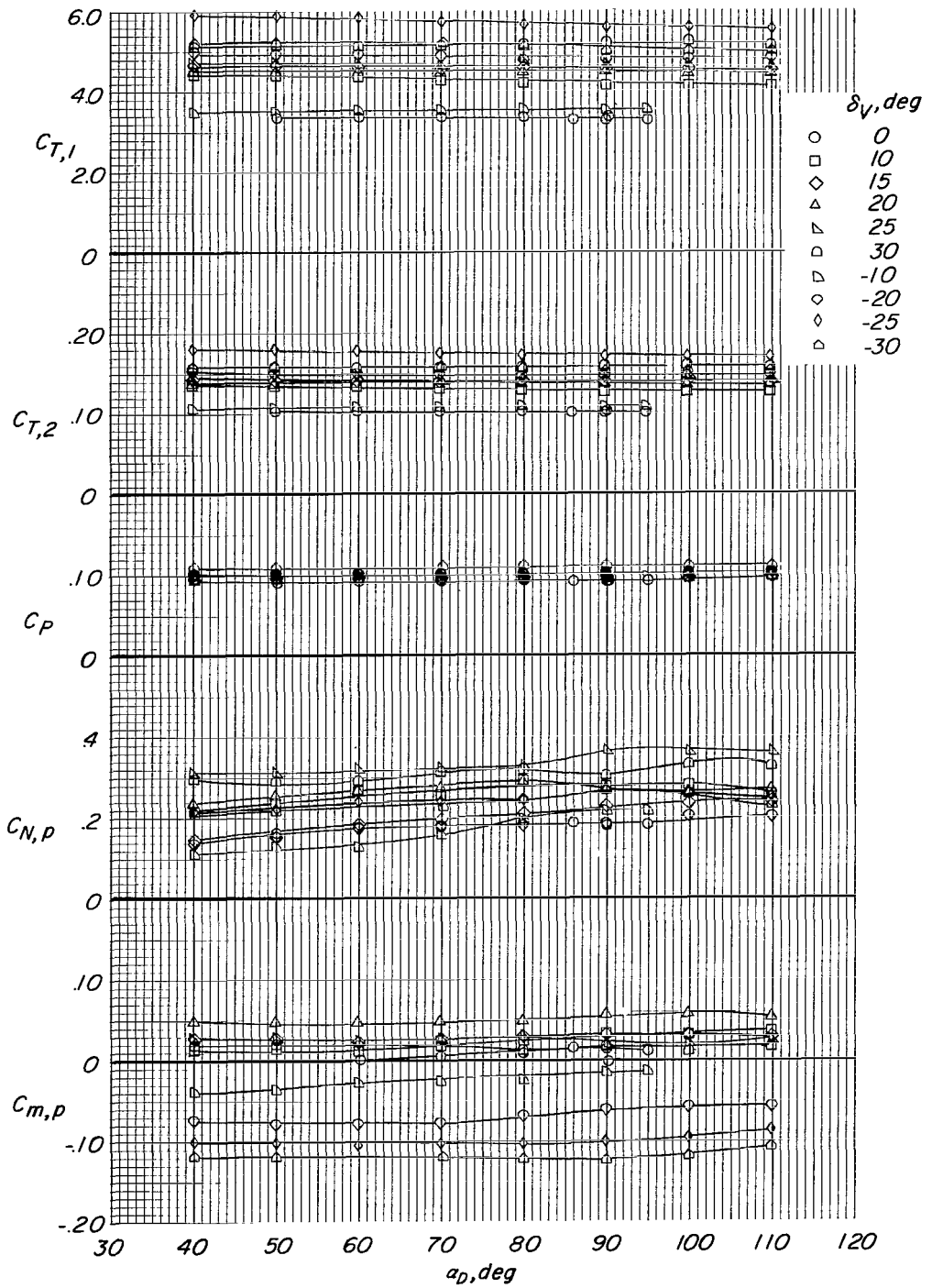


(f) Concluded.

Figure 25.- Continued.

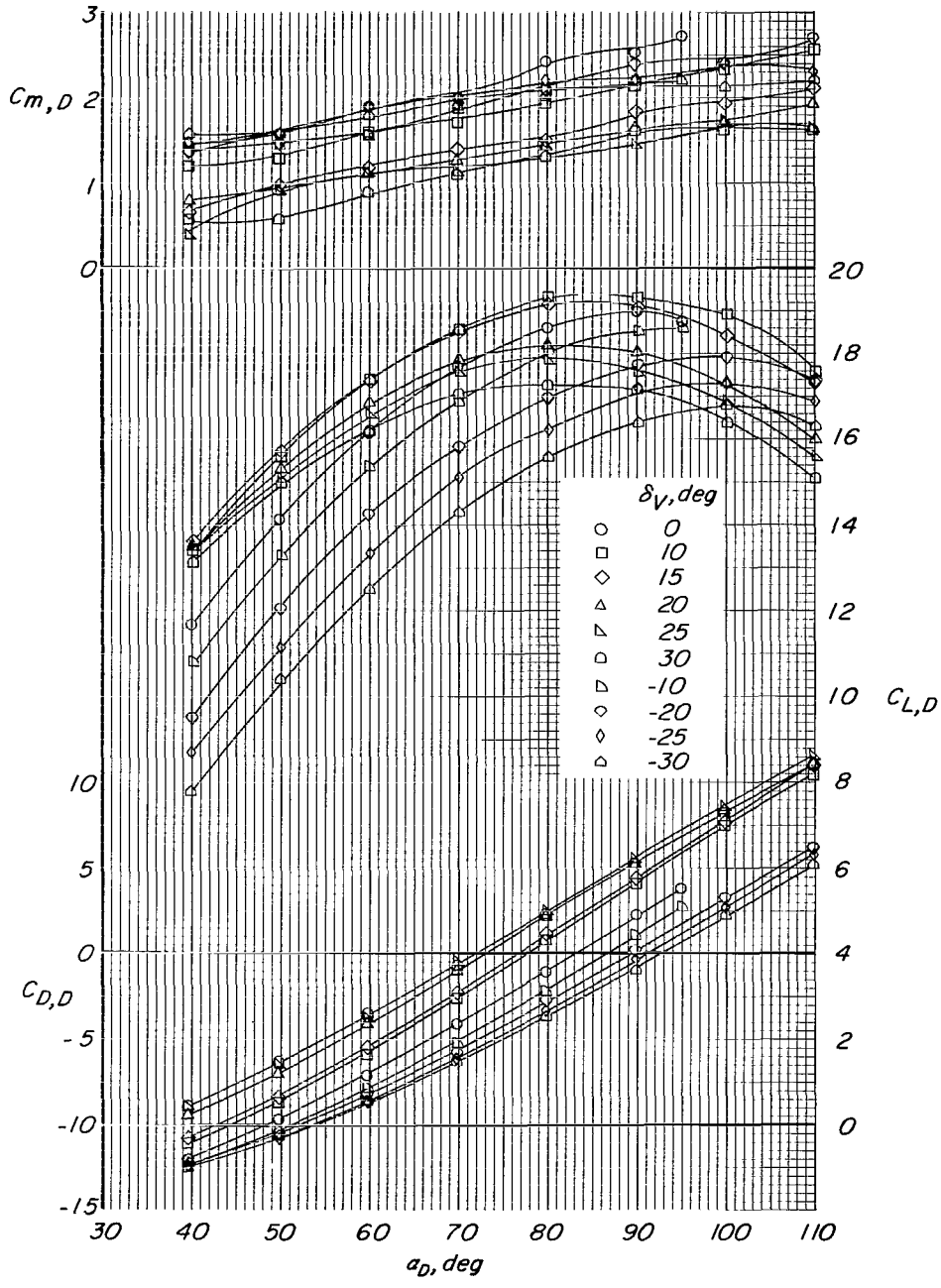


(g) $C_T = 60$.

Figure 25.- Continued.

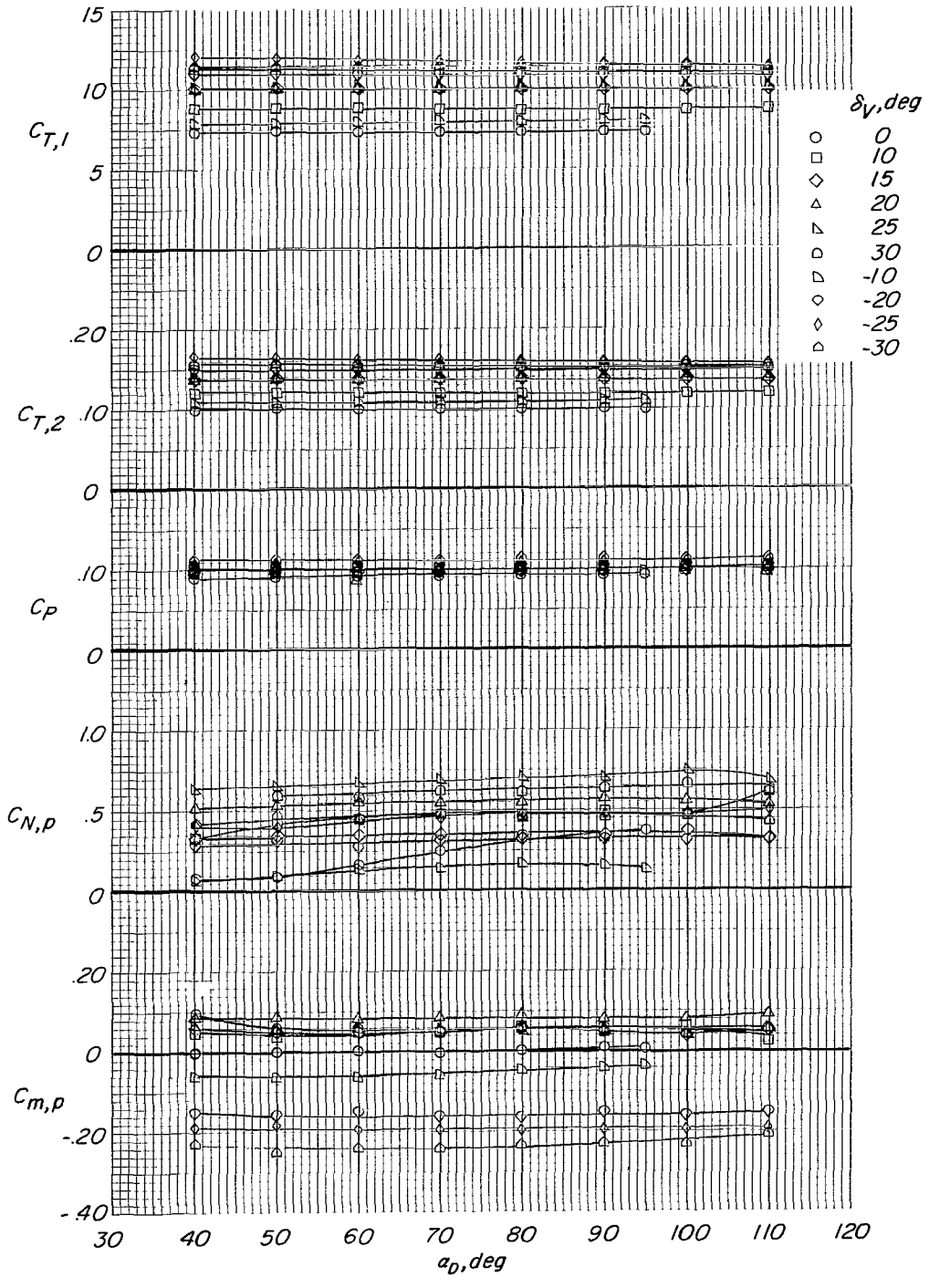


(g) Concluded.

Figure 25.- Concluded.

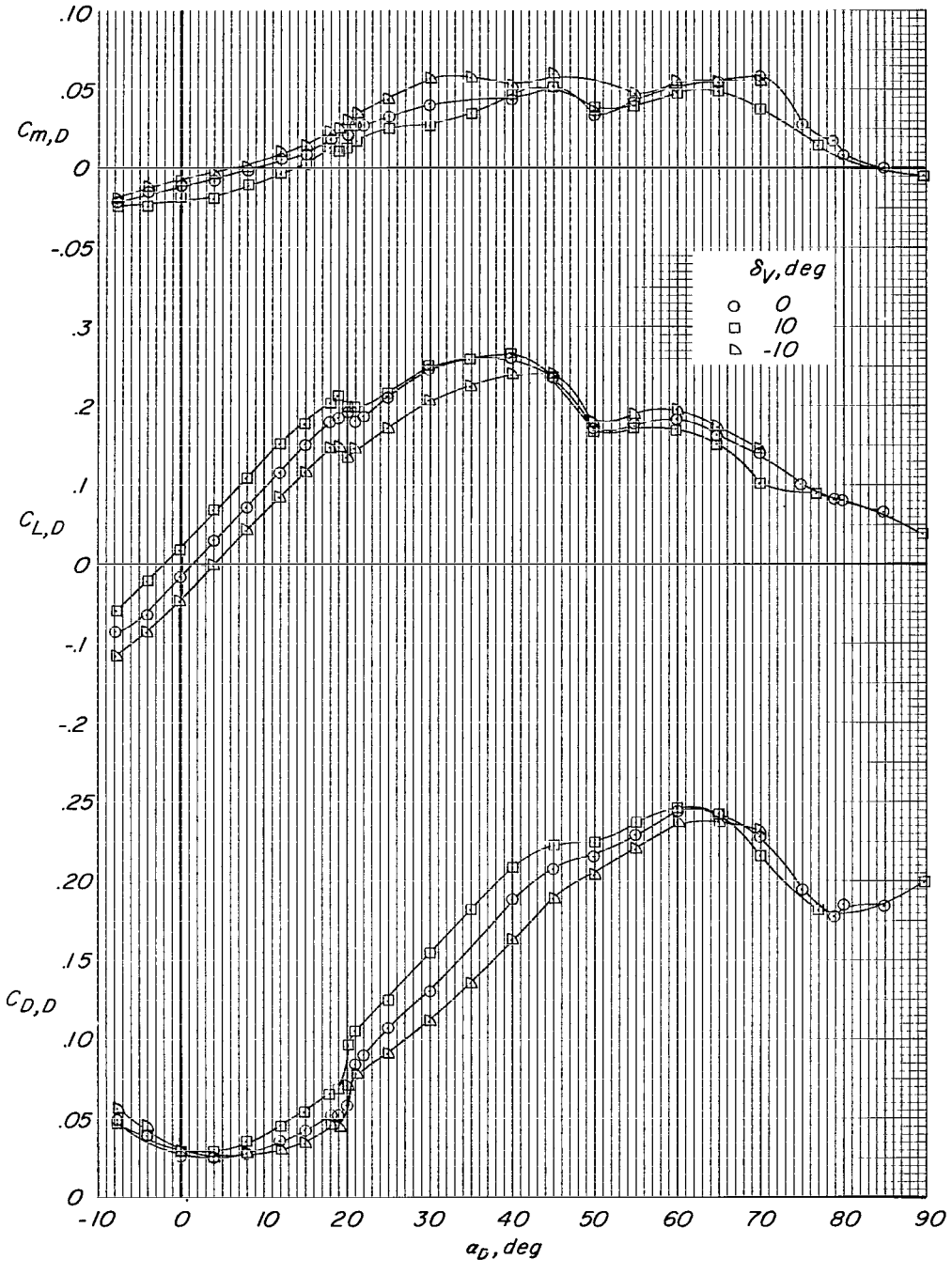


(a) $C_T = 0$; propellers windmilling.

Figure 26.- Effects of vane deflection on the aerodynamic characteristics of the isolated ducted propeller with small vane at various thrust coefficients and with modified duct lips.

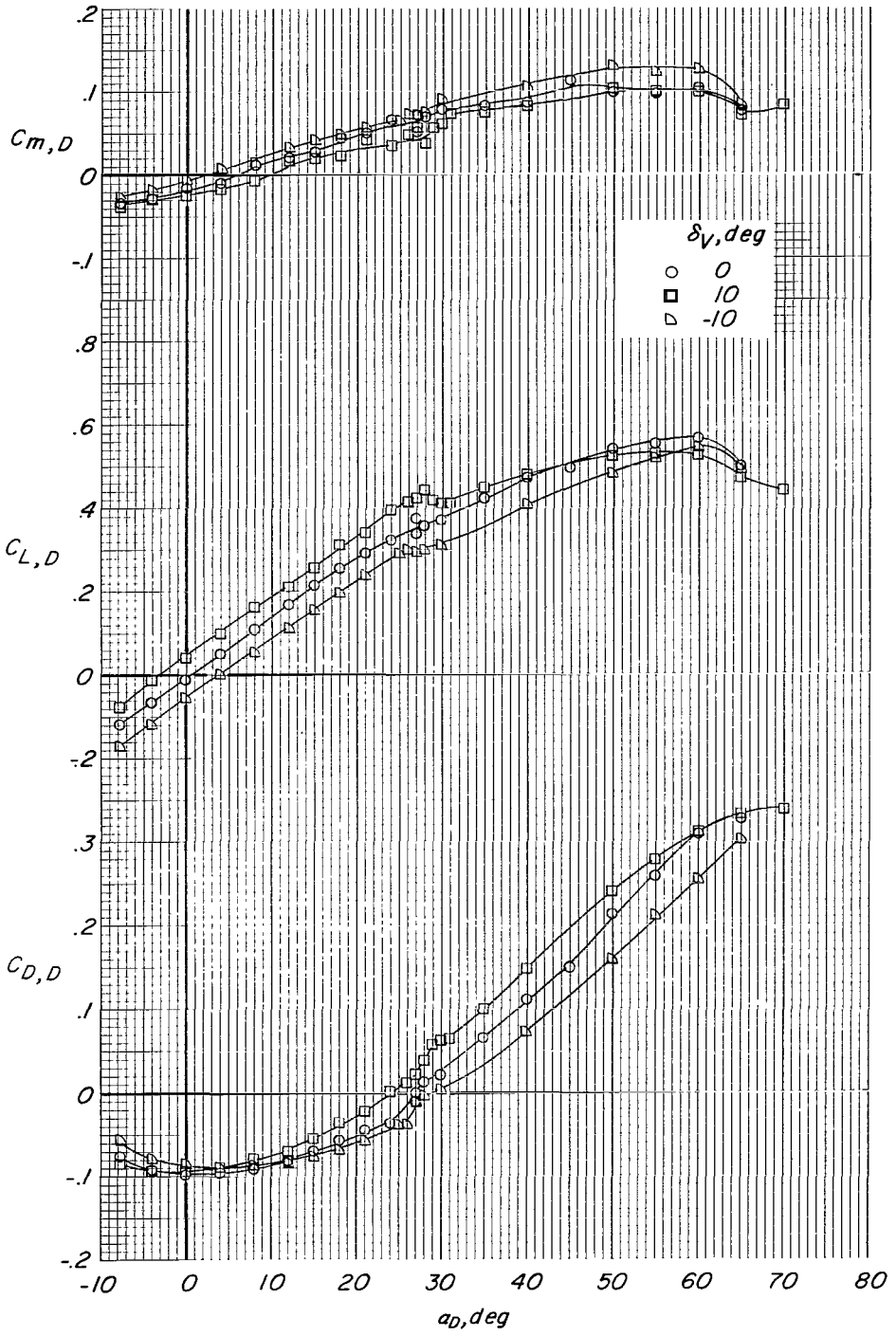


(b) $C_T = 0.4$.

Figure 26.- Continued.

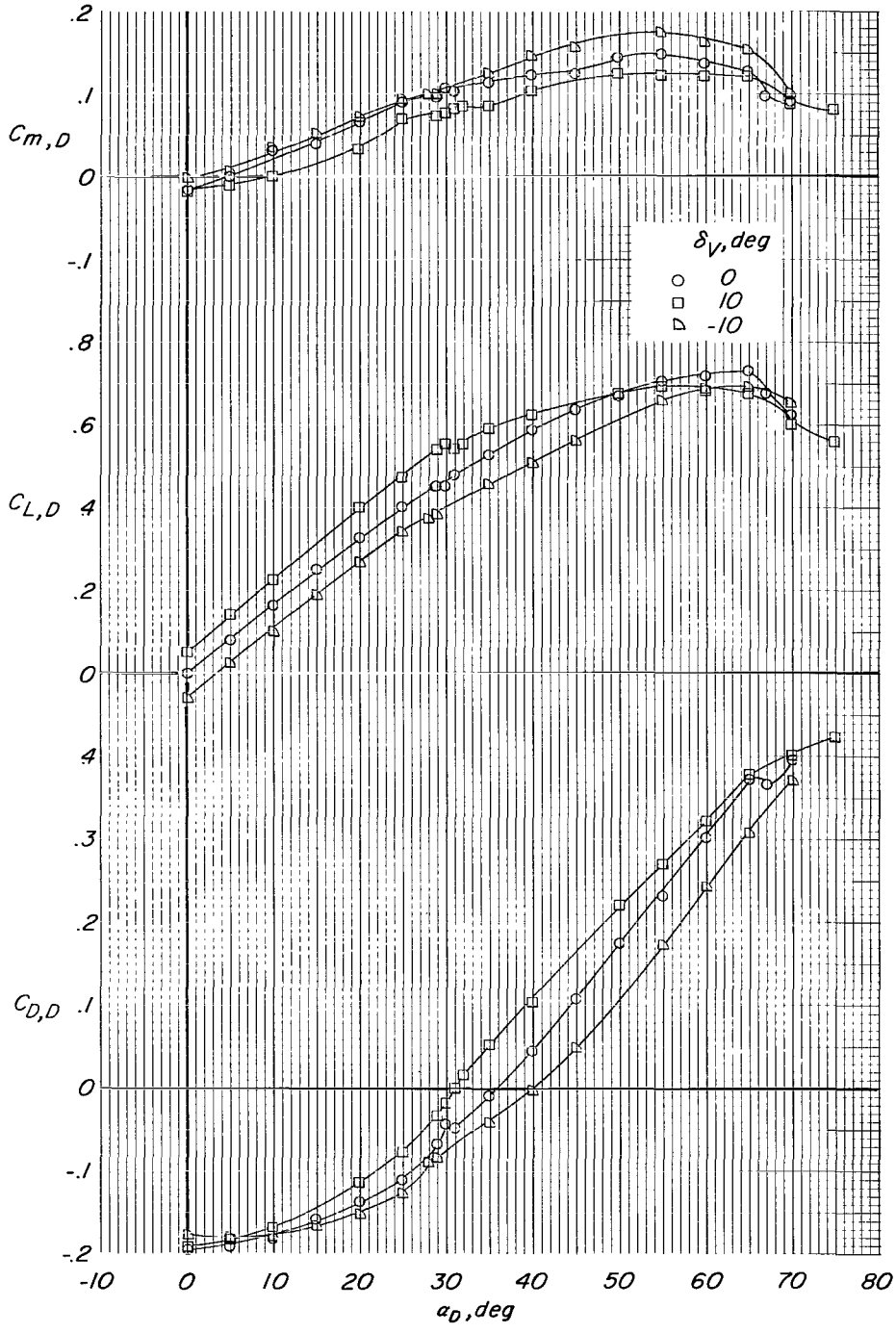


(c) $C_T = 0.8$.

Figure 26.- Continued.

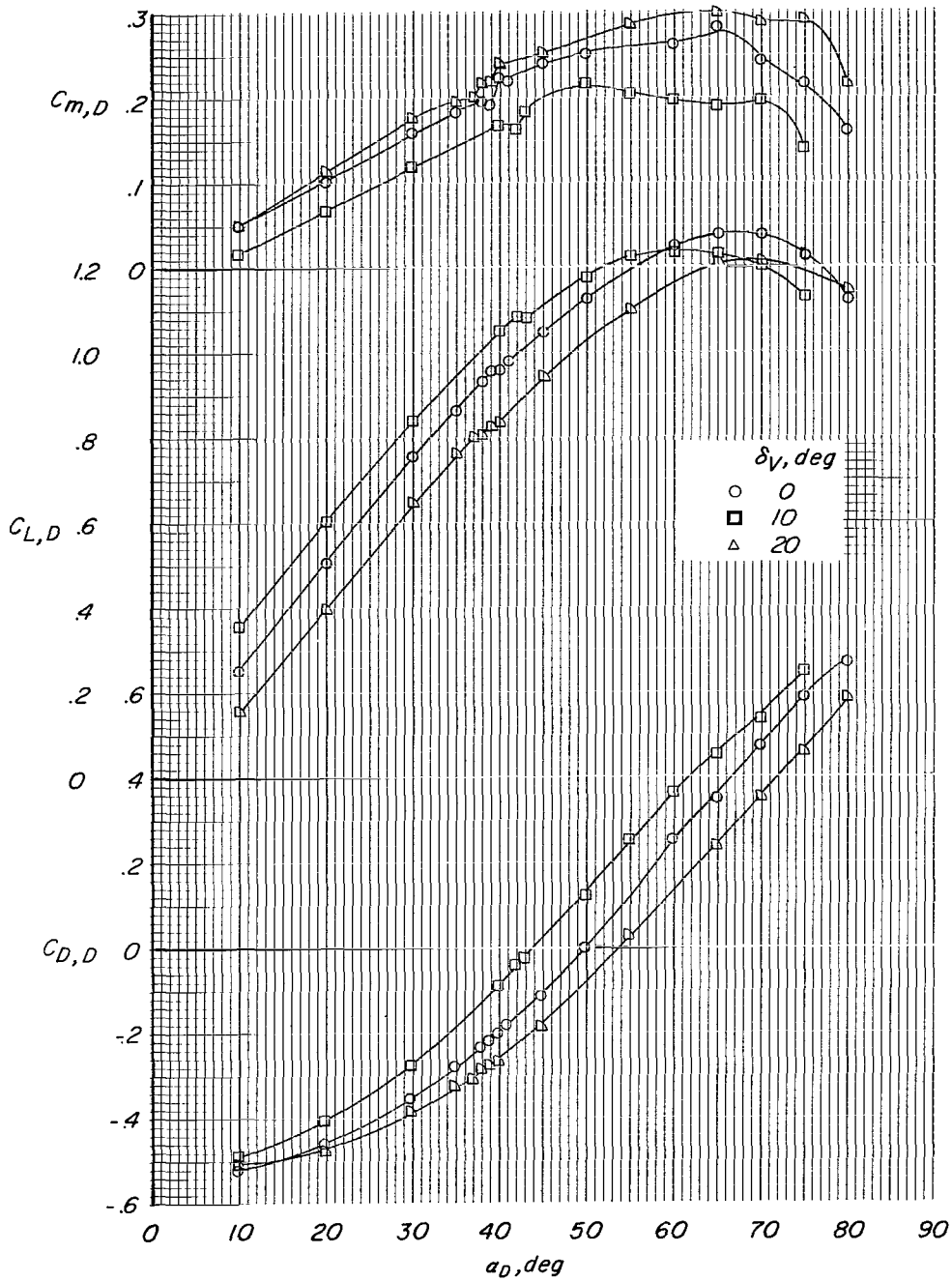


(d) $C_T = 2.1$.

Figure 26.- Continued.

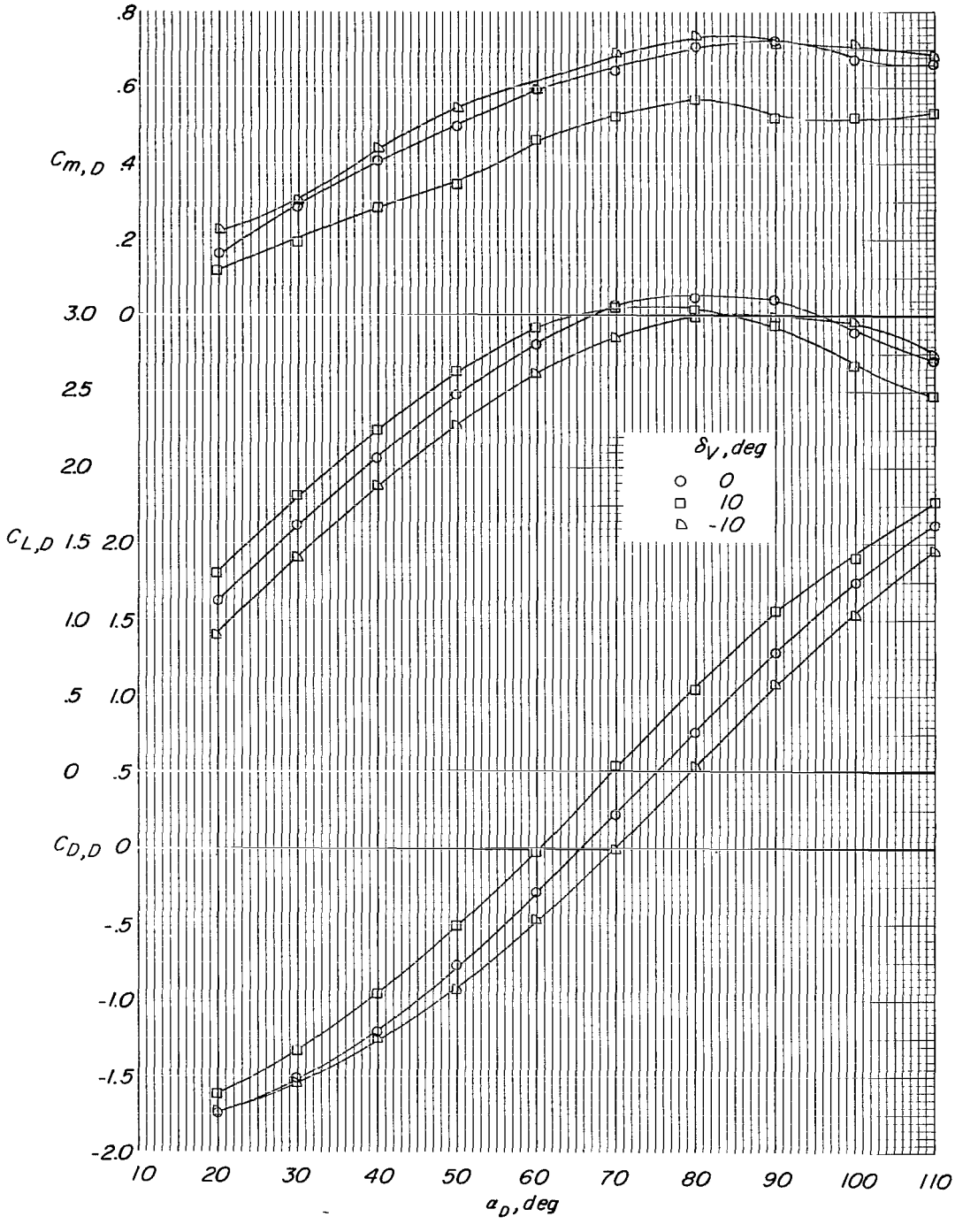


(e) $C_T = 7.0$.

Figure 26.- Continued.

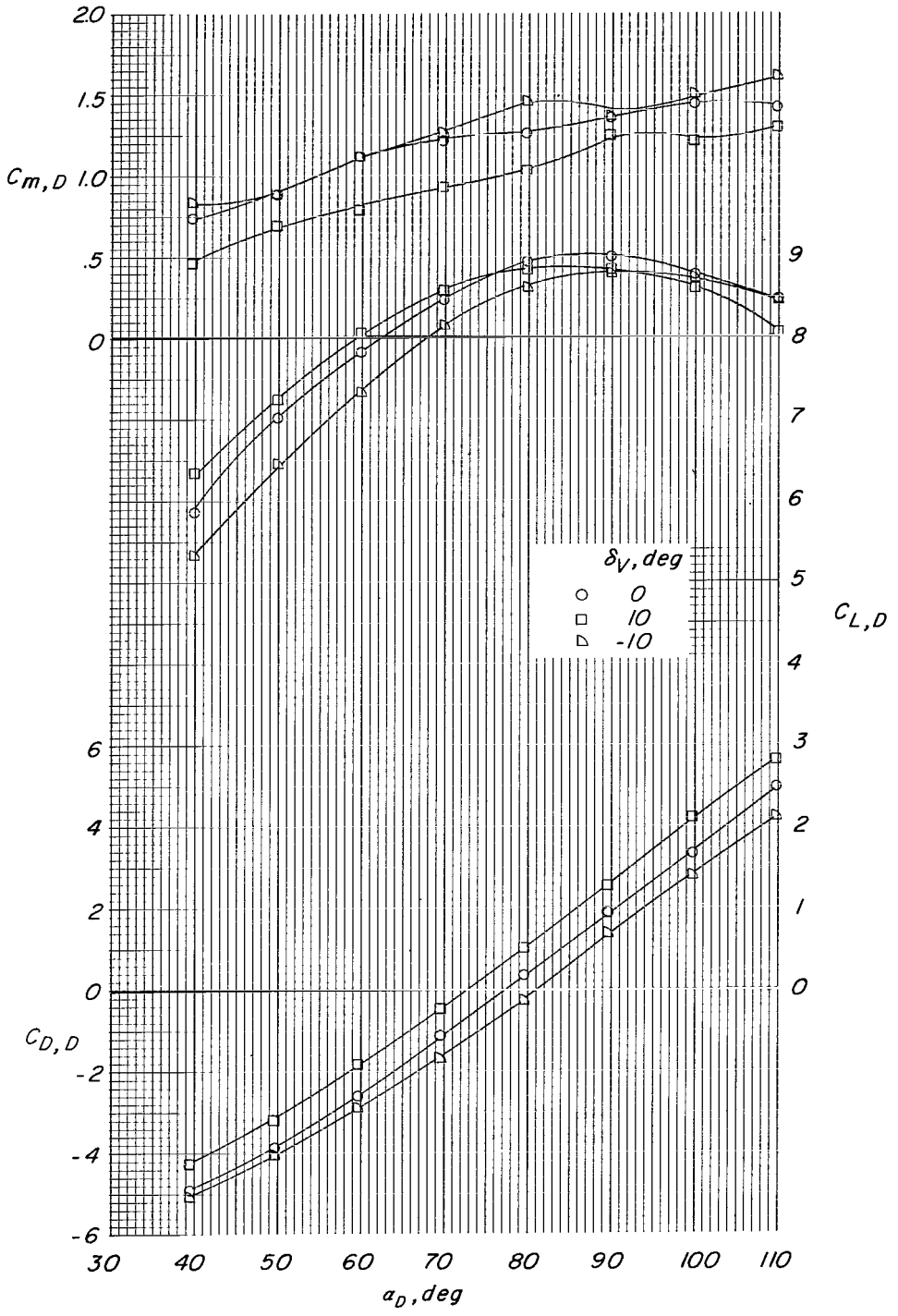


(f) $C_T = 25$.

Figure 26.- Continued.

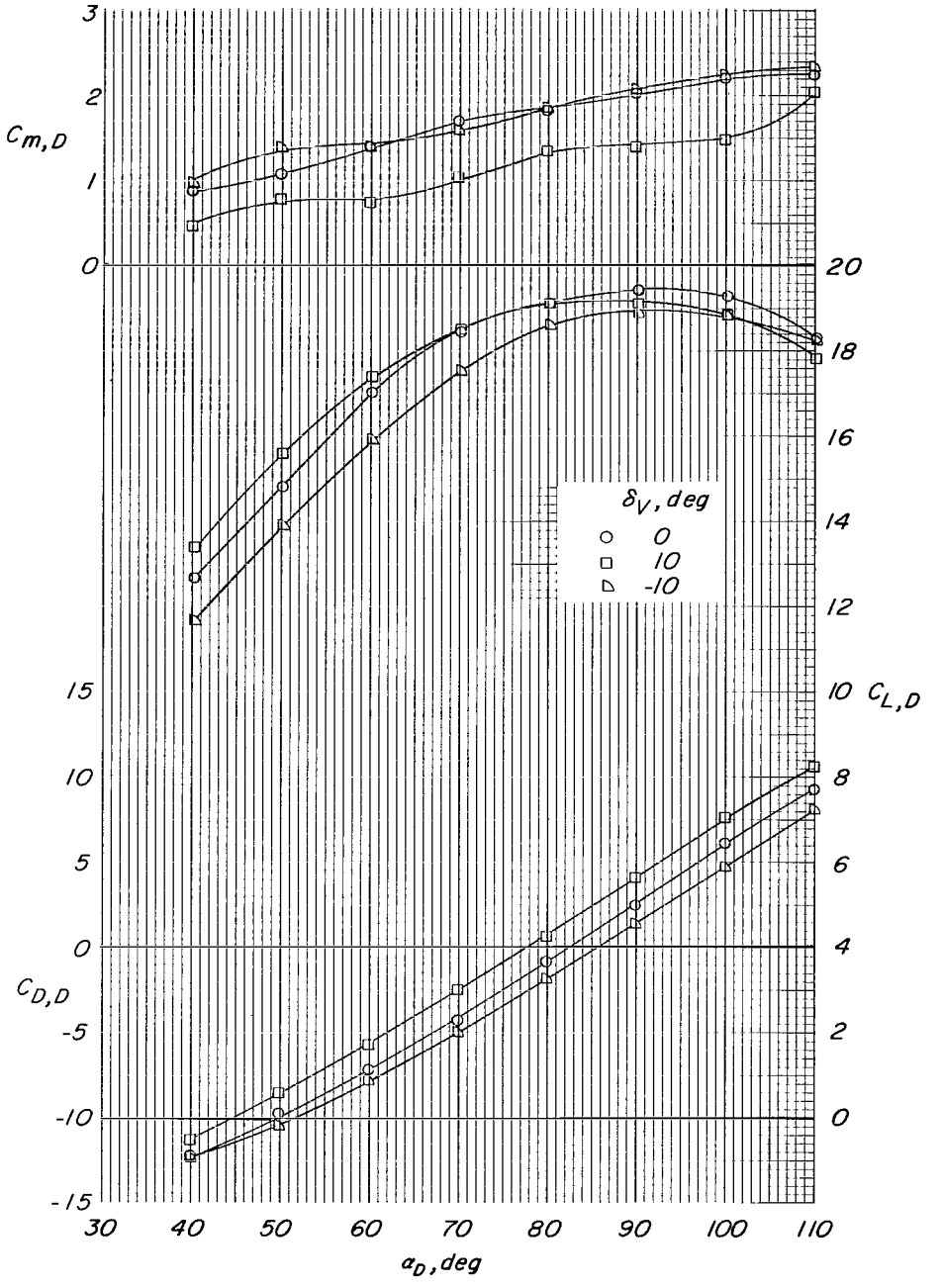


(g) $C_T = 60$.

Figure 26.- Concluded.

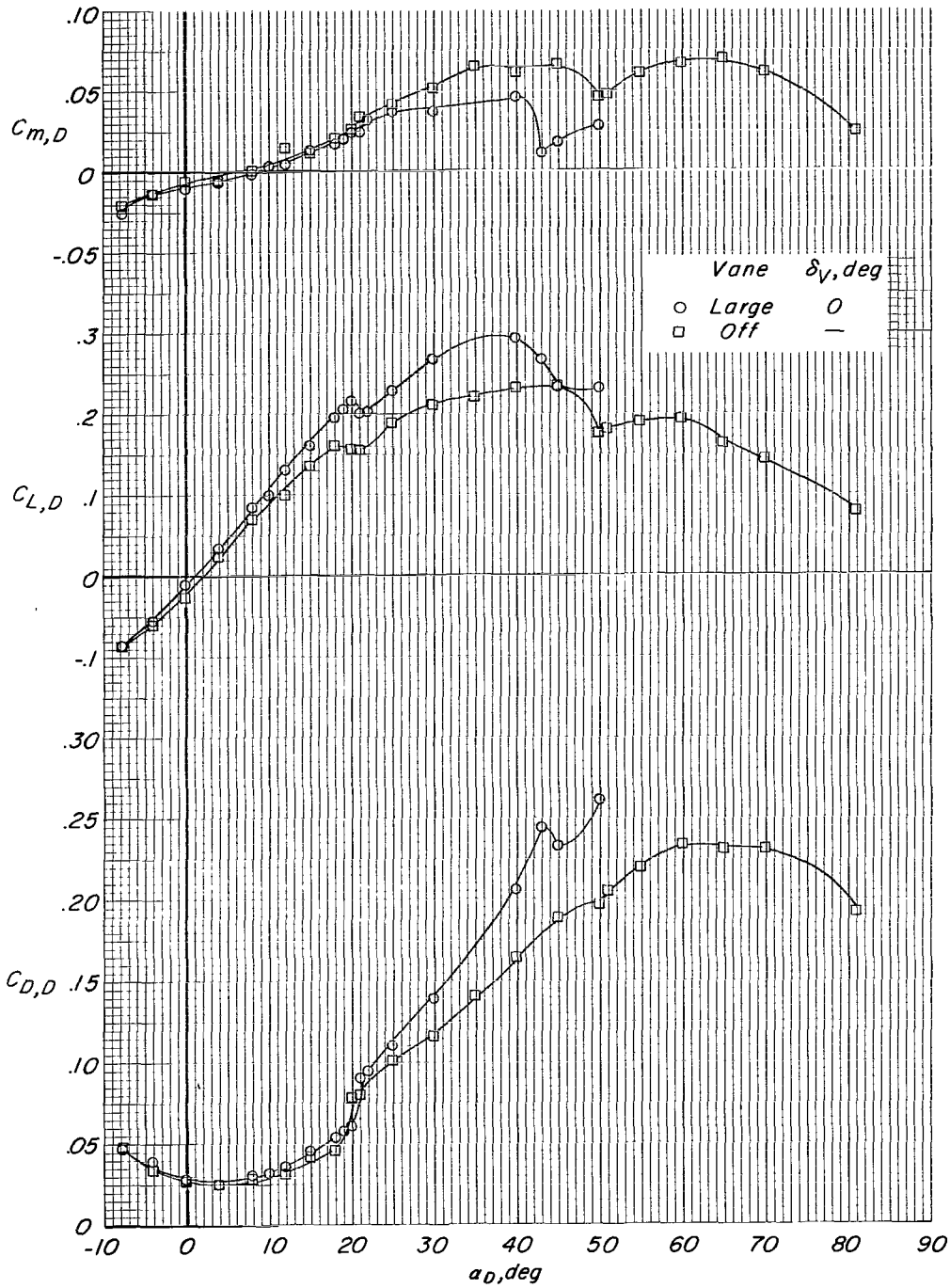


(a) $C_T = 0$; propellers windmilling.

Figure 27.- Effects of vane on and off on the aerodynamic characteristics of the isolated ducted propeller at various thrust coefficients and with modified duct lips.

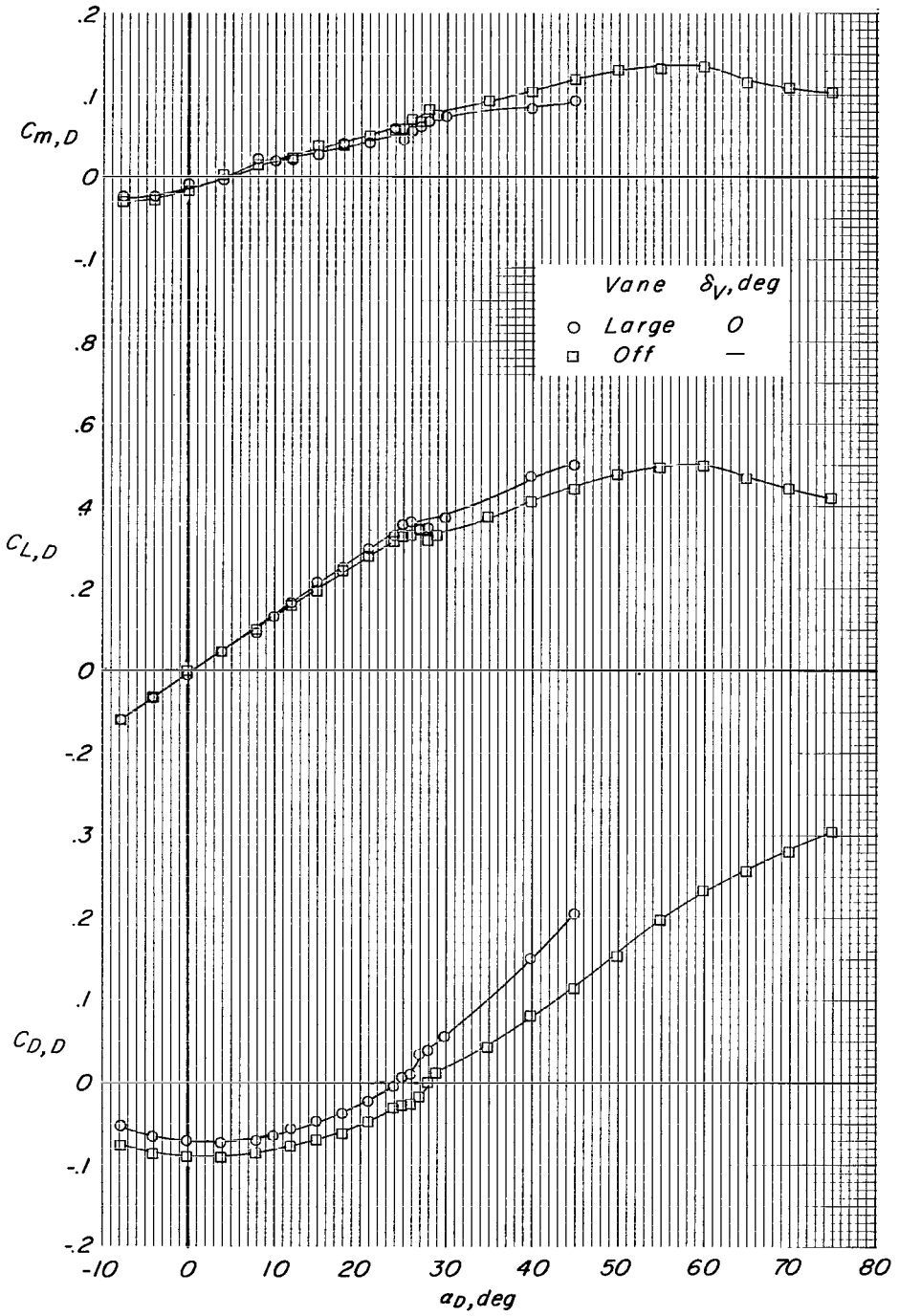


(b) $C_T = 0.4$.

Figure 27.- Continued.

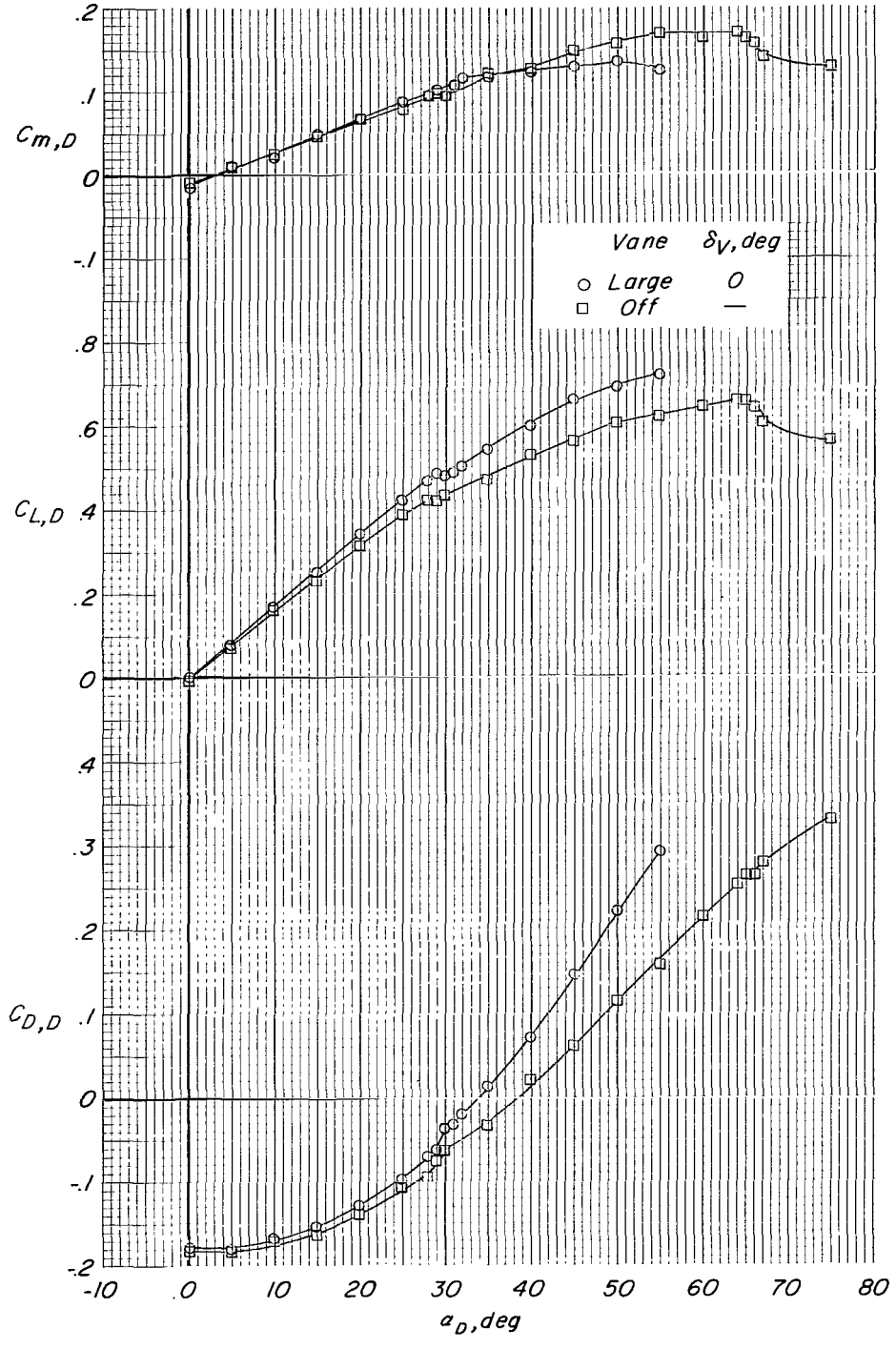


(c) $C_T = 0.8$.

Figure 27.- Continued.

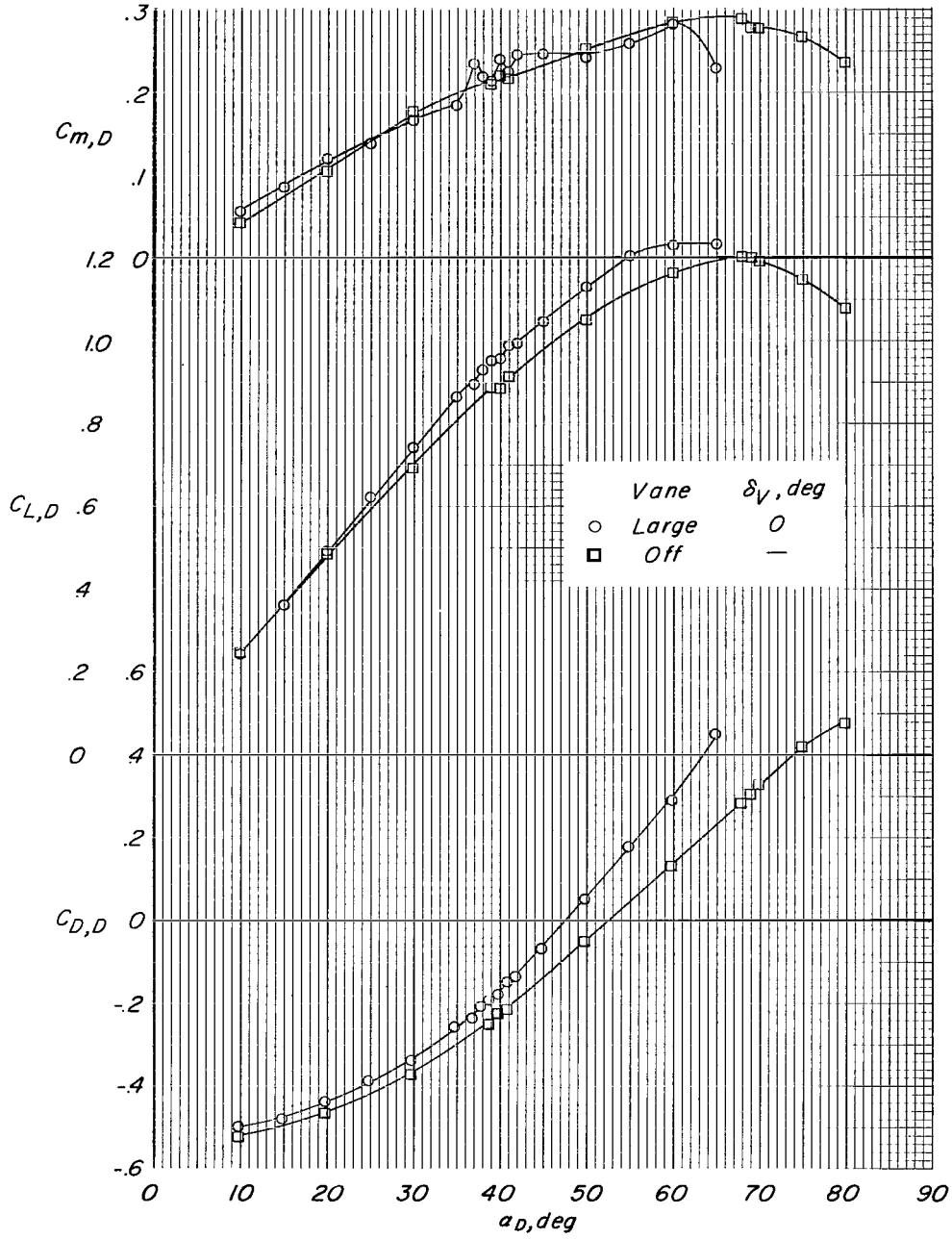


(d) $C_T = 2.1$.

Figure 27.- Continued.

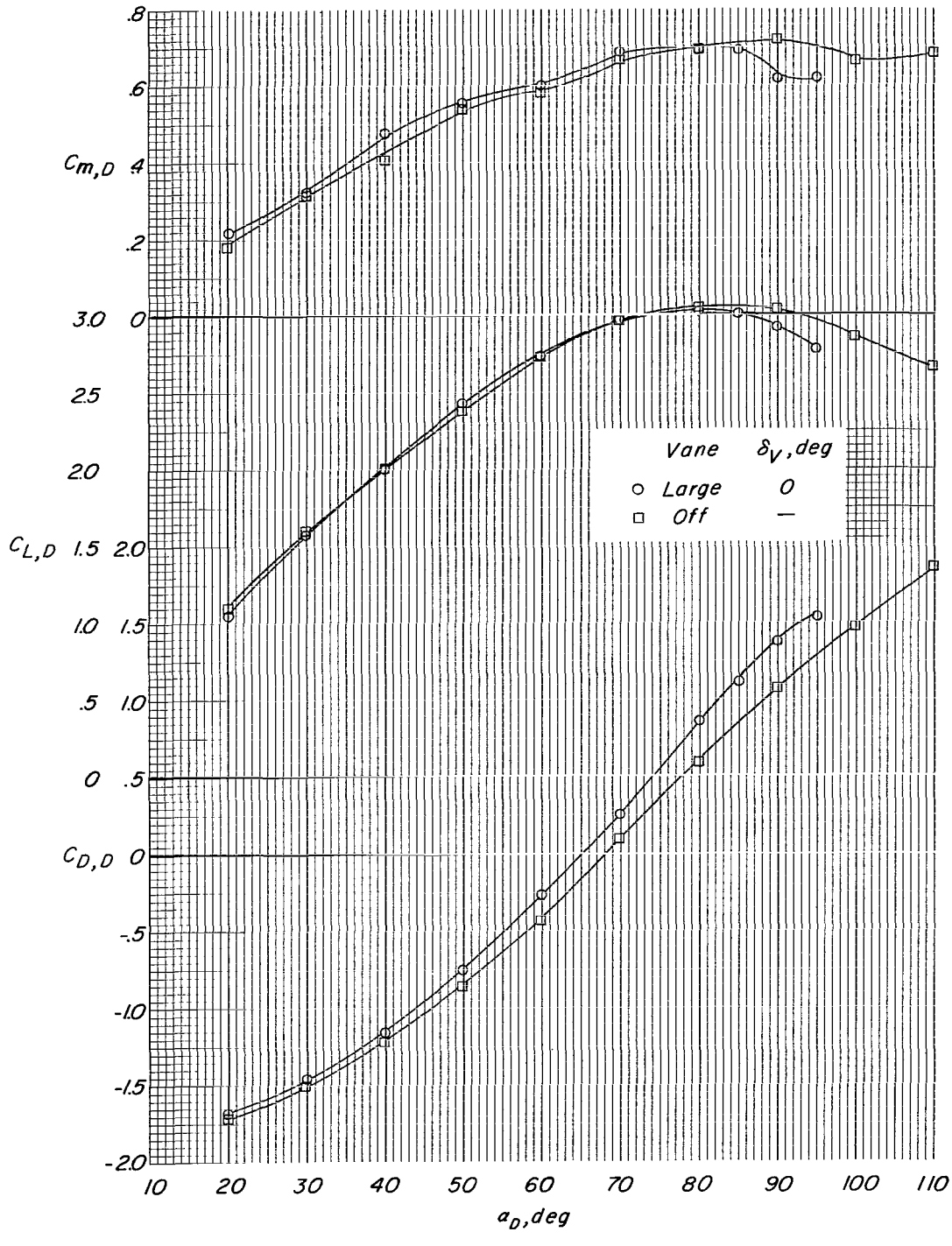


(e) $C_T = 7.0$.

Figure 27.- Continued.

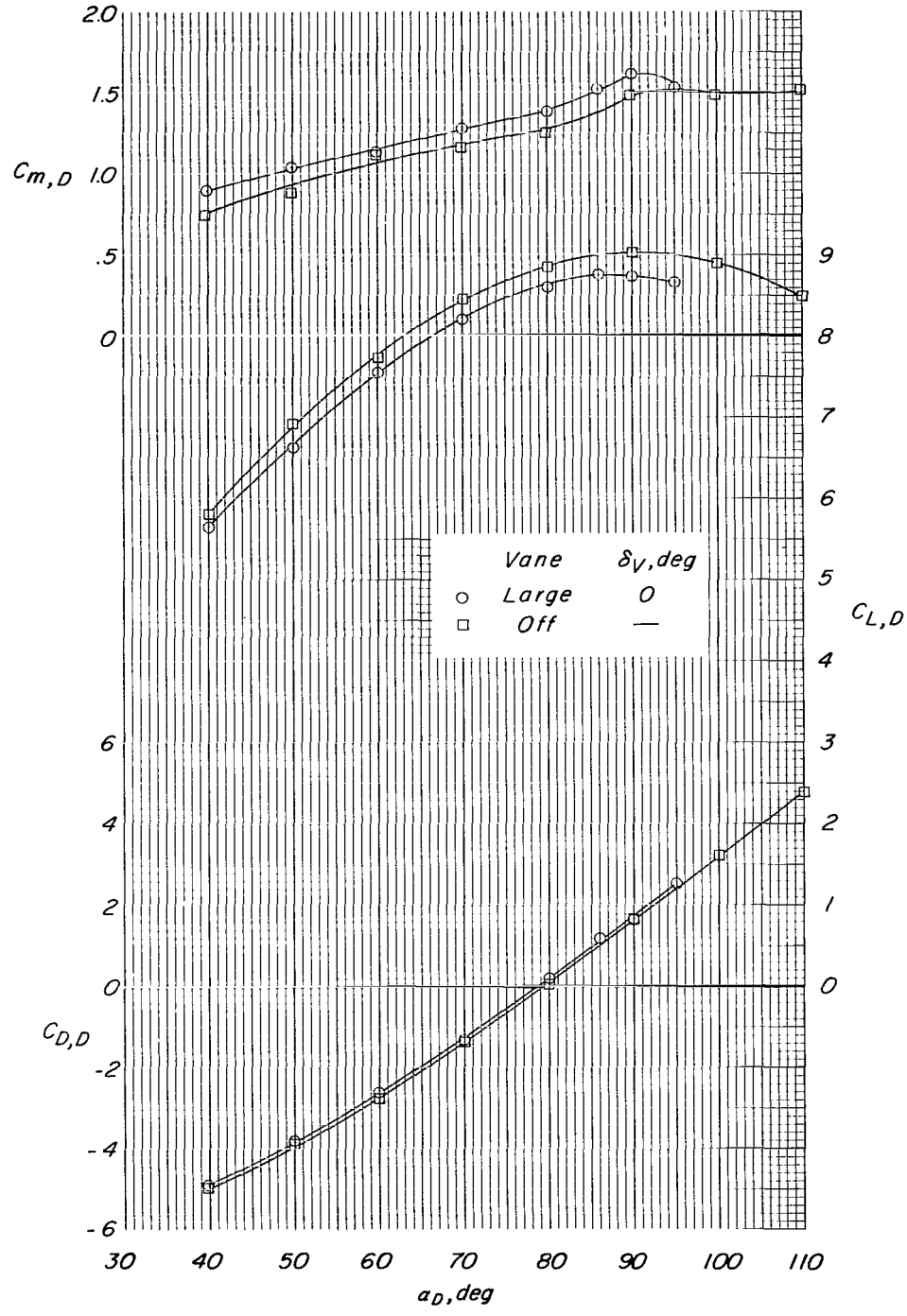


(f) $C_T = 25$.

Figure 27.- Continued.

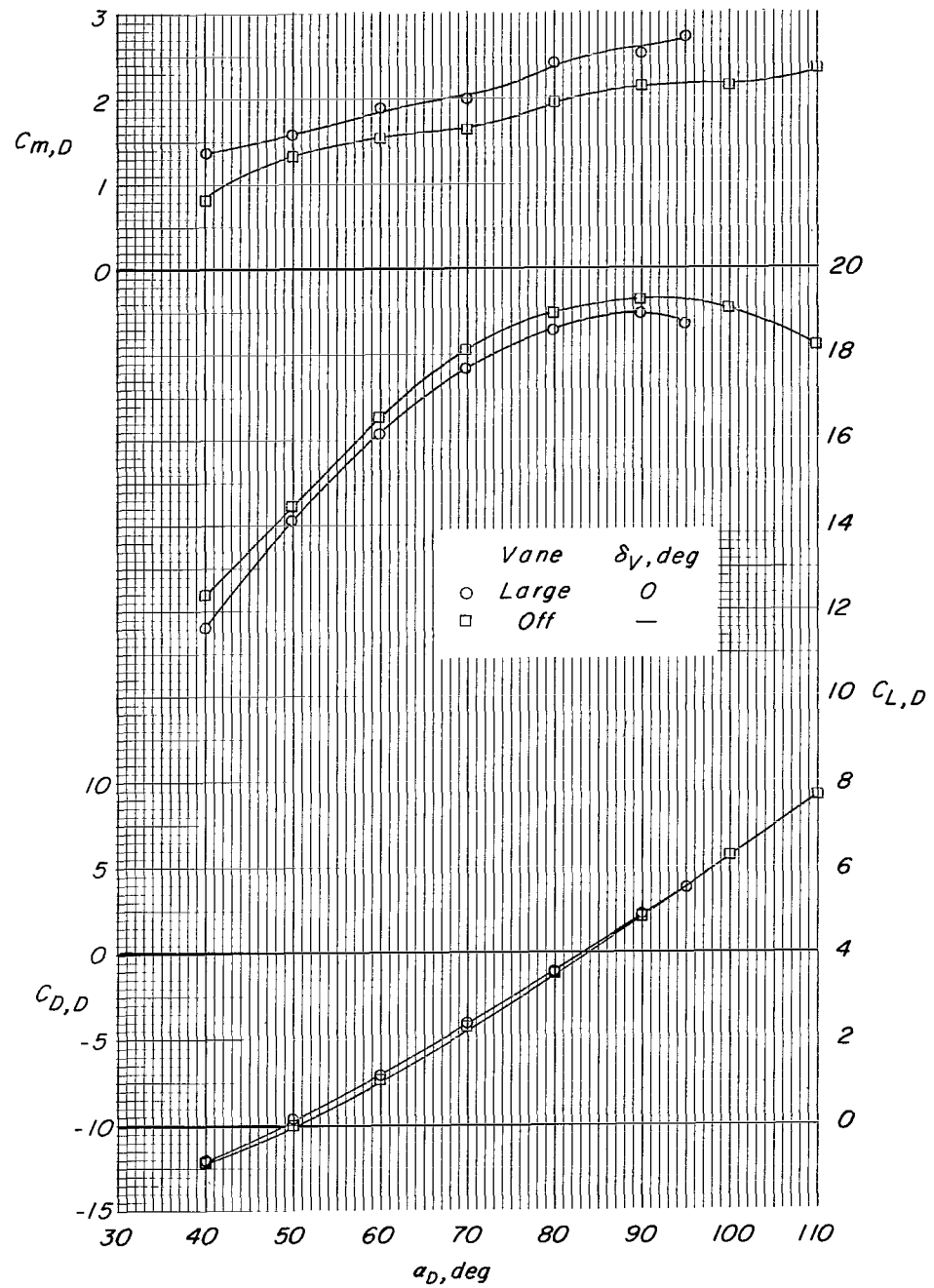


(g) $C_T = 60$.

Figure 27.- Concluded.

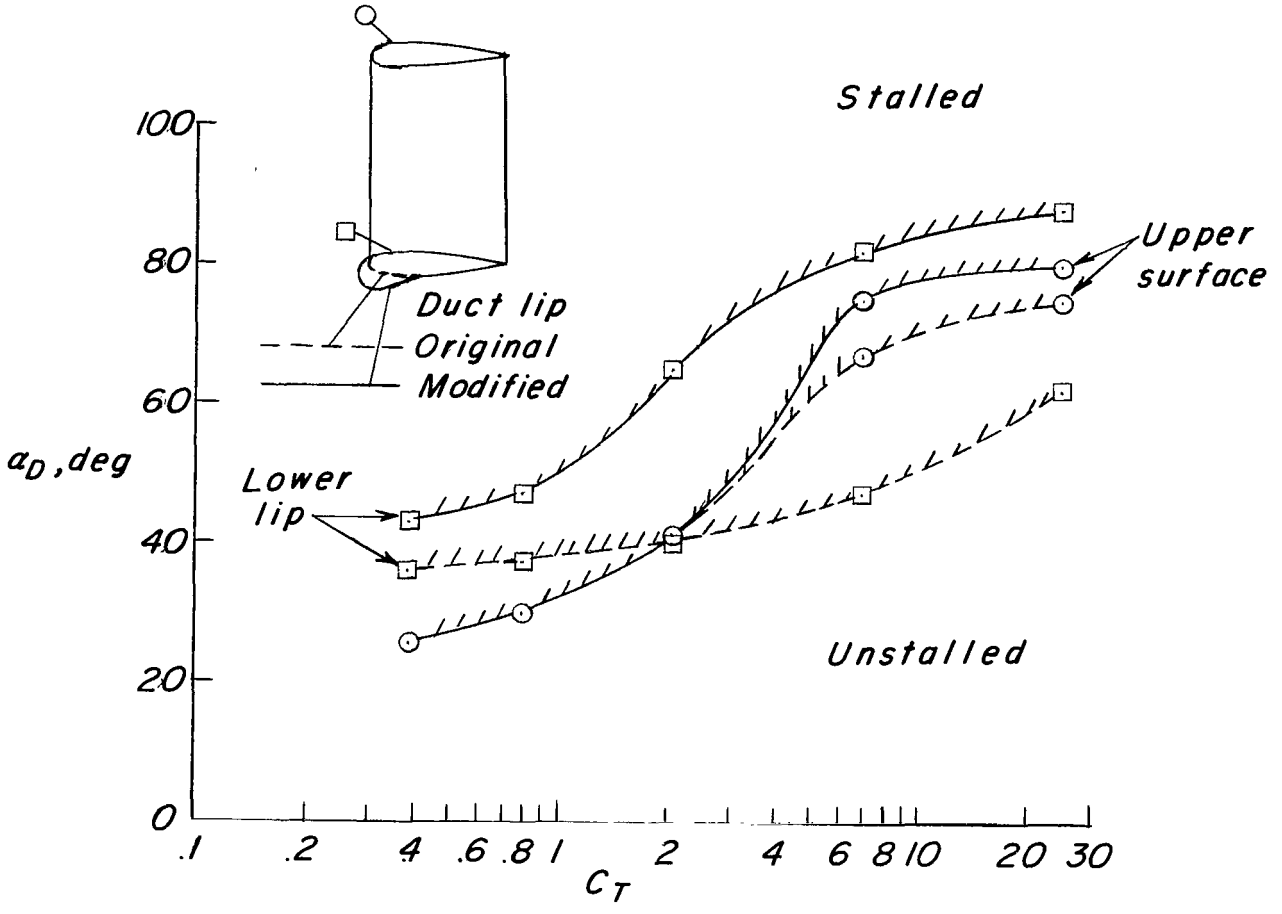


Figure 28.- Summary of isolated-ducted-propeller stall through the thrust coefficient range.

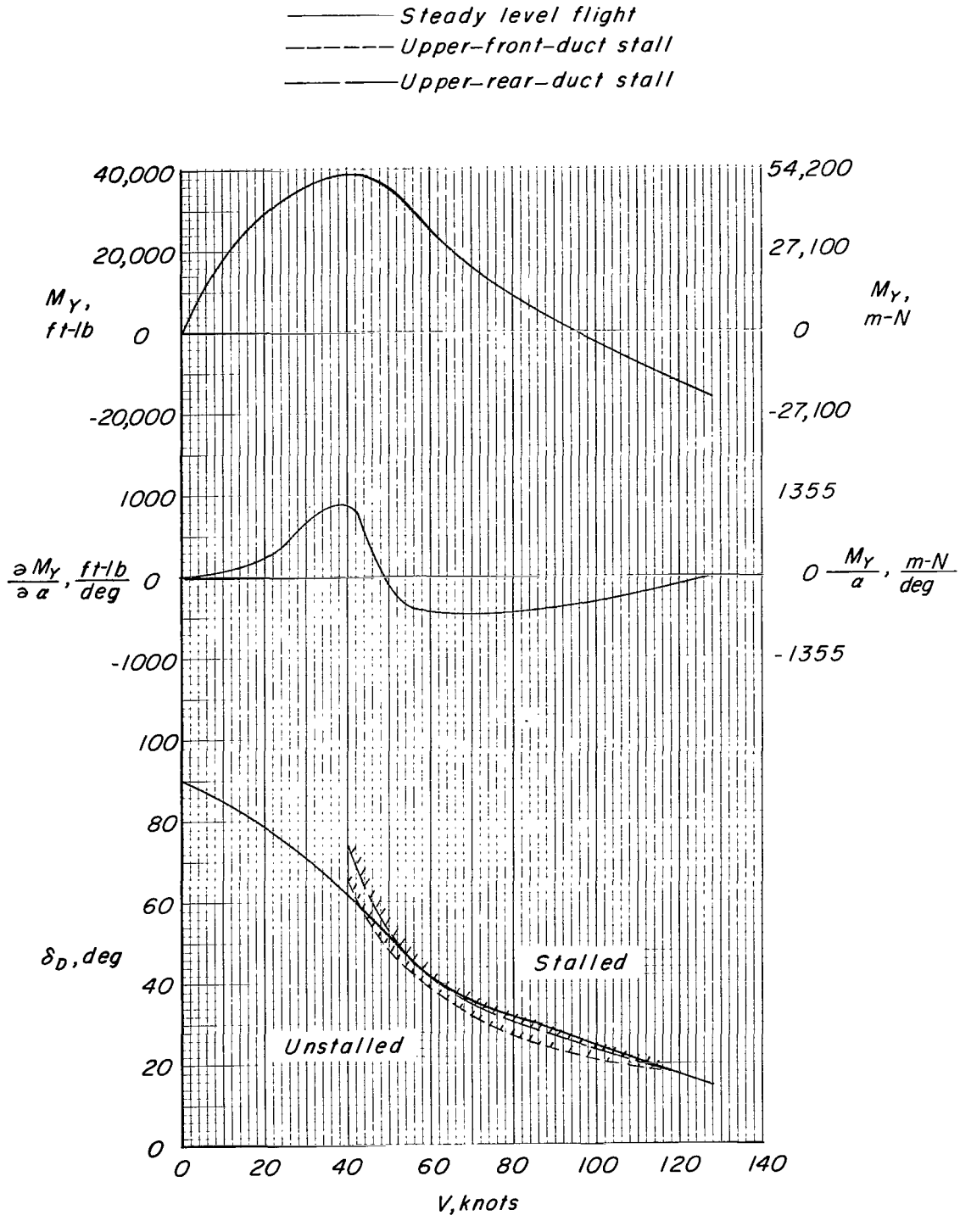


Figure 29.- Pitching moment and duct deflection angles required through the transition speed range for an assumed 15 000-pound (66 720-newton) airplane. $\alpha = 0^{o}$; Thrust = Drag; $\delta_{D,F} = \delta_{D,R}$.

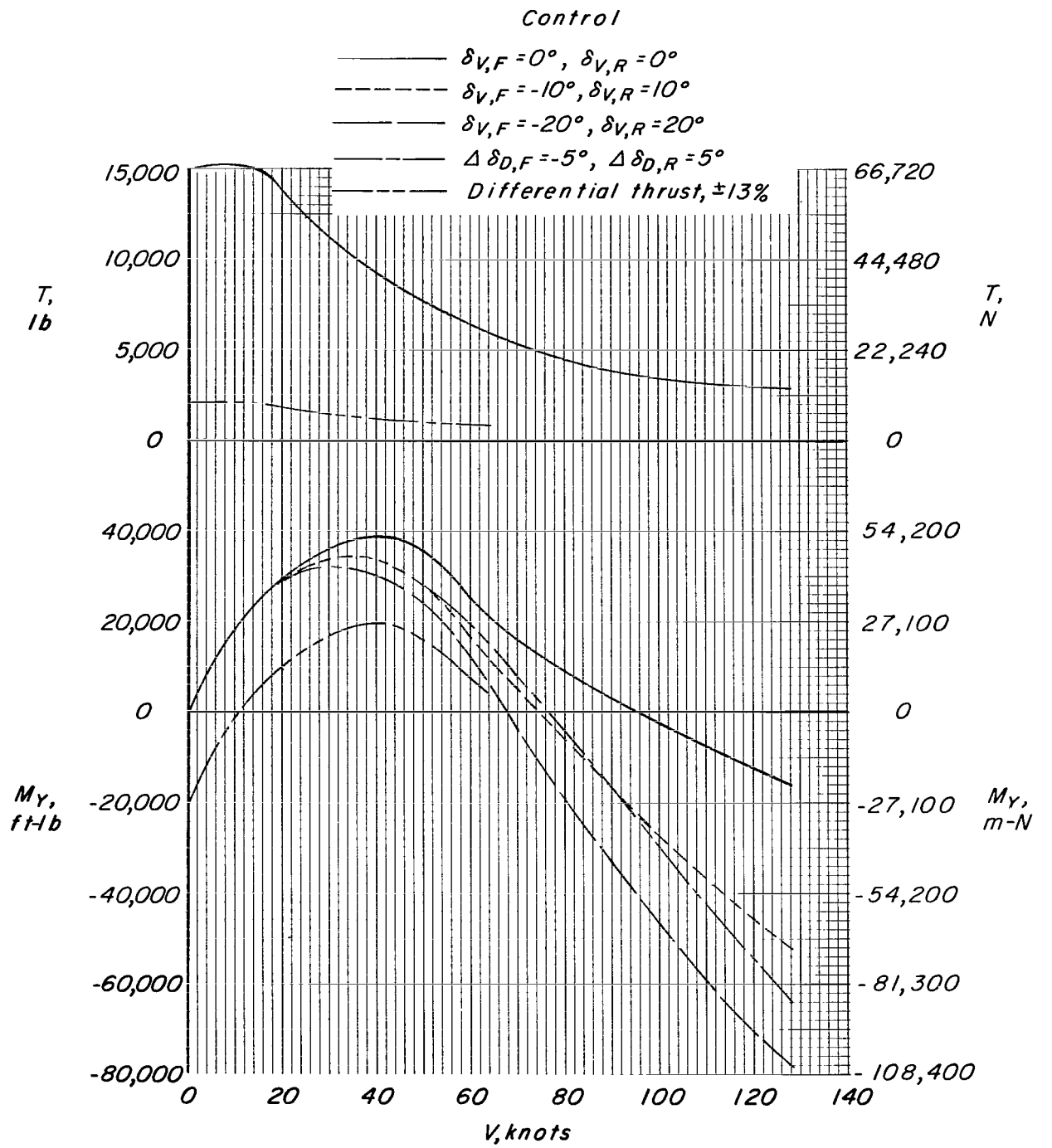


Figure 30.- Pitching moment and thrust required through the transition speed range for an assumed 15 000-pound (66 720-newton) airplane. $\alpha = 0^0$; Thrust = Drag.

*"The aeronautical and space activities of the United States shall be conducted so as to contribute . . . to the expansion of human knowledge of phenomena in the atmosphere and space. The Administration shall provide for the widest practicable and appropriate dissemination of information concerning its activities and the results thereof."*

—NATIONAL AERONAUTICS AND SPACE ACT OF 1958

# NASA SCIENTIFIC AND TECHNICAL PUBLICATIONS

TECHNICAL REPORTS: Scientific and technical information considered important, complete, and a lasting contribution to existing knowledge.

TECHNICAL NOTES: Information less broad in scope but nevertheless of importance as a contribution to existing knowledge.

TECHNICAL MEMORANDUMS: Information receiving limited distribution because of preliminary data, security classification, or other reasons.

CONTRACTOR REPORTS: Technical information generated in connection with a NASA contract or grant and released under NASA auspices.

TECHNICAL TRANSLATIONS: Information published in a foreign language considered to merit NASA distribution in English.

TECHNICAL REPRINTS: Information derived from NASA activities and initially published in the form of journal articles.

SPECIAL PUBLICATIONS: Information derived from or of value to NASA activities but not necessarily reporting the results of individual NASA-programmed scientific efforts. Publications include conference proceedings, monographs, data compilations, handbooks, sourcebooks, and special bibliographies.

***Details on the availability of these publications may be obtained from:***

SCIENTIFIC AND TECHNICAL INFORMATION DIVISION

NATIONAL AERONAUTICS AND SPACE ADMINISTRATION

**Washington, D.C. 20546**